Characterisation and functional analysis of fission yeast tropomyosin mutants and development of quantum dot-antibody conjugates for cellular imaging.

Thesis submitted to the University of Kent for the degree of Doctor of Philosophy (Ph.D.) in the faculty of Science, Technology and Medical Studies.

2010

Daniel East.

Declaration

No part of this thesis has been submitted in support of an application for any degree or qualification of the University of Kent or any other University or Institute of learning.

Signed:

Daniel East.

Abstract

Tropomyosin (Tm) is an evolutionarily conserved dimeric α-helical coiled-coil protein, which interacts end-to-end to form polymers capable of associating with and stabilising actin-filaments and thereby regulate myosin function. The fission yeast, *Schizosaccharomyces pombe*, possesses a single Tm, Cdc8, an essential protein which can be acetylated on its amino terminus to increase its affinity for actin and enhance its ability to regulate myosin function. During this study extensive analyses on the physical properties of acetylated and unacetylated Cdc8 protein, together with a series of novel amino terminal Cdc8 mutants were undertaken in an attempt to explore the effects of amino terminal modification on the Cdc8 protein. In addition, a series of experiments were undertaken to develop fluorescent quantum dot (QD)-antibody (IgG) conjugates for visualising Cdc8 localisation in *S. pombe* cells.

Modifications to the amino terminus altered the stability of the Cdc8 protein, its ability to form end-to-end interactions and its affinity for actin. Changes in actin affinity were reflected in the ability of the Cdc8 proteins to regulate myosin S1 ATPase activity. Despite changes to their biochemical properties, Cdc8 proteins expressed in a temperature sensitive *S. pombe* strain were capable of complementing function at the restrictive temperature. However, when expressed in a Nα-acetyltransferase deficient *S. pombe* strain, the mutant Cdc8 proteins were unable to rescue the growth defects associated with this strain. The QD-IgG conjugates produced during this study produced superior images when compared to organic fluorophores and were significantly more resistant to photobleaching.

This work has provided insights into the importance of acetylation and the structure of the amino terminus for the function of fission yeast Tm and has highlighted the importance of reaction stoichiometry, the difficulties arising from non-specific binding and quenching of fluorescence intensity when coupling QDs to IgG complexes.

Contents

List of tables and figures

List of abbreviations

ADF: Actin depolymerisation factor

APB: Actin binding protein

BSA: Bovine serum albumin

CAR: Contractile actomyosin ring

CD: Circular dichroism

dH$_2$O: Deionised water

EDC: 1-ethyl-3-(3-dimethylaminopropyl) carbodiimide

EM$_{\lambda 495}$: Emission at 495 nm

EX$_{\lambda 468}$: Excitation at 468 nm

F-actin: Filamentous actin

FITC: Fluorescein isothiocyanate

Fluor: Fluorescence at 495 nm

FPLC: Fast protein liquid chromatography

FT: Flow-through

G-actin: Globular actin

HMW: High molecular weight

IgG: Immunoglobulin G (antibody)

LDH: Lactate dehydrogenase

LMW: Low molecular weight

MES: 2-(*N*-morpholino)ethanesulfonic acid

MOPS: 3-(N-morpholino)propanesulfonic acid

MTOC: Microtubule organising centre

OD$_{260}$: Optical density at 260 nm

OD$_{280}$: Optical density at 280 nm

OD$_{600}$: Optical density at 600 nm

PBS: Phosphate buffered saline

PEP: Phosphoenolpyruvate

Pi: Inorganic phosphate

PK: Pyruvate kinase

QD: Quantum dot

R: Retentate

RT: Room temperature

S1: Myosin II sub-fragment 1

SDS-PAGE: Sodium dodecyl sulfate polyacrylamide gel electrophoresis

SIN: Septation initiation network

SPB: Spindle pole body

Tm : Tropomyosin

Tris: tris(hydroxymethyl)aminomethane

WT: Wild type

Chapter 1: Introduction

1.1. Cells and cell growth

The cell is the basic functional unit of life. Cell theory was proposed in 1838 by Theodor Schleiden and Jacob Schwann and stated that all living organisms are composed of one or more cells and that new cells can only arise through the division of existing cells. Viruses are the one exception to cell theory, but are dependent on cells for their reproduction.

In order to grow and divide a cell must have a number of components: the information and facilities to produce new cellular components, a boundary between the cell and the environment, and a mechanism for dividing the cell in two (Murray and Hunt, 1993). The information is encoded in the sequence of the DNA which must be duplicated and segregated into two daughter cells. The genes must also be expressed to produce proteins that control cell growth and that form the components of future cells.

In animals cells the boundary between the cell and its environment is defined by the plasma membrane, composed of lipids and proteins, which mediates interactions between the cell and the environment (Purves et al., 2001). Plant, fungal and often bacterial cells have an extra-membrane cell wall, composed predominantly of cellulose and pectin in plants (Raven et al., 1992), chitin in fungi and peptidoglycan in bacteria (Madigan et al., 2003). Cell walls provide structural support and protection.

As cells replicate their DNA, and produce new components for the next generation of cells they must grow to accommodate these new components. Animals cells expand by deposition of new plasma membrane (Purves et al., 2001). Growth in plants, fungal and bacterial cells occurs by deposition of new cell wall materials and the turgor driven expansion of the membrane (Madigan et al., 2003; Raven et al., 1992). Cell growth is regulated by the Rho/Rac superfamily of proteins which act as molecular 'switches' activating signalling pathways that stimulate

various essential cellular processes (Aznar and Lacal, 2001). Once cells reach a critical size (Nurse, 1975) a complex and precise series of events divides the cell into two identical daughter cells (Pollard and Wu, 2010). The synthesis of new cellular components and cell division occur at discrete points in the cell cycle.

1.2. The cell cycle

The eukaryotic cell cycle can be divided into two fundamental parts: interphase, which occupies the majority of the cycle in which much of the cell's growth occurs and mitosis, which lasts for a significantly shorter period of time and results in the division of the cell in to two identical daughter cells. Interphase can be further subdivided in to 3 phases, G1, S and G2. The cell cycle therefore has four distinct phases (Figure 1.1) much of the cell growth occurs during interphase including synthesis of new membranes ribosomes, mitochondria and most cellular proteins. Cells that do not divide are normally arrested in G1 in a quiescent state also known as G0. Synthesis of DNA is carried out during S phase, it is preceded by a gap called G1 and followed by a gap called G2 The transitions between these four phases are mediated by cyclin dependent kinases (Cdks) and their regulatory subunits, cyclins. For example, Cdk2-cyclin E acts at the G1-S boundary initiating DNA replication, while Cdk1-cyclin B acts at the G2-M boundary initiating mitosis (Purves et al., 2001).
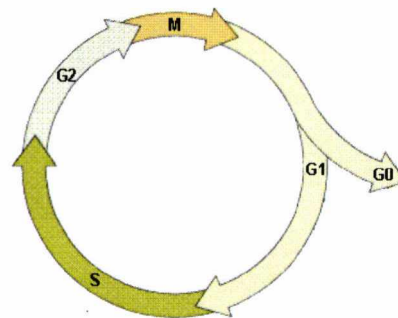
Figure 1.1. Stages of the cell cycle

Mitosis (M) represents only 5% of the cell cycle. There is a substantial G1 gap between mitosis and DNA synthesis (S) and a second G2 gap between replication and mitosis Adapted from (Purves et al., 2001)

In a typical animal cell, G1 lasts approximately 12 hours, S phase 6 hours, G2 6 hours and mitosis roughly 30 minutes (Murray and Hunt, 1993) Although mitosis is a continuous process it is more convenient to divide it in to several sub-phases (Figure 1.2). Upon transition into mitosis the cell enters prophase during which chromatin condenses inside the nucleus to form chromosomes comprised of two identical chromatids. Polar microtubules form between the replicated centrosomes and make up the developing spindle. During prometaphase, the nuclear membrane breaks down, kinetochore microtubules appear and connect the kinetochores of each chromosome to a centrosome.
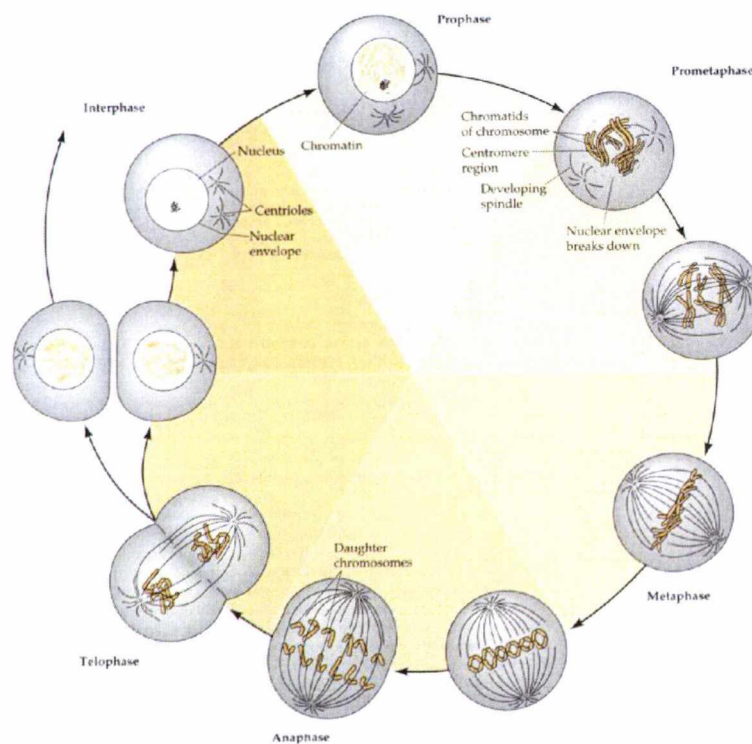
Figure 1.2. The stages of mitosis

The diagram shows the condensation of chromosomes in prophase and alignment of chromosomes along the cells equator by the spindle in metaphase. The daughter chromatid linkages are broken by DNA topoisomerase II and the chromatids are pulled to opposite poles of the cell during anaphase. In telophase chromosomes de-condense and nuclear membranes reform. At the same time the cell undergoes cytokinesis dividing the cytoplasm to create two daughter cells. Adapted from (Purves et al., 2001)

The cell is said to be in metaphase once the chromosomes have aligned along the equatorial plane, cohesion proteins connecting the chromatids break down and interconnected DNA at the centromere is unravelled by DNA topoisomerase II. During anaphase, the chromatids migrate to opposite poles, driven mainly by molecular motors at the kinetochores and also by shortening of the microtubules at the poles. As the chromosomes reach the poles the cell enters telophase and the nuclear envelope re-forms. The process of cytokinesis occurs concurrently where a contractile ring divides the cytoplasm to create two daughter cells (Murray and Hunt, 1993; Purves et al., 2001). Strict coordination of the cytoskeletons and cell growth are crucial for the successful execution of each cell division cycle.

1.3. An overview of *Schizosaccharomyces pombe* and its life cycle

Fission yeast was isolated in 1893 from East African millet beer and the species name is derived from the Swahili word for beer. It was first developed as an experimental model organism in the 1950s for studying cell physiology by Murdoch Mitchison and Urs Leupold (Leupold, 1957; Mitchison, 1957).

S. pombe is a unicellular eukaryote, whose rod-shaped cells typically measure 2 to 3 micrometers in diameter and 7 to 14 micrometers in length. Its cell cycle has distinct G1, S, G2 and M phases (Mitchison, 1970) and a generation time of between 2 to 4 hours. In contrast to animal cells *S. pombe* has a long G2 phase making up approximately 70% of the cell cycle. The remaining phases are each roughly 10% of the cell cycle (Moreno et al., 1991). The genome size of *S. pombe* is 12.4Mbp in length and was originally predicted to contain 4824 genes (Wood et al., 2002) although currently 5027 have been identified (Sanger Institute website as of 24/02/2010). These genes are organised into three fission yeast chromosomes (Robinow, 1977), of 5.7 4.6 and 3.5 Mb in size (Smith et al., 1987a)

Wild type strains of *S. pombe* used routinely in the laboratory grow as haploids and can be one of two mating types, h^+ (P) or h^- (M). When starved of nutrients, especially nitrogen (Yamamoto, 1996), cells of opposite mating types mate to form zygotes which can then directly undergo meiosis to form ascospores which germinate when nutrients become available to produce haploid clones (Leupold, 1970). In specific conditions the zygote can enter mitosis thereby creating a diploid strain. This happens for instance, if the cells are transferred to a nutrient rich environment before they are committed to meiosis. Wild type *S. pombe* cells isolated from the wild are homothallic (h^{90}) and switch mating type every other generation (Gutz et al., 1976). This ensures that a colony which has arisen from a single cell contains both h^+ and h^- cells, therefore an h^{90} strain is able to mate with itself. Mutations in the mating type locus
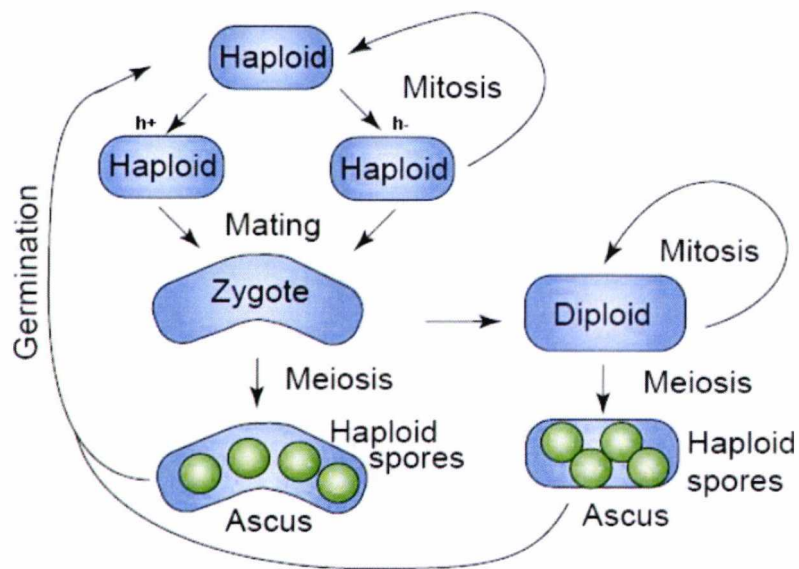
Figure 1.3. The life cycle of *S. pombe*

Fission yeast can exist in both haploid and diploid forms. Nutritional starvation and the heterozygous diploidy (h^+ /h^-) of the cells are essential requirements for meiosis. Adapted from (Dalgaard and Klar, 2001)

of, h⁺ or h⁻ cells that are unable to switch mating type and are used routinely in the lab.

The mechanisms which control the cell cycle were originally elucidated in fission yeast during the 1970s (Nurse, 1975; Nurse et al., 1976) Its similarity to higher eukaryotes, in addition to it's recently sequenced genome (Wood et al., 2002) make it a powerful tool for studying DNA damage and replication, cell cycle controls, cell growth and the cytoskeletons.

1.3. Cytoskeletons.

The cytoplasm of eukaryotes contains a system of long fibres known as the cytoskeleton which has several important roles. The cytoskeleton supports and maintains cell morphology, is important for various types of cell movement and some of the fibres act as 'tracks' for motor proteins, which transport cellular cargoes throughout the cytoplasm (Purves et al., 2001). The cytoskeleton is comprised of microfilaments, intermediate filaments and microtubules (figure 1.4.).

Microtubules are polymers of the protein tubulin. During interphase, microtubules organise the cytoplasm, anchor the nucleus and organelles in place, and are the major components of cilia and flagella. During mitotic division a large array of microtubules form the mitotic spindle, which orientates the plane of division, arranges the individual chromosomes and separates them into the daughter cells (Purves et al., 2001). Tubulin heterodimers of α-tubulin and β-tubulin (Weisenberg et al., 1968) polymerise into protofilaments. Typically, the protofilaments arrange themselves in an imperfect helix with one turn of the helix containing 13 tubulin dimers, each from a different protofilament (Tilney et al., 1973). Tubulin polymerizes end-to-end with the α-subunit of one tubulin dimer contacting the β-subunit of the next, as a result microtubules have polarity. The end with exposed β-subunits is referred to as the *plus*

end, while the α-subunit exposed end is called the *minus* end (Allen and Borisy, 1974).

Microtubules radiate from a microtubule organizing centre (MTOC), known as the centrosome in animal cells and the spindle pole body (SPB) in yeast. MTOCs contain γ-tubulin (Oakley et al., 1990) which nucleates $\alpha\beta$-tubulin for microtubule polymerisation. Microtubules are highly dynamic structures that constantly shrink (catastrophe) and grow (recovery) from the plus end (Walker et al., 1988). This is controlled by the nucleotide status of tubulin; GTP bound tubulin is incorporated into the growing plus end, where it is hydrolysed to GDP tubulin promoting catastrophe (David-Pfeuty et al., 1977; Weisenberg and Deery, 1976). Dynamics are regulated by the stabilising effects of a group of microtubule associated proteins (MAPs) (Mandelkow and Mandelkow, 1995). Two classes of molecular motors associate with microtubules and are responsible for carrying vesicles and cellular cargoes throughout the cytoplasm. Dynein and kinesin typically move towards the minus end and plus ends, respectively (Ross et al., 2008).

Intermediate filaments are found only in multicellular organisms and are composed of fibrous proteins of the keratin family. In cells, these proteins are organised into coiled-coil filaments (Qin et al., 2009) of 8-12 nm in diameter (Ishikawa et al., 1968). Intermediate filaments have several structural functions: they stabilise the cell structure (Herrmann et al., 2007) and maintain the positions of the nucleus and other organelles in the cytoplasm. They also resist tension (Wang and Stamenovic, 2002) and provide strength and rigidity in connective and epithelial tissues.

Microfilaments are helical filaments composed of actin monomers, which are discussed in detail below.
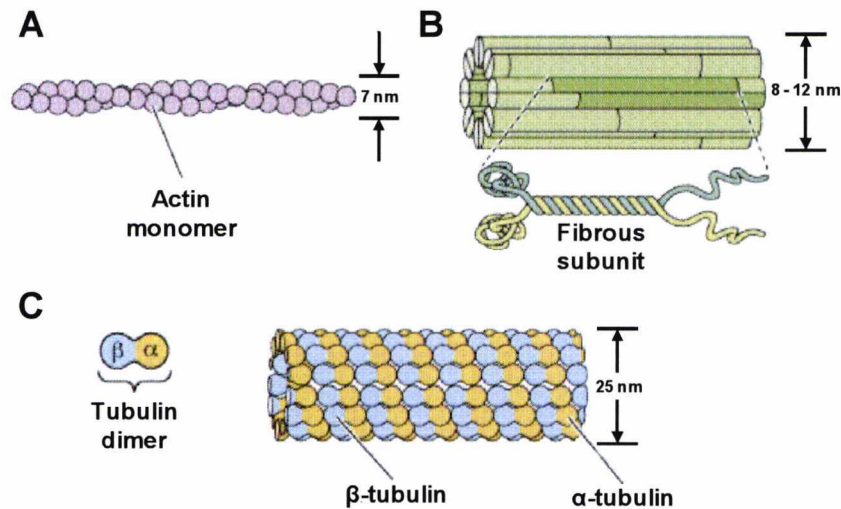
Figure 1.4. Components for the cytoskeleton

(A) Microfilaments are polymers of actin monomers (B) Intermediate filaments are composed of fibrous subunits of keratin family proteins bundled together (C) Microtubules are composed of bundles of tubulin protofilaments. Adapted from (Purves et al., 2001)

1.4. Actin

Actin is found in two mains forms, globular (G) actin in its monomeric state and filamentous (F) actin as a helical polymer. The crystal structure of this 43 kDa protein was first determined in 1990 (Kabsch et al.) and it was seen to be a monomeric, asymmetrical molecule consisting of two major domains. These domains can be further divided into two subdomains giving the molecule 4 subdomains numbered 1-4 (Figure 1.5.). Located between the two major domains is a nucleotide binding cleft, in which ATP or ADP+Pi is tightly bound. ATP binds as a complex with Mg^{2+} or Ca^{2+} (Carlier et al., 1994) and the ionic strength determines how tightly the nucleotide binds.

When decorated with myosin subfragment 1 (S1) filamentous actin has an arrowhead like appearance (Huxley, 1963) and for this reason opposite ends of actin filaments have been described as either barbed or pointed. These ends correspond to exposed subdomains 1 and 3 (barbed) and subdomains 2 and 4 (pointed) respectively. Actin filaments polymerise predominantly by incorporation of ATP bound actin monomers
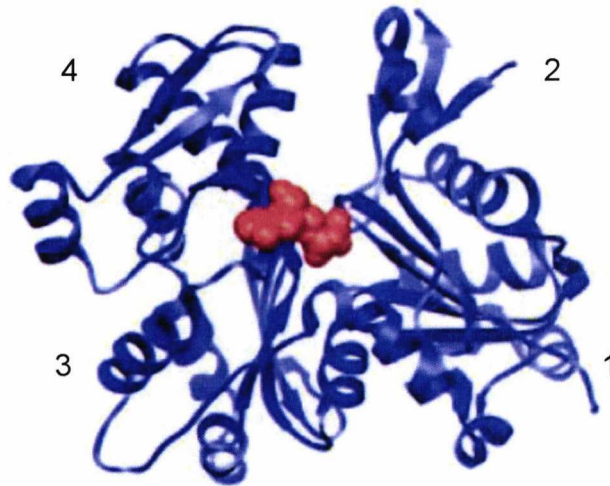
Figure 1.5. The crystal structure of an actin monomer.

A ribbon diagram representation (blue) of the crystal structure of actin monomers. Subdomains are numbered 1 to 4.. ATP binds as a complex with Mg^{2+} or Ca^{2+} and is shown as a red space filling representation. Adapted from (Reisler and Egelman, 2007)

into the barbed (+) end of the filament forming a helical polymer. ATP is then hydrolysed relatively quickly (0.05-0.3 s) to ADP+Pi (Blanchoin and Pollard, 2002) and the inorganic phosphate slowly dissociates. Disassociation of ADP bound actin subunits occurs principally at the pointed (-) end of the actin filament.

The helical nature of f-actin is incompatible with any crystal space group, and as such a crystal structure for F-actin has not yet been determined and only models exist. The most important model was described by Holmes et al. (1990) using a rotational and translational search for a placement of the actin monomer crystal structure into a helical filament so as to best match the observed x-ray fibre diffraction pattern from an oriented F-actin gel. This model is based on the assumption that no large scale conformational change is needed between a G-actin monomer and an F-actin filament.

Humans have 6 actin genes. ACTA1 and ACTC1 are expressed in skeletal and cardiac muscle respectively, ACTA2 and ACTG2 are expressed in smooth muscle tissue, while ACTB and ACTG1 are

cytoskeletal isoforms. Actin filaments can be broadly classified into three categories: actin patches, actin filaments and contractile rings (CARs). *Actin patches* are branched networks of short actin filaments. They typically associated with membranes and are involved cell migration, adhesion and endocytosis (Chhabra and Higgs, 2007; Robertson et al., 2009). *Actin filaments* composed of longer actin polymers bundled together by actin binding proteins. They span the cytoplasm and serve as 'tracks' for actin associated motors (myosins) for intracellular cargo delivery (DePina and Langford, 1999). In association with specific myosins they can generate the forces which modulate cell morphology (Pellegrin and Mellor, 2007), and also have structural roles in cellular protrusions such as filopodia and microvili (Chhabra and Higgs, 2007). CARs are specialised structures comprised of actin and many other components (Pollard and Wu, 2010), that guide the ingression and deposition of new membrane during cytokinesis (Noguchi et al., 2001).

1.5. Actin distribution in *S. pombe*

S. pombe has a single actin gene, *act1$^+$* (Mertins and Gallwitz, 1987). The fission yeast actin cytoskeleton consists of three simple actin structures; cortical patches, cables and a contractile actomyosin ring (CAR) (Marks and Hyams, 1985). The *S. pombe* actin cytoskeleton is highly dynamic and reflects the pattern of growth and cytokinesis (Arai et al., 1998; Marks and Hyams, 1985). Actin patches localise to the growing cell tips and are thought to be involved in deposition of cell wall materials (Kobori et al., 1989) After the fission yeast cell divides, growth occurs exclusively at the old cell end, a process known as old end take off. Once the cell reaches a critical size, between 9 and 9.5 microns and has passed early G2 phase, growth begins at the new end, termed new end take off (Mitchison and Nurse, 1985). Actin patch localisation reflects this growth pattern and immediately after cell division patches are only observed at the old end of the cell (Marks et al., 1986), later on in the cell cycle patches are observed at both cell tips.

During interphase actin cables run the length of the cell and are attached to actin patches (Arai et al., 1998). At the onset of mitosis actin patches disappear from the cell ends, an aster like structure branches from longitudinal actin cables at the cell equator (Arai and Mabuchi, 2002) and F-actin cables accumulate at the medial cortex. As the aster extends to form the primary ring and accumulated actin cables are linked to it and longitudinal actin cables are also seen attached to the growing ring.
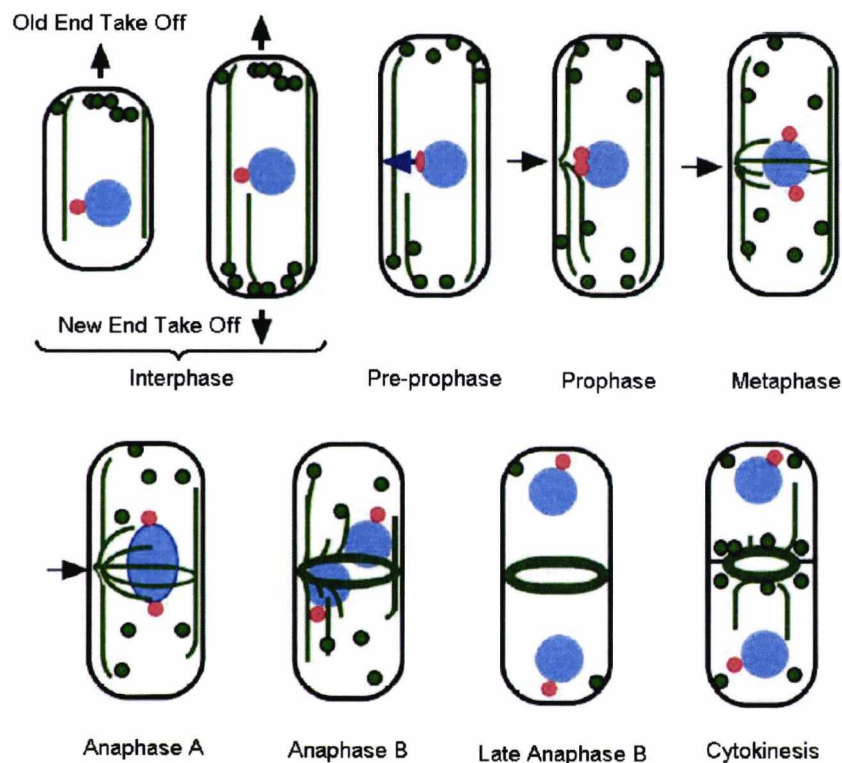
Figure 1.6. Distribution of f-actin through out the cell cycle.

After cell division actin patches are observed at the old end of the cell, after new end take off, patches are localised to both cell tips and actin cables run the length of the cell. Positional signals (blue arrow) from the nucleus promote the formation of an aster like structure (black arrow) which extends into a primary ring. Actin cables are incorporated into the CAR and patches disappear from the tips. A septum forms behind the constricting ring and actin patches localise to the site of new cell wall synthesis Actin: green, nuclear membrane: blue, SPB: red, cell wall: black. Adapted from (Noguchi et al., 2001).

1.6. Actin binding proteins

The dynamic nature of actin polymers are regulated by a variety of actin binding proteins (ABPs). These include the arp2/3 complex, profilin, formins, ADF/cofilin, actin capping proteins and bundling proteins which will be discussed briefly below, and tropomyosin which will be discussed in depth later in this chapter. These proteins can be grouped broadly into 4 categories although some have overlapping functions:

- o Actin polymerisation factors.
- o Actin depolymerisation factors
- o Actin stabilising proteins.
- o Actin bundling proteins.

1.6.1. The Arp2/3 complex

The Arp2/3 complex was first isolated from *Acanthoamoeba* (Machesky et al., 1994), and consists of seven subunits: two actin related proteins Arp2 and Arp3 and 5 other proteins p40, p35, p19, p18, and p14. These proteins are conserved though evolution and have homologs in all eukaryotes (Welch et al., 1997).

The Arp2/3 complex initiates the formation of actin filaments with free barbed ends by nucleating new actin filaments (Mullins et al., 1998a) and prevents dissociation of actin monomers from the pointed end by binding tightly. In addition the Arp2/3 complex promotes actin branching at a constant 70^0 angle by binding the side of an existing filament and nucleating a new filament, or by attaching pointed ends of filaments to the sides of other filaments. The nucleation activity of the Arp2/3 complex is regulated by the WASP (Wiskott-Aldrich syndrome protein) protein family (Machesky and Insall, 1998) which is in turn regulated by the GTPase CDC42 and membrane lipid phosphatidylinositol 4,5-bisphosphate (PIP_2) (Rohatgi et al., 2000) and transduce signals from extracellular stimuli to the actin cytoskeleton. In *S. pombe* the Arp2/3 complex localises to actin patches at growing cell ends, actin cables running the length of the cell
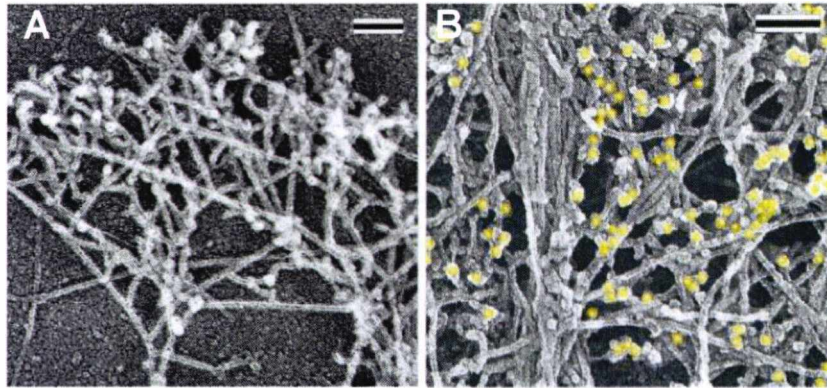
Figure 1.7. Actin and the Arp2/3 complex

(A) Electron micrograph of branched actin filaments in lamellipodia
(B) Electron micro graph of the Arp2/3 complex (yellow) associated
with branched actin filaments visualised by immuno-gold labelling
Scale bar= 0.1 µm. Adapted from (Svitkina and Borisy, 1999)

and to the medial ring during cytokinesis (Balasubramanian et al., 1996;
McCollum et al., 1996)

1.6.2. Profilin

Profilins are small ABPs with an approximate molecular weight of 19 kDa
(Ampe et al., 1988) and bind the 'barbed' end of cytoplasmic actin
monomers promoting the exchange of ADP for ATP (Vinson et al., 1998),
thereby maintaining a pool of actin monomers with high affinity for the
growing barbed end of filaments. Profilin can bind to the Arp2/3 complex
(Mullins et al., 1998b), and dissociation of profilin from actin is stimulated
by PIP2 (Goldschmidt-Clermont et al., 1990); suggesting profilin may play
a role in transmitting signals between the cell membrane and the actin
cytoskeleton.

S. pombe has a single profilin encoded by the *cdc3*[+] gene and it was
originally identified as a temperature sensitive cell division cycle mutant
(Nurse et al., 1976). Cdc3 is required for actin ring assembly and
overexpression results in cell cycle arrest and no observable actin
structures, due to sequestration of actin monomers by the profilin
(Balasubramanian et al., 1994).
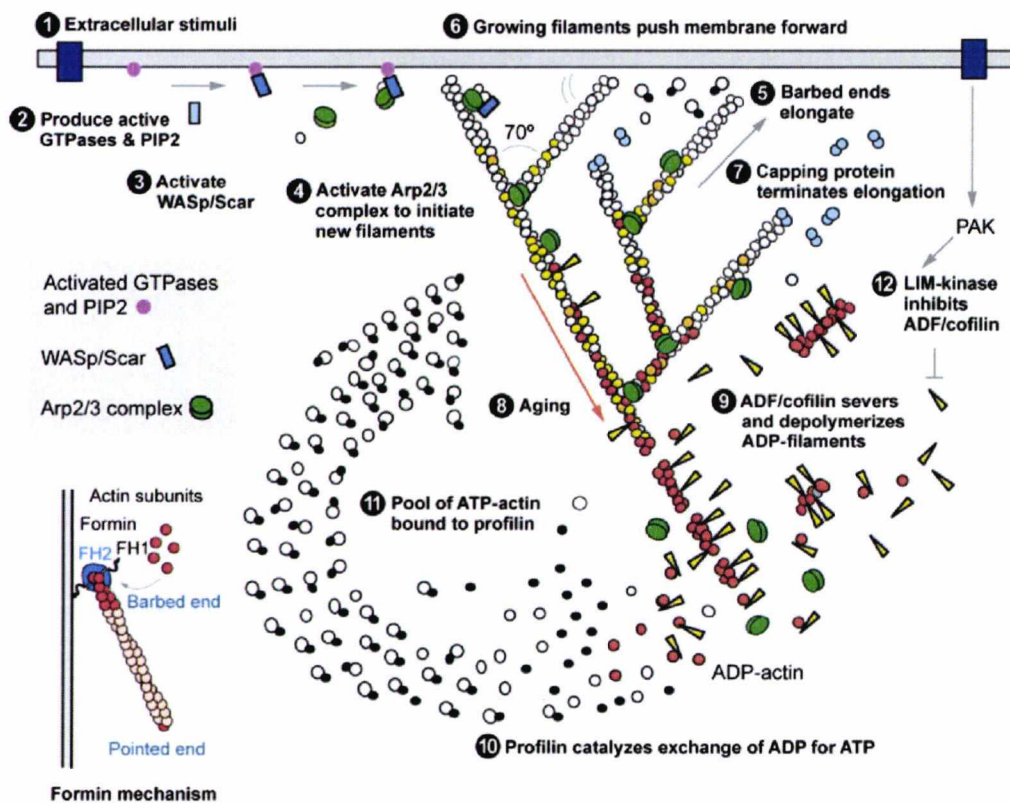
Figure 1.8. Actin nucleation and dynamics.

WASp family proteins activate the Arp2/3 complex to initiate nucleation of new actin filaments. Arp2/3 also initiates branching by binding to the sides of existing filaments. Filaments grow by incorporation of profilin bound actin monomers into the barbed end until barbed end capping limits elongation. As filaments mature severing and depolymerisation is induced by ADF/cofilin. Formins nucleate unbranched filaments and remain attached to their barbed ends as they polymerise. Adapted from (Pollard, 2007)

1.6.3. Formins

Formins are a family of key actin filament nucleators that are involved in the assembly of many actin containing structures. Originally identified in mice as a gene that was disrupted in animals with limb deformity defects (Woychik et al., 1990), formins appear to be universally present in eukaryotic cells (Higgs and Peterson, 2005). Formins have two conserved formin homology (FH) domains (Castrillon and Wasserman, 1994), the FH1 and FH2 domains. The FH2 domain, essential for actin

cable assembly in yeast (Evangelista et al., 2002; Sagot et al., 2002a), binds and nucleates actin monomers (Sagot et al., 2002b) and associates with the barbed ends of f-actin polymers (Pruyne et al., 2002). As filaments elongate formins remain associated with the growing barbed end. The FH1 domain, rich in proline residues allows for profilin binding (Chang et al., 1997; Watanabe et al., 1997) which increases the rate of formin-mediated barbed end elongation (Romero et al., 2004).

S. pombe has 3 formins each fulfilling a distinct cellular role. For3 is required for actin cable assembly and polarized cell growth (Feierbach and Chang, 2001), Cdc12 an essential CAR component (Chang et al., 1997) and Fus1 which is required for mating (Petersen et al., 1995). Cdc12 has a unique property compared to other formins; it binds barbed ends of actin filaments, but will not allow addition of actin monomers unless profilin is present (Kovar et al., 2003). This property is known as 'profilin gating'.
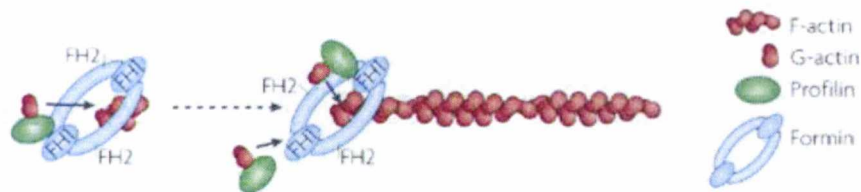
Figure 1.9. Formin mediated actin polymerisation

Profilin bound G-actin monomers are incorporated into a growing F-actin filament by formin which remains associated with the growing end.

1.6.4. ADF/Cofilin

The actin depolymerisation factor (ADF)/cofilin family are conserved actin binding proteins that promote disassembly of actin filaments. ADF/cofilin was first isolated from embryonic chicken brains as a protein that promoted depolymerisation of actin filaments (Bamburg et al., 1980) and cofilin was isolated as a small protein that cosedimented with filamentous actin (Maekawa et al., 1984). These proteins appear to be ubiquitous among eukaryotes and homologs with a variety of names have been

isolated from numerous species, including invertebrate depactin, porcine destrin, *Acanthamoeba* actophorin, *Dictyostelium* coactosin, *Drosophila* twinstar, and *Xenopus* Acs (dos Remedios et al., 2003). Despite the nomenclature there are only genes for two types, ADF and cofilin. Although distinctly different they are often considered synonymous.

ADF/cofilin binds to F-actin, contacting two actin monomer and imparting a conformational twist on the actin filament (McGough et al., 1997). The action of ADF/cofilin is suggested to be concentration dependent. At low concentrations of cofilin the tensional strain between twisted regions of the actin filament and non-twisted regions may be at a maximum and promote filament severing. At moderate concentrations where the filament is largely decorated with cofilin no severing is observed and at high concentrations ADF/cofilin is capable of nucleating new actin filaments (Andrianantoandro and Pollard, 2006). ADF/cofilins are inactivated by phosphorylation on serine 3 by a signal transduction pathway (PAK and LIM kinases) (Van Troys et al., 2008).

S. pombe has a single ADF/cofilin gene adf[+] and the protein is required for formation and maintenance of the CAR (Nakano and Mabuchi, 2006b). During mitosis Adf depolymerises F-actin patches at the cell tips by dissociating arp2/3 associated branched filaments from actin, and also by filament severing (Chan et al., 2009). F-actin assembles at the medial region, where Adf can sever long filaments into shorter ones that are more easily incorporated into the CAR (Nakano and Mabuchi, 2006b). A balance between the destabilising effects of Adf and the stabilising action of other APB help maintain the CAR.

1.6.5. Actin capping proteins

Actin capping proteins bind to the ends of F-actin and are involved in regulating filament dynamics. Capping proteins suppresses both the association and dissociation of actin monomers from filament ends. The most abundant barbed end capping protein, present in all eukaryotic cells

is CapZ (Schafer and Cooper, 1995). CapZ is a heterodimer comprising an α and a β subunit both of which are required for effective barbed end capping (Casella and Torres, 1994). The protein prevents the exchange of actin monomers from the barbed of the actin filament as well as annealing of two f-actin filaments (dos Remedios et al., 2003). In addition CapZ can enhance actin polymerisation by binding to and stabilising actin forming nuclei for elongation into filaments (Casella et al., 1987).

In mammals the most predominant pointed end capping protein is tropomodulin. Tropomodulin has a weak actin affinity, but this increases approximately 1000 fold (Weber et al., 1999) when tropomyosin is present. The molecule has two domains that are tilted 40^0 relative to each other. The amino terminus binds to tropomyosin while the carboxyl terminus protrudes from the pointed end bending towards the terminal actin subunit, thus capping the pointed end (Fujisawa et al., 2001).

The actin capping protein in *S. pombe* is a heterodimer formed from the products of the *acp1⁺* and *acp2⁺* genes. Capping protein competes with formins for actin filament barbed ends and cells lacking capping protein display excess actin filaments in actin patches, as well as depolymerised actin cables (Kovar et al., 2005). Capping protein is involved is assembly of the CAR in conjunction with ADF, profilin and actin crosslinking proteins (Nakano and Mabuchi, 2006a). Fission yeast does not possess a tropomodulin and to date, no proteins with obvious similarities have been identified.

1.6.6. Actin cross-linking proteins

Assembly of actin filaments into bundles and networks is essential for cytoskeletal function and is dependent upon actin crosslinking proteins. Cross-linking proteins with homologs in *S. pombe* will be summarised here, namely α-actinin, fimbrin and IQGAP. Fimbrin, which is found from yeast to humans (Matsudaira, 1994a) is the simpler of the three, a monomeric protein containing two tandem actin binding sites, and a

calcium binding carboxyl domain consisting of two EF hand motifs. α-actinin is a dimeric protein, with the amino terminal actin binding domain of each polypeptide followed by 4 α helical repeats or 'spacers' and an EF hand containing carboxyl terminus (Matsudaira, 1994a). The dimer is arranged in a anti-parallel fashion (Djinovic-Carugo et al., 1999) and the number of 'spacers' determines the separation between cross-linked actin filaments. Fimbrin and α-actinin both bind to the same region on actin, at a site overlapping subdomains 1 and 2 (Matsudaira, 1994b).

IQGAPs are homodimeric proteins (Bashour et al., 1997), and their subunits contain several protein interacting domains. These include an actin binding calponin homology domain, several IQ motifs and a GTPase activating protein (GAP) domain. GAPs inhibit GTPases by increasing their GTPase activity, cycling them to an inactive, GDP bound state. IQGAP bind two GTPases but does not act as a GAP. Instead it appears to inhibit GTPase activity of GTPases, maintaining them in an active state (Tirnauer, 2004). Binding to both actin and GTPases suggests that IQGAPs serve as a direct molecular link between these regulatory signalling pathways and the actin cytoskeleton

Actin filaments with actinin | 50 nm | Actin filaments with fimbrin
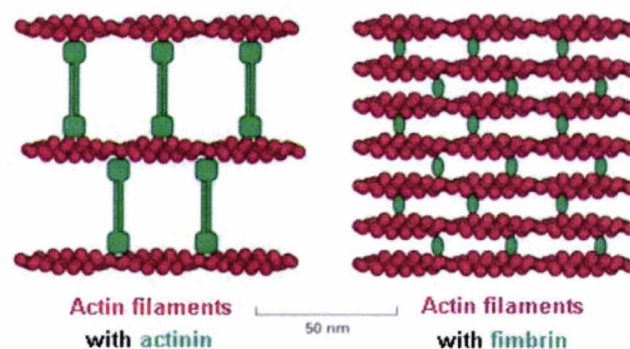
Figure 1.10. Bundling of actin filaments by fimbrin and actinin

Actinin, which is a homodimer, cross-links actin filaments into loose bundles, which allow the motor protein myosin II (not shown) to participate in the assembly. Fimbrin cross-links actin filaments into tight bundles, which exclude myosin. Fimbrin and actinin tend to exclude one another because of the very different spacing of the actin filament bundles that they form. Adapted from (Alberts et al., 1994)

Actinin and fimbrin have been identified in *S. pombe* as products of the *ain1⁺* and *fim1⁺* genes (Wu et al., 2001). Fim1 localises to cortical actin patches and CAR in an actin dependent manner whereas Ain1 is seen only at the CAR. Individual deletions of *ain1* or *fim1* have no observable effects, however the double mutant is synthetically lethal, suggesting overlapping function of the two proteins. The *S. pombe* IQGAP, Rng2 bundles f-actin into linear arrays of filaments and is required for assembly and regulation of filaments into the CAR (Takaine et al., 2009).

1.7. Myosins

A highly specialised group of ABPs are the myosins. Myosins are actin-based molecular motors known or hypothesized to play fundamental roles in processes as diverse as cell motility, cytokinesis, phagocytosis, polarised growth, maintenance of cell shape, and organelle/particle trafficking. Myosins are typically made up of three functional domains: a head or motor domain, a neck domain and a tail domain (Krendel and Mooseker, 2005). The relatively conserved head domain is involved in binding actin and ATP hydrolysis while the neck domain consists of up to six helical IQ motifs of the consensus sequence IQXXXRGXXXR (Cheney and Mooseker, 1992). Myosin light chains and/or calmodulin bind these IQ domains and can not only regulate but also amplify conformational changes with in the head domain. Tail domains are the most varied and their structure depends on the specific function of the myosin. They are involved in anchoring, cargo binding and/or dimerisation of two myosin molecules (figure 1.4).

There are at least 35 different classes of myosin grouped according to head and tail domain structure (Odronitz and Kollmar, 2007) and are described as conventional (filament forming) or unconventional (non-filamentous). The human genome has in the order of 40 myosin genes, grouped into approximately 12 classes (Berg et al., 2001), while yeast have only 3 classes of myosin, type I, type II and type V and these will be discussed in more detail below
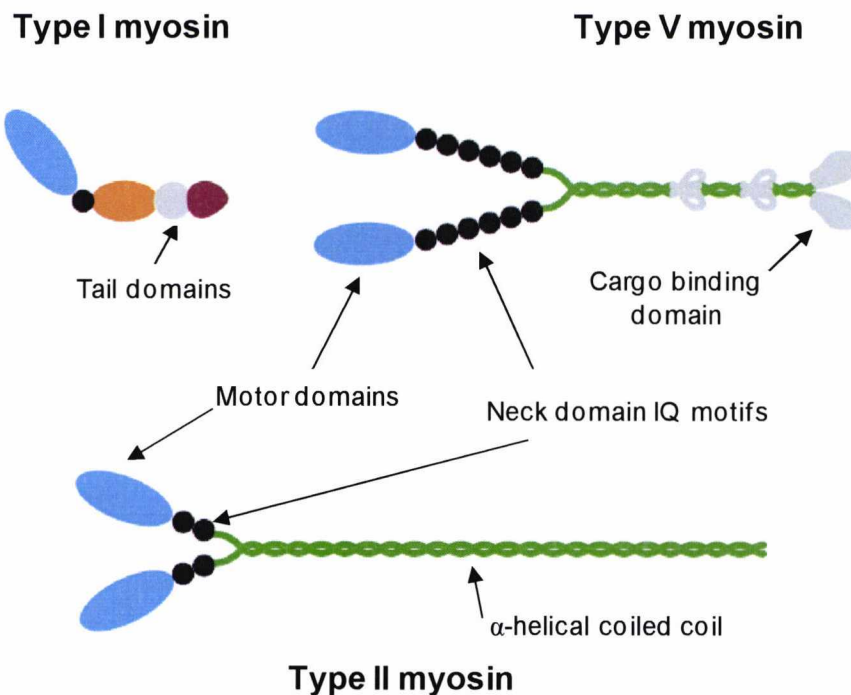
Figure 1.11. Cartoon diagrams of class I, II and V myosins.

Unconventional type I myosins are non-processive and consist of a single motor and IQ domain and up to three tail domains. The heavy chains of Conventional type II myosins consist of a motor domain followed by two IQ domains, to which light chains bind, and a long a-helical tail required for dimerisation. Type V myosins are unconventional and typically processive, each heavy chain contain a motor domain six IQ domains, an α-helical region for dimerisation and a globular cargo binding domain. Adapted from (Krendel and Mooseker, 2005)

1.7.1. Type I myosins

Type I myosins are the largest class of non-filamentous (unconventional) myosins and were first identified and purified from *Acanthamoeba castellanii* (Pollard and Korn, 1973). Type I myosins can be divided into short and long forms. Short forms have a single amino terminal motor domain, one or more IQ motifs that bind regulatory light chains, and a TH1 (tail homology) domain rich in basic residues that bind acidic phospholipids (Doberstein and Pollard, 1992). Long forms have an additional Glycine/Proline/Alanine-rich TH2 domain and an *src* homology

3 (SH3) domain called TH3 (Kim and Flavell, 2008). Type I myosins are frequently associated with membranes, involved in processes such as endocytosis (Titus, 2000), tethering of the cytoskeleton to intestinal microvilli membranes (Tyska et al., 2005) and even in hair cells of the inner ear regulating the opening of ion channels by controlling the tension transmitted the channel (Gillespie et al., 1993).

S. pombe has a single type I myosin encoded my the *myo1*$^{+}$ gene (Lee et al., 2000) that partially co-localises with actin at the growing cell tips and at the cell equator during cytokinesis. Disruption of the *myo1*$^{+}$ gene leads to loss of polarized growth and disorganised actin patches. Myo1 and WASP have overlapping functions in activating actin nucleation by the Arp2/3 complex. Formin mediated actin filament assembly is also linked to Myo1 as the fission yeast formin Cdc12 associates with Myo1 via the PCH family protein Cdc15 (Carnahan and Gould, 2003). Myo1 also has a role in actin mediated endocytosis (Attanapola et al., 2009).

1.7.2. Type II myosins.

The heavy chain of type II myosin motors typically have an actin-binding catalytic head domain followed by two IQ domains, to which essential and regulatory light chains bind. Type II myosins are two-headed structures due to the homodimerisation of their long coiled-coil forming tail domains (Krendel and Mooseker, 2005). Type II myosins are the best studied due to their involvement in muscle contraction, but also have important functions in non-muscle cells.

In the sliding filament theory of muscle contraction proposed in 1954 (Huxley and Niedergerke, 1954; Huxley and Hanson, 1954) 'thin' actin filaments slide past 'thick' filaments composed of myosins. The mechanism of contraction involves a cross bridge cycle first elucidated by Lymn and Taylor (1971). In this cycle ATP binds to myosin rapidly dissociating it from actin and 're-primes' the myosin to its pre-power-stroke position, which is followed by ATP hydrolysis. The Myosin·ADP·Pi
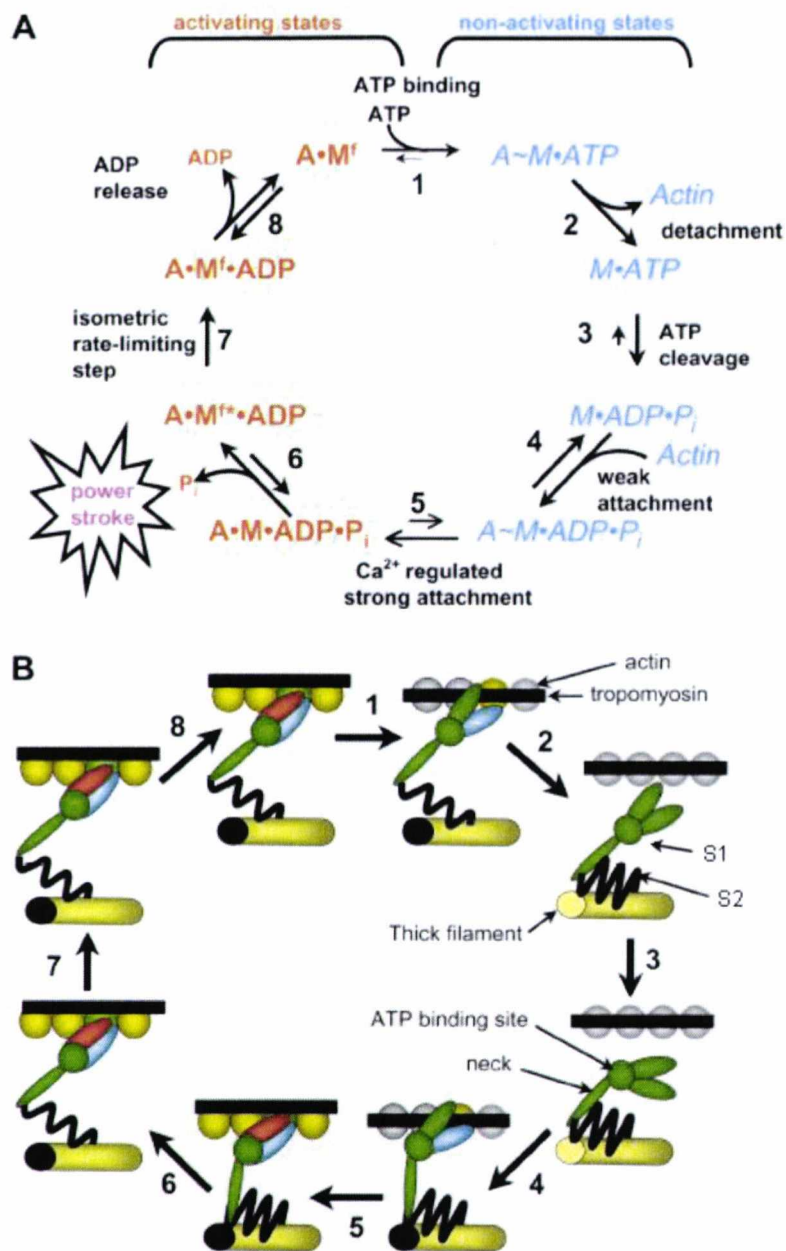
Figure 1.12 A diagram of the cross bridge cycle

(A) The cross-bridge cycle is composed of 8 basic events. Strong binding is designated by "·" between two species and weak binding by "~". A, actin; M,myosin; Pi, inorganic phosphate. Cycle begins at the top, with a cross-bridge strongly bound to actin ($A \cdot M^f$, where ^{f} is a cross-bridge exerting force) and its neck region in an extended position. (B) The same cross-bridge cycle with structural changes to convey how force and motion occur. Non-interacting cross-bridge-actin pairs are shown as gray actin and green myosin, weak interactions as yellow actin and light blue myosin, and strong interactions as green actin and red myosin. Adapted from (Gordon et al., 2001)

complex rebinds to actin, initially weakly and then strongly inducing the dissociation of Pi and the power stroke causing sliding of the actin filament, this is followed by ADP release and a return to the rigor-like complex.

In non-muscle cells, type II myosins have roles in several important cellular functions. Myosin II is essential for cytokinesis and is a known component of the contractile ring (Fujiwara and Pollard, 1976; Win et al., 2002; Yonemura and Pollard, 1992). The microinjection of antibodies to myosin II blocks cytokinesis (Mabuchi and Okuno, 1977). Cells lacking myosin II are capable of migration, albeit at a reduced rate (Wessels et al., 1988). It is thought that type II myosins contribute to cell migration through the regulation of cytoskeleton dynamics and cell adhesion (Vicente-Manzanares et al., 2009). A role for non-muscle myosin II in the polarity of neuronal growth cones and their response to nerve growth factors has also been demonstrated (Loudon et al., 2006)

S. pombe has two type II myosin genes, *myo2*$^+$ (Kitayama et al., 1997; May et al., 1997) and *myp2*$^+$ (Bezanilla et al., 1997). Myo2 appears to be a conventional two-headed dimer, while myp2 has a group of proline residues in the centre of its tail region which split the tail into two subdomains. Although the catalytic domain of Myp2p is highly homologous to known myosin IIs, and phylogenetic analysis places Myp2 in the myosin II family, structural and biophysical analysis suggests that the Myp2 tail subdomains may fold back on themselves, making myp2 a monomeric myosin II (Bezanilla and Pollard, 2000). Both Myo2 and Myp2 share the essential light chain Cdc4 (McCollum et al., 1995) and the regulatory light chain Rlc1 (Le Goff et al., 2000) and all four proteins localise to the CAR during mitosis. Myo2 is essential for cytokinesis and timing of its assembly in the CAR is regulated by the phosphorylation status of two serine residues in the tail region by kinases that make up the septation initiation network (SIN) (Motegi et al., 2004; Mulvihill et al., 2001a). Myp2 is not essential for cytokinesis except during stress

conditions such as high salt (Bezanilla et al., 1997), but may contribute to the structural integrity of the CAR during contraction (Win et al., 2002).

<u>1.7.3. Type V myosins</u>

Type V myosins are motors involved in the transport of organelles, secretory vesicles, mRNA, lipids and proteins on actin cables (Trybus, 2008). Although typically processive there are some exceptions. Reck-Peterson et al (2001) suggest a non-processive budding yeast myosin V (Myo2p) can act processively if at least five molecules of the motor are present per cargo. Whereas Hodges and coworkers (2009) showed that a Myo2p can drive cargo processively when a kinesin related protein is present on the cargo. Similarly a *Drosophila* myosin V (DmV) is individually non-processive but can participate in organelle transport if several motors are present (Toth et al., 2005).

The heavy chains of this dimeric myosin can be divided into 4 regions: the motor domain containing the actin and nucleotide binding sites, the neck domain consisting of 6 IQ domains to which light chains bind, a coiled coil region which facilitates dimerisation and a globular tail which binds cargoes. Myosin 5 'walks' along actin cables using a hand over hand mechanism (Trybus, 2008). When both heads are bound the leading head is in a strained pre-powerstroke conformation, while the trailing head is in a post powerstroke position. The trailing head binds ATP releasing it from actin and is thrust forward as the leading head completes its powerstroke. The new leading head then searches for a new actin binding site (figure 1.13). The step size of this motion is approximately 36 nm which corresponds to the helical repeat of actin (Mehta et al., 1999).

Myosin V tail domains can attach to several type of cargo and organelle-specific myosin V receptors are important for the regulation of cargo attachment (Trybus, 2008). A recent structural study of budding yeast Myo2p (Pashkova et al., 2006) revealed separate binding regions in the

tail domain responsible for binding different cargoes. In the absence of bound cargoes, myosin V tail domains can fold back and bind to the motor domains. This binding inhibits ATPase activity, reduces actin affinity and allows the motor to target new cargoes (Li et al., 2006; Thirumurugan et al., 2006)

S. pombe has two type V myosin genes myo51⁺ and myo52⁺. Myo51 is a non-essential component of the CAR (Win et al., 2001) and appears to have no role in vegetative growth. It localises to the spindle pole body during meiosis independently of actin and the SIN, but requiring a stable microtubule cytoskeleton (Doyle et al., 2009). It is also important for spore formation following meiosis. Myo51 plays a role in maintaining the SPB and ensuring meiotic segregation is coordinated with spore wall synthesis. Its also has an important role in cell fusion during mating facilitating cell wall breakdown as over expression of the tail region disrupts cell fusion (Doyle et al., 2009)
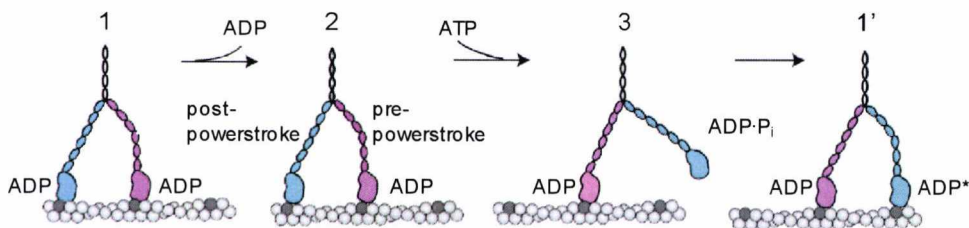
Figure 1.13. A model of myosin V processive movement.

In state 1 both heads are strongly bound to actin with ADP bound. ADP is released from the trailing head (2), then ATP binds and dissociated it from actin. The trailing head it moved forward (3) as the leading head completes its power stroke, at the same time hydrolysing ATP. The detached head then binds to the next actin binding site (dark grey) in the pre-powerstroke conformation (1'), weakly at first then strongly as Pi is released. Adapted from (Trybus, 2008).

Myo52 is an essential protein and cells lacking it show a loss of cell polarity and are defective in cell separation (Motegi et al., 2001; Win et al., 2001). Myo52 is involved in the delivery of cell wall components to the

growing cell tip, and to the septum during cell division (Motegi et al., 2001; Win et al., 2001). It also has a role in vacuole distribution (Mulvihill et al., 2001b) and fusion, and in microtubule dynamics by regulating turnover of a microtubule associated protein (Martin-Garcia and Mulvihill, 2009). Myo52 binds the fission yeast calmodulin via its IQ (neck) domain, however removal of the neck domain has no effect on function or velocity *in vivo* (Grallert et al., 2007).

1.8. Cytokinesis in fission yeast

At the end of mitosis *S. pombe* cells divide by forming a new cell wall, known as the division septum at the centre of the cell. The contractile actomyosin ring constricts and divides the cytoplasm while the septum is synthesised behind it (Jochova et al., 1991). The CAR is comprised of many components (Pollard and Wu, 2010) and is precisely positioned at the middle of the cell. The septation initiation network, a signal transduction pathway is required for temporal regulation of the onset of septum formation.

1.8.1. The *S. pombe* contractile ring

As in many eukaryotic cells, *S. pombe* cells require a contractile ring for cell division. The protein kinase Plo1 triggers the release of a protein, Mid1p, from the nucleus (Bahler et al., 1998) and Mid1p forms a broad band around the cell cortex surrounding the nucleus marking the cell equator. Work by Tran et al (2001) suggests that the nucleus is maintained at the cell centre by bundles of antiparallel microtubules attached on either side. When these microtubules contact the cell ends, the small force generated pushes back on the nucleus causing it to oscillate. The balanced forces on each side keep the nucleus in the centre of the cell. Earlier work by Hagan and Yanagida (1997) suggests a different mechanism whereby the SPB leads the nucleus to its correct position in response to positional cues.

The fission yeast contractile acto-myosin ring (CAR) consists of actin filaments (Marks and Hyams, 1985) and the two type II myosins, the essential Myo2p (Kitayama et al., 1997) and Myp2 (Bezanilla et al., 1997) which is non-essential except under stress conditions such as high salt. Despite being referred to as the CAR the ring contains many other components besides actin and myosin. These include the myosin light chains Cdc4 (McCollum et al., 1995) and Rlc1 (Le Goff et al., 2000) actin crosslinking proteins Ain1p (a-actinin) and Fim1p (fimbrin) (Wu et al., 2001) as well as a PCH protein Cdc15 (Fankhauser et al., 1995). A formin Cdc12 (Chang et al., 1997) profilin Cdc3 (Balasubramanian et al., 1994) and tropomyosin (Balasubramanian et al., 1992) Cdc8 are also required for ring assembly.

The ring is assembled at the cell equator from mid-interphase through to late anaphase in sequential stages (Wu et al., 2003a). At the G2/M transition the board band of Mid1 is joined by Myo2, Cdc4, Rlc1p, Cdc15 and Cdc12. A complex of Cdc15 and Cdc12 recruits actin (Carnahan and Gould, 2003) during a brief stage in early anaphase and through nucleation by the formin, initiates the assembly of short F-actin cables. Ain1 and Fim1 also localise during anaphase. Kamasaki et al (2007) showed that the early ring consists of two semicircular populations of actin filaments showing opposite directionality, at later stages the ring filaments show mixed directionality. Myp2 localises to the ring last and upon signalling from the septation initiation network (SIN) the ring contracts, although the mechanism of this contraction is unknown. It is presumably by the joint actions of forces generated by type II myosins, and timely depolymerisation of the shrinking ring by ADF/cofilin. As myosin II is required and active in ring formation, a second activation for constriction seems unlikely. It has been proposed that anillin and septin proteins at the division site cortex might physically block ingression of the plasma membrane. At the time of SIN signalling, these proteins disperse from the membrane immediately overlying the contractile ring, freeing the plasma membrane to ingress (Wolfe and Gould, 2005).

The fission yeast SIN, is a signal transduction network that is required for septum formation. Its activity is tightly regulated through the cell cycle, to ensure proper co-ordination of mitosis and cytokinesis. SIN signaling requires three protein kinases for its function which assemble on a protein scaffold anchored to the SPB. Regulators of the SIN include the protein kinase Plo1 (Ohkura et al., 1995; Tanaka et al., 2001), and cdc2p-cyclinB, (Nurse, 1990) which when inactivated allows the SIN to adopt its active conformation.

1.9. Tropomyosin

Tropomyosin (Tm) is an α-helical coiled-coil actin binding protein and was first discovered as a component of the skeletal muscle contractile system (Bailey, 1948). Because of its biochemical properties it was incorrectly believed to be a myosin precursor and therefore named 'tropomyosin' (from Greek *tropos*, meaning to turn, or in this case, change).

Tm is a dimer, consisting of two α-helices that coil around each other. Dimers interact in an end-to-end fashion to create a continuous polymer that binds in the helical grooves of actin filaments. Tm stabilises actin filaments and in muscle tissue is part of the regulatory unit controlling contraction (Perry, 2001). In all eukaryotes (except plants) Tm has an important role in maintaining the actin cytoskeleton and regulating its interaction with other ABPs.
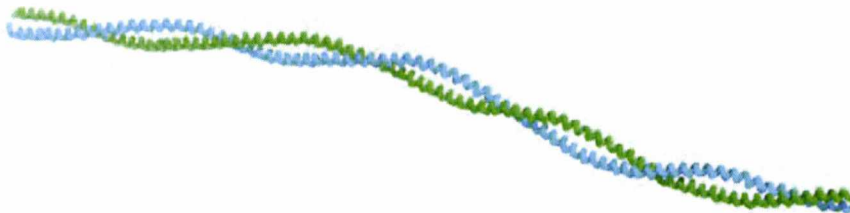
Figure 1.14. Tropomyosin

A diagrammatic representation of a tropomyosin dimer detailing each α-helix (green and blue) of the coiled-coil.

1.9.1. Tropomyosin genes and isoforms

Tm genes have been found in all eukaryotic phyla, except plants, and show an increasing number of genes and greater isoform diversity from lower eukaryotes to vertebrates. The ancestral Tm gene has been hypothesised to have arisen from repeated duplications of a 21 amino acid sequence (Wieczorek et al., 1988) forming a gene with a number of exons. Alternative splicing of different exons and the use of different

promoters are mechanisms by which many Tm isoforms can be generated by one Tm gene.

S. pombe has a single Tm gene *cdc8*[+] (Balasubramanian et al., 1992), it contains a single intron that is spliced out during transcription therefore fission yeast is capable of producing only one Tm isoform. The budding yeast *Saccharomyces cerevisiae* has two Tm genes, *TPM1* and *TPM2* (Drees et al., 1995; Liu and Bretscher, 1989a). In the *TPM1* gene a tandem duplication of 38 residues lengthens the Tpm1p protein (Drees et al., 1995), neither gene contains an intron, and as such each gene can generate only one Tm isoform.

The Nematode worm *Caenorhabditis elegans* has a single Tm gene, *tmy-1* (Kagawa et al., 1995) but is able to generate 4 different isoforms by use of a distal and an internal promoter and alternative splicing of its 15 exons. The fruit fly *Drosophila melanogaster* has two Tm genes *TmI* and *TmII* with different exon/intro structures that probably arose through gene duplication (Karlik and Fyrberg, 1986). From these two genes *D. melanogaster* can generate at least 8 Tm isoforms.

Vertebrates including amphibians, birds and mammals have 4 Tm genes thought to have arisen through two rounds of whole genome replication in the lineage leading to the vertebrates (Holland, 1999), whereas fish have 6 Tm genes two of which are paralogs of the 4 genes corresponding to other vertebrate Tm genes (Toramoto et al., 2004). Mammals use these 4 genes to generate over 40 Tm isoforms, the structure of each human Tm gene shown in figure 1.15. Human Tm genes, through the use of two promoters and alternative splicing generate at least 22 isoforms. Transcription begins at either at exon 1a or 1b and historically Tms have been described as high molecular weight (HMW), approximately 284 aa (amino acids) long, or low molecular weight (LWM), approximately 248 aa long. They differ by the use of exons 1a and 2, or 1b at the amino terminus and all human Tm contain exons 3 to 8. Exons 6a and 6b are mutually exclusive and the carboxyl terminus is provided by one of the exon 9s.
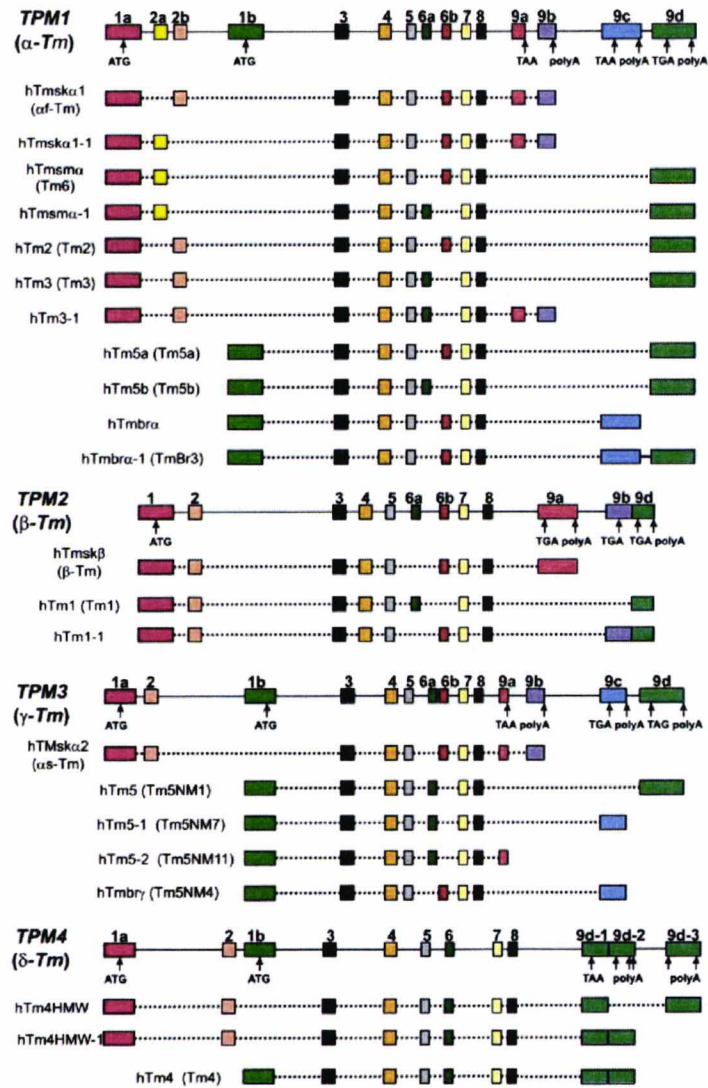
Figure 1.15. Diagram of human tropomyosin genes and isoforms

For the 4 human Tm genes, TPM1-4, exons are represented by coloured boxes and introns by a solid black line. By splicing out the introns (dotted lines) each gene is capable of producing multiple Tm isoforms, with variation occurring at the amino and carboxyl termini as well as the internal exon 6. Corresponding isoforms in rodents are included in brackets. Reproduced from (Lin et al., 2008).

In addition to multiple promoters and alternative splicing, further isoform diversity is achieved through dimerisation. A Tm monomer can form homo- and heterodimers with other monomers, although heterodimers between HMW and LMW Tms are unstable and do not occur naturally. Specificity of dimer formation is partially determined by the thermostability of possible dimer combinations; Skeletal and smooth muscle α and β Tms assemble preferentially into the thermodynamically more stable αβ hetero dimer (Brown and Schachat, 1985; Lehrer and Qian, 1990). Isoform expression also has a role; cardiac muscle expresses only one α Tm therefore only αα homodimers can form (Lees-Miller and Helfman, 1991). There is also evidence that information for homo and heterodimer formation is contained with in the Tm molecule itself and conveyed in part by alternatively spliced exons and area of the carboxyl terminus known as 'trigger sequences'(Araya et al., 2002; Gimona et al., 1995; Kammerer et al., 1998).

Tms exhibit isoform specific accumulation at different intracellular sites in many cell types including neurones (Gunning et al., 1998), skeletal muscle (Kee et al., 2004) and epithelial cells (Dalby-Payne et al., 2003). The sorting of isoforms into distinct compartments, which is dynamic (Schevzov et al., 1997) is unlikely to be due to an intrinsic sorting signal that specifies destination, and more attributable to a 'molecular sink' model (Martin and Gunning, 2008). In this mechanism Tm isoforms accumulate in (actin) structures where they have the highest affinity and are most stable. The regulation of APBs and their interaction with Tm at these sites therefore, also contributes to Tm isoform sorting.

1.9.2. Tropomyosin structure

Tm was first recognised as belonging to the alpha helical *k-m-e-f* (keratin-myosin-epidermin-fibrinogen) class of proteins by Astbury (1948) owing to its characteristic x-ray diffraction pattern. A model for α-helical coiled coils was proposed by Crick in 1953 in which two alpha helices with seven fold

(heptad) pseudo-repeating sequence periodicity (where the 7 residues are termed *a, b, c, d, e, f, g*) associate to form a coiled coil. Residues in the *a* and *d* positions are generally hydrophobic and lock together in a "knobs into holes" fashion, with further stabilisation of the dimer achieved by ionic interactions between charged residues in the *e* and *g* positions (see figure 1.16.)

When the first full length Tm sequence from rabbit skeletal muscle was published (Stone and Smillie, 1978) it confirmed Cricks proposed heptapeptide repeat of hydrophobic amino acids. The "knobs into holes" packing at the core interface of the dimer, and ionic interactions between charges residues was confirmed in Tm by the crystal structure of an 81 aa peptide fragment of the amino terminus of muscle α-Tm (Brown et al., 2001).

Crystal structures of full length Tm have been resolved to 15, 9 and 7 angstroms (Phillips et al., 1986; Whitby et al., 1992; Whitby and Phillips, 2000) but resolutions greater than this have not been possible due to factors including high solvent content, polymerisation and flexibility.
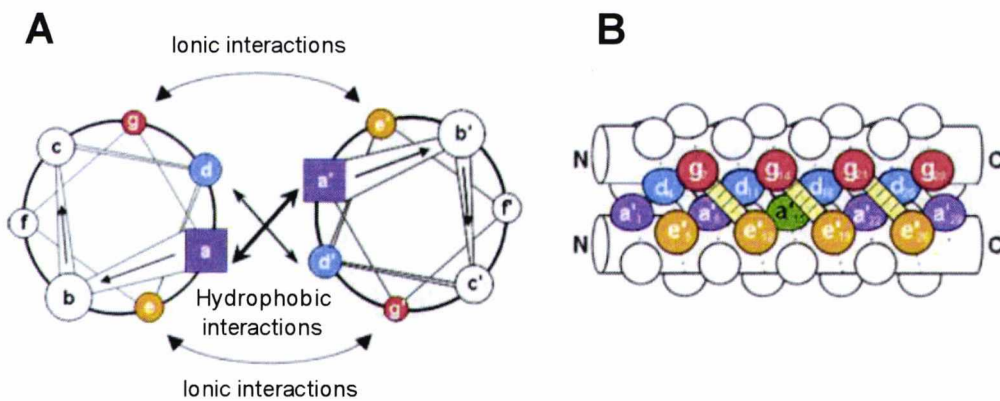
Figure 1.16. Diagram of coiled coil interactions

(A) A diagrammatic representation of the two α-helices of a coiled coil when viewed from the amino terminal end highlighting hydrophobic and ionic interactions. (B) Side view of the coiled coil in which the protein backbones are represented by white cylinders. Residues in the *a* and *d* position lock against each other at the coiled coil interface. Residues in the *g* position can form ionic interactions with *e* position residues in the next heptad if they are oppositely charged. Adapted from (Mason and Arndt, 2004).

Crystal structures of shorter Tm fragments however have given greater insights in to the tertiary structure of the Tm dimer. Brown and colleagues (2001; 2005) noticed that groups of alanines or alanines next to large and generally non polar residues, at core (*a* and *d* positions) positions of the α-helix cause bends in the Tm molecule and suggested this facilitated its superhelical shape when bound to actin.

Actin binding sites on the Tm molecule are poorly understood. From the linear Tm amino acid sequence, McLachlan and Stewart (1975) identified 7 pairs of alternating, α and β 'zones' containing charged and hydrophobic amino acid residues and proposed that they may correspond to actin binding sites in the two positions of Tm on actin in the steric blocking model (covered later in this chapter). Later analysis that took into account the azimuthal position of amino acid side chains (Phillips, 1986) identified a seven fold repeat of charged and hydrophobic amino acid residues in non interface positions (*b*, *c* and *f* positions) that corresponded approximately to the α-zones, referred to as consensus residues.

More recent mutagenesis studies have given support to the Phillips consensus residue hypothesis. Loss of the 5th period of rat striated muscle α-Tm abolishes its actin binding properties (Hitchcock-DeGregori et al., 2002), and although deletion of the second period had little effect, loss of function increased as the deletion was shifted towards the carboxyl terminus. There is a dual requirement for the actin binding consensus residues and localised areas of instability in the Tm dimer (Singh and Hitchcock-DeGregori, 2003; Singh and Hitchcock-DeGregori, 2006). Poor interface packing achieved by clusters of alanine residues in the core positions result in areas of local flexibility that are required for actin binding. The consensus regions however are quasi-equivalent with the period 1 and period 2 consensus sites being able to substitute for period 5 with respect to actin binding (Singh and Hitchcock-DeGregori, 2007). This suggests that the global structure of the Tm dimer and local instability are more important for actin binding than specific sequences. Supporting this, the recently proposed 'gestalt' model of actin-tropomyosin interaction (Holmes and Lehman, 2008) argues that the

overall behavior of Tm on F-actin cannot be easily discerned by examining the smallest interacting units. Instead the association of Tm on actin can only be fully explained after considering the entire actin-Tm system.

1.9 3. The tropomyosin overlap complex

The affinity of individual Tm dimers for actin is weak (Vilfan, 2001). In order to bind actin, Tm must associate end to end to form a continuous polymer along the actin filament (Cho et al., 1990; Dabrowska et al., 1983; Mak and Smillie, 1981). The amino and carboxyl termini are essential for end to end binding and actin affinity, demonstrated by the enzymatic cleavage of the carboxyl terminus (Johnson and Smillie, 1977) and mutagenesis of the amino terminus (Cho et al., 1990). Many studies of wild type and recombinant Tms have established that modifications to the amino and carboxyl terminal sequences alter end to end interactions (Hitchcock-DeGregori and Heald, 1987; Sano et al., 2000) actin affinity (Cho and Hitchcock-DeGregori, 1991; Novy et al., 1993; Pittenger et al., 1995) , and interaction with myosin on the actin filament (Hammell and Hitchcock-DeGregori, 1996; Moraczewska et al., 1999)

An important post translational modification of Tm is acetylation. *In vivo* Tms are acetylated on the amino terminal methionine. Amino terminal acetyltransferases are only present in eukaryote and when recombinantly expressed in *E. coli,* Tms are unacetylated and the first 2 residues are non-helical (Brown et al., 2001). Acetylation of α- skeletal Tm is essential for binding to actin (Urbancikova and Hitchcock-DeGregori, 1994), however β-skeletal Tms and α- smooth Tms do not require acetylation to bind strongly to actin (Cho and Hitchcock-DeGregori, 1991; Pittenger et al., 1995).

The structure of the Tm overlap complex has been solved by NMR (Greenfield et al., 2006) using amino and carboxyl terminal peptides from rat striated α-Tm. In this complex the chains on the carboxyl terminus, the

last 5 residues of which are non helical, spread apart and allow the insertion of 11 amino acids from the amino terminus. The planes of the amino and carboxyl termini are rotated by 90^0 relative to each other, and as a consequence allow the position of the hypothesised actin interacting repeats to be retained from one dimer to the next.

This structure gives an insight into the intermolecular side chain interactions within the overlap. There are ionic interactions between amino terminal Lys 5 and carboxyl terminal Asp 280 and hydrophilic interactions of Lys 7 with Ser 283 and Ile 284 (see figure 1.17). In addition there are several hydrophobic interactions between aliphatic side chains in the a and d positions including Met 1, Ile 4, Met 8 and Leu 11 from the amino terminus, and Leu 274, Ala 277, Met 281 and Ile 284 from the carboxyl terminus. As well as this hydrophobic contacts between residues in non-'core' positions and intra-chain interactions along the helices between charged residues were also observed.
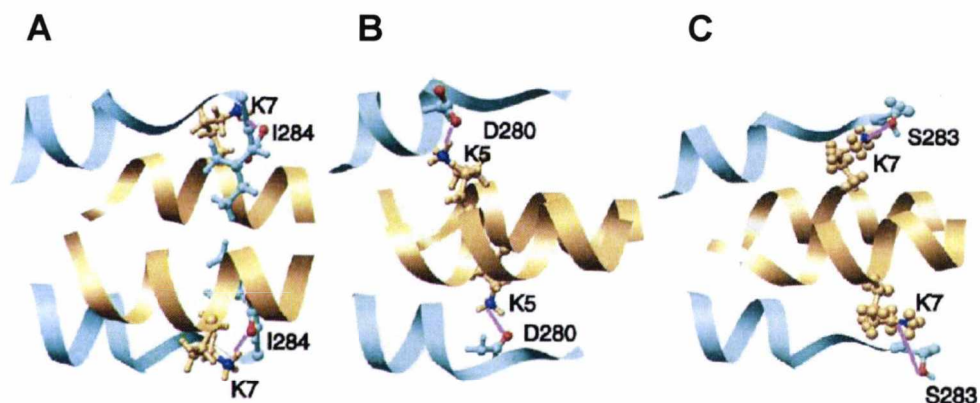
Figure 1.17. Major side chain interactions in the tropomyosin overlap complex.

Diagrams detailing bonds between the 11 overlapping residues from the amino (gold) and the carboxyl (green) termini of rat striated α-tropomyosin. (A) Hydrophilic interaction between the carboxyl terminal of I284 and side chain amino of K7. (B) Ionic interaction between side chain amino of K5 and side chain carboxyl of D280. (C) Hydrophilic interaction between the side chain amino of K7 and free oxygen of S283. Adapted from (Greenfield et al., 2006).

1.9.4. Tropomyosin and the mechanism of skeletal muscle regulation.

In skeletal and cardiac muscle, Tm has another specialised role in addition to stabilising F-actin. In conjunction with the calcium sensitive protein troponin, Tm regulates actin-myosin interaction in the process of muscle contraction. Troponin was first identified as a separate component from Tm by Ebashi and Kodama in 1965 and is in fact a complex of three proteins: the inhibitory subunit TnI which binds to actin and inhibits myosin ATPase activity, the calcium sensitive TnC, and TnT which links the whole complex to Tm (Greaser and Gergely, 1971; Hitchcock et al., 1973; Potter and Gergely, 1974). The troponin complex binds along the Tm coiled-coil and bridges the Tm head to tail overlap. This enhances Tm binding and stability on actin, presumably by reinforcing the interaction between adjacent Tm dimers (Hinkle et al., 1999; Wegner and Walsh, 1981). Tm exons 2b, 6b, 9a and 9b are unique to skeletal muscle Tm isoforms and are proposed to be adapted for
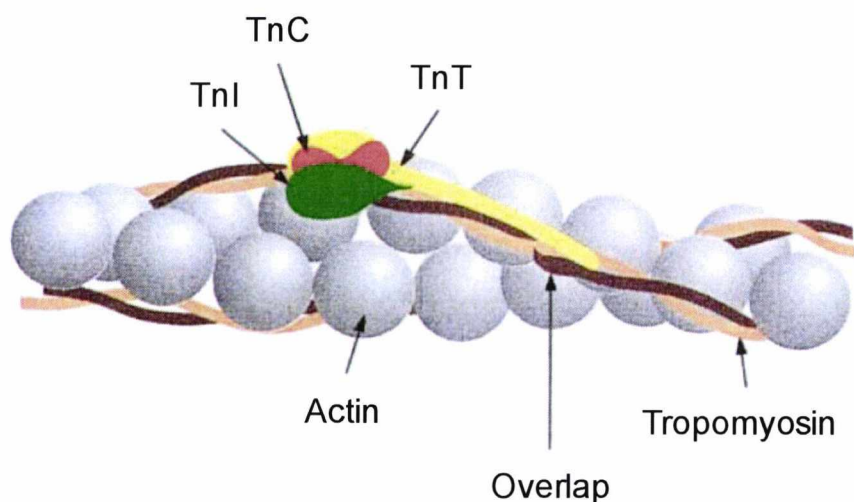
Figure 1.18. Components of the thin filament.

A diagram showing the components of the troponin complex (TnI: green, TnC: red and TnT: yellow) and its position with respect to actin (grey) and tropomyosin (dark red & pink). The amino terminus of TnT bridges the Tm overlap complex, while the carboxyl terminus interacts with TnC and TnI, which in turn interact with actin. Adapted from (Gordon et al., 2000)

interaction with troponin (Colote et al., 1988; Maytum et al., 2004) In skeletal muscle 7 actins, 1 Tm dimer and 1 troponin complex form the 'regulatory unit' of the thin (actin) filament.

Early x-ray diffraction studies (Haselgrove, 1975; Parry and Squire, 1973) on intact muscle suggested that calcium ions (Ca^{2+}) influenced the position of Tm on actin and this formed the basis of the steric blocking model of muscle regulation (Hanson and Lowy, 1964; Hitchcock et al., 1973). In this model Tm blocks myosin binding sites on actin in the relaxed state, and exposes them when the muscle is activated.

Three dimensional reconstructions from electron micrographs showed that in the absence of Ca^{2+} Tm was constrained in a 'blocked' position that covered the myosin binding sites (Lehman et al., 1994; Lehman et al., 1995). In the presence of Ca^{2+}, Tm moves approximately 25^0 around the actin filament into a 'closed' position exposing some, but not all of the myosin binding sites. The partial binding of myosin causes Tm to shift a further 10^0 into an 'open' position fully exposing the myosin binding site (Vibert et al., 1997; Xu et al., 1999). These structural observations support the kinetic evidence that led McKillop and Geeves (1993) to propose the three state model of muscle regulation. Therefore in the three state model Ca^{2+} binding to TnC causes a conformational change in TnI which releases Tm from the blocked position. This allows partial binding of myosin to actin, which in turn, causes further Tm movement allowing full binding and activity.

When myosin interacts with actin during muscle contraction, a cleft at the tip of the myosin head must close for strong binding to actin (Rayment et al., 1993). Molecular modelling by Poole and co-workers (2006) suggested in the relaxed state Tm might act as a molecular 'gag' preventing the closure of the cleft. Tm may therefore regulate myosin interacting with actin by obstructing myosin binding site and by preventing the conformational change required for myosin to bind actin.
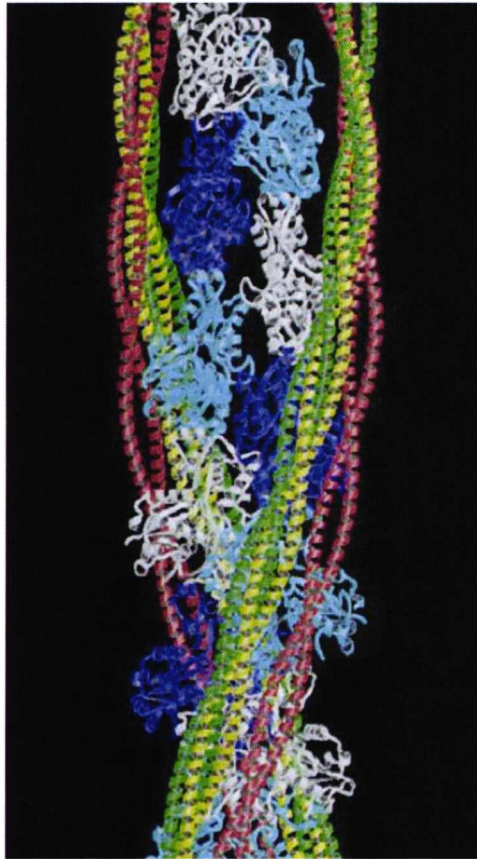
Figure 1.19. The positions of tropomyosin on actin

A molecular model of tropomyosin on actin (blue & white), in the blocked position (red), closed position (yellow) and the open position (green) as deduced from EM reconstructions. From (Poole et al., 2006).

The movement of Tm over the surface of actin is cooperative, in that the movement of one tm dimer can be transmitted to the next through the Tm overlap complex (Geeves and Lehrer, 1994; Phillips and Chacko, 1996). The manner in which Tm moves over the surface of actin is debated. There are two simple structural models consistent with this repositioning of Tm. Firstly a rolling of Tm over the actin surface (Bacchiocchi and Lehrer, 2002; Holthauzen et al., 2004), which implies that Tm is a rather flexible molecule, and secondly a sliding of Tm (Poole et al., 2006; Poole et al., 1995), which implies that Tm is more rigid. A recent study (Li et al.,

2010a) taking into account the natural curvature of Tm in calculations of rigidity lends support to the sliding model of Tm movement.

1.9.5. Tropomyosin and the mechanism of smooth muscle regulation

In humans, smooth muscle tissue is found in a variety of locations including, the walls of arteries and veins, the gastrointestinal and respiratory tracts as well as the bladder and uterus. Like skeletal muscle, smooth muscle contains both actin and Tm. Troponin however is absent and replaced by caldesmon and the calcium binding protein calmodulin. Actin, Tm, caldesmon and calmodulin are present in ratios of 14:2:1:1 (Marston and El-Mezgueldi, 2008). The primary mechanism of regulation in smooth muscle is by activation of myosin by phosphorylation of myosin light chains by a calcium sensitive kinase (Hirano et al., 2003), however caldesmon, and Tm have a secondary role in 'fine tuning' the system.

Smooth muscle Tm is predominantly a heterodimer of the α- and β-smooth isoforms (Jancso and Graceffa, 1991). In α-smooth muscle Tm exons 2a and 9d replace exons 2b, 9a and 9b of skeletal muscle (see figure 1.15). In β-smooth Tm exons 6a and 9d are expressed in the place of skeletal muscles exons 6b and 9a (Marston and El-Mezgueldi, 2008). Exon 9d confers strong end-to-end interactions between Tm dimers and consequently smooth muscle Tm increases myosin S1 activation compared to skeletal muscle isoforms

Caldesmon is an elongated protein consisting of three helical domains and a fourth globular domain. Domain 4 contains the actin and calmodulin binding domains and is responsible for the regulatory property of the molecule (El-Mezgueldi et al., 1998; Szpacenko and Dabrowska, 1986). *In vitro* caldesmon has been shown to bind Tm however structural evidence from 3D helical reconstructions of smooth muscle actin filaments indicate caldesmon forms a continuous polymer along f-actin, parallel to Tm but separated by approximately 90^0 (Lehman et al., 1997). Despite no apparent physical interaction there is a strong functional

interaction. The actin binding and ATPase inhibition by caldesmon are significantly increased by Tm (Dabrowska et al., 1985; Smith et al., 1987b), and caldesmon enhances the affinity of Tm for actin (Yamashiro-Matsumura and Matsumura, 1988).

Figure 1.20. Location of caldesmon and tropomyosin on actin

A three dimensional reconstruction of caldesmon (green wire cage) and tropomyosin (red wire cage) on F-actin (solid purple). Caldesmon lies on the extreme periphery of the outer domains of actin monomers and tropomyosin on the outer edges of the inner domains. Adapted from (Lehman et al., 1997)

The inhibitory effect of caldesmon on myosin S1 is negated by calcium-bound calmodulin (Smith et al., 1987b), however the involvement of Tm in caldesmon inhibition remains unclear. Several groups have demonstrated levels of caldesmon inhibition of ATPase activity in the absence of Tm from none to full, depending on ionic concentration (Marston and El-Mezgueldi, 2008). A hypothesis proposed by Ansari and colleagues (2003), suggest that the action of caldesmon predominantly takes place from actin to actin, by charge-charge interaction, and that Tm protects the actin surface from surrounding solvent allowing these interactions to take place at physiological pH.

1.9.6. Tropomyosin as a regulator of the actin cytoskeleton.

In non-muscle cells, actin cytoskeleton dynamics are central to many fundamental cellular processes, including cytokinesis, cell motility, contractibility, cell morphology and organelle transport. In humans approximately 40 isoforms (Gunning et al., 2005) are generated by 4 Tm genes and the majority of these isoforms are expressed in non-muscle cells. Different Tm isoforms have altered affinities for actin and bind at slightly different positions on actin filaments (Lehman et al., 2000; Pittenger et al., 1994). Different Tm isoforms can regulate the impact of various actin binding proteins on actin filaments and therefore have a role in regulating filament dynamics.

1.9.6.1. Tropomyosin and ADF/Cofilin.

In vitro, Tm and ADF/cofilin compete for actin binding although they do not share the same binding site (McGough, 1998). Actin filaments saturated with skeletal muscle Tm are resistant to severing and depolymerisation by ADF (Bernstein and Bamburg, 1982). Tm added to F-actin simultaneously with ADF offers little protection from severing indicating that Tm must be bound to actin to block the effects of ADF (Kuhn and Bamburg, 2008). If the concentration of ADF is high enough however, it will displace Tm from F-actin (Nishida et al., 1984). ADF binding imparts a conformational 'twist' on the actin filament, and binds preferentially to this subsequent form of actin, Tm however, tends to straighten F-actin and preferentially binds the 'non-twisted' form (Kuhn and Bamburg, 2008). These conformational binding preferences explain the competitive interactions of Tm and ADF with actin. Tm associated actin filaments interact well with myosin II, but displacement of Tm by ADF disrupts myosin binding (Nishida et al., 1984). Tm also inhibits the formation of branched actin network promoted by the actions of ADF and the arp2/3 complex (Blanchoin et al., 2001) suggesting that the competitive actions of Tm and ADF influence the binding of other actin binding proteins.

In addition to their role in regulating the interaction of actin binding proteins, Tm and ADF are also involved in modifying cell morphology. In a study expressing different levels of two non muscle Tms, TmBr3 and Tm5NM1 in a neuronal cell line Bryce and co-workers (2003) showed that overexpression of Tm5NM1 stimulated the assembly of longer, myosin associated stress fibres which are involved in cell adhesion. Overexpression of TmBr3 however caused the loss of stress fibres and increased the formation of arrays of shorter ADF associated actin filaments that are involved in lamellipodia structure and cell migration.
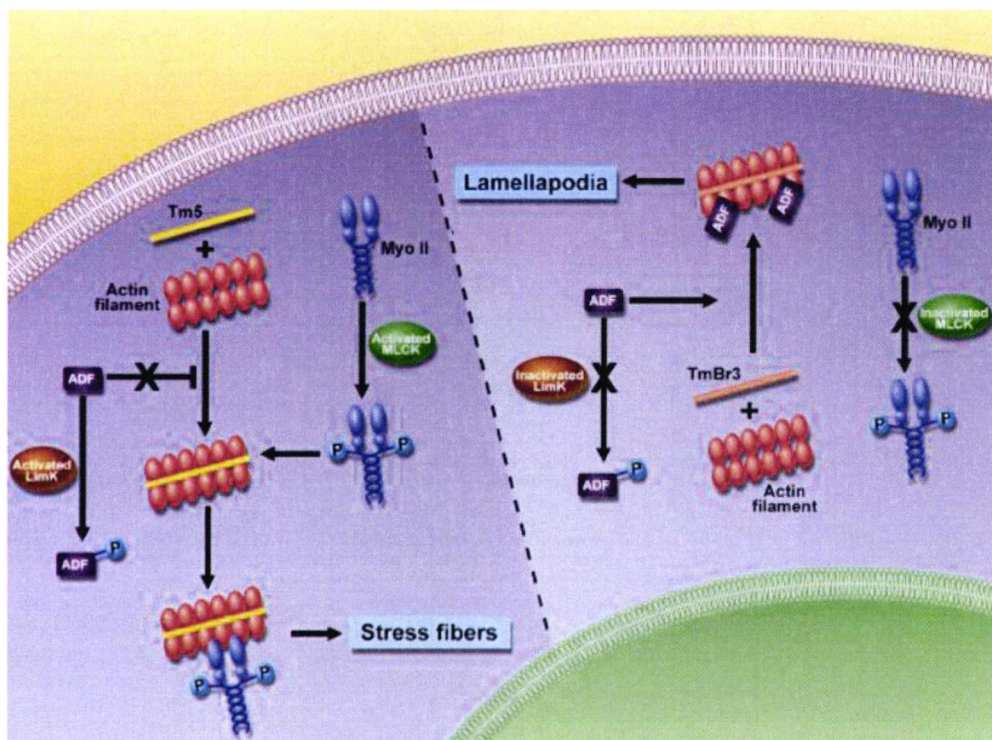
Figure 1.21. Actin filament regulation and tropomyosin sorting

When Lim and MLC kinases are active ADF is inactive and removes competition for Tm5NM1 binding to actin. Active (phosphorylated) myosin II binds to Tm5NM1 associated filaments and promotes the formation of stress fibres. If LimK and MLCK are inactive ADF competes with Tm5NM1 for binding, but collaborates with TmBr3 promoting the formation of shorter filaments and lamellipodia. From (Gunning et al., 2008).

A model of actin morphology regulation and Tm isoform sorting proposed by Gunning et al. (2008) involving actin, Tm, ADF myosin and regulatory kinases suggests that while some Tm isoforms compete with ADF for actin binding, others can collaborate to achieve a different end (figure 1.21)

1.9.6.2. Tropomyosin and formins.

Polymerisation of actin by formins increases the flexibility of actin filaments through long-range allosteric interactions (Bugyi et al., 2006). Formins however increase the affinity of Tm for actin (Skau et al., 2009) Therefore a mechanism exists in which Tm binds and stabilises newly formed f-actin polymerized by formins (Ujfalusi et al., 2009) and the conformational change imparted on actin by formins promotes cooperative binding of Tm to actin filaments.

Tm also regulates actin filament dynamics at the barbed end. The carboxyl terminus of Tm binds to the FH2 domain of formin and modulates the capping action of barbed end associated formins by relieving inhibition of elongation (Wawro et al., 2007). Tm does so in an isoform specific manner, providing another mechanism by which multiple Tm isoforms can regulate actin cytoskeleton dynamics.

It has recently been demonstrated in fission yeast (Skau et al., 2009) that Tm increases actin filament polymerisation by preventing actin monomer disassociation from the barbed end and allowing formin nucleated actin filaments to anneal end-to-end. Upon annealing, formin may be displaced, or sequestered between annealed filaments (figure 1.22). In the latter case no more actin monomer can be added at the site of annealing and this may ultimately 'switch off' formin mediated elongation (Skau et al., 2009).
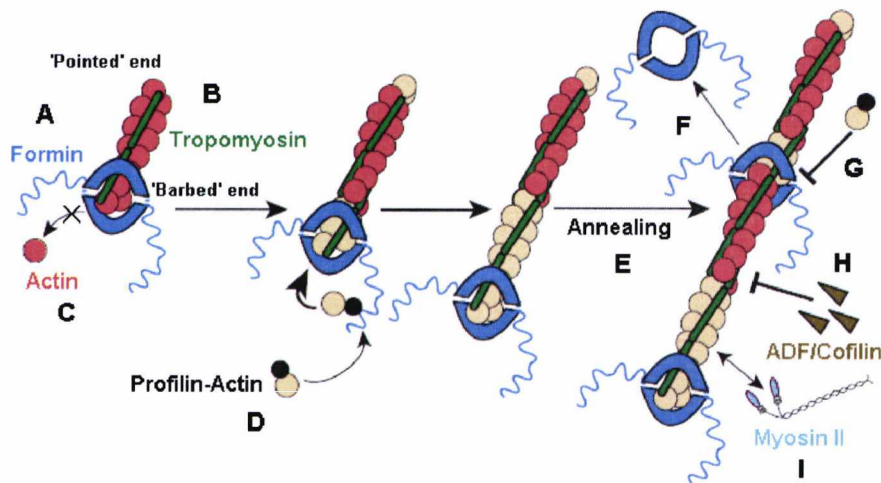
Figure 1.22. Tropomyosin regulates formin mediated actin assembly

(A) Formins nucleate actin filaments and remain processively associated with the growing 'barbed' end. (B) Formins increase the affinity of Tm for actin filaments. (C) Tm prevents actin disassociation from the barbed end. (D) Tm increases the rate at which formin adds profilin-actin to the barbed end (E) Tm allows formins nucleated filaments to anneal end-to-end. (F) Formins may be displaced by annealing or remain trapped in the filaments, new profilin-actin cannot be incorporated into annealed barbed ends. (H, I) Tm protects against the severing activity of ADF and regulates myosin II binding to actin filaments. Adapted from (Skau et al., 2009)

1.9.6.3. Tropomyosin and tropomodulin.

The affinity of tropomodulin for the pointed end of actin filaments is low in the absence of Tm, but increases substantially when Tm is present (Weber et al., 1999). Both Tm polymers associated with an actin filament bind (Kostyukova et al., 2006), via their amino termini, to two separate binding sites (Kostyukova et al., 2007) in the amino terminal half of tropomodulin. The affinity of Tm for binding sites on tropomodulin is isoform specific, and therefore may contribute to the efficiency of pointed end capping by tropomodulin.

1.9.6.4. Tropomyosin and myosins.

Tm interactions with myosin are most studied in striated muscle contraction (see section 1.5.4.) where Tm regulates actin-myosin II binding via a steric blocking mechanism. But Tm is also involved in regulating other myosin types in muscle and non-muscle cells, and this section will focus briefly on myosins I, II and V.

Type I myosins are characterised by their exclusion from actin filaments containing Tm suggesting Tm may play a role in regulating myosin I localisation (Collins and Matsudaira, 1991). In vitro experiments have shown that Tm inhibits myosin I ATPase activity and actin filament gliding in motility assays (Fanning et al., 1994). Injection of a HMW Tm isoform into epithelial cells caused retrograde translocation of organelles towards the nuclear area where as a LWM isoform had no effect. The suggested mechanism is that Tm prevents myosin I, in an isoform specific manner, from binding actin and 'anchoring' organelles in their correct location and as such they are translocated towards the nucleus by microtubule motors (Pelham et al., 1996). Further *in vivo* evidence (Tang and Ostap, 2001) with GFP tagged myosin I shows its localisation to Tm free membrane associated actin filaments, but not with Tm containing stress fibres. The molecular mechanism of Tm regulation of myosin I is not clear. One possibility is that a surface loop on myosin I (loop 4) is larger than in other myosins and has been proposed to sterically clash with Tm (Kollmar et al., 2002) Leito-Trivedi and colleagues (2007) replaced loop 4 with the shorter loop of a myosin II. The chimera could translocate actin filaments in an *in vitro* motility assay but were able to localise to actin *in vitro*. Another factor may be myosin I kinetics. Type I myosins are 'low duty ratio' (duty ratio refers to the percentage of the ATPase cycle spend bound to actin) motors in that the equilibrium constants for weak and strong actin bound states are low. The probability of myosin I binding in the strongly bound state is low and would result in no actin induced activation of ATPase activity (Ostap, 2008).

Type II myosins in non-striated muscle cells are regulated predominantly by the phosphorylation state of their heavy and regulatory light chains however Tm also has a role in regulating myosin II activity. The ATPase activity of smooth muscle myosin II increases in the presence of smooth muscle Tm (Chacko, 1981) and actin gliding velocity is increased by smooth muscle tm in *in vitro* motility assays (Umemoto et al., 1989). Two HMW Tm isoforms, one striated and one non-muscle have no effect on skeletal muscle myosin II induced actin filament motility, but inhibit myosin II ATPase activity at low myosin concentrations (Fanning et al., 1994). Conversely in the same study a LMW non-muscle Tm increased both ATPase rate and actin gliding activity of the skeletal muscle myosin II. Two Tms from budding yeast, Tpm1p and Tpm2p moderately increase actin filament gliding when skeletal muscle myosin II is present (Strand et al., 2001). When budding yeast myosin II is present however, Tpm1p has no effect on actin gliding where as Tpm2p inhibits gliding by approximately 40% (Huckaba et al., 2006). This is paralleled *in vivo* where yeast cell expressing only Tpm2p retrograde actin cable flow was reduced where as cell expressing only Tpm1p had normal retrograde flow rates.

The mechanism by which Tm inhibits or increases myosin II activity has not been fully determined although it is likely that in cases of increased activity (rate limiting) ADP release is accelerated by some Tm isoforms (Ostap, 2008). Since different Tms can occupy different positions on actin filaments (Lehman et al., 2000), the equilibrium position of a TM on actin, and the kinetics of different type II myosins could regulate actomyosin interaction.

Type V myosins transport vesicles and cellular cargoes along actin filament, but there is little literature regarding their interaction with Tm. One study shows that Tm does not affect the motility of myosin V coated beads. Since type V myosin are 'high duty ratio' motors (Sellers and Veigel, 2006), having large equilibrium constants for the strong binding position, the inability of Tm to inhibit myosin V is not unreasonable. In budding yeast Tm affects myosin V indirectly. In cells lacking Tm actin

filaments are absent, and polarised delivery of myosin V cargoes is abolished (Pruyne et al., 1998)

1.9.7. Tropomyosin in yeast.

Historically Tm has been studied longest as a regulator of actin and myosin interaction in muscle cells, and more recently in its roles in cell motility and morphology in non-muscle cells. Yeast cells have rigid cell walls and do not undergo the same morphological changes as animal cells, therefore the presence of Tm might be considered unlikely. However discovery of actin and myosin in yeast suggested that Tm like proteins might exist in non-metazoan cells. As Tm is a coiled-coil, sequence homology searches using animal templates return matches to coiled coil proteins of many sorts. The first non-metazoan Tm was isolated by subjecting yeast cells to a protocol for isolating non muscle Tm (Liu and Bretscher, 1989b). Tms from the budding yeast *Saccharomyces cerevisiae*, and the fission yeast *Schizosaccharomyces pombe* are the most widely studied in non-metazoans.

1.9.7.1. Tropomyosin in *Saccharomyces cerevisiae*

S. cerevisiae has two Tms, encoded by the *TPM1* and *TPM2* genes. Tpm1p was first isolated using a method for extracting Tm from non-muscle cells (Liu and Bretscher, 1989b) while Tpm2p was identified through sequence homology and first isolated from a Tpm1p deletion strain (Drees et al., 1995). The two proteins are similar to other Tms, being heat stable, alpha helical dimers, that bind to actin. Tpm2p is only 166 amino acids in length while an internal 38 residue duplication has lengthened the Tpm1 protein to 199 amino acids. Tpm1p and Tpm2p show approximately 65% sequence homology to each other but only 20% homology to vertebrate Tms and although shorter than animal Tms the proteins share the characteristic actin binding pseudo repeats (McLachlan and Stewart, 1975). The shorter yeast Tms have fewer

repeats and span fewer actin subunits (figure 1.5.7.2); 5 and 4 for Tpm1p and Tpm2p respectively, compared to 6 for LWM Tms and 7 for HMW Tms (Drees et al., 1995)

Like skeletal muscle Tms, Tpm1p (and presumably Tpm2p) are acetylated at the amino terminus (Maytum et al., 2000) by the budding yeast N-acetyltransferase NatB (Polevoda et al., 2003; Singer and Shaw, 2003) and like skeletal Tms this modification is required for the Tm to bind actin (Maytum et al., 2000). A short dipeptide (Ala-Ser) amino terminal extension or longer 5 and 9 amino acid extensions similar to those found in fibroblast Tms, are able to restore actin binding in bacterially expressed budding yeast Tm (Maytum et al., 2000; Monteiro et al., 1994)

In budding yeast cells the two Tms share similar localisation to actin cables and the CAR (figure 1.23), where they stabilises actin by enhancing actin-actin interactions (Wen et al., 2000) and protects against ADF/cofilin mediated severing (Okada et al., 2006). Tm does not colocalise to cortical actin patches, presumably because Arp2/3 induced branching in cortical actin networks is incompatible with Tm binding, disrupting end to end interactions (Pruyne, 2008). Although they share similar localisation within the cell, the two Tm isoforms have distinct but overlapping functions. Cells lacking Tpm1p are sickly and display growth defects (Liu and Bretscher, 1992; Liu and Bretscher, 1989a). In *S. cerevisiae* growth occurs apically and the type V myosin, Myo2p, guides secretory vesicles along actin filaments to the site of growth. When Tpm1p is absent, actin cables are lost and growth occurs isotropically (Pruyne et al., 1998).

While cells lacking Tpm2p have no easily discernable morphological phenotype, (Drees et al., 1995) overexpression of Tpm2p induces bipolar growth, suggesting that maintenance of proper ratios of Tpm1p and Tpm2p are important for polarised growth (Drees et al., 1995). In budding yeast type II myosin associated retrograde flow of actin cables from the cortical growth site to the cell interior is important for polarised growth and

organelle targeting. Deletion of *TPM2* increases the speed of actin filament retrograde flow *in vivo* and inhibits actin gliding *in vitro* (Huckaba et al., 2006), Deletion of *TPM1* has no effect on retrograde flow, and does not inhibit actin gliding suggesting that myosin II and Tpm2p act antagonistically in regulating retrograde actin filament flow. This is supported by the observation that Tpm2p binds with greater affinity to actin filaments (Drees et al., 1995)

Although the loss of either Tm gene products alone is tolerated in *S. cerevisiae*, deletion of both Tms is lethal suggesting that these Tms may overlap for some essential functions, or that they are structurally similar enough to compensate for the absence each other.

1.9.7.2. Tropomyosin in *Schizosaccharomyces. pombe*

S. pombe has a single Tm gene, $cdc8^+$ first identified in 1992 (Balasubramanian et al., 1992) by sequence identity and the ability to complement a cell division cycle mutation . The gene contains one intron and encodes a protein of 161 amino acids. While it is identical in length to *S. cerevisiae* Tpm2p, it shares greater sequence similarity to Tpm1p, including actin interacting pseudorepeats (figure 1.24.).

Cdc8 expression levels do not vary throughout the cell cycle and at any given point approximately 80% of Cdc8 dimers are acetylated (Skoumpla et al., 2007) Acetylation greatly increases the affinity of Cdc8 for actin, the unacetylated protein still binds to actin albeit weakly. Interestingly and unlike budding yeast Tms, the addition of a amino terminus dipeptide extension (Ala-Ser), does not mimic amino terminal acetylation on *S. pombe* (Skoumpla et al., 2007). In cells lacking the regulatory subunit of the NatB acetyltransferase complex, all Cdc8 remains unacetylated (Arthur Coulton, personal communication). Cells can still grow and divide at temperatures lower than 25^{0}C, but display multiple growth and cytokinesis defects.
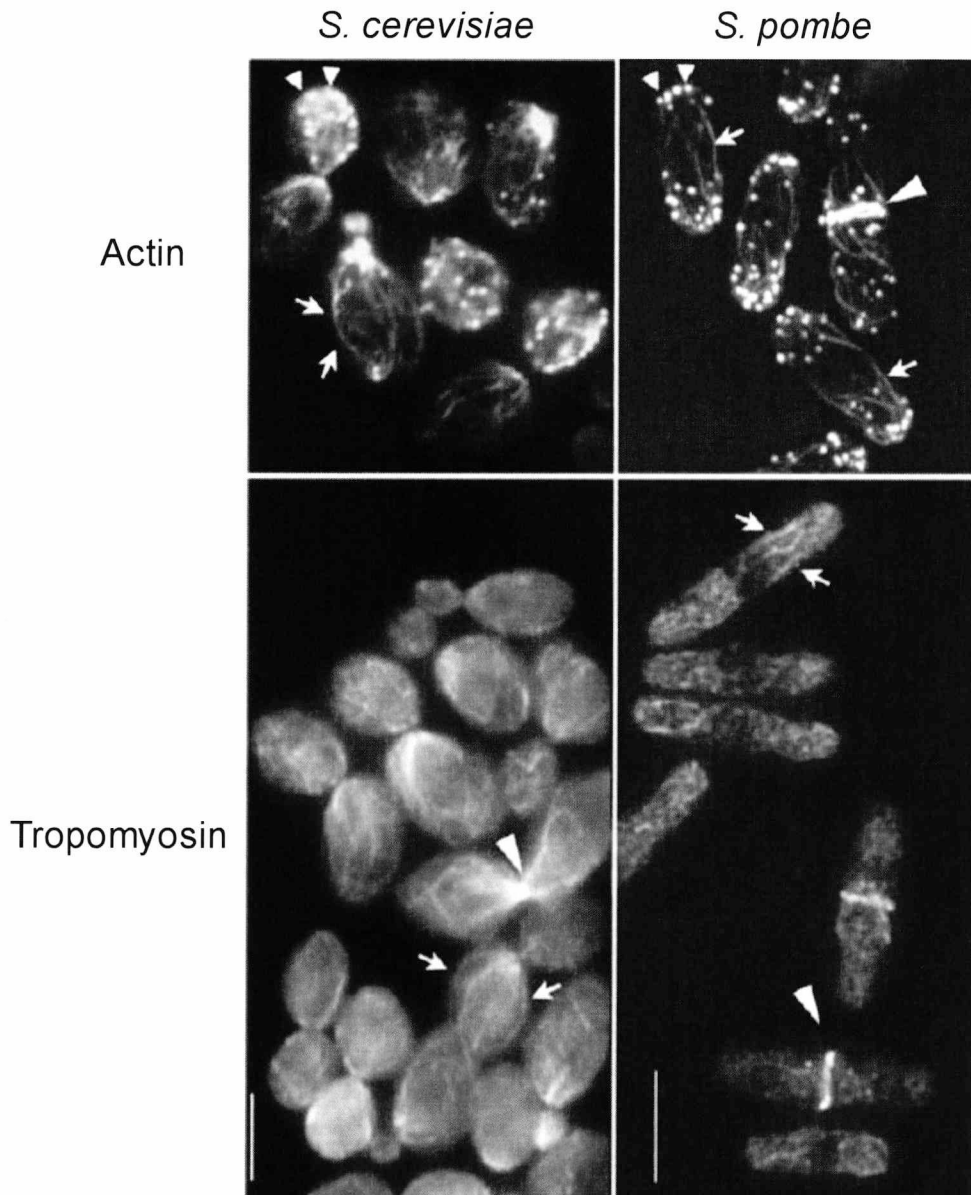
Figure 1.23. Organisation of yeast actin cytoskeletons

Actin staining (top panels) in the budding yeast *Saccharomyces cerevisiae* and the fission yeast *Schizosaccharomyces pombe* reveals three distinct actin structures. Cortical actin patches (small arrow heads) associate with sites of growth. Long actin filaments (arrows) extend the length of the cell in both species. During mitosis a contractile actin ring forms at the bud neck in *S. cerevisiae* and at the cell equator in *S. pombe* (large arrow heads). During cytokinesis the rings constrict and dive the two daughter cells. Tropomyosin (bottom panels) associates only with actin filament and the actin ring. Scale bars equal 5 µm for *S. cerevisiae* and 10 µm for *S. pombe*. Reproduced from (Pruyne, 2008)

Cdc8 localises to cytoplasmic actin filaments and to the CAR (figure 1.23). Cdc8 is also seen as patches in the cytoplasm, but these patches do not colocalise with cortical actin patches (Arai et al., 1998; Skoumpla et al., 2007). Cdc8 is required to stabilise actin filaments and maintain polarised cell growth (Chang et al., 1996; Pelham and Chang, 2001). As in budding yeast, actin filaments, stabilised by Cdc8, serve as 'tracks' upon which a type V myosin guides secretory vesicles to the sites of cell growth (i.e. cell tips) (Grallert et al., 2007). Cells lacking functional Cdc8, and actin filaments, continue to grow but are characterised by swollen 'dumbbell' shaped tips.
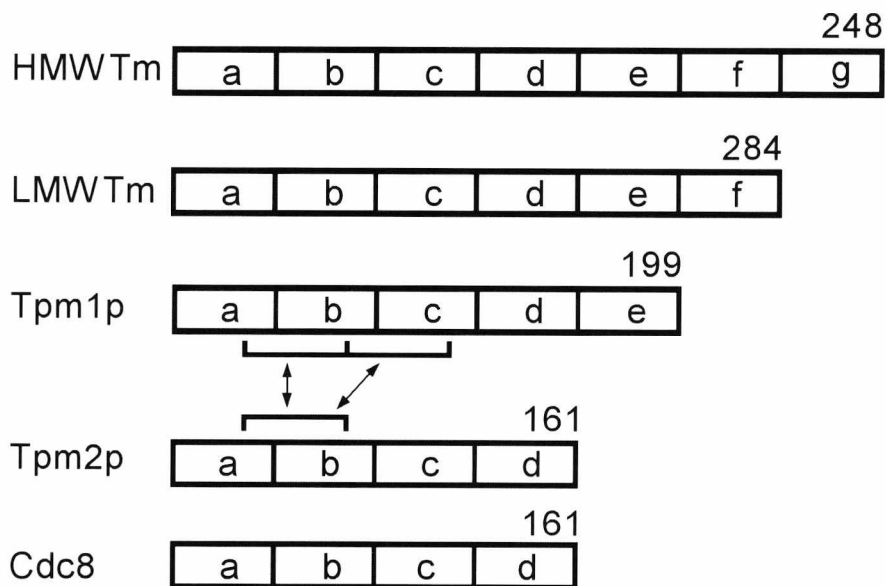
Figure 1.24. Animal and fungal tropomyosins' actin binding pseudorepeats.

Diagramatic representations of the primary sequence of high and low molecular weight vertebrate tropomyosins, budding yeast Tpm1p and Tpm2p and fission yeast Cdc8 showing overall length in amino acids and approximate boundaries between predicted actin binding The region of duplication within Tpm1p and its corresponding region within Tpm2p are highlighted with arrows. Reproduced from (Pruyne, 2008).

The fact that only partial depolarisation is observed may be due to vesicle transport along microtubules, or some vesicle capturing mechanism at the cortex (Pruyne, 2008) Cdc8 is also essential for formin mediated assembly of actin into the CAR, and subsequent   ring constriction (Balasubramanian et al., 1992; Skau et al., 2009). Cells lacking Cdc8 are unable to divide and septate, but continue to undergo nuclear division resulting in long multinucleate cells lacking septa. In addition to defects in growth and division during the mitotic life cycle, Cdc8 also has been shown to affect cell fusion during mating (Kurahashi et al., 2002). This study identified several Cdc8 mutations that not only impair cell fusion during meiosis but also mitotic growth suggesting that the function of Cdc8 and actin filaments is not separate in these two processes.

Three dimensional helical reconstructions from EM micrographs of acetylated Cdc8 bound to actin reveal that it occupies the 'closed' (see figure 1.25.) position on actin filaments, and consistent with this is able to regulate type II myosin interaction with actin (Skoumpla et al., 2007). What is more fibroblast and smooth muscle Tm can rescue a loss of Cdc8 function *in vivo* (Balasubramanian et al., 1992; Skoumpla et al., 2007), suggesting similarities to Tms in higher organisms. The study of Cdc8 could be useful in understanding Tm's role in cytoskeletal regulation in non-muscle cells of higher eukaryotes.
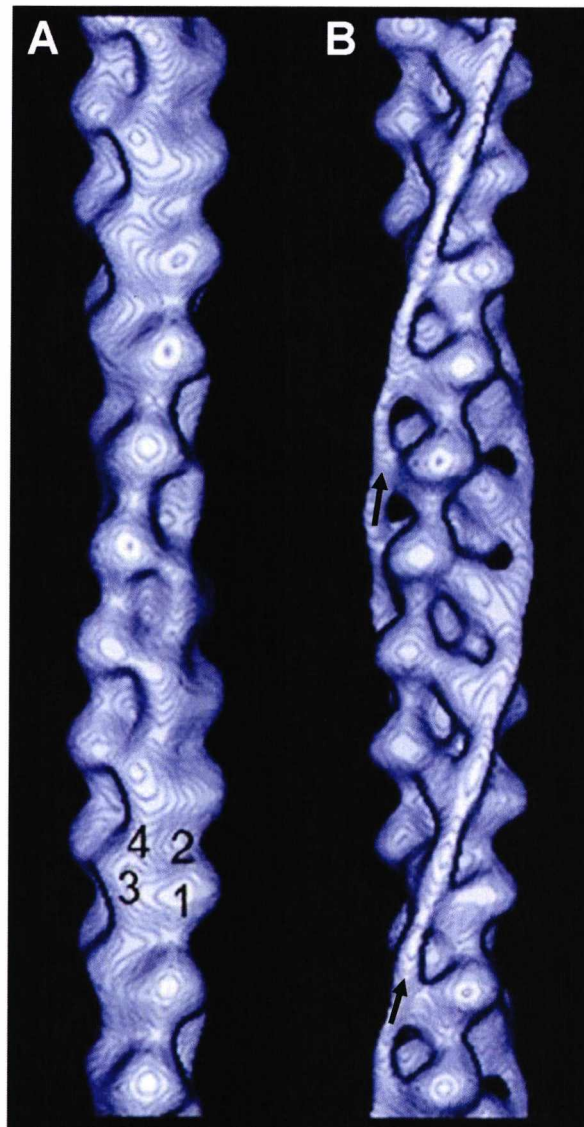
Figure 1.25. Three-dimentional reconstruction of Cdc8 bound to F-actin.

(A) F-actin filaments without Tm. Actin subdomains 1 to 4 are marked on one actin monomer (B) F-actin decorated with Cdc8. Additional density corresponding to tropomyosin is marked with arrows. Cdc8 occupies the 'closed' position on actin, i.e. it localises on the outer edge of actin subdomains 3 and 4 next to the cleft separating the inner (subdomains 3 and 4) and outer (subdomains 1 and 2) domains of actin. Adapted from (Skoumpla et al., 2007).

1.10. Quantum dots

Fluorescent probes are widely using in cell biology, most commonly in fluorescence microscopy, where fluorescence in is achieved by exciting delocalised electrons typically in the carbon-carbon double bonds of the fluorophore molecule. As a result 'traditional' organic fluorophores can suffer from photobleaching, wide overlapping emission spectra and the need to be excited at a specific wavelength. Quantum dots (QDs) are nanometer size fluorescent crystals, made of semiconducting materials and measure between 2 and 10 nm in diameter (10 to 50 atoms). QDs fluoresce in a manner related to the material from which they are made, and their size and shape, and do not suffer these drawbacks. They are bright, photostable structures and available with a variety of emission wavelengths (colours) that make then attractive for use in biological imaging.

1.10.1. Fluorescence and quantum dots

Traditional organic fluorophores typically contain one or more aromatic ring structure (figure 1.26). Atoms in the ring are bonded by strong covalent sigma bonds, and also by weaker pi bonds. Electrons occupy discrete 'orbitals' or energy levels and when a pi electron absorbs a photon of light, it can become excited and 'jump' to a higher energy level. As the electron relaxes and 'falls' back to its original level, or ground state, it emits some energy as light, this effect is referred to as fluorescence (Lakowicz., 1999).

Atoms in organic fluorophores are relatively isolated, in contrast atoms in crystalline semiconductor quantum dots are closely packed (figure 1.26) and the number of orbitals becomes exceedingly large. The difference in energy between them becomes small, so the levels may be considered to form continuous 'bands' of energy rather than the discrete energy levels of atoms in isolation (McQuarrie and Simon., 1999). There are also some energy levels that contain no orbitals, leading to the formation
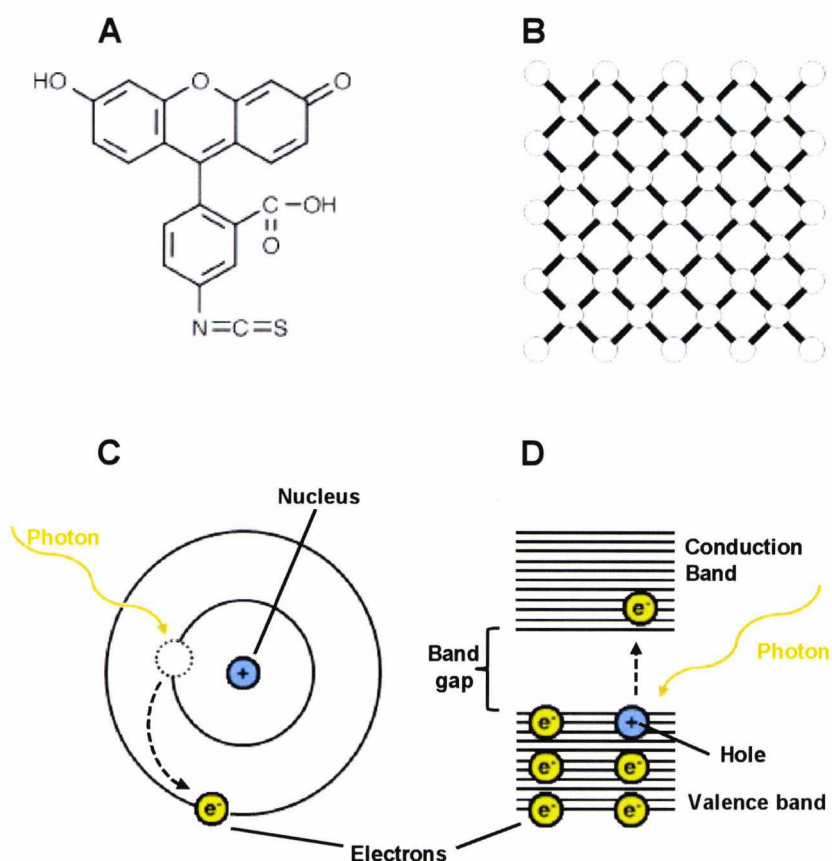
Figure 1.26. Comparison of fluorescence in organic fluorophores and quantum dots.

(A) The arrangement of atoms in a molecule of FITC in contrast to (B) the closely packed and uniform arrangement of atoms in an CdSe semiconductor. (C) For a relatively isolated atom in an organic fluorophore absorbtion of a photon by an electron permits the electron to occupy a higher energy level. (D) In the closely packed arrangement of a semiconductor energy levels between atoms are 'shared' as discrete bands. Absorbtion of a photon by an electron in the valence group of bands allows the electron to cross the band-gap and the conduction band.

of a band gap, an energy level which electrons are 'forbidden' to occupy. Electrons in a semiconductor normally occupy the 'valence' group of energy levels and are associated with a single atom. When an electron absorbs a photon of light it can 'jump' into the conduction group of energy levels and can move freely in the semiconductor, leaving behind a positively charged 'hole'. The recombination of the electron-hole pair is accompanied by the emission of radiation as fluorescence (Alivisatos,

1996). The wavelength of fluorescence depends on the size of the band gap, which in turn depends on the size of the QD (Bruchez et al., 1998; Peng et al., 1998).

1.10.2. Structure and optical properties of quantum dots.

The crystalline semiconductor core of QDs is typically composed of cadmium sulphide (CdS) cadmium selenide (CdSe) or cadmium telluride (CdTe) (Peng and Peng, 2001). A shell of a structurally related non-emissive material, typically zinc sulphide (ZnS) is synthesised around the core and increases the quantum yield (efficiency) of the QD to around 80% (Hines and Guyot-Sionnest, 1996). CdSe QDs are most commonly used in imaging as their emission wavelengths are in the visible spectrum, CdS and CdTe emit in the UV-blue and far red-infrared spectra respectively

The size of QDs can be controlled during their synthesis by adjusting the amount of QD precursor material and crystal growth time (Peng et al., 1998), and QD emission spectra are related to crystal size. Small CdSe nanocrystals (~2 nm diameter) fluoresce in the range between 495 and 515 (Murray et al., 1993), where as larger nanocrystals (~5 nm diameter) fluoresce between 605 nm and 630 nm (Bruchez et al., 1998). The ability to precisely control QD size allows the production of QDs that emit at any wavelength, and therefore colour.

The inorganic crystalline structure of QDs offer optical advantages over 'traditional' fluorophores. Photo bleaching in organic fluorophores occurs as covalent bonds between carbon atoms are broken by radiation used to excite the fluorophore. In QDs this type of bond is absent and fluorescence occurs via a different mechanism, making QDs extremely resistant to photobleaching (Nirmal and Brus, 1999). In addition, the molar extinction coefficient of QDs is 10 to 50 times larger than that of organic fluorophores, QDs therefore can absorb 10 to 50 times more
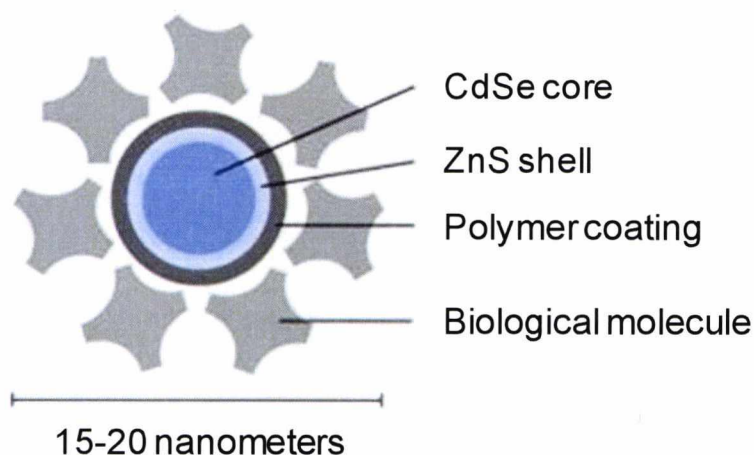
Figure 1.27. Structure of a quantum dot conjugate.

A diagram showing the composition of CdSe-ZnS core/shell quantum dot soluabilised in water with a polymer coating and conjugated to a biological molecule. Dimensions are drawn approximately to scale. Adapted from online URL: invitrogen.com

photons per unit area than organic dyes, at the same excitation energy. As a result, in imaging applications QDs have been found to be 10 to 20 times brighter than 'traditional' fluorophores (Gao et al., 2004).

Another favourable property of QDs is their unique optical spectra. Organic fluorophores have narrow excitation spectra, and can only be excited at specific wavelengths (figure 1.28.). In addition they have broad emission spectra. The Stokes shift (distance between excitation and emission maxima) is often small with organic fluorophores which can lead to background in imaging applications. In addition when imaging multiple fluorophores, care must be taken to avoid overlapping emission wavelengths. Conversely QDs have narrow emission spectra, broad excitation spectra and a large Stokes shift (figure 1.28). As such multiple QDs, with varying emissions, could be excited at a single wavelength and fluorescence signal overlap is reduced (Bruchez et al., 1998).
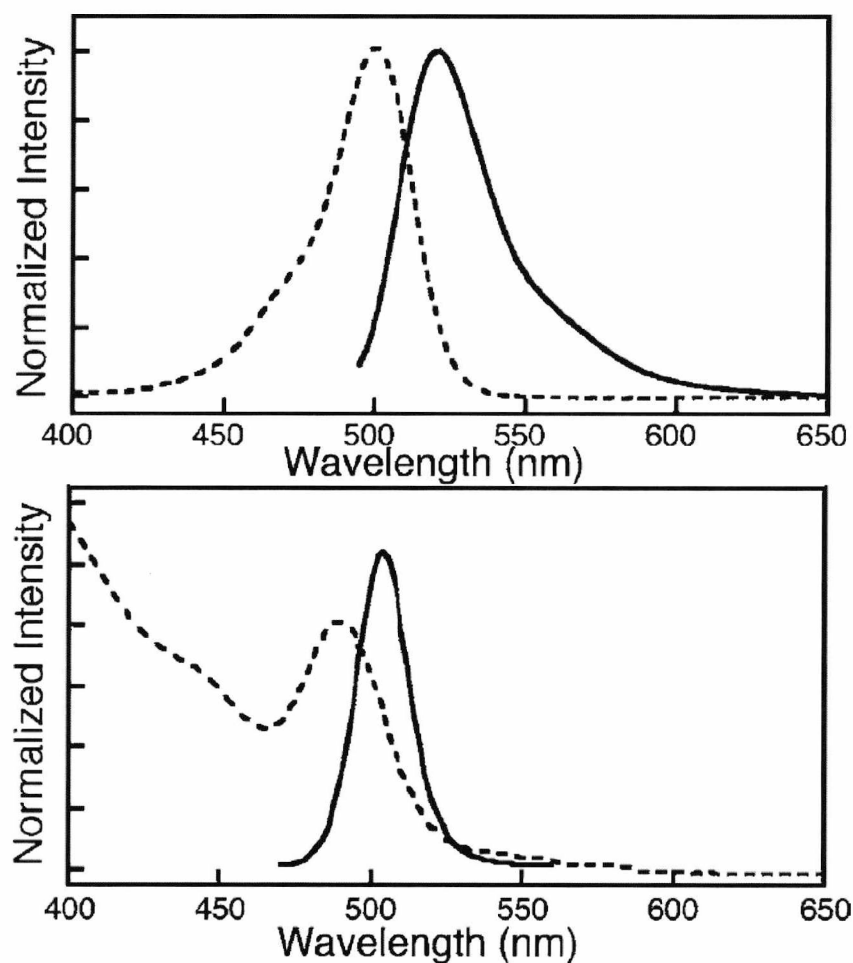
Figure 1.28. A comparison of optical spectra

Excitation (dotted line) and emission (solid line) of fluorescein (top) and a water soluble quantum dot (bottom) Reproduced from (Bruchez et al., 1998)

1.10.3. QD biocompatibility and conjugation to biological molecules.

CdSe QDs are synthesised by injecting liquid precursors into hot organic solvents (Murray et al., 1993) and stabilised in the solvent by surrounding them (capping) in an organic surfactant. However for biological applications QDs must be soluble in water which can be achieved by displacing the hydrophobic surfactant molecules with biofunctional molecules that are hydrophilic at one end and hydrophobic at the other (Alivisatos et al., 2005). Molecules containing thiols (-SH) such as

mercaptocarbonic acids (SH-...-COOH) or cysteamines (SH-...-NH$_2$) are often used in this context; the thiol group binds the ZnS shell while the carboxyl or amine group provides water solubility (Alivisatos et al., 2005). Alternatively the surface of QD can be coated with amphiphilic (possessing both hydrophilic and lipophilic groups) polymers (Pellegrino et al., 2004). Rather than displacing the surfactant coating, the hydrophobic groups in the polymer intercalate with the surfactant molecules while the hydrophilic groups ensure water solubility.

To make water soluble QDs useful for biological applications they must be coupled to biological molecules. Several successful approaches have been used to link biological molecules to QDs. Simple small molecules such as oligonucleoties readily adsorb to the surface of water soluble quantum dots (Mahtab et al., 2000), however binding is non specific and depends on ionic strength, temperature and surface charge. Alternatively QDs can be coated with a negatively charged polymer, which attracts naturally positively charged proteins, (Goldman et al., 2002) or proteins engineered with positive charges (Mattoussi et al., 2000), via electrostatic interactions and results in stable QD protein conjugates.

Biological molecules containing thiol (-SH) groups can be conjugated directly to QDs. The thiol group is able to bind directly to the ZnS shell of the QD (Chan et al., 2002; Willard et al., 2001). However the bond between ZnS and –SH groups is not very strong and biomolecules can detach causing QDs to become insoluble. A more stable method is to covalently link biological molecules to QD surface functional groups using cross-linking molecules. If the QD surface has –COOH, -NH$_2$ or –SH groups then biological molecules containing these groups can be linked to the QD. The water soluble cross-linker 1-Ethyl-3-(3-dimethylaminopropyl)carbodiimide (EDC) which functions by converting carboxyl groups to amine-reactive groups, is commonly used to link –COOH and NH$_2$ groups, where as Sulfosuccinimidyl 4-[N-maleimidomethyl] cyclohexane-1-carboxylate (Sulfo-SMCC) is used to link –SH and NH$_2$ groups (Yu et al., 2009).

1.10.4. Application of quantum dot bio-conjugates

This study is concerned with the conjugation of QDs to antibodies (IgG) and as such this part of the project concentrated predominantly on the application of QD-IgG conjugates, in cellular imaging with emphasis on microscopy. QDs were first used for *in vitro* fluorescence microscopy by Bruchez and colleagues (1998) to label the actin cytoskeleton of mouse fibroblast cells, this early experiment however did not use antibodies to specifically label actin. It relied on the high affinity of the protein streptavidin for the B-complex vitamin, biotin. A biotinalyated actin binding protein was incubated with the cells, followed by streptavidin and finally biotinalyated QDs to fluorescently label the actin cytoskeleton. Subsequently quantum dots have been successfully conjugated to various biological molecules including biotin, oligonucleotides, peptides and proteins (Alivisatos et al., 2005) and used successfully in fluorescence microscopy to visualise several distinct cellular components (figure 1.29).

Wu and co-workers (2003b) simultaneously labelled microtubules and nuclear antigens in mouse fibroblast cells with considerable increases in brightness and photostability compared to organic fluorophores. Organelles including vesicles in neuronal cells (Ness et al., 2003) and mitochondria in a HeLa (immortal cell line used in research) cell line (Derfus et al., 2004) have also been visualised using QD-IgG conjugates. Several groups have successfully visualised cell surface and membrane proteins using QD-IgG conjugates; Jaiswal and colleagues (2003) labelled a membrane transport protein on HeLa cells and demonstrated that the cells remained fluorescently labelled for over a week as they grew and developed. Tokumasu & Dvorak (2003) labelled a membrane anion exchanger protein on the surface of erythrocytes and used multiple images to create 3D reconstructions of the cells and to show the distribution of the protein in the lipid membrane. The breast cancer cell surface growth factor receptor, Her2 has been visualized using QD-IgG conjugates (Wu et al., 2003b) and Kaul (2003) and colleagues used
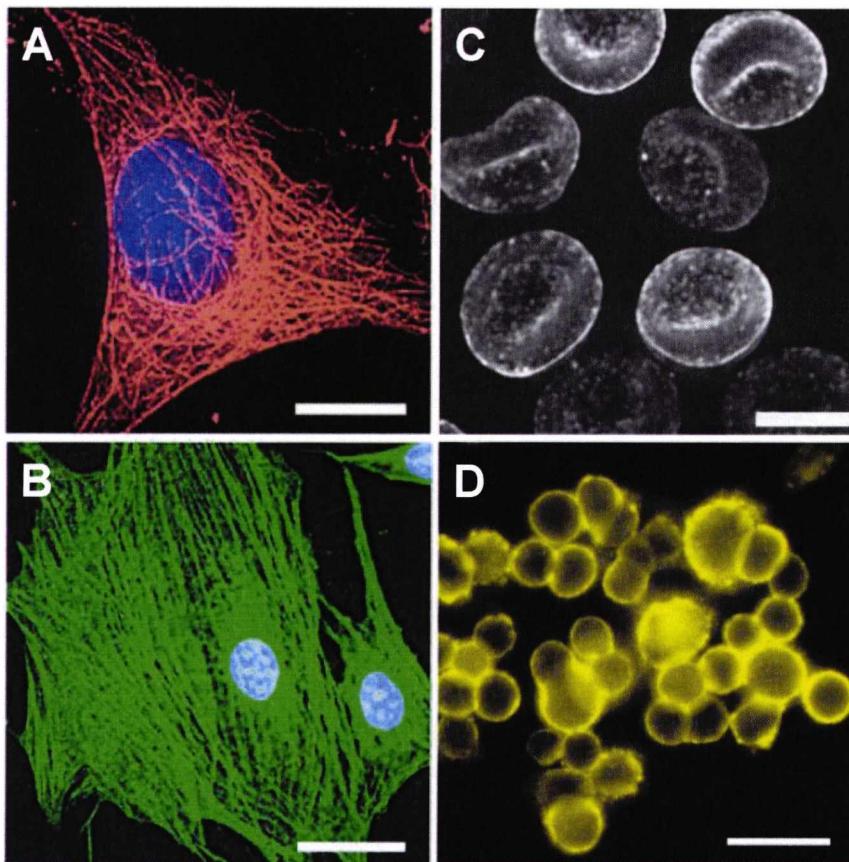
Figure 1.29. Fluorescence imaging with quantum dots

(A) Microtubules (red) in mouse fibroblast cells labeled with QD conjugates. Scale bar = 10 μm. (B) Actin filaments (green) in mouse fibroblast cells labeled with QD conjugates. Scale bar = 24 μm. (C) Erythrocyte cell surface anion exchanger labeled with QD conjugates. Scale bar = 5 μm (D) Human growth factor receptor on the surface of breast cancer cells labeled with QD conjugates Scale bar = 20 μm. Images adapted from (Tokumasu and Dvorak, 2003; Wu et al., 2003b)

QD-IgG conjugates to study the redistribution of heat shock protein 70 in osteogenic sarcoma cells during heat stress.

In fluorescence imaging applications using QD-IgG probes, the most commonly used conjugation approach has been based on biotin-streptavidin interaction. In addition, many visualisation protocols use a three step approach. That is, an unlabeled primary antibody specific to the cellular target, and biotinylated general secondary antibody (anti-

mouse, anti-goat etc) and finally a streptavidin coated quantum dot are used to visualised intracellular structures/processes. Direct attachment of antibodies to QDs is not widely reported and the use of EDC to couple carboxyl modified QDs to free amino groups on antibodies has the potential to produce coupled conjugates for use in one step probing of cellular targets. Reports of this method are limited and details of the specifics of the coupling process are typically vague. There is currently there is no literature on the use of QD-IgG conjugates for fluorescence imaging in the model organisms *Saccharomyces cerevisiae* or *Schizosaccharomyces pombe*.

1.10.5 Carbodiimide for bioconjugation

A carbodiimide is a functional group consisting of the formula $RN=C=NR$ and are often used as dehydration reagesnt to activate carboxylic acids for amine bond formation with amine groups. Bioconjugation using carbodiimides is widely performed (Nakajima and Ikada, 1995) and 1-ethyl-3-(3-dimethylaminopropyl) carbodiimide (EDC) is water soluble making it preferable for biological applications.

The formation of an amide using a EDC is uncomplicated, but with several side reactions can produce unwanted products (figure 1.30). The acid (**1**) will react with the carbodiimide to produce the key intermediate: the O-acylisourea (**2**), which can be viewed as a carboxylic ester with an activated leaving group. The O-acylisourea will react with amines to give the desired amide (**3**) and urea (**4**).

The side reaction of the O-acylisourea (**2**) produce both desired and undesired products. The O-acylisourea (**2**) can react with an additional carboxylic acid (**1**) to give an acid anhydride (**5**), which can react further to give the desired amide (**3**). The main undesired reaction pathway involves the rearrangement of the O-acylisourea (**2**) to the stable N-acylurea (**6**) (Nakajima and Ikada, 1995; Sam et al., 2009)
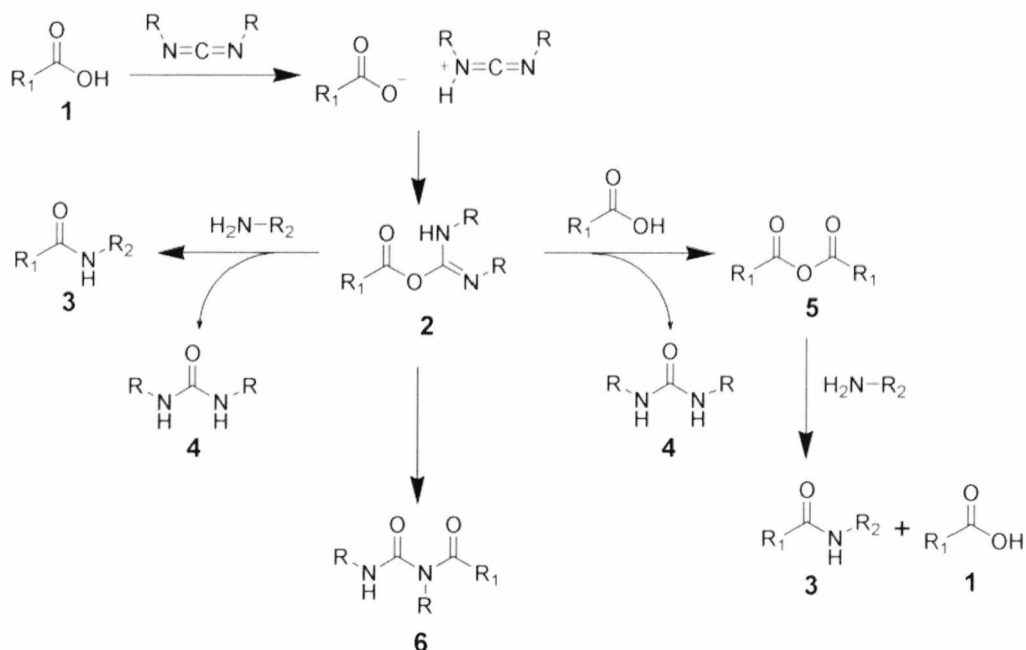
Figure 1.30. Amide formation by EDC

A cartoon of the reaction mechanisms between carboxylic acid and amine groups in aqueous solution in the presence of carbodiimide.

1.11. Aims of this project

The role of TM in vertebrate muscle is well known and has been studied extensively (Perry, 2001) however there are at least 18 TM isoforms expressed in mammalian non-muscle cells that are less well understood (Gunning et al., 2008). The fission yeast *Schizosaccharomyces pombe* has a single TM, Cdc8 and its similarity to higher eukaryotes makes it and excellent system to study this non-muscle TM.

Although several mutations that affect the function *in vivo* of Cdc8 have been reported (Balasubramanian et al., 1992; Kurahashi et al., 2002; Nurse et al., 1976), mutations in the important amino terminal region of Cdc8, and detailed biochemical studies have not been undertaken. The primary aim of this project was to create several amino terminal mutations in the Cdc8 protein and investigate the effects these mutations have on

the physical properties of the protein, including thermal stability and the ability to form end-to-end interactions and polymerise. The aim was then to investigate and potentially correlate these observations with ability each Cdc8 mutant to interact with actin, regulate acto-myosin interactions and function *in vivo*.

Quantum dots have been widely used for *in vitro* fluorescence microscopy and have been reported to produce brighter signals that are more resistant to photobleaching than organic fluorophores (Alivisatos et al., 2005). EDC mediated coupling is widely used in bioconjuagtions (Nakajima and Ikada, 1995) however its use for coupling antibodies to QDs is not widely reported, furthermore there are few detailed studies of the variables involved are available.

Direct coupling of antibodies to QD using EDC would be beneficial for *in vitro* multiplex fluorescence microscopy, therefore the secondary aim of this project to was develop a QD-IgG conjugate for use in fluorescent imaging of *S. pombe* cellular components whilst simultaneously undertaking a detailed study of factors influencing the efficiency of EDC mediated coupling.

Chapter 2: Materials & Methods

2.1. Cell culture

2.1.1. *S. pombe* cultures

Fission yeast strains used in this study are listed in table 2.1 Standard culture methods were used as described by Moreno et al. (1991). Cells were grown in either Yeast Extract plus Supplements (YES) media, 10x YES (YES containing 10 fold concentrations of each component or Edinburgh Minimal Media (EMM), with appropriate amino acid supplements (Table 2.2). Repression of the nmt41 promoter (Maundrell, 1993) was achieved by supplementing EMM with thiamine to a final concentration of 4 μM. Solid media for plates was prepared by the addition of 2% agar to liquid media before autoclaving.

2.1.2. *E. coli* cultures

All bacterial cultures were grown in Luria Bertani (LB) broth at 37°C. Plasmid selection was achieved by supplementing with ampicillin to a final concentration of 50 μg/ml.

2.1.3. Cdc8 expression in *S. pombe*

1 L of YES, 10X YES or EMM was inoculated from an overnight starter culture. Cells were incubated at 30 °C with shaking until late log phase. Cells were harvested by centrifugation at 3000 rpm for 10 minutes at 4 °C, and resuspended in STOP buffer (150 mM NaCl, 50mM NaF, 10 mM EDTA, 1 mM NaN$_3$, pH 7.0). Cells were then centrifuged at 3000 rpm for 10 minutes at 4 °C and resuspended in *S. pombe* lysis buffer. (50 mM Tris pH 7.5, 50 mM EDTA, 1% SDS, pH 7.5).

Table 2.1. *S. pombe* strains used in this study

Lab Stock Number	Strain name	Genotype description
244	wt	*his2- ura4.d18 leu1.32*
331	*cdc8-110*	*cdc8-110 (IH3417)*
360	TM011	*TM011 (ts) leu1-32 ura+ (Protease deficient mutant)*
761	*ura4-d18*	*ura4-d18*
1227	*arm1::kanMX6*	*arm1::kanMX6-ura4-d18 leu1-32 ade6-*
1443	*cdc8-110 pREP41*	*cdc8-110 his2- ura4.d18 leu1.32 pREP41*
1444	*cdc8-110 pREP41cdc8⁺*	*cdc8-110 his2- ura4.d18 leu1.32 pREP41cdc8⁺*
1445	*cdc8-110 pREP41cdc8-E6K*	*cdc8-110 his2- ura4.d18 leu1.32 pREP41cdc8-E6K*
1446	*cdc8-110 pREP41cdc8-D16A*	*cdc8-110 his2- ura4.d18 leu1.32 pREP41cdc8-D16A*
1447	*cdc8-110 pREP41cdc8-E6A*	*cdc8-110 his2- ura4.d18 leu1.32 pREP41cdc8-E6A*
1448	*cdc8-110 pREP41cdc-LKL*	*cdc8-110 his2- ura4.d18 leu1.32 pREP41cdc8-LKL*
1449	*cdc8-110 pREP41cdc8-D2A*	*cdc8-110 his2- ura4.d18 leu1.32 pREP41cdc8-D2A*
1450	*wt pREP41*	*his2- ura4.d18 leu1.32 pREP41*
1451	*wt pREP41cdc8⁺*	*his2- ura4.d18 leu1.32 pREP41cdc8⁺*
1452	*wt pREP41cdc8-E6K*	*his2- ura4.d18 leu1.32 pREP41cdc8-E6K*
1453	*wt pREP41cdc8-D16A*	*his2- ura4.d18 leu1.32 pREP41cdc8-D16A*
1454	*wt pREP41cdc8-E6A*	*his2- ura4.d18 leu1.32 pREP41cdc8-E6A*
1455	*wt pREP41cdc-LKL*	*his2- ura4.d18 leu1.32 pREP41cdc8-LKL*
1456	*wt pREP41cdc8-D2A*	*his2- ura4.d18 leu1.32 pREP41cdc8-D2A*
1464	*arm1::kanMX6 pREP41*	*arm1::kanMX6-ura4-d18 leu1-32 ade6-pREP41*
1465	*arm1::kanMX6 pREP41cdc8⁺*	*arm1::kanMX6-ura4-d18 leu1-32 ade6-pREP41cdc8⁺*
1466	*arm1::kanMX6 pREP41cdc8-E6K*	*arm1::kanMX6-ura4-d18 leu1-32 ade6-pREP41cdc8-E6K*
1467	*arm1::kanMX6 pREP41cdc8-D16A*	*arm1::kanMX6-ura4-d18 leu1-32 ade6-pREP41cdc8-D16A*
1468	*arm1::kanMX6 pREP41cdc8-E6A*	*arm1::kanMX6-ura4-d18 leu1-32 ade6-pREP41cdc8-E6A*
1469	*arm1::kanMX6 pREP41cdc8-LKL*	*arm1::kanMX6-ura4-d18 leu1-32 ade6-pREP41cdc8-LKL*
1470	*arm1::kanMX6 pREP41cdc8D2A*	*arm1::kanMX6-ura4-d18 leu1-32 ade6- pREP41cdc8-D2A*

Table 2.2. Media and stock solutions

YES media		
Component	Amount	Final concentration
Yeast extract	5 g/l	0.5% w/v
Glucose	30 g/l	3.0% w/v
Supplements	-	*

50 x salt stock		
Component	Amount	Final concentration
$MgCl_2.6H_2O$	52.5 g/l	0.26 M
$CaCl_2.2H_2O$	0.735 g/l	4.99 mM
KCl	50 g/l	0.67 M
Na_2SO_4	2 g/l	14.1 mM

EMM media		
Component	Amount	Final concentration
Potassium hydrogen phthallate	3 g/l	14.7 mM
Na_2HPO_4	2.2 g/l	15.5 mM
NH_4Cl	5 g/l	93.5 mM
Glucose	20 g/l	2% w/v
Salts	20 ml/l	-
Vitamins	1 ml/l	-
Minerals	0.1 ml/l	-
Supplements	-	*

1000 x vitamin stock		
Component	Amount	Final concentration
Pantothenic acid	1 g/l	4.20 mM
Nicotinic acid	10 g/l	81.2 mM
Inositol	10 g/l	55.5 mM
Biotin	10 mg/l	40.8 µM

10000 x mineral stock		
Component	Amount	Final concentration
Boric acid	5 g/l	80.9 mM
$MnSO_4$	4 g/l	23.7 mM
$ZnSO_4.7H_2O$	4 g/l	13.9 mM
$FeCl_2.6H_2O$	2 g/l	7.40 mM
Molybdic acid	0.4 g/l	2.47 mM
KI	1 g/l	6.02 mM
$CuSO_4.5H_2O$	0.4 g/l	1.60 mM
Citric acid	10 g/l	47.6 mM

LB media		
Component	Amount	Final concentration
Bacto Peptone	10 g/l	1% w/v
Yeast Extract	5 g/l	0.5% w/v
NaCl	10 g/l	171 mM

* Appropriate supplements of adenine, histidine, leucine, uracil and thiamine were added to final concentrations of 200 µg/ml (leucine & histidine), 100 µg/ml (adenine & uracil) and 5 mM (Thiamine) as required.

2.1.4. Cdc8 expression in *E. coli*

1 L of LB media containing 0.05 mg/ml ampicillin was inoculated with 2.5 ml of an overnight starter culture. Cells were incubated at 37 ^{0}C with shaking at 220 rpm until optical density at 600 nm reached between 0.3 and 0.5. Expression from the T7 promoter was induced with the addition of Isopropyl β-D-1-thiogalactopyranoside (IPTG) to a concentration of 0.1 mg/ml and the cells were incubated at 37 ^{0}C with shaking at 220 rpm for

2 hours. The cells were harvested by centrifugation at 5000 rpm for 30 minutes at 4 $^{\circ}$C. Pellets were frozen at -20 $^{\circ}$C or resuspended for protein extraction.

2.1.5. *S. pombe* growth curves

10 ml cultures of *S. pombe* cells were grown to mid-log phase overnight in EMM lacking leucine, in 50 ml flasks at 25°C with shaking at 200 rpm. Cells were diluted to 0.1 OD_{600} and 1 ml pipetted into wells of a 24 well CellStar® plate (Greiner Bio-One). Growth curves were generated by monitoring OD_{600} at 25°C or 36°C with shaking at 200 rpm using a Fluostar Optima plate reader (BGM labtech) connected to a PC running Optima v2.2 control software.

2.2. Biochemical techniques

2.2.1. SDS-PAGE

SDS-PAGE was performed using 12% polyacrylamide gels, and Bio Rad Mini Protean II and III gel apparati. Glass plates were cleaned with 70% ethanol before use. The resolving gel was poured to approximately ¾ of the height of the plates and overlaid with isopropanol. Once set isopropanol was aspirated and residual traces removed by washing with dH$_2$O and blotting with filter paper. The stacking gel was poured and an appropriate sized comb inserted. Once set the comb was removed, wells were washed with dH$_2$O, and the gels were assembled in the gel tank containing SDS-PAGE running buffer (250 mM Tris base, 2 M glycine, 0.1% SDS). Samples were mixed with SDS loading buffer (150mM Tris, 25% w/v glycerol, 5% w/v SDS, 12.5% v/v β-mercaptoethanol , 0.025% w/v Bromophenol Blue.) at a ratio of 6:1, heated at 85 $^{\circ}$C for 10 minutes and loaded using a Hamilton microsyringe. Gels were run at 150V for 90 to 120 minutes.

Table 2.3. Polyacrylamide gel conditions

	Resolving gel	Stacking gel
dH$_2$O	1.75 ml	7 ml
1.5 M Tris pH 8.7/ 1 M Tris pH 6.8	3.75 ml	1.25 ml
10% SDS	0.1 ml	0.05 ml
30% Acrylamide/Bis, 29:1	4 ml	1.7ml
APS	0.1 ml	0.1 ml
TEMED	0.015 ml	0.015 ml

2.2.2. Coomassie Staining

Following SDS-PAGE, gels were immersed in coomassie stain (0.1% coomassie brilliant blue, 50% methanol, 10% acetic acid) and incubated at RT for 1 hour to overnight with gentle agitation. After staining, gels were immersed in destain solution (50% methanol, 10% acetic acid) for 1 hour to overnight.

2.2.3. Cdc8 extraction from *E. coli* and *S. pombe.*

E. coli pellets were resuspended in bacterial lysis buffer (0.2 M NaCl, 20 mM Tris pH 7.5, 5 mM EGTA, 1% PMSF) and lysed by sonication. Frozen *S. pombe* droplets were lysed in a SPEX SamplePrep 6770 Freezer Mill under liquid nitrogen. Lysates were heated at 85 ^{0}C for 10 minutes. Cell debris and denatured proteins were removed by centrifugation at 4500 rpm for 15 minutes at 4 ^{0}C. Soluble Cdc8 was isolated by isoelectric precipitation at pH 4.55. The solution was centrifuged at 4500 rpm for 15 minutes at 4 ^{0}C. The supernatant was discarded and crude Cdc8 pellets were frozen at -20 ^{0}C or resuspended for purification.

2.2.4. Cdc8 purification by fast protein liquid chromatography.

Crude Cdc8 pellets were resuspended in FPLC running buffer (5 mM Tris 100 mM NaCl pH 7) with 10 mM MgCl$_2$ and 10 mg/l DNase and RNase and incubated at 4 ^{0}C overnight with stirring. The Cdc8 was purified by FPLC using two 5 ml Pharmacia HiTrap-Q columns in tandem and eluted with a 100-900 mM NaCl gradient. Cdc8 was isolated from the protein containing fractions (determined monitoring absorbance at 260 nm and 280 nm), by isoelectric precipitation at pH 4.55 and centrifugation, then resuspended in FPLC running buffer for subsequent purification, typically three times in total. After the final elution Cdc8 was resuspended in 5 mM Tris pH 7 and stored at -80 ^{0}C. Concentration was determined by spectroscopy at 280 mn, using an extinction coefficient of 2980 M^{-1} cm^{-1} determined using the ExPASy proteomics server ProtParam tool, based on protein sequence.

2.2.5. Cosedimentation and quantitative electrophoresis

Cosedimentation assays were performed at 25 ^{0}C by mixing 10 µM actin with increasing concentrations of Cdc8 in cosedimentation buffer (20 mM MOPS, 100 mM KCl, 5 mM MgCl$_2$, pH 7.0) in a total volume of 100 µl. Reactions were incubated for 30 minutes. Actin along with any bound Tm was pelleted by centrifugation at 100 000 RPM for 20 minutes (Beckman Instruments TLA-100.1). Equal volumes of resuspended pellet and supernatant were separated by SDS-PAGE. Gels were scanned using an Epson perfection 1640SU scanner with a transparency adaptor attached to a PC and total band intensity analysis was performed using Scion Image software (Scion Corp). The K$_{50\%}$ values were determined after fitting the curves with the Hill equation (below), where h is the Hill coefficient, [Tm] is the free Tm concentration, K$_{50\%}$ is the Tm concentration required for 50% saturation of actin and θ is the fractional saturation of actin with Tm calculated from gel data.

$$\theta = \frac{[Tm]^h}{K_{50\%}^{\,h} + [Tm]^h}$$

2.2.6. Western blots

Cdc8 proteins were separated in a 12% SDS polyacrylamide gel at 140 V for 90 minutes and blotted onto a methanol activated PVDF membrane using a BioRad Trans-Blot® semi-dry electro blotter at 10 V for 30 minutes. After blotting membranes were blocked with 3% skimmed milk powder in PBS for 1 hour at room temperature with gentle agitation. Subsequently membranes were incubated at room temperature with this laboratory's anti-Cdc8 antibody (Skoumpla., et al. 2007) (1 in 1000 dilution) in PBS with 3% skimmed milk powder for 1 hour with gentle agitation, then washed 3 times in PBST (PBS+ 0.2 % tween[20]) for 10 minutes with gentle agitation. Membranes were then incubated at room temperature with a alkaline phosphatase conjugated anti-rabbit secondary antibody (Sigma-Aldrich) in PBS with 3% skimmed milk powder for 1 hour with gentle agitation. Membranes were subsequently washed 3 times in PBST for 10 minutes with gentle agitation followed by incubation with development buffer (0.1 M NaCl, 0.1 M Tris pH 9.6, 5 mM $MgCl_2$) for 1 minute. Excess buffer was discarded and 3 mls of BCIP®/NBT-Purple Liquid Substrate (Sigma) was added to membranes and incubated at room temperature with gentle agitation. The reaction was stopped by washing in deionised water.

2.2.7. Circular Dichroism

Circular dichroism studies of Cdc8 proteins were performed by Dr Steven Martin at the NIMR in Mill Hill using a Jasco 715 spectropolarimeter. Cdc8 proteins (section 2.2.3.) were diluted in CD buffer (10 mM Potassium phosphate , 500 mM NaCl, 5 mM $MgCl_2$ pH 7.0) to a concentration of 0.4 mg/ml. Thermal data were obtained automatically as ellipticity values at 222 nm at a scan speed of 1 deg/min. The sample was measured in a 1 mm cuvette.

CD data were analyzed by Dr Steven Martin as a simple two-state equilibrium between the folded dimer (F_2) and the unfolded monomer (U).

$$F_2 \overset{K}{\rightleftharpoons} 2U$$
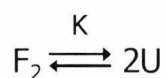
The unfolding constant is defined as $K = [U]^2/[F_2]$ and the total concentration of protein (P_0) is given by $P_0 = [U] + 2[F_2]$. The fraction of unfolded monomer present can be defined as $F_U = [U]/P_0$. Therefore:

$$F_U = \frac{-K + \sqrt{K^2 + 8KP_0}}{4P_0}$$

(1)

F_U at the mid-point of the unfolding transition (T_m) is equal to 0.5 by definition.

Therefore: $\quad K_{Tm} = P_0$ and $\Delta G_{Tm} = \Delta H_{Tm} - T_m \Delta S_{Tm} = -RT_m Ln(P_0)$.

If one assumes that $\Delta C_p \sim 0$ then for all temperatures one has $\Delta H_T = \Delta H_{Tm}$ and

$$\Delta S_T = \Delta H_{Tm}/T_m + RLn(P_0).$$

Therefore: $\quad K_T = P_0 \exp\left(\frac{\Delta H_{T_m}}{R}\left(\frac{1}{T_m} - \frac{1}{T}\right)\right)$

(2)

CD data collected as a function of temperature were analyzed using the following equation:

$$CD_T = (a+bT)(1-F_u) + (c+dT)F_u$$

Where a,c and b,d are the intercepts and slopes of the of the pre- (a,b) and post-transition (c,d) regions and F_u is obtained from equation (1) with K_T from equation (2).

2.2.8. Mass spectroscopy

Cdc8 (section 2.2.3) molecular weights were determined by electrospray mass spectroscopy by staff at the University of Kent in-house Biomolecular Science Facility using a Finnegan Mat LCQ ion-trap mass spectrometer.

2.2.9. Viscosity

Cdc8 samples (20 µM) were run in a Cannon-Manning semi-microviscometer at 20 ± 1 ^{0}C in a 1 ml of viscometry buffer (20 mM MOPS, 5 mM MgCl$_2$, pH 7.0) with the NaCl concentration increasing from 0 to 250 mM. Kinematic viscosity was calculated using the kinematic viscosity constant for the viscometer and the average efflux time, calculated from 5 observations per sample at each NaCl concentration.

2.2.10. Actin preparation

Purified rabbit F-actin kindly provided by Nancy Adamek was purified as described previously (Spudich and Watt, 1971). It was separated from endogenous Tm by incubating with 600 mM KCl at 25^{0}C for 5 hours with periodic gentle agitation. Actin was centrifuged at 100 000 rpm for 20 minutes at 20^{0}C. The pellet was resuspended in Actin buffer (100 mM KCl, 20 mM MOPS, 5 mM MgCl$_2$, 1 mM NaN$_3$, pH 7.0). The actin was dialysed in dialysis tubing against actin buffer at 4^{0}C, overnight with gentle stirring. Concentration was determined by spectroscopy at 280 nm, using an extinction coefficient of 46536 M^{-1} cm^{-1}

2.2.11. S1 preparation

Myosin S1 was kindly provided by Sam Lynn was prepared by chymotryptic digest, purified and processed as described previously (Margossian and Lowey, 1982; Weeds and Taylor, 1975) 150 µg of

freeze dried myosin S1 powder was resuspended in S1 buffer (30 mM KCl, 20 mM MOPS, 5 mM $MgCl_2$, 1 mM NaN_3, pH 7.0) The S1 was dialysed in dialysis tubing against S1 buffer at 4^0C, overnight with gentle stirring. S1 was centrifuged at 12 000 rpm for 5 minutes at 4^0C and the supernatant retained. Concentration was determined by spectroscopy at 280 nm using an extinction coefficient of E= 7.9 cm $^{-1}$ and a molecular weight of 115 kDa.

2.2.12. ATPase assay

Reactions were prepared in ATPase buffer (10 mM MOPS, 30mM NaCl, 5 mM $MgCl_2$ pH 7) containing 150 µM phosphoenolpyruvate (PEP), 150 µM NADH, 150 µM ATP, 10µl of pyruvate kinase/lactate dehydrogenase enzyme mix (Sigma-Aldrich) and varying concentrations of rabbit myosin II sub-fragment 1 (S1) were added to 1ml plastic cuvettes (Sarstedt) and allowed to equilibrate for 1 minute at 25^0C. Actin or actin saturated with Cdc8 proteins (30 minute pre-incubations of actin and Cdc8 were performed at 25^0C) was added to the reactions and mixed with a plastic stir-rod. Total reaction volume was 500 µl. Absorbance at 340 nm was monitored using a UV/Visible spectrophotometer (Varian Cary 50 Bio) connected to a PC and rates calculated from the slope of the curve.
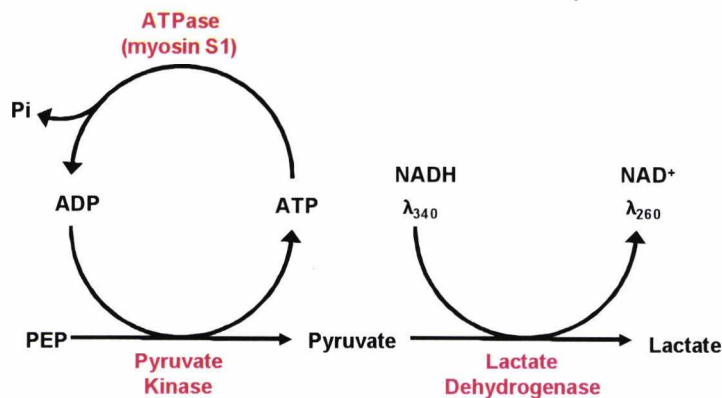
Figure 2.1. Coupled enzyme ATPase assay

PEP is converted to pyruvate by Pyruvate Kinase, converting ADP to ATP. ATP is hydrolysed by S1 yielding one molecule of ADP and one of inorganic phosphate (Pi). Pyruvate is reduced to lactate by lactate dehydrogenase which oxidises NADH to NAD^+. One molecule of released Pi corresponds to oxidation of one molecule of NADH.

2.3. Molecular biology techniques

2.3.1. Site directed mutagenesis

Site directed mutagenesis of the *cdc8⁺* gene was performed using Quikchange® reagents (Agilent Technologies). Following mutagenesis, plasmids were amplified and purified in *E. coli* and mutations confirmed by sequencing (Eurofins MWG operon) Reactions and thermal-cycler conditions were typically as follows:

Plasmid template:	1 μl
Primer mix (1 in 10 dilution):	1 μl
5xBuffer:	10 μl
dH$_2$O:	36.5 μl
Polymerase:	0.5 μl

STEP	TEMPERATURE	TIME	
Initial denaturation	94^{0}C	2 min	
Hot start	94^{0}C	-	
Denaturation	94^{0}C	30 sec	
Annealing	55^{0}C	1 min	30 cycles
Extension	68^{0}C	4 min	
Final extension	68^{0}C	5 min	
Hold	10^{0}C	∞	

2.3.2. *S. pombe* transformation

Mid-log *S. pombe* cells were washed in 0.1 M lithium acetate pH 4.9, and resuspended in lithium acetate at 2x10^8 cells/ml. Cells were incubated at the permissive temperature for 1 hour. 5 μl of DNA was added to 100 μl of 70% PEG 4000, 100 μl of cells were added to the PEG and mixed by vortexing. Cells were incubated at the permissive temperature for 1 hour

then heat shocked at 42 ^{0}C for 10 minutes. Cells were washed, resuspended in sterile dH$_2$O, then plated onto EMM agar with appropriate supplements.

2.3.3. *E. coli* transformation

100 µl aliquots of chemically competent *E. coli cells* (stored at -80^{0}C) prepared as described previously (Hanahan, 1983) were thawed on ice. Up to 5 µl of plasmid DNA was added to the cells, mixed gently and incubated on ice for 30 minutes. Cells were heat shocked at 42^{0}C for 90 seconds then placed on ice for 2 minutes. Cells were plated onto LB agar containing ampicillin and placed at 37 ^{0}C. Negative controls were performed using identical methods but lacking DNA.

2.3.4. *S. pombe* genomic DNA preparation

1.5 ml of mid-log phase *S. pombe cells* were pelleted in an eppendorf tube at 13 000 RPM for 2 minutes. Cells were resuspended in 1 ml of lysis buffer (50 mM Tris pH 7.5, 50 mM EDTA, 1% SDS), and transferred to a 2 ml screw-top mechanical lysis tube with 0.5ml of glass beads. Cells were lysed by two runs in a FastPrep$^®$ Instrument at full power for 30 seconds with 2 minutes on ice between runs. 300ul of phenol-chloroform solution (1:1 phenol:chloroform) was added to the lysate and mixed by vortex. Lysate was centrifuged at 13 000 rpm for 10 minutes at 4^{0}C, and the aqueous layer transferred to a clean microcentrifuge tube. An equal volume of chloroform was added and mixed by inversion. The tube was centrifuged at 13 000 rpm for 10 minutes at 4^{0}C and the upper aqueous layer transferred to a clean microcentrifuge. 3 volumes of ice cold ethanol and 1/10 volume of 3M sodium acetate was added to the tube, mixed by inversion and DNA precipitated at -20^{0}C overnight. Precipitated DNA was pelleted by centrifugation at 13 000 rpm for 10 minutes at 4^{0}C. The pellet was washed in 70% ethanol for 5 minutes and centrifuged at 13 000 rpm for 10 minutes at 4^{0}C. The supernatant was removed and the pellet

allowed to air dry. The pellet was resuspended in 50 µl of sterile distilled water with 1 µl of RNase and stored at -20^{0}C.

2.3.5. Plasmid DNA preparation

Plasmid DNA from *E. coli* was extracted using a 'QIAprep Spin Miniprep Kit' from (Qiagen) following the manufacturers instructions for the microcentrifuge protocol. Plasmid DNA was eluted in 50 µl of sterile elution buffer (10 mM Tris-Cl, pH 8.5) and stored at -20^{0}C.

2.3.6. Cloning of *cdc8* mutants cDNAs into an *S. pombe* expression vector

Mutants *cdc8* genes were excised from the *E. coil* expression vector (pJC20) using a sequential double digest with Sma1 (25^{0}C 1 hour) and Nde1 (37^{0}C 1 hour) restrictions enzymes (New England Biosciences) The destination vector was cut in the same manner. Typical reaction conditions were as follows:

Plasmid:	10 µl
10x buffer	10 µl
dH$_2$O:	76 µl
Sma1:	2 µl
Followed by:	
Nde1:	2 µl

DNA fragments were separated by electrophoresis on a 1% agarose gel and visualised by a low power UV transilluminator. Desired bands were cut from the gel using a razor blade and purified using a GeneClean® kit with the supplied protocol (Qbiogene). The purified DNAs were ligated into the destination vector (pREP41) with T4 DNA ligase (New England Biolabs) at 4^{0}C over night, using the following reaction:

Vector:	2 µl	
Insert:	6 µl	
10x buffer:	1 µl	
Ligase	1 µl	

Negative controls were performed using identical methods but lacking insert DNA. Following ligation, reactions were amplified and purified from *E. coli*. Inserts were confirmed by Sma1/Nde1 digests and subsequent electrophoreses on a 1% agarose gel.

Table 2.4. Plasmids used in this study

Lab stock number	Plasmid	Source
2	pREP41	Basi et al, 1993
80	pJC20cdc8	This Lab
99	pREP41cdc8	This Lab
141	pREP41n3SkTm	Arthur Coulton
312	pJC20cdc8-D2A	This Study
313	pJC20cdc8-D16A	This Study
316	pJC20cdc8-E6A	This Study
352	pJC20cdc8-LKL	This Study
370	pJC20cdc8-E6K	This Study
391	pREP41cdc8-E6K	This Study
409	pREP41cdc8-D16A	This Study
410	pREP41cdc8-E6A	This Study
411	pREP41cdc8-LKL	This Study
417	pREP41cdc8-D2A	This Study
447	pGEM -T-*cdc8-110*	This Study

2.3.7. Agarose gel electrophoresis

1% w/v of agarose was dissolved in TAE (40 mM Tris-acetate, 1mM EDTA) by heating in a microwave oven. The solution was allowed to cool slightly then ethidium bromide was added to a final concentration of 0.5 µg/ml. Gels were poured in casting trays of appropriate sizes and allowed to set. DNA loading buffer (0.25% bromophenol blue and 40% (w/v) sucrose in dH$_2$O) was diluted 1 in 5 in sample DNA and samples pipetted into the gel wells. Samples were run at 50 v for 30 to 60 minutes, and gels visualised using a UV transilluminator.

2.3.8. Amplification of the *cdc8-110* gene

The *S. pombe cdc8-110* gene was amplified by PCR using the Expand High Fidelity PCR system (Roche). Following amplification, mutations were identified by sequencing (Eurofins MWG operon) three independent clones. Reactions and thermal-cycler conditions were as follows:

Genomic DNA (1 in 10 dilution):	1 µl
Primers	1 µl
10xBuffer:	5 µl
dH$_2$O:	42.75 µl
Polymerase:	0.25 µl

STEP	TEMPERATURE	TIME	
Initial denaturation	92^{0}C	1 min	
Hot start	92^{0}C	-	
Denaturation	92^{0}C	30 sec	
Annealing	40^{0}C	30 sec	35 cycles
Extension	72^{0}C	5 min	
Final extension	72^{0}C	10 min	
Hold	10^{0}C	∞	

Table 2.5. Oligonucleotide primers used in this study

Lab Stock Number	Name	Sequence	Conc
117	cdc8downstreamR	5′ TTC ATC TAT GTT CGT CAA GC 3′	0.1 µg/µl
131	cdc8100bpUS	5′ AAT AGA ACT TTC TTG TAC CG 3′	0.1 µg/µl
197	cdc8D2AJC20F	5′ GAG ATA TAC ATA TGG CCA AGC TTA GAG AG 3′	1.0 µg/µl
198	cdc8D2AJC20R	5′ CTC TCT AAG CTT GGC CAT ATG TAT ATC TC 3′	1.0 µg/µl
199	cdc8E6AF	5′ GGA TAA GCT TAG AGC GAA AAT TAA TGC CG 3′	1.0 µg/µl
200	cdc8E6AR	5′ CGG CAT TAA TTT TCG CTC TAA GCT TAT CC 3′	1.0 µg/µl
201	cdc8D16AF	5′ CGT GCT GAG ACT GCA GAG GCT GTC GC 3′	1.0 µg/µl
202	cdc8D16AR	5′ GCG ACA GCC TCT GCA GTC TCA GCA CG 3′	1.0 µg/µl
232	cdc8LKLF	5′ GAG AAA ATT ATT GCC TTA AAA CTC GAG ACT GAT GAG GC 3′	1.0 µg/µl
233	cdc8LKLR	5′ GCC TCA TCA GTC TCG AGT TTT AAG GCA TTA ATT TTC TC 3′	1.0 µg/µl
258	cdc8E6KF	5′ GGA TAA GCT TAG AAA GAA AAT TAA TGC C 3′	1.0 µg/µl
259	cdc8E6KR	5′ GGC AAT AAT TTT CTT TCT AAG CTT ATC C 3′	1.0 µg/µl

2.4. Microscopy

2.4.1. Light microscopy sample visualisation

Samples were visualised using an Olympus IX71 microscope with PlanApo 100xOTIRFM-SP 1.45 NA lens mounted on a PIFOC z-axis focus drive (Physik Instrumente, Karlsruhe, Germany), and illuminated using an automated 300 W Xenon light source (Sutter, Novato, CA) with ET-sedat filters (Chroma, Bellows Falls, VT). Samples were visualised via a QuantEM CCD camera (Photometrics) and the system was controlled with Metamorph software (Molecular Devices). Digital deconvolution was performed using MediaCybernetics 'Autoquant X' software.

2.4.2. Cdc8 Immunofluorescence in *S. pombe* cells

Mid-log *S. pombe* cells were fixed by the addition of formaldehyde solution (30 % paraformaldehyde in PEM; 0.1 M PIPES, 1 mM $MgCl_2$, 1 mM $MgSO_4$, pH 6.9). Formaldehyde was added to cells while shaking on an orbital shaker, 1.25 ml per 10 ml cells and incubated at RT for 30 minutes with constant agitation . Cells were harvested by centrifugation at 3000 rpm for 2 minutes and washed 3 times in PEM. Cells were resuspended in 1 ml PEMS (PEM + 1 M sorbitol) with 1.2 mg of zymolase and incubated at 37 $^{\circ}$C for 30 minutes. Cells were then resuspended in PEMS + 1% Triton for 30 sec, then washed 3 times in PEM. Cells were resuspended in PEMBAL (PEM + 1% BSA, 0.1% NaN_3, 100 mM lysine hydrochloride, pH 6.9) and placed on a rotating wheel at RT for 30 minutes. Cells were resuspended in 100 µl PEMBAL with 1 µl of anti-Cdc8 serum and incubated at RT overnight. Cells were washed 3 times in PEM, resuspended in 100 µl PEMBAL with 1 µl anti-rabbit FITC secondary antibody (Sigma-Aldrich) and incubated on a rotating wheel in the dark at RT overnight. Cells were washed once in PEM, once in PBS and resuspended in PBS. 10 µl was dried onto a coverslip and mounted in glycerol on a glass slide and visualised as described in section 2.4.1.

2.4.3. Rhodamine-phalloidin staining of cdc8-110 S. pombe cells

10 ml cultures of S. pombe cells were grown to mid-log phase overnight, in supplemented EMM lacking leucine, in 50 ml flasks at 25^0C with shaking at 200 rpm. Cells were shifted to the non-permissive temperature of 36^0C for 4 hours, with shaking at 200 rpm. Formaldehyde solution was freshly prepared by adding 3.2 g paraformaldehyde to PM buffer (35 mM KPO_4, 1 mM $MgSO_4$,) and heating to 65ºC degrees for 5 minutes. Drops of 10 M NaOH were added until the solution became almost clear. The formaldehyde solution was centrifuged at 2000 rpm for 5 minutes. 1.5 ml of PM buffer and 3 ml of formaldehyde solution were added to 10 ml of mid log cells shaking at 36^0C, and incubated for 30 minutes. Cells were then centrifuged at 2000 rpm for 3 minutes. Cell pellets were resuspended in 1 ml of PM buffer and transferred to a 1.5 ml microcentrifuge tube. Cells were washed 3 times in 1 ml of PM, once in PM+T (PM, 10% + triton-X100) and a further 3 times in PM. Cells were resuspended in 100 µl of PM with 0.1 µM Rhodamine-Phalloidin (Sigma-Aldrich) and incubated in the dark for 30 minutes with end-over-end agitation. Cells were mounted on a coverslip with equal volumes of soya bean lectin and visualised as described in section 2.4.1.

2.4.4. Electron microscopy of actin filaments

Electron microscopy of Cdc8 decorated actin filaments was performed by Dr Agnieszka Galińska-Rakoczy at The Univeriasty of Massachussets Medical School in Worcester, MA. Endogenous Cdc8 purified from S. pombe and recombinant Cdc8 purified from E.coli (section 2.2.3) (120 uM) was mixed with F-actin (24 uM), to allow Cdc8-actin filament formation, in buffer containing 20 mM MOPS, pH 7.0, 30 mM KCl and 5 mM MgCl2. The actin-Cdc8 filaments were diluted 20-fold in the same buffer immediately prior to applying to carbon-coated electron microscopy grids. Samples were negatively stained, electron microscopy images captured at 45,000x under low-dose conditions ($\sim$12e$^-$/Å)

2.4.5. EM rotary shadowing and persistence length calculation

Rotary shadowing and persistence length calculations were performed by Dr. Duncan Sousa at the University of Boston, MA. Cdc8 samples (section 2.2.3) were diluted to 1.0 µM in a solution consisting of 5 mM Tris (pH 7.0), 5 mM KCl, 5 mM $MgCl_2$ and including 30 % glycerol were sprayed onto freshly cleaved mica. Platinum evaporation and rotary shadowing was carried out as in Sousa et al., 2010. Electron microscopy was carried out on the shadowed molecules using a Philips CM120 electron microscope (FEI, Hillsboro, OR) at 120 kV and images digitized at 28,000 times magnification with a 2Kx2K F224HD slow scan CCD camera (TVIPS, Gauting, Germany). The recorded images of tropomyosin were then skeletonized following manual selection of 0.5 x 0.5 nm points every 4 to 5 nm along the center of the protein's longitudinal axis (Li et al., 2010b; Li et al., 2010c). The persistence length, ξ, was calculated, using the tangent angle correlation method, after determining θ (the deviation angles along tropomyosin molecules and polymers from an idealized straight rod) for segment lengths between 50 and 400 nm. Algorithms specifically tailored to determine ξ and θ were developed previously (Li et al., 2010b; Li et al., 2010c). Plots relating the inverse slope of <ln(cos θ)> to the segment length yields the persistence length values, where the factor of two in $\langle \cos(\theta(s)) \rangle = e^{-s/2\xi}$ accounts for the two dimensionality of the images (Li et al., 2010b; Li et al., 2010c).

2.5. QD-IgG conjugate development methods

2.5.1: Affinity purification of anti-Cdc8 antibodies from serum.

Anti-Cdc8 antibodies were created by immunising an SPF rabbit with purified full-length recombinant Cdc8 protein with Titre Max Gold adjuvant. Serum was collected at 1-month intervals 1 week after each boost (Skoumpla, et al. 2007). Unwanted serum proteins were removed

by affinity purification using a kit from Pierce (Pierce # 44894), following the manufacturers protocol. Concentration of antibody collected was determined by UV absorbance at 280nm using an extinction coefficient of 210 000 $M^{-1} cm^{-1}$.

Fractions observed to have OD_{280} of greater than 0.02 (fractions 3-5, Figure 2.2.A.) were assayed by denaturing 12.5% SDS-PAGE (see section 2.2.1.).and after staining with coomassie blue two bands were observed, one of approximately 55 kDa corresponding to IgG heavy chains and one of approximately 25 kDa equivalent to IgG light chains (figure 2.2.B.). This observation confirmed that the antibody was contained in these fractions and the fractions were pooled. The purified antibody was then assayed for function and specificity. Firstly a western blot (see section 2.2.6) was performed in which recombinant Cdc8 and Cdc8 mutant proteins were immobilised to a membrane. The result can be seen in figure 2.2.C, where a single band of the expected size for Cdc8 was observed. Secondly the antibodies were used in an immunofluorescence experiment (see section 2.4.2) with WT *S. pombe* cells, and FITC labelled secondary antibody (Figure. 2.2.D.). Cdc8 was seen localised at the CAR. These two results in conjunction indicate that the purified antibody was both functional and specific.

2.5.2. Quantum dot-antibody conjugation reaction

Carboxyl modified quantum dots (QDs) (Evident technologies 'lake placid blue' Evitag® or eBioscience's eflour™ nanocrystals) were activated by mixing 1-ethyl-3-(3-dimethylaminopropyl) carbodiimide (EDC) to QDs at molar ratios of 40 000:1, 5000:1, 1000:1, 500:1, 250:1 or 8:1 EDC:QD and incubating for 5 minutes at room temperature. Subsequently affinity purified antibody (section 2.5.1.) was added to the reaction mixture at ratios of 10:2, 10:1, 10:0.5, 10:0.1, 1:2, 1:1 or 1:0.5 QD to IgG, 10 µl of 10X Phosphate buffered saline (PBS) (Sigma) and deionised water to a final volume of 100µl. The reaction incubated at room temperature for 1.5 hours on a rotating wheel, in the dark.

A

B

57.5 KDa –

24.8 KDa –

C   L   WT D2A E6A D16A   **D**

24.8 KDa–
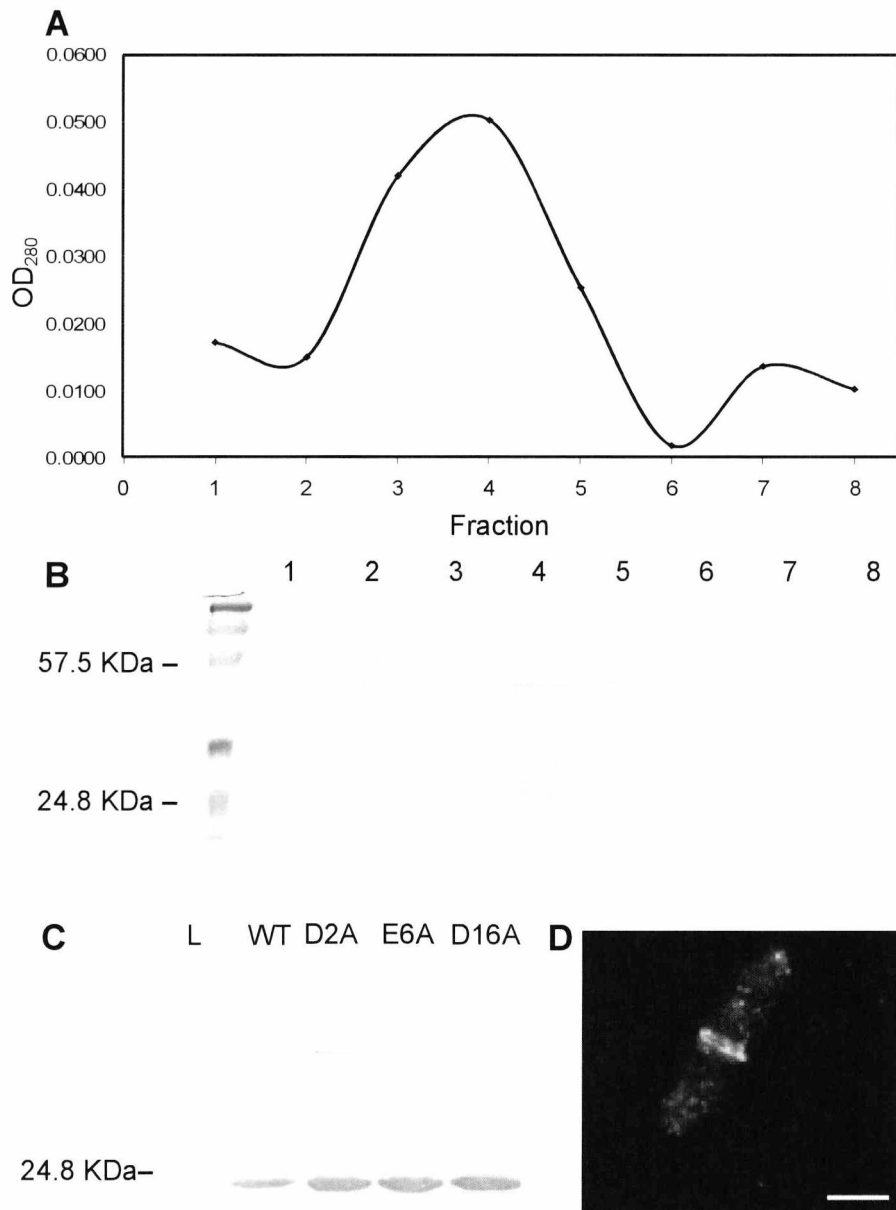
Figure 2.2. Affinity purification of anti-Cdc8 with western blot and immunofluorescence using purified antibody.

(A). Absorbance at 280nm of 1ml fraction of an anti-Cdc8 antibody affinity purification is shown, (B) SDS-PAGE of fractions 1-8 (from A) after affinity purification with molecular weight marker (L). (C) Pooled antibody containing fractions used to probe a western blot of wild type Cdc8 (WT) and 3 Cdc8 mutants (D2A, E6A & D16A). (D) An Immunofluorescence image of *S. pombe* cells using purified antibody. Scale bar = 5 µm.

2.5.3. Separation of conjugates using Evitags protocol.

Once conjugate had been produced it was necessary to purify it from non-reacted reaction components and the Evitags® protocol recommended size exclusion chromatography as for this purpose. The first attempt at conjugate utilised whole serum from rabbits used to produce Cdc8 anti bodies. Subsequent to conjugation the reaction was separated using the Evitags size exclusion protocol. Conjugation reaction was layered onto the column, eluted with PBS and collected as 100 µl fractions which were stored at 4^0C or analysed immediately. Eluted fractions were assayed for absorbance at 280 nm, and fluorescence at 495 nm (See materials and methods 2.6 and 2.7) and both values plotted as graphs.

The manufacturer's literature described that an overlapping peak for OD_{280} and fluorescence would indicate which fractions contained the conjugate, and that a second OD_{280} peak would correspond to un-reacted biomolecules. In the preliminary experiment multiple peaks at 280 nm were observed (Figure 2.3 top), presumably as a consequence of the fact that whole serum proteins were present, not just Cdc8 antibody. No peaks at 495 nm were observed (Figure 2.3 bottom), and despite subsequent elutions of the conjugate from the column with PBS, low pH (PBS pH 2.3) and high salt (1M NaCl) buffers, no fluorescence was ever detected in any fraction eluted.

In a separate experiment to check if it was possible to elute QDs from the column, an undiluted sample of the QDs (10 µl) was applied to the column and eluted with 5 ml of PBS and collected in 100 µl fractions. No fluorescence signal was observed in any of the fractions, suggesting that the QDs and consequently any QD-IgG conjugates may have 'stuck' to the column matrix. These observations suggested that size exclusion chromatography was unsuitable, for separation of my QD-IgG conjugate and an alternative approach supplied by Dr. P. Bachmann (Medical Systems Division, Royal Dutch Philips, Aachen, Germany) was used in all subsequent experiments. This method used centrifugal concentrator
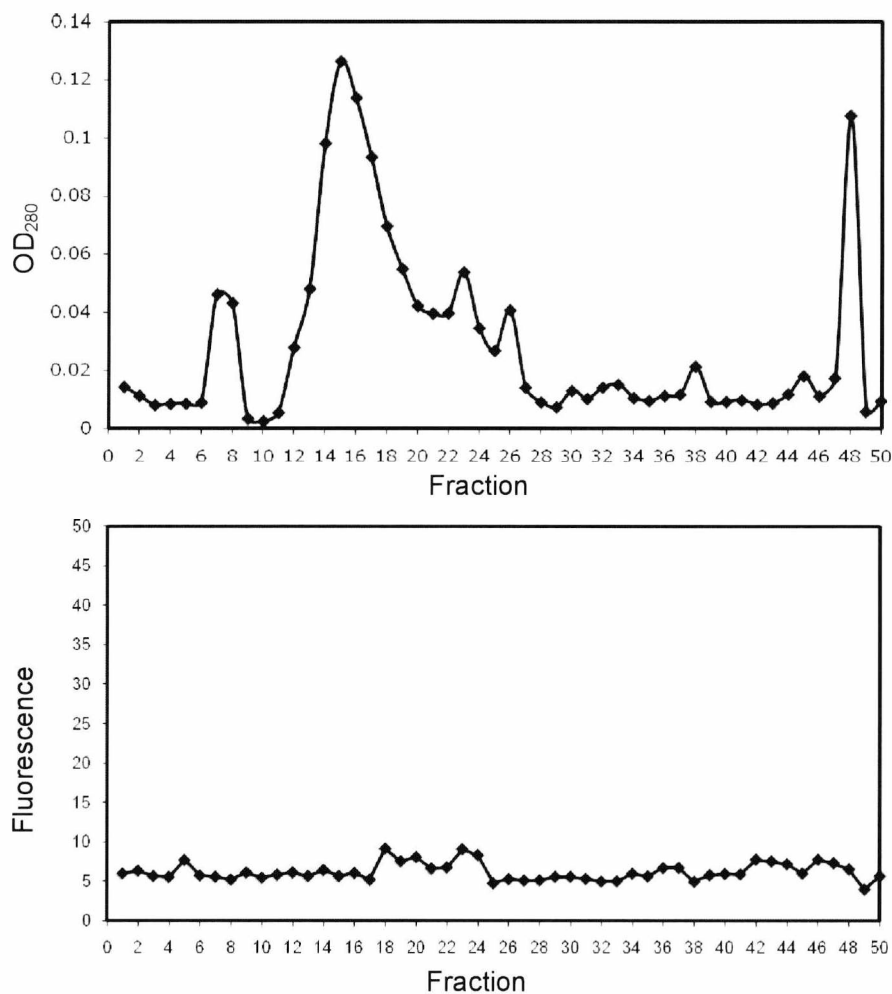
Figure 2.3. OD$_{280}$ and EM$_{\lambda495}$ of fractions collected during size exclusion chromatography of a QD-IgG conjugate.

OD$_{280}$ (top panel) and fluorescence at 495nm (bottom panel) for fractions of QD-IgG conjugate separated by size exclusion chromatography.

cartridges with a molecular weight cut-off of 100 kDa to separate conjugates from non-reacted components, and proved successful in separating the conjugate from un-reacted reaction components and was adopted henceforth in this study (see section 2.5.5.).

2.5.4. QD-IgG size exclusion columns

Superdex 200 resin was used in the preparation of columns for use in size exclusion separation of QD-IgG conjugates in the following manner. A sterile 5 ml plastic syringe was packed with sterile glass wool followed by 5 ml of superdex 200 resin and the column washed with 10 ml of sterile distilled water.

2.5.5. Ultrafiltration

Vivaspin500 filter units (Sartorius) were pre-rinsed 3 times with 200 µl 0.1mM KOH, and centrifuged at 6000g, for 5 to 10 minutes to remove glycerine and sodium azide. The cartridges were then washed 3 times with 200 µl deionised water, at 6000 g, for 5 to 10minutes. QD reaction mixture was then layered into the filter unit, and centrifuged at 6000 g, for 5 to 10 minutes, yielding a retentate of approximately 25 µl. The retentate was washed 3 times with 200 µl PBS at 6000 g, for 5 to 10 minutes and finally approximately 25 µl of separated reaction mixture was recovered and diluted in PBS to a volume of 100 µl.

2.5.6. Assaying OD280nm

100 µl conjugate/fractions were assayed for antibody content at OD_{280nm} using a UV/Visible spectrophotometer (Varian Carey 50 Bio) in micro-volume cuvettes (BrandTech #7592 00) and using the extinction coefficient 210 000 M^{-1} cm^{-1}.

2.5.7. Assaying fluorescence

Fractions were assayed for fluorescence in white 384 well plates (Corning Costar) using a fluorescence spectrophotometer (Varian Carey Eclipse), at 600v with excitation at 468nm and emission at 495nm.

2.5.8. Western blot detection

Cdc8 protein (section 3.2) was electrophoresed in a 12% polyacrylamide SDS gel at 140 v for 90 minutes and blotted onto a methanol activated PVDF membrane using a BioRad Trans-Blot® semi-dry electro blotter at 10 v for 30 minutes. After blotting membranes were blocked with 3% skimmed milk powder in PBS for 1 hour at room temperature with gentle agitation.

Subsequently membranes were incubated at room temperature with either anti-cdc8 antibody (1 in 1000 dilution) or QD-IgG conjugates (total conjugate) in PBS with 3% skimmed milk powder for 1 hour with gentle agitation, washed 3 times in PBST for 10 minutes with gentle agitation and imaged in a FLA-5000 phosphoimager (Fujifilm). Membranes were then incubated with anti-rabbit FITC conjugated secondary antibody (1 in 10 000 dilution) (Sigma) for 1 hour with gentle agitation, washed 3 times in PBST for 10 minutes with gentle agitation and re-imaged using the phosphoimager.

2.5.9. Plate binding assay

100 µl of 1 µg/ml fission yeast Tm (Cdc8) in PBS was added to the wells of a 96 well amino-modified microtitre plate (Nunc Immobilizer™ Amino plate). The plate was sealed and incubated in the dark for 2 hours with gentle agitation on a rocker. Unbound protein was removed and the wells washed 5 times with 200µl of PBS + 0.05% (v/v) Tween20 (PBST). 100µl of QD-IgG conjugate was added to wells and incubated in the dark for 1 hour with gentle agitation. The conjugate was removed and the wells

which were then washed 5 times with 200 µl of PBST. Finally 100 µl of PBS was added to the wells and fluorescence measured using a fluorescence spectrophotometer (Varian Carey Eclipse), at 800v by excitation at 468 nm and for emission at 495 nm.

2.5.10. Standardisation of Cdc8 binding to magnetic nano-beads

10 mg of beads (Dynabeads M-270 Carboxylic Acid – Dynal Biotech) were washed twice in 10 mM NaOH for 2 minutes with end-over-end mixing. The beads were washed in dH_2O three times for 10 minutes with end-over-end mixing. The beads were incubated with 500 µl of 100 mM EDC for 30 minutes with end-over-end mixing. The beads were subsequently washed once with dH_2O and once with 50 mM MES (pH 5.5) for 10 seconds. The beads were divided into 10 microcentrifuge tubes (eppendorf) and incubated with increasing concentrations of Cdc8 (1 µg to 50 µg) for 2 hours with end-over-end mixing. Finally the supernatants were removed, assayed for protein content by spectroscopy (see section 2.5.6.) and compared to starting concentration. 20 µg of Cdc8 was sufficient to saturate 1 mg of the beads.

2.5.11. Membrane spotting assay

A standard curve of antibody concentration was included in each experiment in triplicate: Standards of affinity purified cdc8 antibody were prepared at amounts of 1.23×10^{-2}, 6.15×10^{-3}, 2.46×10^{-3} 1.23×10^{-3} and 6.15×10^{-4} nanomoles.

Conjugates were produced and separated as described above in sections 2.5.2. and 2.5.6. Firstly 100 µl of standards, retentates and flow-through were applied directly to a methanol activated PVDF membrane and dried at 37^0C. Membranes were incubated at room temperature with anti-rabbit alkaline phosphotase secondary antibody (1 in 10 000 dilution) (Sigma) in PBS with 3% skimmed milk powder for 1 hour with gentle agitation then

washed 3 times in PBST for 10 minutes with gentle agitation. Membranes were then incubated with development buffer (0.1 M NaCl, 0.1 M Tris pH 9.6, 5 Mm $MgCl_2$) for 1 minute, excess buffer was discarded. 3 mls of BCIP®/NBT-Purple Liquid Substrate (Sigma) was added to membranes and incubated at room temperature for 10 minutes with gentle agitation. The reaction was stopped by washing in deionised water and membranes were dried and scanned using a Epson perfection 1640SU scanner, then analysed using ImageJ software.

Chapter 3: The design and characterisation of fission yeast tropomyosin mutants.

Introduction

Tropomyosin is a dimeric α-helical coiled-coil protein which polymerises end-to-end along the two grooves of F-actin filaments. Tm modulates actin filament function and provides structural stability. In muscle cells Tm plays crucial roles in regulation of muscle contraction while in non muscle cells it is important role for regulation of actin cytoskeleton dynamics.

Tm dimers polymerise in an end-to-end fashion (Greenfield et al., 2006) and the amino and carboxyl termini of the protein are essential for end to end binding (Cho et al., 1990; Johnson and Smillie, 1977). Additionally, modifications to the amino acid sequence the protein, can alter the stability of the molecule (Kremneva et al., 2006) and its ability to form end-to-end interactions (Hitchcock-DeGregori and Heald, 1987)

S. pombe has only one Tm coded by the cdc8+ gene (Balasubramanian et al., 1992). Because of this, fission yeast provides an excellent system in which to study the influence of structure on the physical properties and function of this protein. A series of mutations at the amino terminus of Cdc8 were created to explore the importance of this region on the physical properties of the protein.

3.1. Creation and expression of WT and mutant Cdc8 proteins.

The first stage of this part of the project was to generate amino terminal mutants of cdc8+. The amino acid sequence for the first 20 residues of Cdc8 were compared (figure 3.1.) with Tms from the budding yeast, S. cerevisiae (Tpm1 and Tpm2) and Tms from G. gallus (chicken) and R. norvegicus (rat) (α- and β-smooth muscle and α- and β-skeletal muscle).

As negatively charged amino acid residues are important for interaction between proteins, conserved acidic residues were chosen, that did not fall in the 'a' or 'd' position of the predicted heptad repeat (see figure 1.16), or the 'e' and 'g' positions, which provide stability through ionic interaction.


```
abcdefgabcdefgabcdef

MDKLREKINAARAETDEAVA    Cdc8    S. pombe
MDKIREKLSNLKLEAESWQE    Tpm1    S. cerevisiae
MEKIKEKLNSLKLESESWQE    Tpm2    S. cerevisiae
MDAIKKKMQMLKLDKENALD    α-sm    G. gallus
MEAIKKKMQMLKLDKENAID    β-sm    G. gallus
MDAIKKKMQMLKLDKENALD    α-sk    R. norvegicus
MDAIKKKMQMLKLDKENAID    β-sk    R. norvegicus
```

Figure 3.1. Sequence alignment of tropomyosin amino termini.

The first 20 amino acid residues of the amino terminus of tropomyosin from fission yeast, budding yeast, chicken smooth muscle and rat skeletal muscle. Highlighted in yellow are the residues chosen for mutation in this study, residues with conserved properties are highlighted in grey. Lower case letters a-g indicate residue position in the heptad repeat.

It was decided to make a number of mutations, firstly three alanine substitutions. Aspartic acid 2 and glutamic acid 6 which are thought to be important in end to end binding of Tm (Greenfield et al., 2006), as well as aspartic acid 16 which falls outside the Tm overlap region and is less likely to have a dramatic effect. The methyl group of alanine is non-reactive and is consequently less likely to be involved in protein function. Therefore mutating these residues to alanine was a way to test the effect of removing the negative charge. Glutamic acid 6 was also mutated to lysine, a change from a negative to a positive charge, as this is the conserved residue at this position in metazoan muscle Tms.

It was also noted from the sequence alignment that Cdc8 residues 11, 12 and 13 have an alanine-arginine-alanine (ARA) motif, whereas all other Tms have a leucine-lysine-leucine (LKL) motif. To explore this difference Cdc8 'ARA' motif was substituted with 'LKL'. A summary of each mutation is presented in table 3.1.

Table 3.1. A summary of amino acid substitutions at the amino termini of Cdc8.

The left column details each amino acid residue selected for mutation and the subsequent substitution. The right column displays the abbreviated name for each mutation. Mutants are referred to by these abbreviations for the remainder of this study.

Amino acid substitution	Allele name
Aspartic acid 2 to Alanine	*cdc8-D2A*
Glutamic acid 6 to Alanine	*cdc8-E6A*
Glutamic acid 6 to Lysine	*cdc8-E6K*
Aspartic acid 16 to Alanine	*cdc8-D16A*
Alanine 11 to Leucine Arginine 12 to Lysine Alanine 13 to Leucine	*cdc8-LKL*

Mutations were introduced into the cDNA coding for Cdc8, by site directed mutagenesis of the $cdc8^+$ gene on a bacterial expression plasmid. Plasmids were introduced into *E. coli* strain DH5α, and plasmid DNA was extracted from successful transformants and sequenced to ensure that mutations had been correctly introduced. Plasmids were introduced into, *E. coli* strain BL21 and Cdc8 protein was subsequently expressed (see materials and methods section 2.1.4.). 1 ml samples of *E. coli*, pre- and post- induction with IPTG, were taken and separated by SDS-PAGE. An example is presented in figure 3.2.A. A large band at 23 kDa (predicted migration for Cdc8) in the post induction samples indicates a substantial level of protein expression.

3.2. Purification of WT and mutant Cdc8 proteins.

Wild type and mutant Cdc8 proteins were purified by isoelectric precipitation and fast protein liquid chromatography (FPLC) (see materials and methods section 2.2.4.). Up to three consecutive runs through the FPLC column were required to eliminate contaminants, especially nucleic acid, from the sample. Figure 3.2.B shows an example of traces from three rounds of purification of the Cdc8-D2A protein. On the first two charts, the red trace, (corresponding to OD_{260}) is above the blue (representing OD_{280}), indicating the presence of nucleic acid contamination. By the third run however, the OD_{280} trace is above the OD_{260} indicating a nucleotide free, purified protein.

Bacterial expressed Cdc8 is not acetylated at the amino terminus, as *E. coli* lacks the cellular 'machinery' to do so. To facilitate a more comprehensive comparison of these proteins, endogenous acetylated Cdc8 (Cdc8[ACE]) was isolated from *S. pombe* cells (see materials and methods section 2.1.3.) and purified using a similar method, previously developed in this lab (Skoumpla et al., 2007)
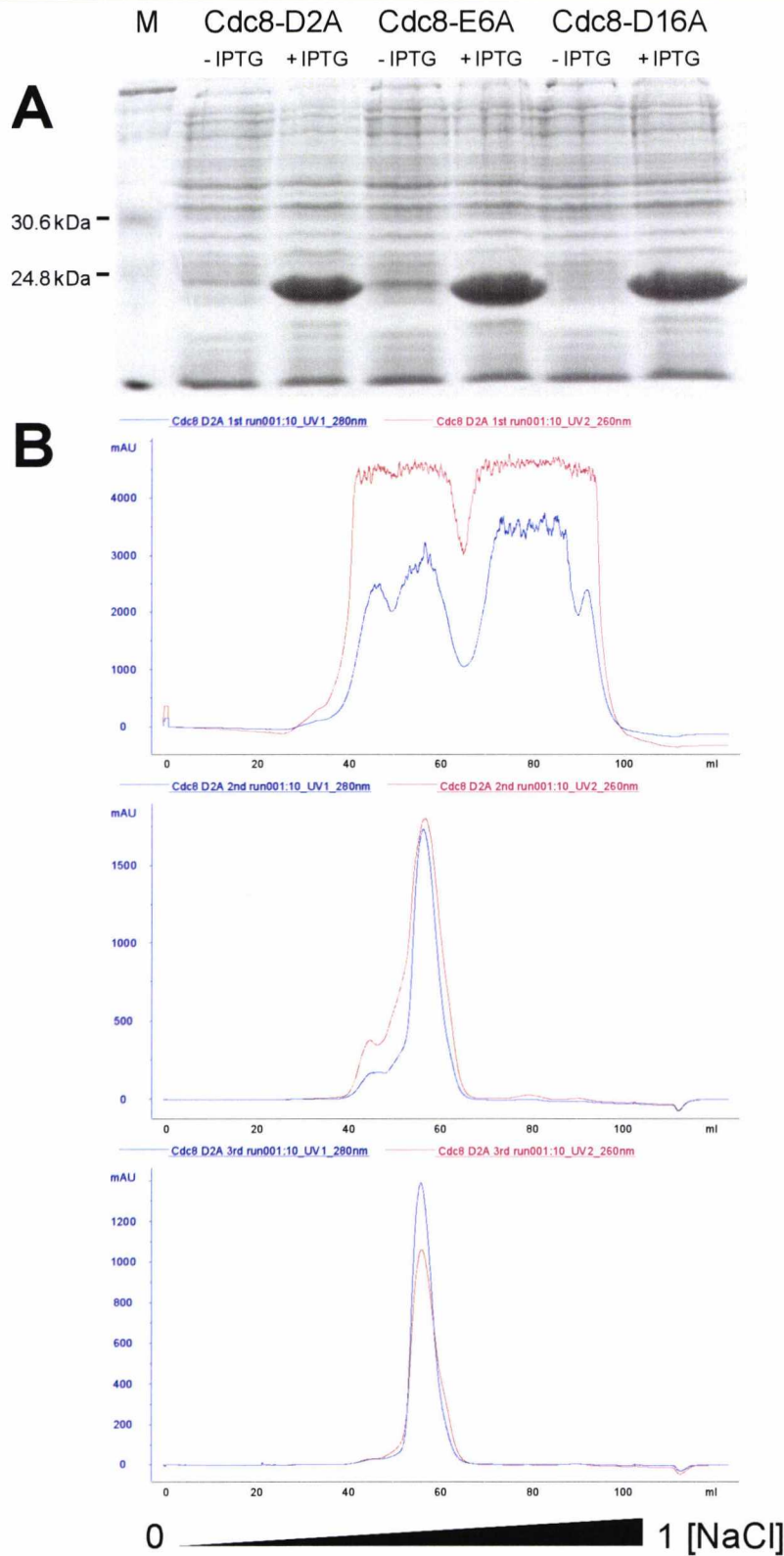
Figure 3.2. Expression and purification of recombinant Cdc8 protein from _E. coli._

(A) An SDS-PAGE gel showing, from left to right, molecular weight marker (M) then pre- and post induction samples of _E. coli_ expressing Cdc8-D2A, E6A and D16A respectively. (B) FLPC traces from top to bottom of three successive FPLC purifications of Cdc8-D2A eluted using a HiTrap Q FF column and gradient of 0 to 0.9 M NaCl. The red trace corresponds to OD_{260}, the blue to OD_{280}.

After purification the concentration of each Tm was determined using a spectrophotometric techniques (see materials and methods section 2.2.4.). The purity of each protein was assayed by two methods. Firstly a sample of each was subjected to SDS-PAGE analysis (figure 3.3.A). Each protein migrated at the predicted size for Cdc8, (~23 kDa). The reduced mobility of Cdc8 (predicted mass 19 kDa) is likely to be a consequence of its coiled-coil nature (Skoumpla et al., 2007). No contaminating protein bands were observed in any of the samples and the equivalent intensity of the cdc8 bands gave confidence that the concentration had been accurately and reproducibly determined. In addition the gel was incubated with ethidium bromide and imaged using UV to check for bands of contaminating nucleic acid; none were observed.

Secondly a sample of each Tm was assayed by mass spectrometry (see materials and methods). An example of the mass spectroscopy data is presented in figure 3.3.B. No products of cleavage or degradation were observed for any of the Tms and the single peak obtained for each matched the predicted mass calculated using the online ExPASy protomics server 'ProtParam' tool, based on amino acid sequence.

Table 3.2. A summary of molecular weight of WT and mutant Cdc8 determined by mass spectrometry.

Tropomyosin	Source	Predicted mass (Da)	Mass (Da)
Cdc8-uACE	*E. coli*	18964.0	18963.8
Cdc8-ACE	*S.pombe*	19007.0	19005.5
Cdc8-D2A	*E. coli*	18788.8	18788.1
Cdc8-E6A	*E. coli*	18905.9	18905.4
Cdc8-E6K	*E. coli*	18963.0	18962.6
Cdc8-D16A	*E. coli*	18920.0	18919.3
Cdc8-LKL	*E. coli*	19020.1	19019.6
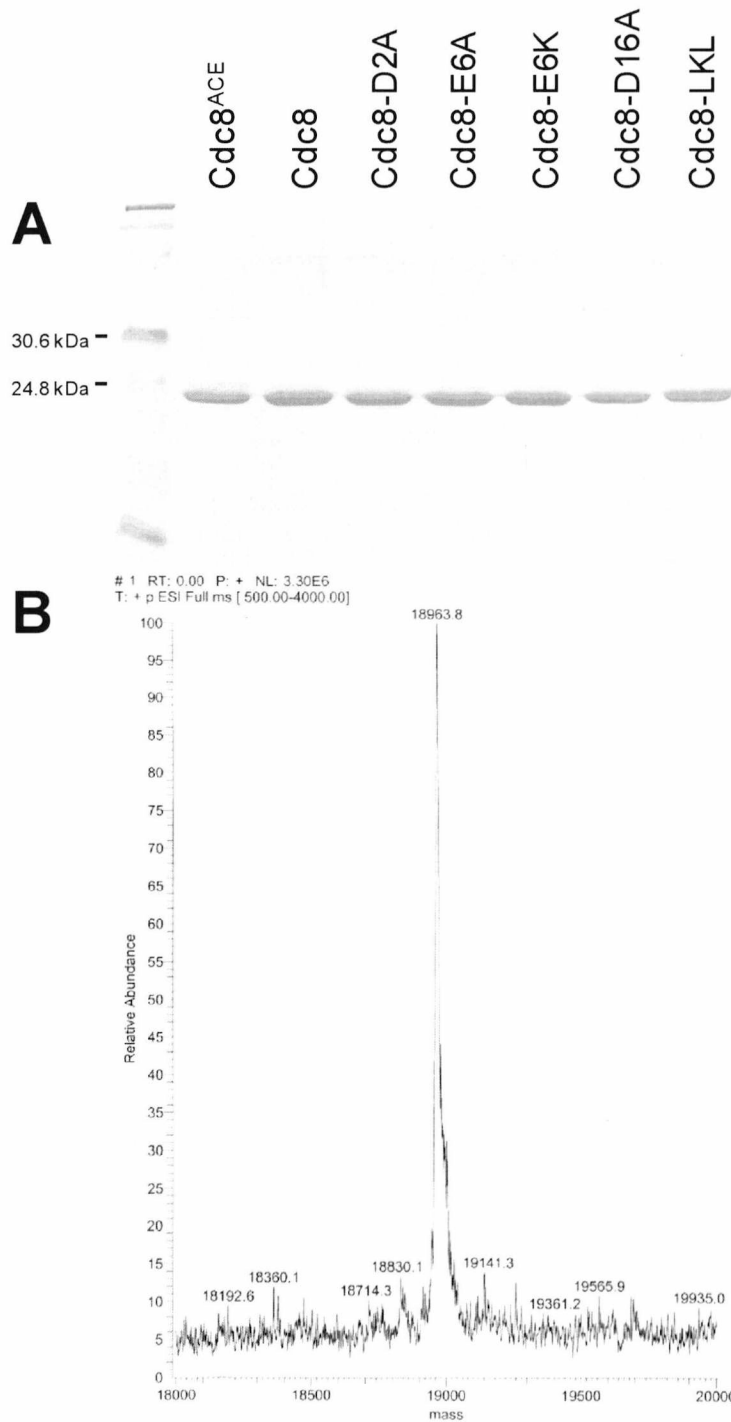
Figure 3.3. Purity and integrity of WT and Cdc8 mutants

(A) A coomassie stained SDS-PAGE gel showing WT and mutant Cdc8 proteins. (B) A mass spectrometer trace showing a single peak for recombinant wild type Cdc8.

The extra mass associated with Cdc8 purified from *S. pombe* corresponds to an acetyl group added post-translationally in fission yeast. Tms with mutations at amino acid residue 2 are typically subject to proteolytic cleavage of the first methionine (Monteiro et al., 1994), when expressed in *E. coli*. Consistent with this, mass spectroscopy analysis revealed the first methionine had been cleaved from the Cdc8-D2A protein. A summary of mass for each protein can be found in table 3.2.

3.3. Amino termini mutations alter the thermostability of Cdc8.

To address the affect of amino acid substitution and acetylation on the thermal stability of Cdc8, thermal unfolding experiments using circular dichroism (CD) were performed (see materials and methods section 2.2.7). The CD spectra for all-α (containing only α-helices), $\alpha+\beta$ (composed of α-helices and β-strands that occur separately along the backbone) and α/β (composed of alternating α-helices and β-strands along the backbone) proteins are characterised by a distinct negative band with minima at 208 nm and 222nm, and a strong positive band between 191 nm and 193nm (Martin and Schilstra, 2008). Cdc8 is an all-α protein, therefore spectra consistent with this were expected. Figure 3.4.A shows an example CD spectrum for unacetylated Cdc8 and the characteristic minima at 208 nm and 222 nm are evident. Spectra were equivalent for all Cdc8 proteins (data not shown)

Figure 3.4.B shows raw data curves of absorbance at 222 nm, at temperatures between 20 ^{0}C and 50 ^{0}C, of three Cdc8 proteins highlighting the most dramatic effects. All had single phase curves which indicated that at this resolution the Cdc8 dimer appeared to dissociate at the same time as the protein denatured. Figure 3.4.C shows examples of first derivative plots for these data, with the peaks correspond to the midpoint melting temperature (T_m), the area under the curves giving a measure of the enthalpy of protein unfolding (see materials and methods section 2.2.7).

The T_m for unacetylated Cdc8 is 34.7 ^{0}C. Acetylation slightly increased the T_m of Cdc8 to 35.4 ^{0}C. For Cdc8-D2A a significant decrease in thermostability was observed, with the T_m for this protein equaling 32.4 ^{0}C. The E6A mutation had little effect on thermal stability, when compared to the WT unacetylated protein, with a T_m of 34.4 ^{0}C. The E6K mutation increased thermostability to equal that of the WT acetylated Cdc8, 35.4^{0}C and the D16A mutation increased the T_m slightly further to 35.9^{0}C. A dramatic increase in thermostability was observed with Cdc8-LKL which has a T_m of 37.3 ^{0}C. A summary of midpoint melting temperature for each Cdc8 protein is presented in table 3.3.

Charged residue interactions affect how much energy is required to cause the protein to become disordered and can be assessed in this system as enthalpy change. The Cdc8^{ACE} protein has a high value for enthalpy of 171 kJ mol^{-1}. It is known for mammalian Tm, that acetylation of the first methionine permits the amino terminus of Cdc8 to form a coiled-coil structure (Brown et al., 2001) and is likely to stabilize the dimer as the unacetylated protein has an enthalpy of 144.7 kJ mol^{-1}. The effect of N-terminal acetylation on the secondary structure of the Cdc8 α-helix may also contribute to this stability. The Cdc8-LKL protein also has a high enthalpy of 177.4 kJ mol^{-1} and the mutations at this position lie in the 'd', 'e' and 'f' positions (see Introduction figure 1.16). It is possible that this mutation affects both the Cdc8 dimer and the secondary structure of the Cdc8 α-helix. All other mutations are in the 'b' and 'f' position, therefore are likely only to affect α-helical structure. With the exception of the E6K mutant there was a positive correlation between T_m and ΔH for the (unacetylated) Cdc8 mutants. A summary of enthalpy change and T_m for each Cdc8 protein is presented in table 3.3.
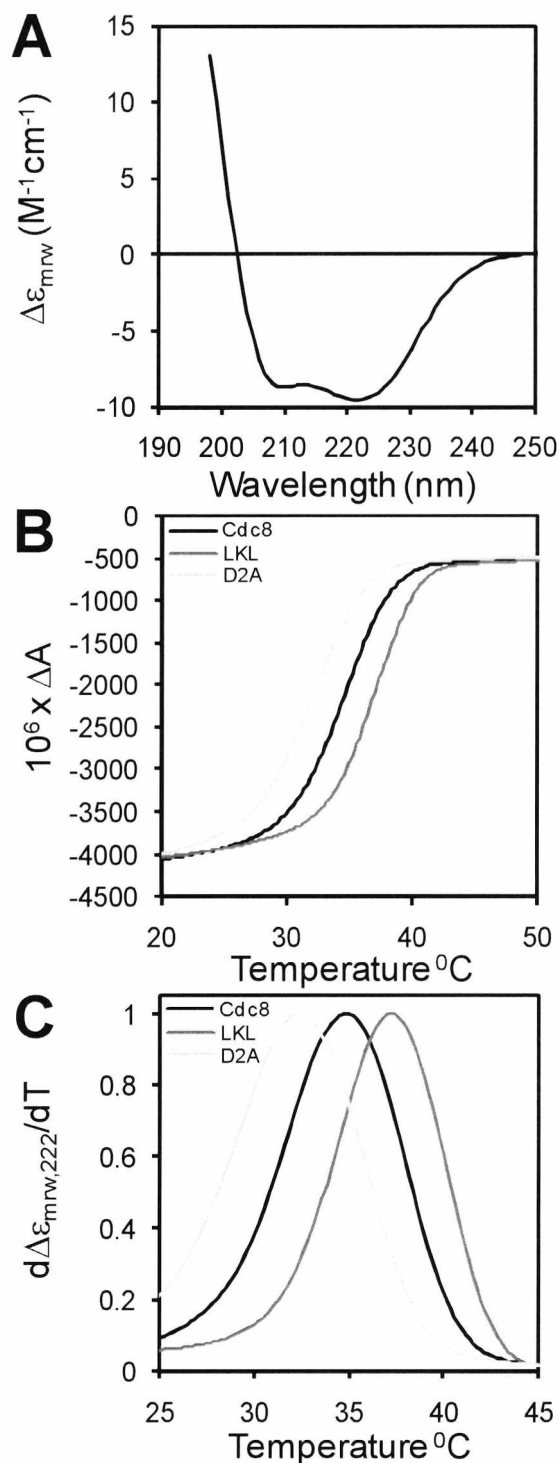
Figure 3.4. Thermostability of WT and mutant Cdc8 proteins.

(A) Circular dichroism spectrum for unacetylated Cdc8. (B) Raw absorbance data for unacetylated Cdc8, Cdc8–D2A, and Cdc8–LKL at 222 nm. (C) First derivative plots for unacetylated Cdc8, Cdc8–D2A, and Cdc8–LKL at 222 nm. The peaks correspond to the midpoint melting temperature.

Table 3.3. A summary of midpoint melting temperature and enthalpy of WT and mutant Cdc8

Mutant	Source	$T_m(^0C)$	ΔH (kJ mol^{-1})
Cdc8	E. coli	34.7	144.7
Cdc8^{ACE}	S.pombe	35.4	171.8
Cdc8-D2A	E. coli	32.4	128.3
Cdc8-E6A	E. coli	34.4	143.5
Cdc8-E6K	E. coli	35.4	130.2
Cdc8-D16A	E. coli	35.9	159.8
Cdc8-LKL	E. coli	37.3	177.4

3.4. Amino termini mutations affect the end-to-end interactions of Cdc8

End-to-end interactions between the amino and carboxyl termini of Cdc8 dimers allow the protein to polymerise. A viscometry assay (see materials and methods section 2.2.8) was used to investigate the effect mutations at the amino terminus of Cdc8 had upon the ability of the protein to form filaments, with a higher viscosity corresponding to a greater propensity to form filaments. Viscosity measurements were taken at increasing NaCl concentrations. The salt disrupts the ionic interactions that facilitate Cdc8 polymerisation and thus can be used to measure the strength of end-to end interactions.

Figure 3.5 shows viscosity data for the Cdc8 proteins, the shape of the curves is indicative of the disruption of end-to-end interactions. This implied the proteins were forming specific end-to-end bonds and not simple aggregating. A summary of viscosity for each of the Cdc8 proteins, in the absence of NaCl is presented in Table 3.4.

In the absence of NaCl Cdc8 has a viscosity of 1.08 centistokes (cSt). Acetylation of Cdc8 had a dramatic effect, increasing viscosity to 1.15 cSt. The effect of the D2A mutant was to render the protein unable to form end-to-end interactions, as Cdc8-D2A had a viscosity of 1.05 cSt,

which is equal to the buffer control containing no protein. The E6A, E6K and D16A mutations increased the viscosity to a value comparable with that of Cdc8[ACE], with recorded values of 1.13 cSt, 1.15 cSt and 1.14 cSt respectively. The most striking effect was observed with Cdc8-LKL. The affect of this mutation was to significantly increase viscosity to 1.22 cSt.

Amino terminal mutations in Cdc8 also had differing effects on the strength of end-to-end interaction. Visosities were said to be equal to the buffer control at 1.06 cSt. The Cdc8 protein has weak interaction, and viscosity was reduced to the level of the buffer at only 20 mM NaCl, whereas viscosity of the Cdc8[ACE] protein equalled the buffer between 150 and 200 mM. The viscosity of Cdc8 –E6A, E6K and –D16A were equivalent to the buffer at 80 mM NaCl, whereas the Cdc8-LKL viscosity was still greater than the buffer at 200 mM.

Table 3.4. A summary of viscosity of WT and mutant Cdc8

Mutant	Source	Viscosity (cSt) [1,2]
Cdc8	E. coli	1.08
Cdc8[ACE]	S.pombe	1.15
Cdc8-D2A	E. coli	1.05
Cdc8-E6A	E. coli	1.13
Cdc8-E6K	E. coli	1.15
Cdc8-D16A	E. coli	1.14
Cdc8-LKL	E. coli	1.22

[1] Standard deviations were less that 0.01
[2] Measured in the absence of NaCl, at pH 7.0, 20 ^{0}C
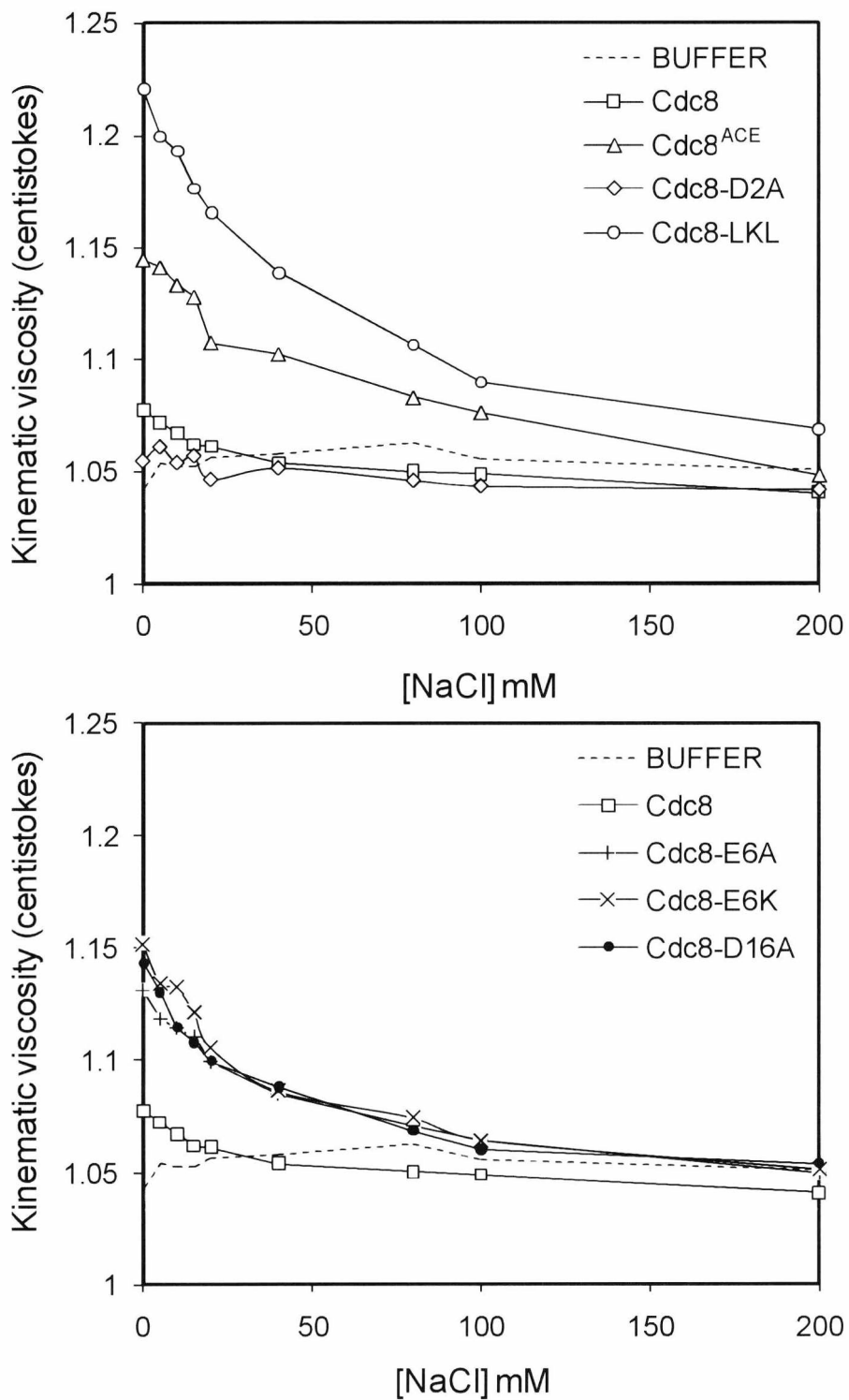
Figure 3.5. Viscosity of WT and mutant Cdc8

Viscosity of 20 μM Cdc8 proteins and buffer control at NaCl concentrations from 0 to 200 mM at 23 $^{\circ}$C.

3.5. Electron microscopy of Cdc8 filaments

To have confidence that the viscosity data was a consequence of specific end-to-end interactions, and not simple aggregation, a travelling grant was applied for, and received from "The Company of Biologists" to fund a trip to the lab of Professor William Lehman at the University of Boston in Massachusetts. During this trip, and the subsequent collaboration, electron microscopy was used to directly observe filaments of Cdc8, Cdc8^{ACE} and Cdc8–LKL Figure 3.6 shows electron micrographs representative of what was typically observed for each protein.

The Cdc8 protein was observed mainly as monomers, or very short filaments, where as the Cdc8^{ACE} protein was seen as distinctly longer filaments. The Cdc8-LKL protein appeared to form longer filaments still From the micrographs it was possible to calculate the percentage of filaments consisting of single or multiple Cdc8 dimers and the persistence length of the filaments (table 3.5). Persistence length is used to describe the "stiffness" or "flexibility" of a rod, is dependent on temperature, and is defined as the length along a rod over which its direction (longitudinal tangent) becomes nearly uncorrelated (Li et al., 2010a). Although the Cdc8-LKL protein was able to form longer polymers than Cdc8^{ACE} persistence length was not correspondingly increased. Overall these observations were consistent with the viscosity data and gave confidence that the observations were a result of end-to-end interaction and not aggregation.
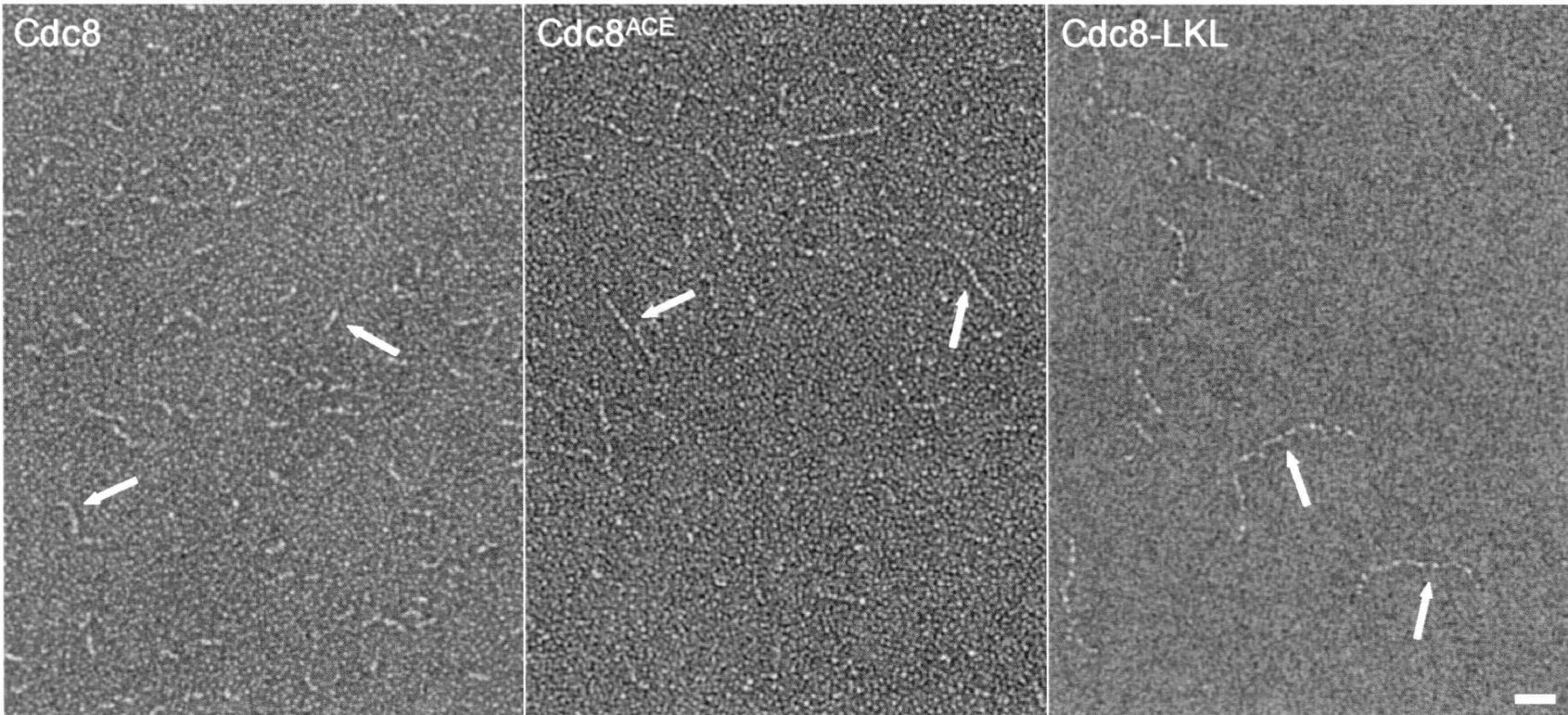
Figure 3.6. Electron microscopy of Cdc8 filaments.

Electron micrographs of Cdc8, Cdc8[ACE] and Cdc8–LKL, negatively stained with uranyl acetate. Example filaments are highlighted with white arrows, although more are present in each image. Scale bar equals 50 nm.

Table 3.5. Cdc8 filament length and filament persistence length.

| Tropomyosin | Source | Percentage of polymer lengths | | | | |
		Single dimer	2 dimers	3 dimers	4 dimers or longer	Persistence length*
Cdc8	*E. coli*	93.33%	6.67%	0	0	50 nm ± 10
Cdc8ACE	*S.pombe*	74.05%	19.62%	5.70%	0.63%	90 nm ± 20
Cdc8-LKL	*E. coli*	62.94%	24.12%	7.06%	5.88%	90 nm ± 20
			*n = >200			

Summary

During this part of the project, several single amino acid substitutions were generated at the amino terminus of Cdc8 using site directed mutagenesis. Wild type Cdc8 and Cdc8 mutants were expressed in, and purified from bacteria; acetylated Cdc8 was purified from *S. pombe*. The purified proteins were assayed for contaminants by gel electrophoresis and mass spectroscopy, and the concentration of each assayed spectrophotometrically.

The physical properties of each protein were then characterised. It was discovered that amino terminal mutations and acetylation state of the protein affected the thermostability of the molecule and its ability to form end-to-end interactions. When Cdc8 proteins were viewed by electron microscopy, the acetylated Tm formed longer polymers than the unacetylated. The Cdc8-LKL mutation caused an increase in filament length compared to the acetylated protein, but did not increase the 'stiffness' of the polymer.

Chapter 4: Functional analysis of wild type Cdc8 and Cdc8 amino termini mutants.

Introduction

Tropomyosin is an actin binding protein that stabilises the actin filaments and regulates myosin interaction with actin in muscle and non muscle cells. Modifications to the amino acid sequence of Tm affect its affinity for actin (Pittenger et al., 1995), and its ability to regulate acto-myosin interaction (Moraczewska et al., 1999) .

In fission yeast Tm is required for the maintenance of actin cables (Pelham and Chang, 2001) and for assembly of the contractile actomyosin ring (Balasubramanian et al., 1992). Loss of Cdc8 function is lethal and mutations in the protein result in defects in cytokinesis and polarised growth (Chang et al., 1996).

The Cdc8 amino termini mutants described in the previous chapter were assayed for their affinity for actin and the capacity to regulate myosin interaction with actin. These mutants were also examined *in vivo* for the capacity to rescue function in a Cdc8 temperature sensitive strain of *S. pombe* and a strain lacking N-acetyltransferase activity.

4.1. Amino termini mutations modify the affinity of Cdc8 for actin.

To address the affect of the amino acid substitutions on the affinity of Cdc8 for actin, co-sedimentation experiments were performed (see materials and methods section 2.2.5.). Increasing concentrations of Cdc8 were incubated with a constant concentration of actin, centrifuged at high speed, then pellets and supernatants were subjected to SDS-PAGE and subsequent gels were stained with Coomassie blue. Examples of SDS-PAGE gels used to determine binding affinity of three Cdc8 mutants are presented in figure 4.1.
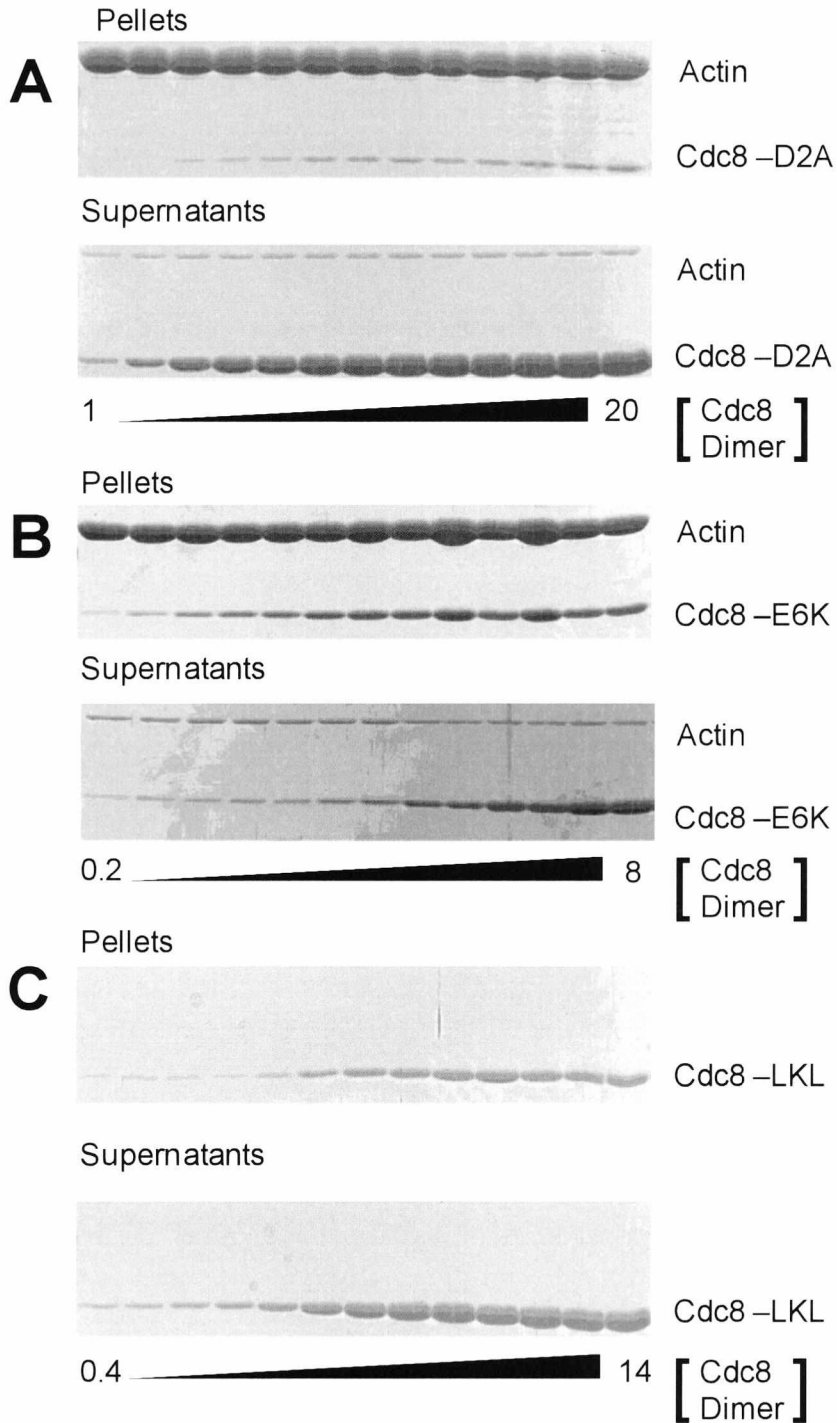
Figure 4.1. SDS-PAGE gels for Cdc8 co-sedimentation with actin

SDS page gels of the pellets and supernatants from co-sedimentation experiments of Cdc8-D2A (A) and Cdc-E6K (B) with 10 mM actin at 100 mM KCl over increasing tropomyosin concentrations (µM). (C) Cdc8-LKL pellets in the absence of actin.

In figures 4.1.A. and B. the top bands are actin and the density remain approximately constant. The bottom bands are Cdc8 protein and the density increases as Cdc8 dimer concentrations increase from left to right. Figure 4.1.A. is an example of a Cdc8 mutant binding weakly to actin. Even at 20 µM Cdc8-D2A, only a small proportion of the protein is observed in the pellet fraction, while a large amount of Cdc8-D2A remains in the supernatant. Conversely Figure 4.1.B. shows an example of a Cdc8 mutant which binds strongly to actin. A faint band can be observed in the pellet with as little as 0.2 µM Cdc8-E6K, a much denser band is visible at 8 µM Cdc8-E6K. Less Cdc8-E6K can be observed in the supernatant at equivalent Cdc8-D2A concentrations.

The gels were subsequently analysed by densitometry, and the values were used to determine the binding coefficients ($K_{50\%}$) of each Tm for actin by fitting the data to binding curves using the Hill equation (see materials and methods 2.2.5.). Typical binding curves for WT and cdc8 mutants are presented in figure 4.2. Unacetylated Cdc8 has a $K_{50\%}$ of 2.76 µM, the acetylated protein has an increased affinity for actin with a $K_{50\%}$ of 0.46 µM. These observations for WT unacetylated and acetylated proteins were consistent with previously published data (Skoumpla et al. 2007).

The Cdc8-D2A protein bound extremely weakly to actin, a binding curve could not be generated as the binding coefficient was found to be greater than 20 µM. The affect of the E6A and E6K mutations was to increase the affinity of these mutant proteins for actin, with values for $K_{50\%}$ of 0.32 µM and 0.45 µM respectively. These values are comparable with the WT acetylated protein. The $K_{50\%}$ for Cdc8-D16A is 2.27 µM, and although lower, overlapping standard deviations indicate no significant difference from the unacetylated wild type protein.
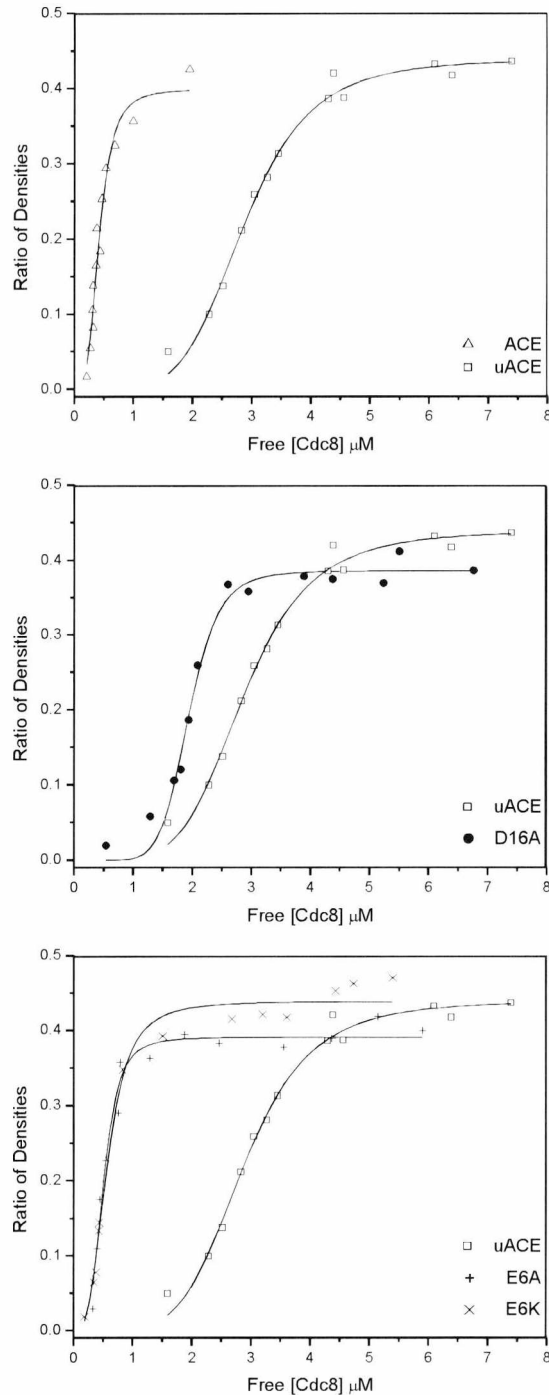
Figure 4.2. Binding curves of wild type and mutant Cdc8 for actin

Binding curves of free Cdc8 concentration against ratio of density of actin/Tm, for WT and mutants Cdc8, measured by densitometry of co-sedimentation SDS-PAGE gels. uACE and ACE refer to unacetylated and acetylated Cdc8 respectively Curves represent Hill equation lines of best fit. Concentration ranges (μM): 0.2-4 $Cdc8^{ACE}$, 1-10 $Cdc8^{uACE}$ 1-20 Cdc8-D2A, 0.5-12 Cdc8-E6A, 0.2-8 Cdc8-E6K and 1-12 Cdc8-D16A.

Surprisingly the Cdc8-LKL protein was observed in the pellet in the absence of actin (figure 4.1.C.). As a result of this a binding curve could not be generated. Several attempts to determine a value using high salt conditions and lower centrifugation speeds were also unsuccessful and it was not possible to determine the actin affinity of this protein using this method. This is potentially a consequence of Cdc8-LKL filament formation. Each $K_{50\%}$ was determined at least 3 times during independent experiments. Averages and standard deviations for WT and Cdc8 mutants were calculated and are summarised in Table 4.1.

Table 4.1. A Summary of WT and mutant Cdc8 actin binding coefficients

Tropomyosin	Source	$K_{50\%}$ (µM)*	Hill coefficient*
Cdc8-uACE	*E. coli*	**2.76** ±0.22	**5.38** ±0.32
Cdc8-ACE	*S.pombe*	**0.46** ±0.10	**3.69** ±0.54
Cdc8-D2A	*E. coli*	**>20**	-
Cdc8-E6A	*E. coli*	**0.32** ±0.14	**1.91** ±0.89
Cdc8-E6K	*E. coli*	**0.45** ±0.10	**3.63** ±0.69
Cdc8-D16A	*E. coli*	**2.27** ±0.31	**5.45** ±2.87
Cdc8-LKL	*E. coli*	n.d.	-
*average of at least 3 independent experiments			

4.2. The acetylation state of Cdc8 affects actin morphology.

During the collaboration with Professor William Lehman at the University of Boston (see Chapter 3.4) attempts were made to reconstruct images of unacetylated Cdc8 bound to actin, using electron microscopy. This proved unsuccessful, largely due to the relatively weak affinity of the unmodified protein for actin. However a number of interesting observations were made on the effect the Cdc8 protein had upon the morphology of actin.

Figure 4.3 shows a typical example of EM micrographs for actin alone and actin decorated with either cardiac Tm, unacetylated Cdc8 or Cdc8^{ACE}. Polymers of actin alone are long, continuous, straight and able to flex without breaking and these properties are retained when decorated with cardiac Tm. When decorated with Cdc8^{ACE} the actin polymer in the same conditions became wavy, however were still long, continuous and
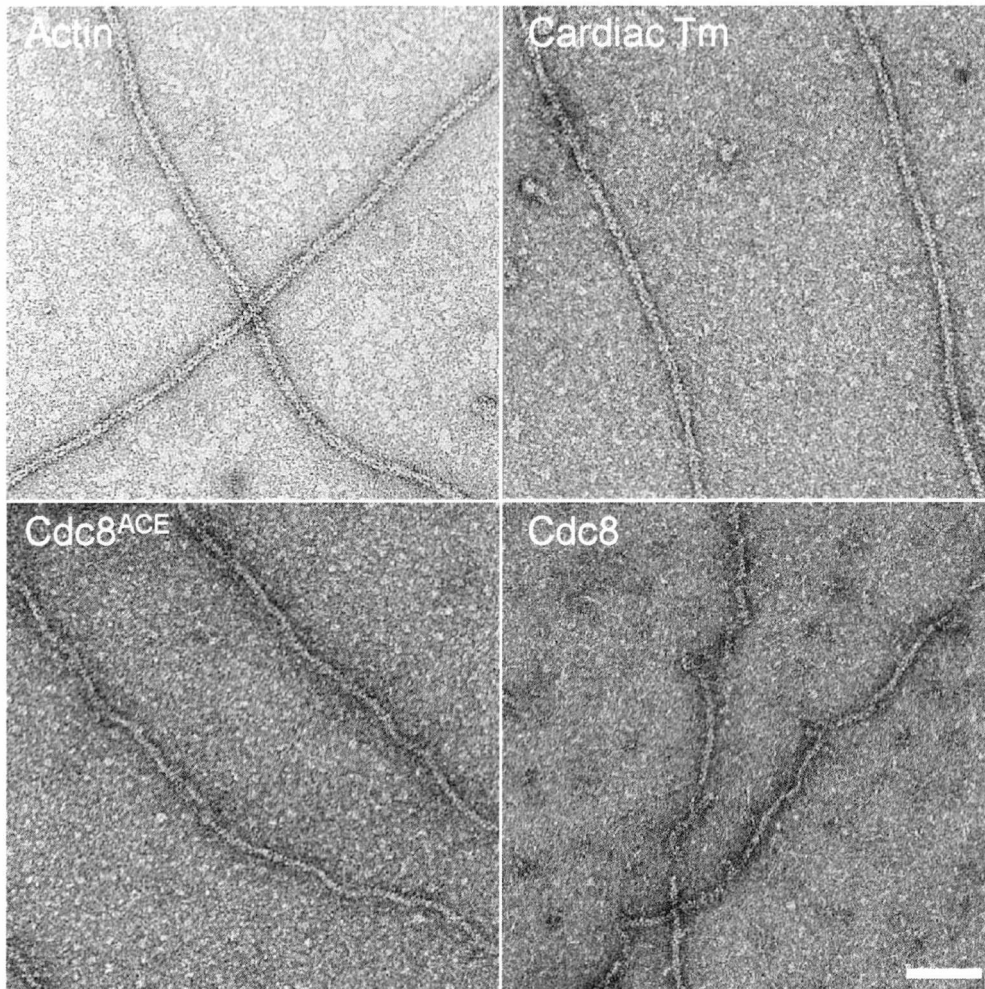
Figure 4.3. Electron microscopy of actin polymers

Uranyl acetate stained actin and actin decorated with tropomyosin on carbon coated copper grids. Images of actin and actin with cardiac Tm courtesy of Agnieszka Galińska-Rakoczy, University of Boston, Massachusetts. Scale bar equals 50 nm.

flexible. When decorated with unacetylated Cdc8, the actin polymers appeared crooked and are cracked and broken resulting in shorter non-continuous polymers. The decoration is weaker with unacetylated Cdc8, with unbound Tm dimers visible in the background. This observation is consistent with previous results showing that although unacetylated Cdc8 can bind actin, its affinity is reduced (Skoumpla et al., 2007; this study section 4.1.). What is more this result suggests that unacetylated Cdc8 may promote actin depolymerisation, or stiffen actin polymers causing them to become brittle

4.3. Amino terminal mutations of Cdc8 affect ATPase activity of myosin sub fragment 1.

In *S. pombe*, type II and type V myosins associate with Tm bound actin filaments. In order to investigate the influence of Cdc8 amino terminal mutations on regulation of myosin ATPase activity, a coupled enzyme ATPase assay was used. Increasing concentrations of myosin sub fragment 1 (S1), which retains the ATPase and actin-binding activities of the myosin, were incubated with constant concentrations of actin and Cdc8. This assay (see materials and methods figure 2.1) is based on the conversion of phosphoenolpyruvate (PEP) to pyruvate by pyruvate kinase (PK), in which a phosphate group from PEP is transferred to ADP to yield one molecule of pyruvate and one of ATP. This reaction is coupled to the conversion of pyruvate to lactate by lactate dehydrogenase (LDH). The latter step requires NADH which is oxidised to NAD^+. NADH absorbs at 340 nm but NAD^+ does not, allowing NADH concentration to be followed by monitoring absorbance at 340 nm. The decrease in OD_{340} can subsequently be converted into ATPase activity where one molecule of NADH oxidized to NAD^+ corresponds to the production of one molecule of ADP and one of inorganic phosphate by the S1 ATPase.

Figure 4.4 shows phosphate release at increasing concentrations of S1 for WT and Cdc8 mutants. The gradient obtained from each curve was
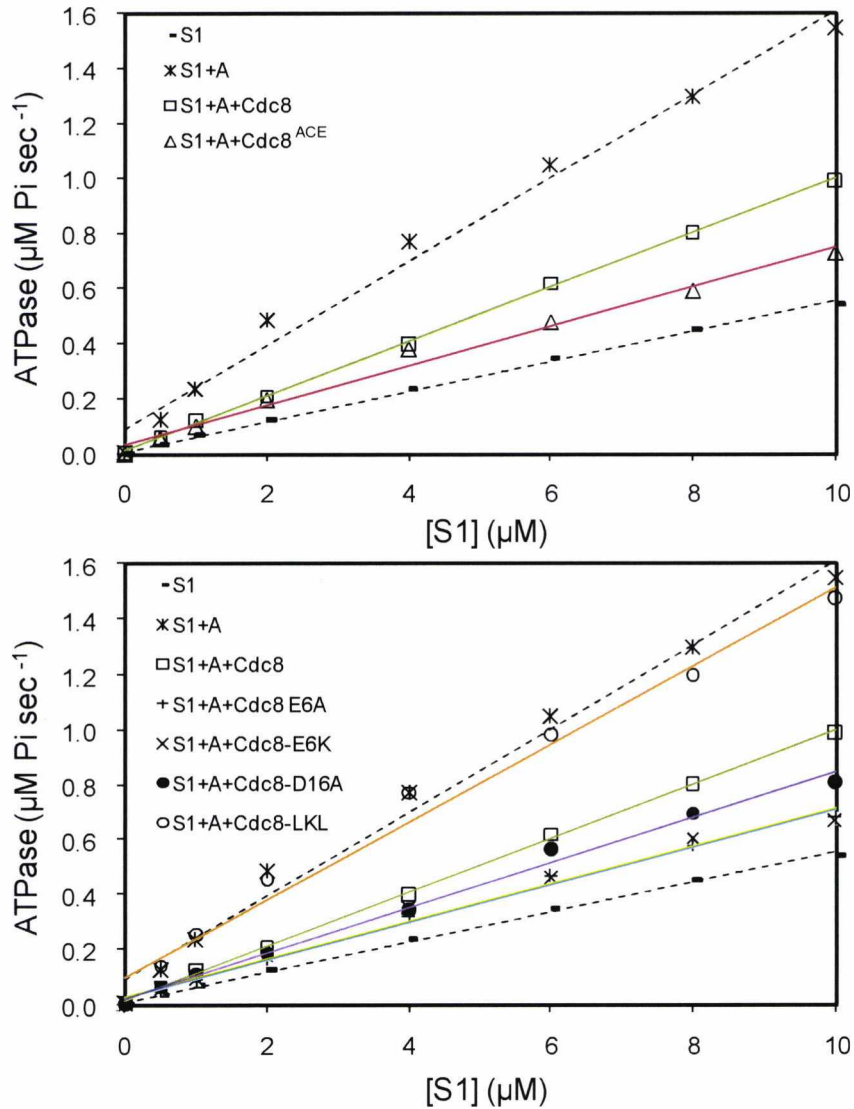
Figure 4.4. Inhibition of acto-S1 ATPase activity by WT and mutant Cdc8.

ATPase rate against S1 concentration for WT and mutant Cdc8 proteins at 25 °C with 30 mM NaCl. Dashed lines correspond to the maximum (S1) and minimum (S1+actin) controls, solid lines represent each protein. The top panel show a comparison between unacetylated Cdc8 and Cdc8^{ACE}, the bottom panel compares unacetylated Cdc8 with mutant Cdc8 proteins. Actin concentration was 1 µM. Cdc8 dimer concentrations were 1 µM for Cdc8^{ACE}, Cdc8-E6A and Cdc8-E6K, 2.5 µM for Cdc8 and Cdc8-D16A and 10 µM for Cdc8-LKL

used to calculate the ATPase rate. A summary of ATPase rates for each protein is presented in Table 4.2. The ATPase rate of S1 when only actin is present was 0.096 μM Pi sec^{-1} μM S1^{-1}. When unacetylated Cdc8 is bound to actin the rate decreased to 0.044 μM Pi sec^{-1} μM S1^{-1} and when Cdc8^{ACE} was bound the rate decreased further to 0.017 μM Pi sec^{-1} μM S1^{-1}. When Cdc8-E6A or Cdc8-E6K were bound to actin, ATPase rates were reduced to 0.014 and 0.015 μM Pi sec^{-1} μM S1^{-1} respectively, rates comparable to that of Cdc8^{ACE}. The Cdc8-D2A protein was not assayed owing to its extremely low affinity for actin (see section 4.1). Cdc8-LKL had only a small inhibitory effect on acto-S1 ATPase rate, reducing it to 0.086 μM Pi sec^{-1} μM S1^{-1}.

As a inhibitory effect was observed for Cdc8-LKL at high (10 μM) concentrations it was decided to use the ATPase assay to determinate an actin binding coefficient for Cdc8-LKL. ATPase rates were recorded in the presence of increasing Cdc8-LKL concentrations and a binding curve fit using the Hill equation (see materials and methods section 2.2.5.). The $K_{50\%}$ for Cdc8-LKL was determined as the Cdc8-LKL concentration producing half of maximum inhibition.

Table 4.2. A Summary of WT and mutant Cdc8 inhibition of S1 ATPase activity

Protein	Source	ATPase rate[1] (μM Pi sec^{-1} μM S1^{-1})	Normalised[2] rate
Actin alone	Rabbit	0.096 ±0.014	1.00
Cdc8	E. coli	0.044 ±0.002	0.46
Cdc8^{ACE}	S.pombe	0.017 ±0.001	0.18
Cdc8-D2A	E. coli	-	-
Cdc8-E6A	E. coli	0.014 ±0.003	0.15
Cdc8-E6K	E. coli	0.015 ±0.003	0.15
Cdc8-D16A	E. coli	0.028 ±0.001	0.29
Cdc8-LKL	E. coli	0.086 ±0.008	0.90

[1]Rate of S1 alone subtracted from values
[2]Relative to ATPase rate of S1+Actin alone

A value of 5.19 µM was calculated using this method which is approximately 2-fold weaker than that of unacetylated Cdc8 calculated using the standard co-sedimentation assay (section 4.1). As a control the same method was used to calculate the $K_{50\%}$ of Cdc8^{ACE}. A value of 0.41 µM was determined, comparable to the value obtained using cosedimentation. This gave confidence that this method was reliable for determiing affinty for actin.
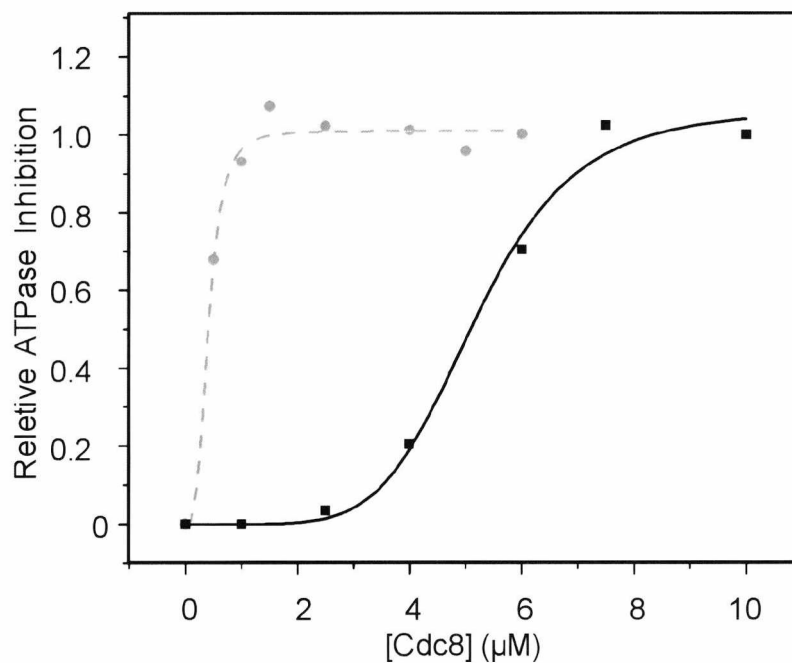
Figure 4.5. Affinity of Cdc8-LKL for actin.

Binding curves for Cdc8-LKL (black squares) and Cdc8^{ACE} (grey circles) calculated from ATPase measurements at at 25 ºC with 30 mM NaCl, 1 µM actin, 10 µM S1 and increasing concentrations of Cdc8. Curves represent Hill equation lines of best fit.

4.4. Overexpression of WT and mutant Cdc8 proteins is not toxic in WT *S. pombe.*

Having acquired detailed information on the physical properties, and interactions with actin and myosin for the Cdc8 amino terminal mutants, it was important to relate these properties to the behaviour of the Cdc8 mutant proteins *in vivo*. To achieve this, mutant *cdc8* cDNAs were cloned

into an *S. pombe* expression plasmid (see materials and methods section 2.3.6.) under the control of the medium strength nmt41 (no message with thiamine) promoter (Maundrell, 1993). In the presence of thiamine, expression levels using this promoter are approximately equal to the WT level (Skoumpla et el., 2007). Over expression is achieved by removing thiamine from the *S. pombe* growth media.

S. pombe expression plasmids containing the mutant *cdc8*⁺ alleles were introduced into a WT *S. pombe* strain (see materials and methods section 2.3.2.). In order to investigate whether over expression of mutant Cdc8 proteins was toxic, wild type *S. pombe* cells expressing mutant cdc8 genes were grown on solid media in the presence and absence of thiamine (Figure 4.6). In this experiment *S. pombe* cells expressing the wild type *cdc8*⁺ gene and an empty vector were also included as controls.

When thiamine was present, cells of each strain grew normally. Overexpression of each Cdc8 protein did not have a significant effect on growth of the wild type cells and indicates that overexpression is not toxic to the cells.
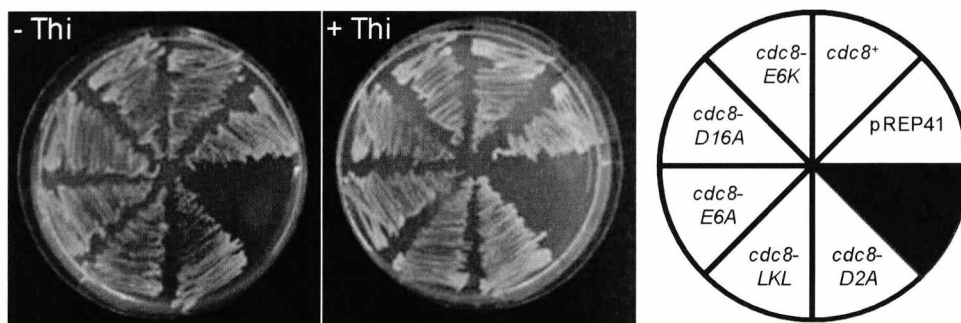
Figure 4.6. Over expression of WT and mutant Cdc8 in *S. pombe*

WT *S. pombe* cells expressing (+ Thi) and over expressing (- Thi) WT and mutant Cdc8 proteins at 25°C on EMM -leucine agar plates. An empty pREP41 plasmid was used as the negative control.

4.5. Mutant Cdc8 proteins complement *cdc8*⁺ function

To assess the ability of the mutant Cdc8 proteins to complement wild type *cdc8* function (i.e. to test functionality), *S. pombe* expression plasmids containing the mutant *cdc8* alleles were introduced into a *cdc8-110* temperature sensitive strain (see materials and methods section 2.3.2), in which the mutant genomic *cdc8* allele renders the Cdc8 protein non-functional at 36^{0}C.

Figure 4.7 shows a comparison of *cdc8-110* cells expressing WT and mutant Cdc8, grown at 25^{0}C and 36^{0}C. At the permissive temperature (25^{0}C) the *cdc8-110* gene product is functional and all strains grew normally. When grown at the restrictive temperature (36^{0}C), cells containing empty pREP41 plasmids lacked a functional Cdc8 protein and
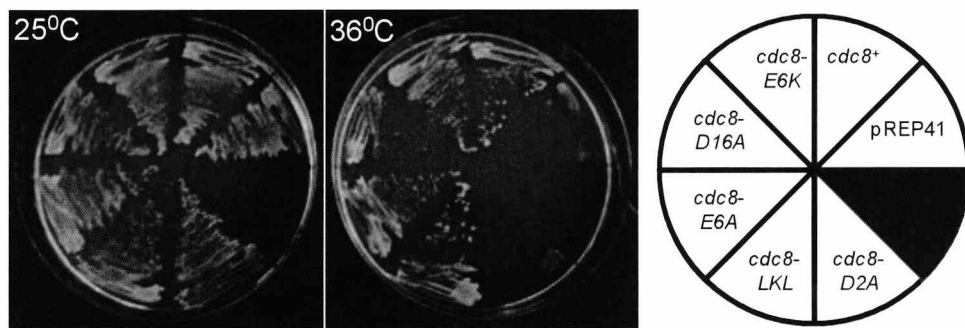
Figure 4.7. Growth of *cdc8-110* cells expressing WT and mutant Cdc8.

cdc8-110 cells expressing WT and mutant Cdc8 under the control of the *nmt41* promoter grown on EMM agar plates, lacking leucine and containing thiamine at 25^{0}C and 36^{0}C.

were unable to grow. In contrast cells expressing *cdc8*⁺ from a plasmid were able to grow at the restrictive temperature. *cdc8-110* cells expressing *cdc8-E6A*, *cdc8-E6K*, *cdc8-D16A* and *cdc8-LKL*, were also capable of growth at 36^{0}C although growth in cells expressing *cdc8-D16A* appeared slower. However expression of *cdc8-D2A* did not rescue *cdc8-110* function and the cells were unable to grow.

To compare the rate of growth in each of these strains, growth curves (figure 4.8.A) were generated at 36^0C (see materials and methods section 2.1.5.). Growth rates were calculated by measuring the slope of each curve in the middle of the exponential growth phase. Cells expressing the WT Cdc8 protein grew at a rate of 0.050 ΔOD$_{600}$ hours^{-1}, and little increase in growth rate was observed in cells expressing Cdc8-E6A. Cells expressing Cdc8-E6K grew slightly faster than cells expressing the WT protein, and cells expressing Cdc8-D16A grew slightly slower. Cells containing empty pREP41 plasmids or expressing Cdc8-D2A were unable to grow. Cells lacking functional Tm do continue to grow in length for a while, but are unable to divide (Chang et al., 1996; Pelham and Chang, 2001). This accounts for the initial increase in cell density for these two strains (figure 4.8.A.). Surprisingly, cells expressing Cdc8-LKL grew approximately 50% faster than the WT cells. A summary of growth rates is presented in figure 4.8.B.

Cell length, and septation index (proportion of cell population with visible division septa) were also determined for *cdc8-110* cells expressing each mutant Cdc8 protein. Cells expressing Cdc8-D2A had a longer average length than cells expressing other Cdc8 mutants, which are similar in length, and standard deviations suggested any variation in length observed was not significant. Cells expressing Cdc8-D2A did however exhibit a marked reduction in septation index, consistent with their inability to undergo cell division. Cells expressing mutant Cdc8 each had misplaced septa to some degree, suggesting these proteins were not fully functional *in vivo*.

A

B

Allele	Growth rate (Δ OD$_{600}$ hours^{-1})	Growth rate relative to $cdc8^+$
$cdc8^+$	**0.050** ±0.003	1.00
$cdc8$-D2A	-	-
$cdc8$-E6A	**0.052** ±0.001	1.04
$cdc8$-E6K	**0.061** ±0.003	1.22
$cdc8$-D16A	**0.040** ±0.004	0.80
$cdc8$-LKL	**0.075** ±0.004	1.49
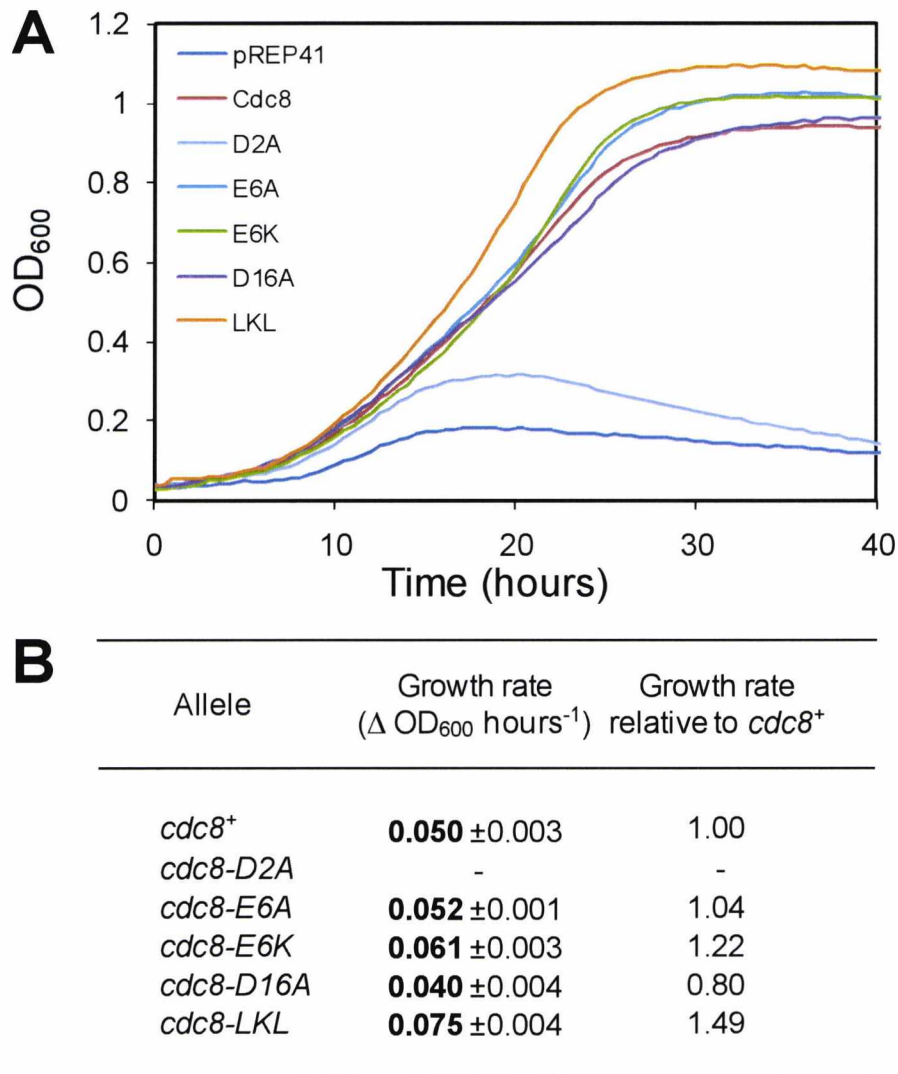
Figure 4.8. Growth rates of *cdc8-110* cells expressing WT and mutant Cdc8.

(A) The OD$_{600}$ for *cdc8-110* cells expressing WT and mutant Cdc8 over 40 hours at 36^{0}C. Cells were grown in liquid EMM lacking leucine and containing thiamine.(B) Growth rates for each strain calculated from the steepest section of each curve (~18-24 hours).

Table 4.3. Summary of septation index and cell length for cdc8-110 cells at 36^{0}C

Allele	Septation Index (%)	Misplaced Septa (%)	Average cell length (µm)
cdc8$^+$	12.87	0.00	**13.76** ±3.25
cdc8-D2A	3.23	4.52	**16.04** ±3.88
cdc8-E6A	9.52	1.19	**12.58** ± 3.14
cdc8-E6K	10.47	0.58	**13.25** ± 3.18
cdc8-D16A	11.24	2.81	**14.14** ±3.14
cdc8-LKL	9.52	1.79	**13.68** ±3.52

4.6. Actin morphology is affected by Cdc8 amino terminal mutations.

To see what effect expression of mutant Cdc8 had on the actin cytoskeleton, actin was labelled with rhodamine conjugated phalliodin in cdc8-110 cells expressing wild type and mutant cdc8 alleles grown at the restrictive temperate, (see materials and method 2.1.1.). Figure 4.6 shows images of typical cells of each strain stained with rhodamine-phalliodin.

In cdc8-110 cells containing the empty pREP41 plasmid, actin patches appear diffuse throughout the cell and no actin cables could be observed. Cells expressing WT Cdc8 exhibited normal actin morphology with cortical actin patches, actin cables and CARs visible. Actin in cells expressing Cdc8-D2A resembled cells with an empty plasmid, with diffuse patches and no visible cables. The actin morphology in the cells expressing all other mutant Cdc8 appears largely unaffected, cortical actin patches actin cables and CARs were observed in each.
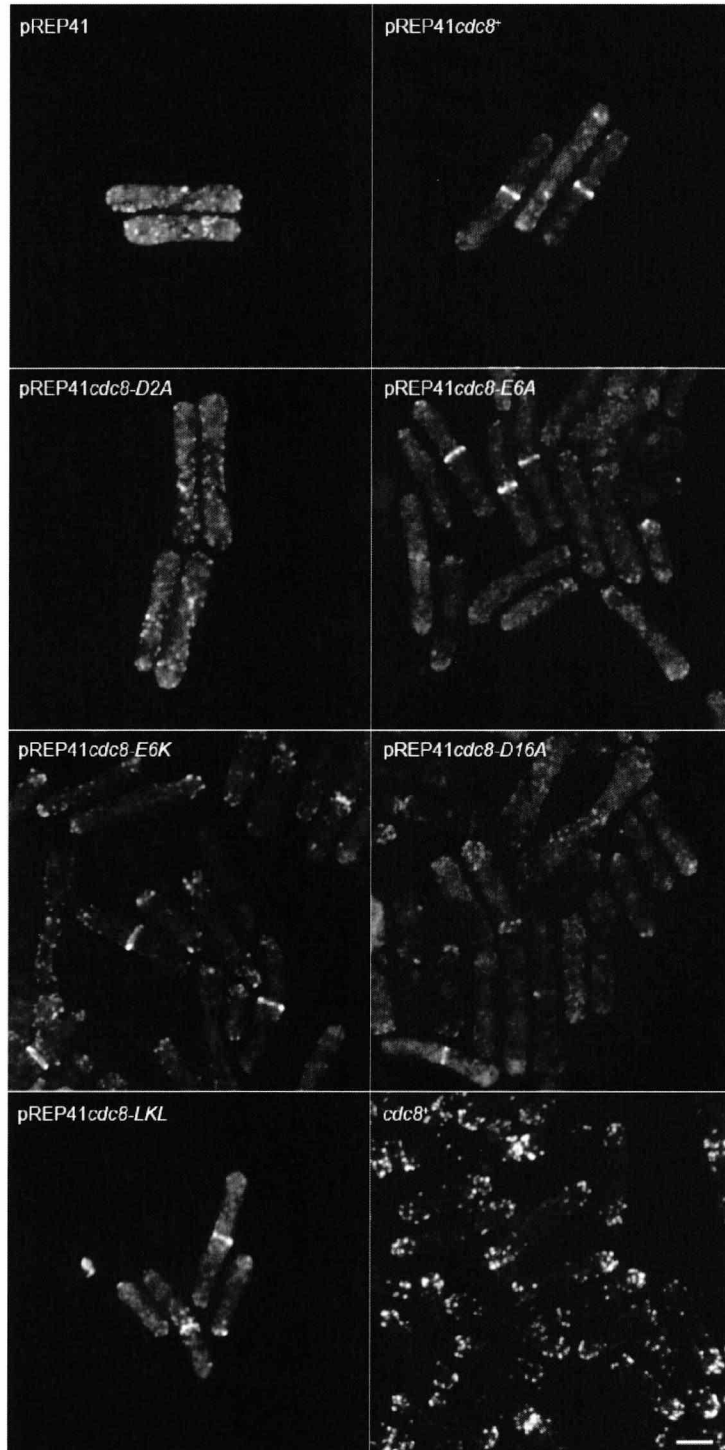
Figure 4.9. Rhodamine Phalloidin staining of *cdc8-110* cells

Fluorescence microscopy of actin in *cdc8-110 S. pombe* cells expressing mutant Cdc8 from pREP41 plasmids. Cells were stained with rhodamine-phalloidin after 4 hours at 36°C. The bottom right panel shows WT cells lacking plasmids. Scale bar equals 5 microns.

4.7. Cdc8 amino terminal mutations do not compensate for loss of Nα-acetlytransferase activity.

In *S. pombe* the homolog of the *S. cerevisiae* NatB amino terminal α-acetyltransferase regulatory subunit (Singer and Shaw, 2003) is expressed by the *arm1⁺* gene. An *arm1Δ* deletion strain lacks NatB N-terminal α-acetyltransferase activity, therefore Tm is not acetylated (Arthur Coulton, personal communication). These cells have a slow growing phenotype at 25^0C, with cytokinesis defects, and are unable to grow at 36^0C. To examine whether any of the Cdc8 amino terminal mutants were able to rescue the *arm1Δ* phenotype, *S. pombe* expression plasmids containing WT and mutant *cdc8* genes were introduced (see
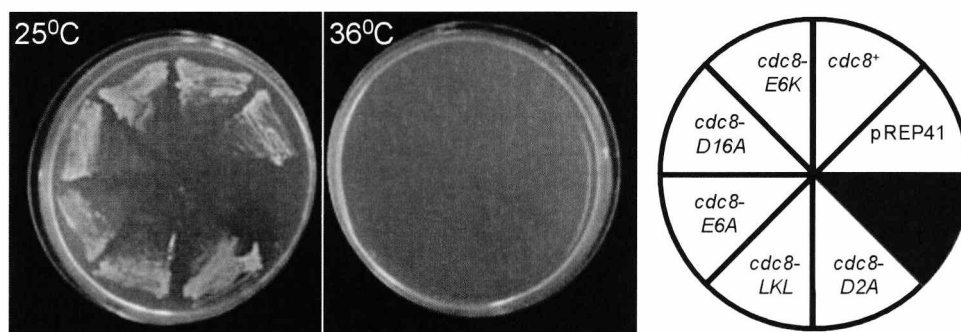
Figure 4.10 Growth of *arm1Δ* cells expressing WT and mutant Cdc8

arm1Δ cells expressing WT and mutant Cdc8 under the control of the nmt41 promoter grown on EMM agar plates, lacking leucine and containing thiamine at 25^0C and 36^0C.

materials and methods section 2.3.2.) into the *arm1Δ* strain. Figure 4.10 shows plates allowing growth comparison of *arm1Δ* cells expressing WT and mutant Cdc8, at 25^0C and 36^0C. None of *arm1Δ* cells expressing extragenomic wild type or mutant *cdc8* were able to grow at the restrictive temperature and *arm1Δ* cells overexpressing wild type and mutant *cdc8* were similarly unable to grow at the restrictive temperature (data not shown). Figure 4.11 shows a phenotype comparison of *arm1⁺* cells, *arm1Δ* cells and *arm1Δ* cells expressing extragenomic wild type Cdc8.
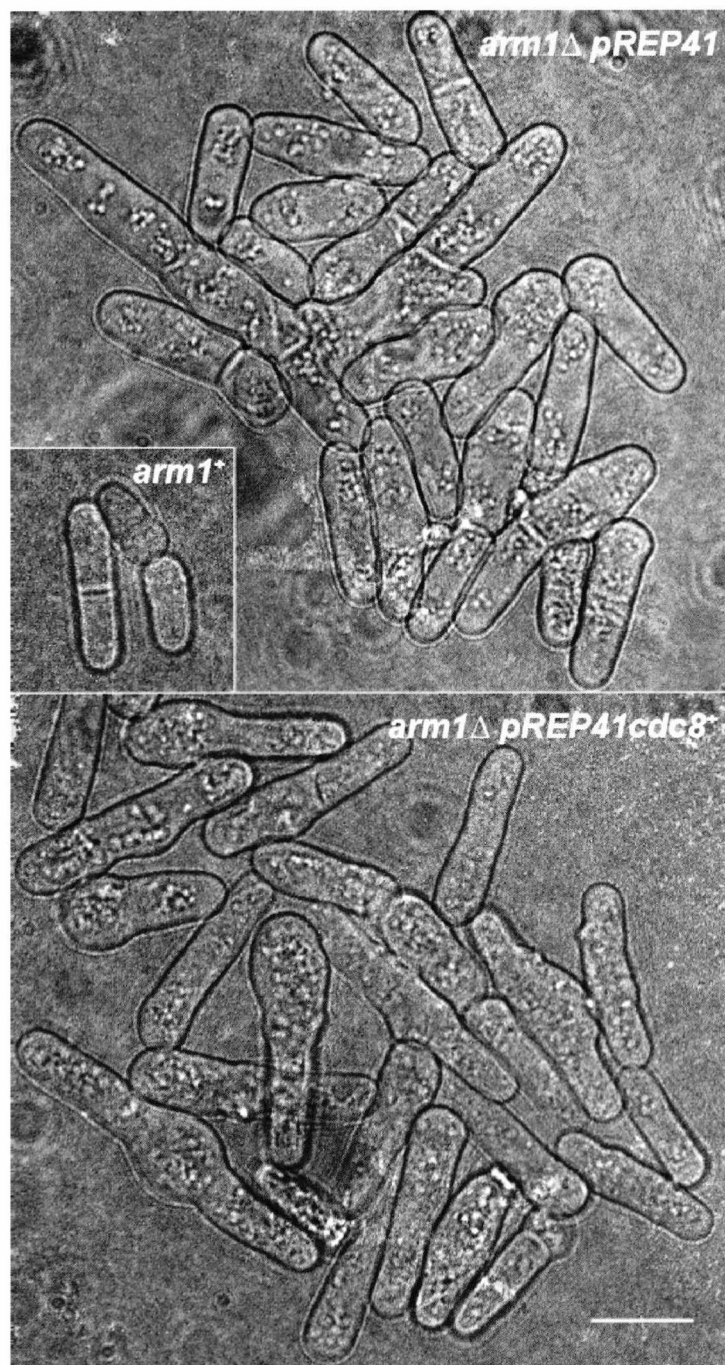
Figure 4.11. The wild type and *Δarm1* phenotype of S. pombe.

Phased contrast microscopy of *arm1Δ* containing empty expression vector (top panel), *arm1Δ* cells expressing wild type Cdc8 (bottom panel) and Wild type cells (inset). The *arm1Δ* phenotype is not rescued by extrachromosomal Cdc8 expression. Scale bar = 10 microns

Allele	Growth rate (Δ OD_{600} hours^{-1})	Growth rate relative to *pREP*
pREP	**0.039** ±0.002	1.00
cdc8^{+}	**0.042** ±0.002	1.08
cdc8-D2A	**0.044** ±0.003	1.13
cdc8-E6A	**0.039** ±0.003	1.00
cdc8-E6K	**0.031** ±0.002	0.79
cdc8-D16A	**0.043** ±0.002	1.10
cdc8-LKL	**0.044** ±0.003	1.13
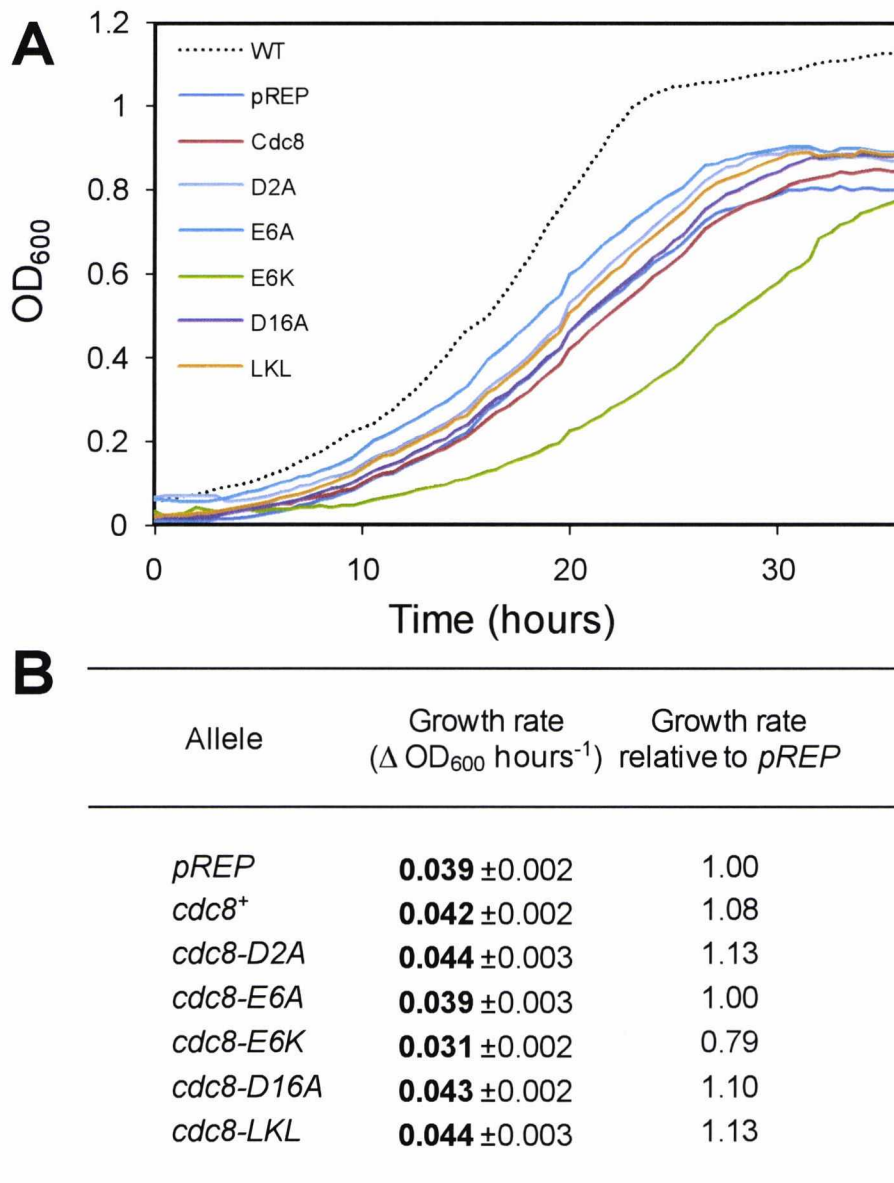
Figure 4.12. Growth rates of *Δarm1* cells expressing WT and mutant Cdc8.

(A) The OD_{600} for *Δarm1* cells expressing wild type and mutant Cdc8 over 35 hours at 25^{0}C. Cells were grown in liquid EMM lacking leucine and containing thiamine. A growth curve for wild type cells (WT) grown in the same conditions from a separate experiment is overlaid (dotted line) for reference. (B) Grown rates for each strain calculated from the steepest section of each curve, expressed as change in OD600 per hour and relative to an *arm1Δ* strain carrying empty expression vector (pREP). Growth rate for the WT strain was calculated as 0.074 Δ OD_{600} hours^{-1}.

Extragenomic expression of WT or mutant Cdc8 proteins did not rescue the arm1Δ phenotype at 25^{0}C.

To compare the rate of growth in each of these strains, growth curves (figure 4.12A) were generated at 25^{0}C (see materials and methods section 2.1.5.). Growth rates (figure 4.12B) were calculated by measuring the slope of each curve in the middle of the exponential growth phase. The growth rate was not significantly altered in cells expressing WT Cdc8 and Cdc8 mutant proteins, apart from Cdc8-E6K. Cells expressing Cdc8-E6K surprisingly grew slower by approximately 20% in contrast to the effect observed in *cdc8-110* cells.

Summary

During this section of the project, the affect of amino terminal mutations on the functional properties of Cdc8 were assessed. Modification of the amino terminal increased and decreased the affinity of Cdc8 for actin to varying degrees and the affinity of each Cdc8 mutant was correspondingly reflected in its ability to regulate the actin induced ATPase activity of myosin II S1. When Cdc8 bound to actin was observed directly by electron microscopy unexpected actin morphology was observed. Actin decorated with acetylated Cdc8 appeared more 'wavy' compared to actin decorated with cardiac Tm. Binding of unacetylated Cdc8 to actin caused the filament to become brittle and fractured.

All Cdc8 proteins except Cdc8-D2A were able to complement loss of Cdc8 function in a temperature sensitive *S. pombe* strain. Additionally cells expressing *cdc8-E6K* and *cdc8-LKL* genes were able to grow faster than cells expressing the wild type gene. In *Δarm1* cells wild type and Cdc8 mutants were unable to compensate for loss of amino terminal acetyltransferase activity The growth rate was not significantly altered in *Δarm1* cells expressing wild type Cdc8 or Cdc8 mutant proteins, except for Cdc8-E6K which grew slower.

Chapter 5: Research, development and optimisation of quantum dot-antibody conjugates for imaging tropomyosin localisation in *S. pombe*.

Introduction

Conjugates of inorganic fluorescent nanocrystals and biological macromolecules, chiefly antibodies and oligonucleotides, have been used in research and diagnostic applications for imaging of disease, cellular processes and structures both *in vitro* and *in vivo* where it has been reported that they can produce stronger signals, which are more resistant to photobleaching than traditional fluorophores (Gao et al., 2004; Wu et al., 2003b).

A thorough investigation into the variables involved in producing quantum dot-antibody conjugates, has yet to be undertaken, and this study aimed to do so. A series of conjugates of anti-Cdc8 antibodies and a commercially available QD were produced with the aim of determining optimal conditions for conjugation, and the study yielded detailed information on the intrinsic chemical properties, and biological activity of the conjugates, and has lead to the establishment of a standardised protocol for conjugate production.

5.1. Optimisation of QD-IgG conjugation

The first stage of this part of the project was to produce QD-IgG conjugates using a standard, optimised protocol and involved a number of experiments to identify and control variables relevant to the conjugation reaction and purification of reaction (QD-IgG) products. As a starting point, and simply to prove conjugates could be produced from the materials available, the Evitag® generic protocol (manufacturers instructions) was employed to investigate the effect of relative EDC:QD:IgG ratios on conjugation efficiency as measured by production

of QD-IgG conjugate. In carrying out these experiments it was assumed that each QD had 8 –COOH surface groups (see manufacturers literature) and that the reaction stoichiometry was 1:1:1, COOH:EDC:IgG.

A series of experiments was conducted using ratios of 40 000:1, 5000:1, 1000:1, 500:1, 250:1 and 8:1 EDC:QD. This equates to a ratio of 5000:1, 625:1, 125:1, 62.5:1, 31.25:1 and 1:1 with respect to –COOH groups. Ratios of 10:2, 10:1, 10:0.5, 10:0.1, 1:2, 1:1 and 1:0.5 QD:IgG were also used and control reactions included QD reacted without IgG and QDs with IgG but no EDC. Reactions were performed in PBS pH 7.0, at RT for 90 minutes with end-over-end mixing.

5.2. Assaying QD:IgG conjugates for fluorescence and antibody content.

After separation by ultrafiltration (see materials and methods section 2.5.5.) the retentate and flow through of all reactions described in section 5.1, were assayed for fluorescence and antibody content by absorbance at 280 nm (see materials and methods sections 2.5.7. & 2.5.6.) In an initial series of single experiments to conjugate QDs and IgG (see materials and methods section 2.5.2.) in which reaction mixtures were separated by ultrafiltration the fluorescence ($EM_{\lambda 495}$) and optical density (OD_{280}) of the 'retentate' and 'flow through' fractions of the reactions were measured to determine if conjugate had been produced.

The results are displayed in table 5.1. and no obvious trends are observable. All fluorescence and OD values reported are very low, however it is possible to comment briefly on the control reactions. The degree of reduction in total fluorescence was greatest in the control containing QD and IgG. This reduction was largely caused by a much lower fluorescence value for the 'retentate' fraction suggesting the possibility that IgG and QD could have become associated by non specific binding mechanisms to form a 'quasi-conjugate' which was retained above the membrane but in which QD fluorescence was 'quenched' by the presence of protein.

Table 5.1. Fluorescence and absorbance of preliminary conjugations.

Fluorescence and OD_{280} data for Retentate (R) flow-through (FT) and washes (W) for conjugations performed under varying conditions. Units are arbitrary fluorescence values. Control reactions are highlighted in grey. Total fluorescence of QDs before separation are highlighted in yellow.

	EDC:QD	QD:AB	R Fluor	R OD_{280}	FT Fluor	FT OD_{280}	W1 Fluor	W1 OD_{280}	W2 Fluor	W2 OD_{280}	W3 Fluor	W3 OD_{280}
1	40000:1	1:0.5	14.85	0.04	9.23	0.16	0.17	0.00	-1.35	0.00	-1.47	0.00
2	5000:1	1:0.5	3.85	0.08	15.07	0.09	11.32	0.00	0.55	0.00	3.39	0.00
3	1000:1	1:0.5	13.22	0.02	11.32	0.07	0.49	0.00	2.59	0.00	1.50	0.00
4	40000:1	1:1	6.18	0.02	17.39	0.06	-2.63	0.00	-5.98	0.00	1.46	0.00
5	5000:1	1:1	11.06	0.02	11.10	0.04	-2.30	0.00	2.12	0.00	0.91	0.00
6	1000:1	1:1	10.61	0.03	10.15	0.23	1.20	0.00	1.06	0.00	1.56	0.00
7	40000:1	1:2	5.08	0.02	9.85	0.08	2.36	0.00	0.99	0.00	2.31	0.00
8	5000:1	1:2	8.24	0.01	17.11	0.05	-1.28	0.00	-1.73	0.00	1.47	0.00
9	1000:1	1:2	1.33	0.01	12.93	0.04	0.53	0.00	1.65	0.00	1.30	0.00
10	5000:1	1:0	26.43	0.02	15.95	0.04	1.34	0.00	-1.61	0.00	-2.76	0.00
11	0:1	1:1	3.72	0.03	13.80	0.22	-2.23	0.01	1.43	0.00	0.06	0.00
12	0:1	1:0	18.73	-	23.99	-	5.69	-	4.46	-	11.60	-
13	0:1	1:0	94.99	-	-	-	-	-	-	-	-	-

When QD's alone were separated by ultrafiltration, much of the fluorescent signal was observed in the 'flow through' and washes suggesting that in the absence of other reactants, the QDs were able to pass through the filter membrane. The sum of fluorescence values from the 'retentate', 'flow through' and washed for QDs alone was not equal to the total QD fluorescence suggesting some of the material has adsorbed non-specifically to the filter membrane.

A replicate experiment was then conducted but where the total amount of QD was increased tenfold so as to hopefully result in higher fluorescence values and therefore make trends more easily identifiable. (IgG concentration was not increased proportionately for two reasons (i) only a limited amount of stock IgG solution was available to perform the experiments and (ii) regarding the hypothesis presented above with respect to quenching it was possible that by increasing IgG concentration in line with that of the QD then the quenching effect would have still rendered low final fluorescence values). Results are displayed in table 5.2.

Firstly it is important to comment on the fact that all fluorescence values measured were much higher than in the previous experiment. However in common with the previous experiment was the observation that fluorescence values were lower in control reactions where QDs were present with either IgG or EDC compared to where QD was present alone. The trend suggested by control reactions where QD:IgG and QD:EDC were present in the first experiment was not seen and in this case the QD:EDC control reaction produced a lower fluorescence value than that for QD:IgG. Interestingly all fluorescence measured remained above the filter in the retentate in this experiment indicating that the QDs, QD:EDC and QD:IgG mixtures and QD-IgG conjugates produced 'materials' which were either above the size exclusion limit of the filter or which had become non specifically absorbed to it removing them from the retentate. No fluorescence was observed in either retentate or flow-through for control reactions where only IgG was present. Results for the

various conjugation reactions shown in table 5.2. indicate a number of discernable trends, listed below.

Table 5.2. Fluorescence and absorbance data for conjugations with increased QD concentration.

Fluorescence and OD_{280} data for Retentate (R) and flow-through (FT) conjugations performed under varying conditions with ten times the quantity of QD per reaction. Units are arbitrary fluorescence values. Control reactions are highlighted in grey. N=3 for each value

	EDC:QD	QD:AB	R Fluor	R OD_{280}	FT Fluor	FT OD_{280}
1	40000:1	10:0.5	8.28±14.34	0.05±0.03	8.22±13.82	0.34±0.07
2	5000:1	10:0.5	297.90±175.23	0.40±0.06	3.94±6.82	0.13±0.01
3	1000:1	10:0.5	331.80±133.53	0.50±0.06	2.78±4.81	0.06±0.01
4	40000:1	10:1	6.62±4.73	0.08±0.06	2.26±1.06	0.44±0.01
5	5000:1	10:1	170.81±128.06	0.26±0.03	0.00±0.00	0.11±0.02
6	1000:1	10:1	217.32±152.25	0.28±0.002	3.61±3.86	0.08±0.04
7	40000:1	10:2	3.45±5.97	0.02±0.01	15.36±25.42	0.24±0.06
8	5000:1	10:2	23.63±23.04	0.10±0.04	3.64±4.29	0.09±0.02
9	1000:1	10:2	58.76±45.23	0.12±0.01	4.61±7.98	0.05±0.01
10	5000:1	10:0	18.19±20.72	0.04±0.02	5.29±5.74	0.08±0.01
11	0:1	10:1	153.94±177.94	0.29±0.03	0.37±0.65	0.04±0.02
12	0:1	10:0	665.72±213.17	0.26±0.03	1.04±0.63	0.02±0.01
13	0:0	0:1	-	0.03	-	-

Trend 1. A decrease in EDC concentration causes an increase in retentate fluorescence at constant IgG concentration

Trend 2. An increase in IgG concentration causes a decrease in retentate fluorescence.

Trend 3. A Decrease in EDC concentration causes an increase in Retentate OD_{280} constant IgG concentration.

Trend 4. An increase in IgG concentration causes a decrease in retentate OD_{280}.

Trend 5. A decrease in EDC concentration causes a decrease in flow-through fluorescence at constant IgG concentration.

Trend 6. A decrease in EDC concentration causes a decrease in flow-through OD_{280} irrespective of IgG concentration.

From table 5.2 greatest fluorescence was observed in those conjugation reactions where EDC and IgG concentration were lowest in terms of ratio to QD (rows 2 and 3). In later experiments (see section 5.3.4.) samples' fluorescence was correlated with IgG content and that conjugate judged to have the best balance in terms of fluorescence and IgG was eventually used in cellular imaging.

On the basis of the above results a third identical single experiment was conducted to investigate whether a further reduction in the concentration of EDC (and IgG) could lead to increased fluorescence of conjugates. Results are presented in table 5.3. It can be observed that in general further reduction of the concentration of EDC in the conjugation reactions led to increased retentate fluorescence values at constant IgG concentration and that reducing IgG had the same effect. There are exceptions, however this series of experiments was performed only once.

Another series of experiment was conducted in order to understand more fully the effects of EDC on QD fluorescence and OD_{280} in 'conjugates'. Firstly, fluorescence and OD_{280} values for the three different EDC solutions used in conjugation reactions were measured (See table 5.4A). It can be seen that fluorescence in all these samples was close to zero, but OD_{280} was EDC concentration dependent.

Secondly the fluorescence and OD_{280} values for mixtures of the three EDC solutions and a single QD concentration were measured (See table 5.4B). It this case it was observed that the presence of QDs increased the OD_{280} values by a similar amount for each EDC concentration, but that fluorescence of the three mixtures was more or less equal.

Table 5.3. Fluorescence and absorbance data for conjugations using lower EDC and IgG concentrations.

Fluorescence and OD_{280} data for Retentate (R) and flow-through (FT) for conjugations performed under varying conditions with lower ratios of EDC:QD and QD:IgG. Units are arbitrary fluorescence values. Control reactions are highlighted in grey.

EDC:QD	QD:AB	R Fluor	R OD_{280}	FT Fluor	FT OD_{280}
5000:1	10:1	267.16	0.20	0.00	0.10
1000:1	10:1	363.35	0.22	0.36	0.02
500:1	10:1	255.54	0.17	0.00	0.00
250:1	10:1	310.55	0.29	2.30	0.00
8:1	10:1	434.55	0.22	0.00	0.00
5000:1	10:0.5	295.52	0.19	4.25	0.03
1000:1	10:0.5	324.86	0.18	0.00	0.00
500:1	10:0.5	377.90	0.16	0.00	0.00
250:1	10:0.5	468.64	0.21	0.00	0.00
8:1	10:0.5	449.06	0.21	0.00	0.00
5000:1	10:0.1	118.02	0.00	14.66	0.00
1000:1	10:0.1	447.95	0.29	3.21	0.01
500:1	10:0.1	535.03	0.18	0.00	0.00
250:1	10:0.1	565.21	0.19	2.34	0.00
8:1	10:0.1	569.99	0.26	0.00	0.00
5000:1	10:0	23.39	0.00	8.45	0.09
0:1	10:1	427.90	0.27	13.56	0.00
0:1	10:0	737.14	0.18	0.00	0.00
0:0	0:1	-	0.03	-	-

Thirdly fluorescence and OD_{280} values for mixtures of the three EDC solutions and a single concentration of QD and IgG were measured before (i) and after separation (ii) by ultrafiltration (See table 5.4C(i)). In the case of (i) it was observed that the addition of IgG reduced fluorescence at the highest EDC concentration and that at the two lower concentrations fluorescence was almost equal. The addition of IgG produced no significant difference in OD_{280} compared to when only EDC and QDs were present.

After separation by ultrafiltration (material and methods section 2.5.5.) retentate and flow-through fractions were assayed for fluorescence and OD_{280}. Table 5.4.C(ii) illustrates results from these experiments where

Table 5.4. Fluorescence and absorbance data for mixtures of EDC, QD and IgG.

Fluorescence and OD_{280} data for different concentrations of EDC (A), mixtures of EDC and QDs (B) and mixtures of EDC, QDs and IgG before (C i) and after separation by ultrafiltration (C ii). R = retentate, FT = flow-through

A

EDC	Fluor	OD_{280}
40 000	5.28±0.76	0.68±0.001
5000	4.10±0.65	0.17±0.007
1000	1.73±0.55	0.02±0.006

B

EDC: QD	Fluor	OD_{280}
40 000:1	717.83±12.30	1.11±0.004
5000:1	810.15±5.87	0.49±0.004
1000:1	700.18±3.29	0.35±0.001

C

i Total		
EDC: QD: IgG	Fluor	OD_{280}
40 000:10:1	345.73±8.51	1.213±0.046
5000:10:1	713.33±63.55	0.471±0.009
1000:10:1	762.41±8.04	0.401±0.040

ii Separated				
EDC: QD: IgG	R Fluor	R OD_{280}	FT Fluor	FT OD_{280}
40 000:10:1	14.6±1.76	0.015±0.007	38.84±3.65	0.214±0.012
5000:10:1	181.73±34.76	0.214±0.020	10.40±4.39	0.041±0.007
1000:10:1	214.20±1.54	0.215±0.010	7.130.49	0.023±0.012

it can be seen that decreasing EDC concentration resulted in increased retentate fluorescence and OD_{280}. As EDC concentration was reduced flow-through fluorescence and OD_{280} decreased. These observations are consistent with the trends observed in tables 5.2. and 5.3.

5.3. Assay development for antibody content and biological activity of QD-IgG conjugates.

Once conjugates had been analysed for their fluorescence and OD_{280}, it was important to correlate these values with 'specific biological activity'. To achieve this, an assay was needed to deduce how much of the OD_{280} value observed actually 'related' to active IgG. A number of approaches were attempted to achieve this goal resulting in a final successful solution.

5.3.1. Well plate assay

In the first attempt at assay development a multi-well plate immunoassay type approach was implemented. In this experiment antigen (Cdc8) was linked to amino modified wells of 96 well NUNC microplate following the manufacturers protocol (materials and methods section 2.5.7.). Conjugates were reacted with antigen immobilised in the wells, the conjugate solution removed, wells were washed to remove any unbound material and fluorescence measured as an indication of bound conjugate.

To determine the amount of antigen required to saturate a well, 100 µl of a range of antigen solutions at varying concentrations (20 to 100 µg ml^{-1}) were incubated a series of wells. Antigen solutions were then removed from the wells and assayed for protein concentration (subtraction assay by Bradford, gel densitometry or OD_{280}). Unfortunately the difference between starting antigen solution concentration and solution concentration post incubation with the wells was too small to measure using these methods. Consequently a large excess in antigen solution

concentration was employed in all experiments so as to ensure complete saturation of the wells.

An indirect measure of confirmation of antigen immobilisation and well saturation involved incubating unlabeled Cdc8 antibody with the antigen coated wells, washing the wells and then adding FITC labelled secondary antibody. Fluorescence detected in the wells indicated the presence of the antigen and confirmed that the wells/plates could be used in QD-conjugate experiments. This experiment was accompanied by a control in which QD alone was incubated with the antigen coated wells, the wells were washed and assayed for fluorescence. Some fluorescence was detected indicating that a small amount of nonspecific binding of the QDs to wells had taken place. To prevent this from occurring a further experiment was undertaken in which QDs were incubated in a similar fashion with the wells with a blocking agent, 0.1%w/v BSA. In this case no fluorescence was observed in the wells. Results are displayed in table 5.5.

Table 5.5. The effect of BSA on non-specific binding of QDs to multi-well plates.

Fluorescence values for wells containing QDs in PBS or PBS alone, with or without 0.1% BSA. Samples were removed and wells were washed prior to measurement. N=3.

	PBS	QD + PBS
- BSA	8.46 ± 1.61	19.61 ± 3.62
+ BSA	6.75 ± 3.13	7.78 ± 8.42

QD-IgG conjugates (5000:1 EDC:QD, 10:1 QD:IgG) were produced (as described previously) and incubated in wells with immobilised antigen (see materials and methods section 2.5.7.) and fluorescence intensity from the QD wells were compared with that from control wells incubated with PBS. Observed values were low and no difference between QD or PBS fluorescence was observed despite repeating the experiment

several times. One possible reason for this lack of fluorescence was that the amount of IgG incorporated in the QD-IgG conjugate was so little that the amount bound to the wells was undetectable.

5.3.2. Western blot detection

In a second attempt at assay development a western blotting type approach was adopted. In this experiment a known quantity of antigen (Cdc8), separated by SDS-PAGE was blotted using a BioRad semi dry electroblotter onto a Polyvinylidene Difluoride (PVDF) membrane. and challenged with conjugates produced using three different IgG concentrations and one EDC concentration (10:0.5, 10:1 and 10:2 QD:IgG and 5000:1 EDC:QD) as previously described (see section 2.5.2).

Specifically 25 µl samples of a 5 µM Cdc8 solution were subjected to electrophoresis on a 12.5% SDS gel and blotted on to a PVDF membrane using a BioRad semi dry electro-blotter, following the manufacturers instructions. The membrane was cut into strips, with one Tm band present on each strip. Each membrane strip was probed (see materials and methods 2.5.8.) with one of the three different QD IgG conjugates. A control strip was also included which was probed with an unlabeled primary antibody. No fluorescence was detected from the QD-IgG conjugate probed strips (figure 5.1A) but all strips (control included) were then incubated with a secondary FITC conjugated antibody and assayed for fluorescence. In this case, fluorescence was visible (figure 5.1B) in the case of all strips, with greatest fluorescence resulting from the strip which had been probed with the QD-IgG conjugate produced using the greatest amount of antibody. This suggests that the QD-IgG conjugates were binding to the immobilised antigen but that their fluorescence was in some way obscured. This could have been due to the quantity of QD in the conjugate being too small to detect by the phosphoimager. Alternatively that binding of the conjugate to the antigen immobilised on the membrane had inhibited their fluorescence.
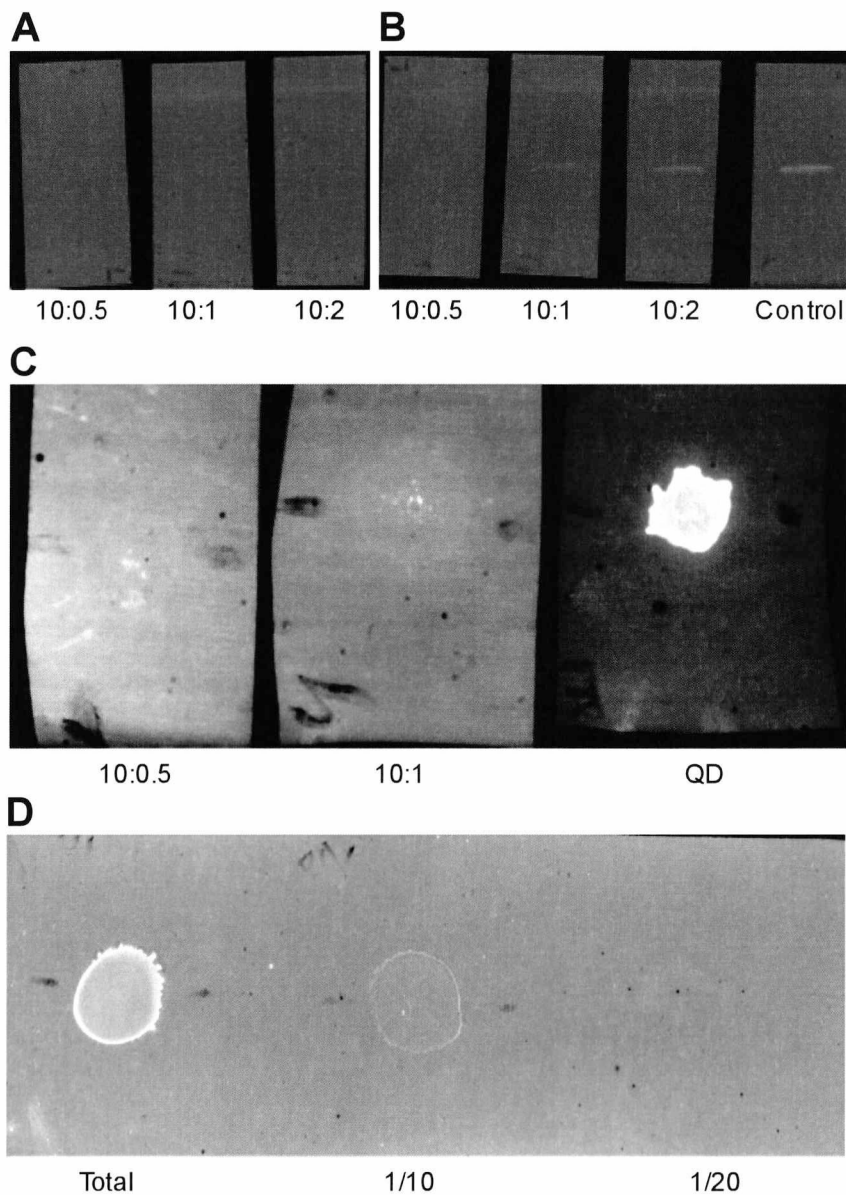
Figure 5.1. Conjugate detection on PVDF membranes

(A) Fission yeast tropomyosin was run on a 12.5% SDS gel and
blotted on to a PVDF membrane. The membrane was cut into strips
and each strip probed with a different QD-IgG conjugate (10:0.5,
10:1 and 10:2 QD:IgG, all produced with 5000:1 EDC:QD), A strip
was also probed with unlabeled anti-Cdc8 (control). Strips were
imaged in a phosphoimager. (B) Strips were probed with an anti-
rabbit FITC secondary antibody conjugate and re-imaged. (C) 20µl
of QD (1 in 10 dilution) and two QD-IgG conjugates (10:0.5 and 10:1
QD:IgG, 5000:1 EDC:QD) were applied directly to an activated
membrane dried and imaged. (D) 100µl of a mixture of QDs and IgG
(10:1 QD:IgG) and two dilutions of that mixture were spotted on to a
membrane, dried and imaged.

To determine if QDs fluoresced on PVDF membrane, an amount of QDs equal to that used in conjugation reactions was spotted onto a PVDF membrane along with two QD-IgG conjugates (10:0.5 and 10:1 QD:IgG, 5000:1 EDC:QD) and allowed to dry. A fluorescent signal was detected from the QD only sample (figure 5.1C) but no obvious fluorescence was observed from the conjugate spots. It seemed probable that something in the conjugate; most likely the antibody was responsible for QD 'quenching'. In a brief attempt to determine if conjugation of IgG to QD or simple presence of IgG and QD together was responsible for the 'quenching' effect a 100 μl mixture (with no conjugation) of QDs and IgG (10:1 QD:IgG) as well as its 1 in 10 and 1 in 20 dilutions were spotted to a PVDF membrane and dried. When placed in the phosphoimager fluorescence was observed from the undiluted mixture (figure 5.1D) but with a much reduced intensity compared to that seen from QDs alone (figure 5.1C). The 1 in 10 dilution produced a very weak signal and the 1 in 20 dilution produced no signal. These results indicated that conjugation of the protein to QD was not necessary to produce the 'quenching' effect.

5.3.3. Magnetic bead agglutination assay.

In a third attempt at assay development a bead agglutination type assay (Suresh and Arp, 1993) was adopted. Superparamagnetic nano-beads coated with antigen were incubated with the QD-IgG conjugates. It was assumed probable that each QD would have more than one IgG molecule conjugated to its surface. As the Cdc8 antibody was polyclonal its various isoforms possess the ability to recognise different epitopes on the antigen. This characteristic could used to cross link the particles in suspension and a resulting decrease in suspension turbidity could be measured by spectroscopy at OD_{595} (see figure 5.2. for a diagrammatic representation of the process)

Binding of antigen to the magnetic beads was standardised (see materials and methods section 2.5.10) and it was found that 20μg of antigen (Cdc8) was sufficient to saturate the surface of 1mg of beads. 1

mg of antigen coupled beads were placed in the wells of a transparent
microtitre plate and 100µl of QD-IgG conjugates (1000:1 EDC:QD, 10:1
QD:IgG) were incubated with the them for 1 hour at room temperature. A
control was included using beads which had not been conjugated with
antibody. At the end of that period turbidity of the samples was measured
by recording optical density at OD_{595}. No differences between wells
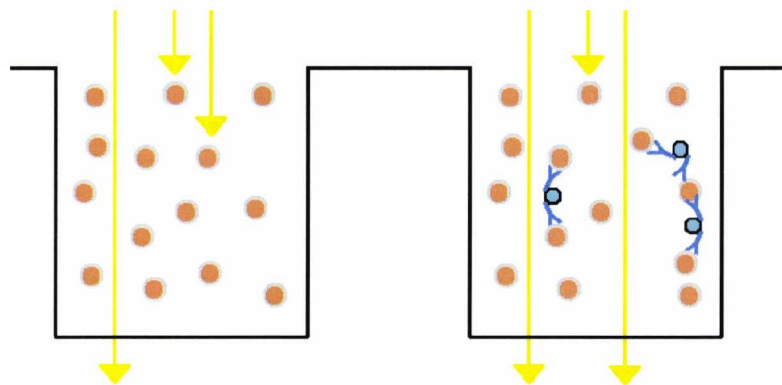
Figure 5.2. Diagram of magnetic bead agglutination

QDs (turquoise) conjugated to multiple polyclonal antibodies (blue)
can react with several antigen coupled nanobeads (orange/grey),
decreasing turbidity and allowing more light (yellow arrows) to pass
through.

containing conjugate and control were detected. In this case one possible
reason for failure was that the amount of IgG incorporated in the QD-IgG
conjugates was so little that degree of agglutination in the solution was
too small to detect.

5.3.4. Membrane spotting assay

In a final and successful attempt at assay development a sandwich type
immuno-assay approached was adopted in which conjugates were dried
directly onto a PVDF membrane then reacted with an alkaline
phosphatase coupled secondary antibody. A soluble uncoloured
substrate was then added which could be converted to an insoluble blue

product by the enzyme. Blue colour development depended on the amount of enzyme present and time of incubation. (see materials and methods section 2.5.11.).

In this assay it was first necessary to produce a standard curve against which blue colour development in samples could be compared. To do so a dilution series (12.3 to 0.6 picomoles in 100 μl) of unlabeled anti-Cdc8 was prepared in PBS and applied to a PVDF membrane. This was then reacted with a solution of anti-rabbit alkaline phosphatase secondary antibody (1 in 10 000 dilution) (Sigma) at 25°C for a period of 60 minutes. Subsequently the membranes were washed in PBS and a solution of the colour development reagent added (BCIP®/NBT Liquid Substrate System – Sigma-Aldrich) and left to develop for 5, 10 and 20 minutes.

After those time intervals the membranes were again washed in PBS and spot intensity determined as described in the materials and methods (see materials and methods section 2.5.11.) When data relating to spot intensity was plotted against antibody concentration the curves were not linear (figure 5.3B). Attempts at linearising the curves first involved plotting log antibody concentration against colour intensity (figure 5.3C) which improved their linearity. Although still not entirely linear the 10 minute curve was selected as optimum and this time was used in all subsequent experiments for colour reagent development. Subsequent attempts at improved linearisation of the data using Lineweaver-Burk and Eadie-Hofstee transformations were unsuccessful.

Chapter 5: Research, development and optimisation of quantum dot-antibody conjugates for imaging tropomyosin localisation in *S. pombe*.

144
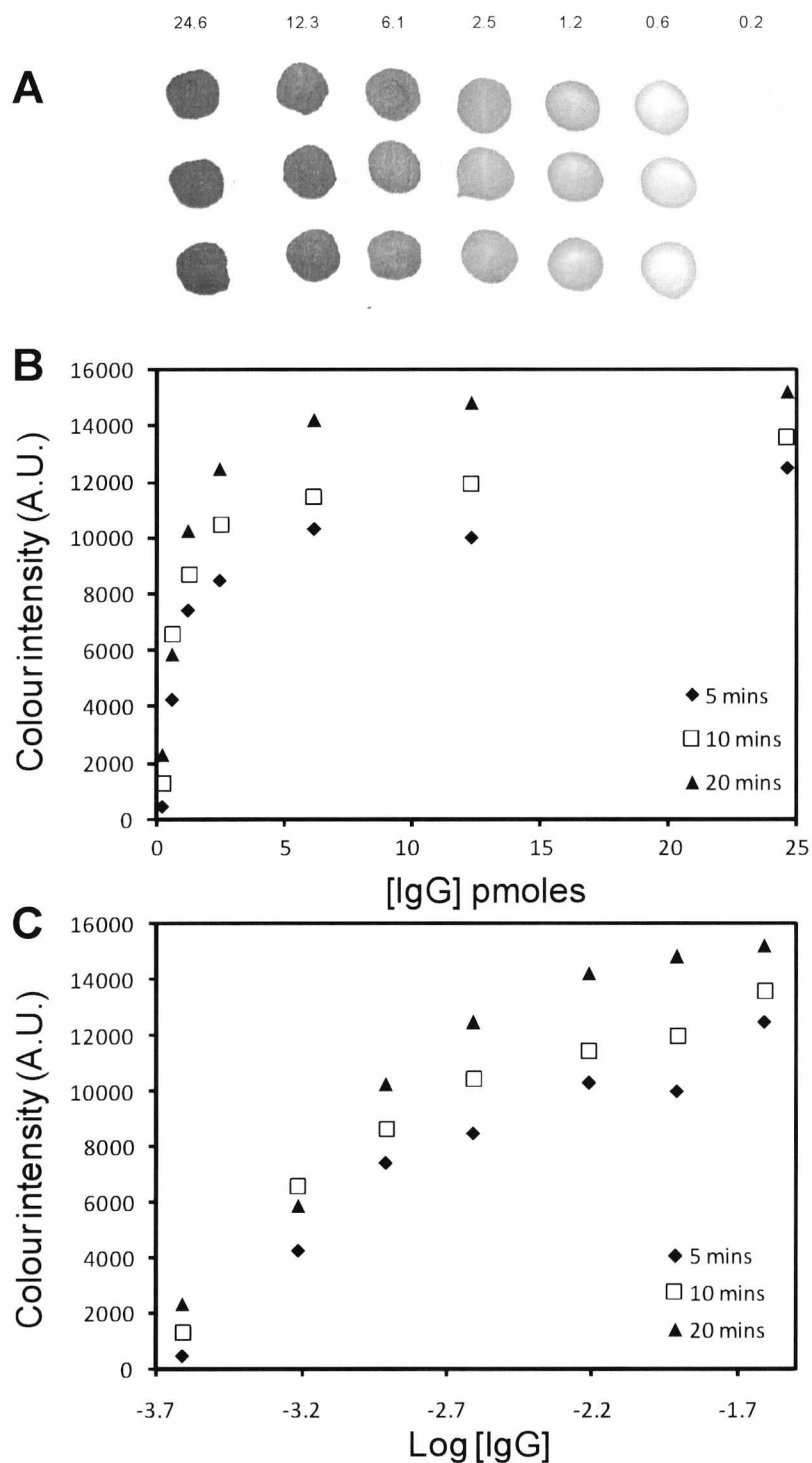
Figure 5.3. Optimisation of membrane development time

(A) An example of a PVDF membrane spotted with known concentrations of anti-Cdc8 antibodies in triplicate developed for 10 minutes. Amounts are in picomoles. (B) Spot intensity against antibody concentration for membranes developed for 5, 10 and 20 minutes (C) Spot intensity against log antibody concentration for membranes developed for 5, 10 and 20 minutes.

Chapter 5: Research, development and optimisation of quantum dot-antibody conjugates for imaging tropomyosin localisation in *S. pombe*.

145

A

| | 1.2×10^{-2} | 6.1×10^{-3} | 2.4×10^{-3} | 1.2×10^{-3} | 6.1×10^{-4} |

Standards

Sample   1   2   3   4   5   6   7   8   9   10   11   12   13   14
Retentate

Flow-through

B

$$y = 7183.2x + 24301$$

Density (A.U.) vs Log [IgG]
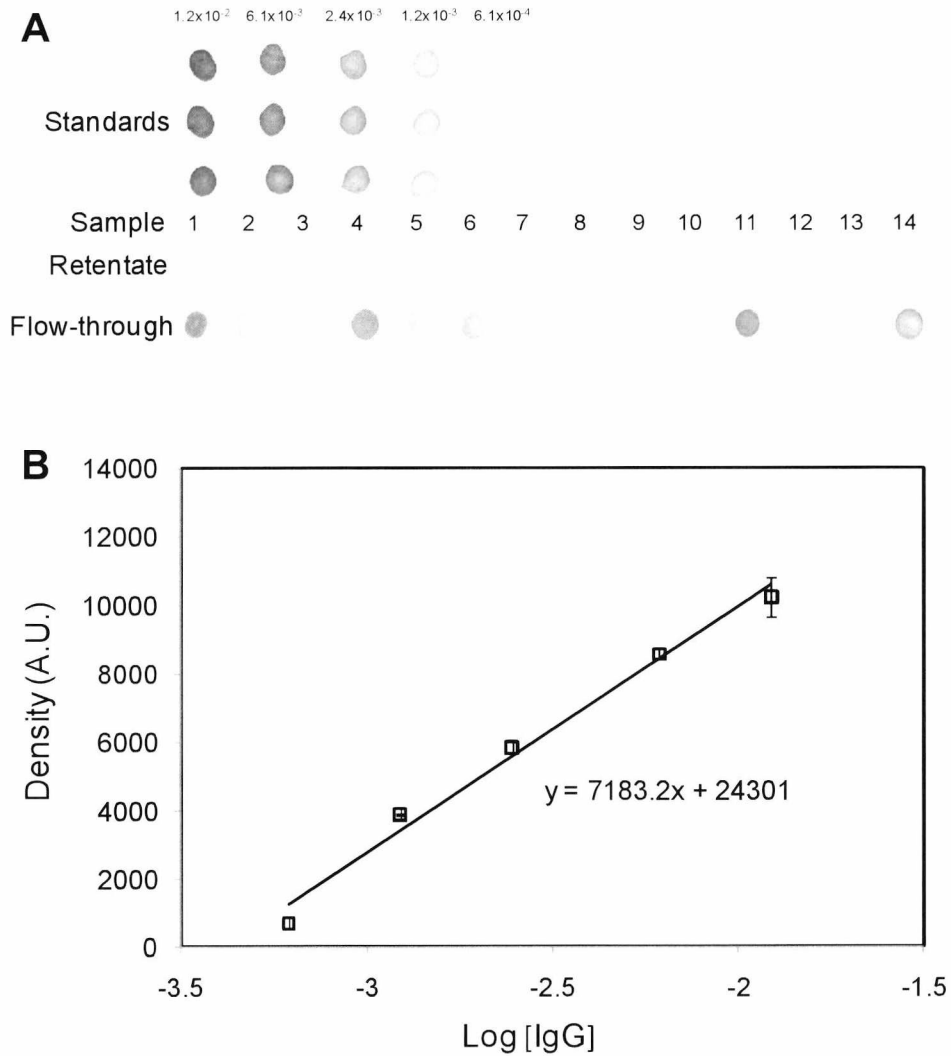
Figure 5.4. Membrane spotting assay

(A) An example of a developed PVDF membrane spotted with known concentrations of anti-Cdc8 antibodies and the retentate and flow-through of 14 samples. (B) A standard of anti-Cdc8 antibody concentration was constructed from the average of 3 values at each antibody concentration. Unknown antibody concentration in each sample was calculated using the gradient of the trend line.

A standard curve was constructed as part of each sample assay to ensure comparability within experiments, samples to standards. A series of conjugates produced under various conditions (40 000:1, 5000:1, 1000:1 EDC:QD and 10:1, 10:0.5, 10:0.1 QD:IgG) were assayed using this method and one example of a developed membrane is presented in figure 5.4A. The standard curve for this experiment is also presented. Table 5.5 integrates data obtained from the QD-IgG conjugation (fluorescence and OD_{280}) with data from the spotting assay.

From table 5.5 a 5000:1 EDC:QD ratio appears to be the optimum for conjugation (highlighted green) regardless of antibody concentration. Ratios of 40000:1 and 1000:1 always resulted in conjugates possessing little to no IgG. The ratio 10:0.5 QD to IgG resulted in a conjugate containing the highest percentage (11.83%) of IgG when compared to the amount added in the reaction, and the greatest amount of IgG, 3.88×10^{-4} nmoles. Lower ratios of QD to IgG result in a greater percentage IgG detectable in flow-through fractions. In addition in these cases none of the retentate/flow-through percentages total 100%, indicating that IgG is probably lost on the filter membrane during separation

Table 5.5. Fluorescence, OD$_{280}$ and quantity of IgG present in QD-IgG conjugates.

Fluorescence and OD$_{280}$ data for retentate (R) and flow-through (FT) of QD-IgG conjugates produced under various conditions. The concentration of IgG present in both retentate and flow-through determined colourimetrically is displayed in nanomoles, and is also expressed as a percentage of the total IgG added to the reaction. Optimum conditions are highlighted in green, control reactions are highlighted in grey. The reaction EDC:QD 0:1, QD:IgG 10:0 (yellow highlight) was not subjected to filtration, but was used in the colourimetric assay.

	EDC:QD	QD:AB	R Fluor	R OD$_{280}$	FT Fluor	FT OD$_{280}$	R [IgG]	FT [IgG]	R % TOTAL	FT % TOTAL
1	40000:1	10:1	17.09	0.01	11.44	0.38	0.00E+00	1.03E-02	0.00	82.72
2	5000:1	10:1	146.94	0.22	13.11	0.14	3.34E-04	3.16E-03	7.53	57.70
3	1000:1	10:1	210.15	0.23	5.43	0.06	1.23E-04	4.28E-04	0.96	14.04
4	40000:1	10:0.5	9.62	0.02	11.04	0.41	0.00E+00	3.89E-03	0.00	85.35
5	5000:1	10:0.5	183.90	0.25	8.35	0.09	3.88E-04	1.00E-03	11.83	39.15
6	1000:1	10:0.5	211.06	0.14	14.65	0.06	3.88E-05	1.36E-03	0.04	44.09
7	40000:1	10:0.1	10.69	0.03	8.31	0.57	0.00E+00	3.74E-04	0.00	25.65
8	5000:1	10:0.1	147.09	0.15	13.91	0.08	1.85E-04	4.41E-05	1.73	1.87
9	1000:1	10:0.1	258.57	0.18	26.72	0.04	3.89E-05	2.24E-04	0.12	1.91
10	5000:1	10:0	66.35	0.10	11.71	0.08	0.00E+00	0.00E+00	0.00	0.00
11	0:1	10:1	291.00	0.23	2.24	0.05	4.11E-04	2.37E-03	8.52	53.98
12	0:1	10:0	299.43	0.20	14.15	0.02	0.00E+00	0.00E+00	0.00	0.00
13	0:1	10:0	804.31	-	1.38	-	0.00E+00	0.00E+00	0.00	0.00
14	0:0	0:1	4.73	0.00	-0.86	0.04	0.00E+00	3.03E-03	0.00	58.73

5.4. A comparison QD-IgG conjugate and a FITC-IgG conjugate photobleaching characteristics

A well reported property of quantum dots is their resistance to photobleaching (Alivisatos et al., 2005; Bruchez et al., 1998). This property is advantageous in biological imaging applications as QDs potentially allow imaging over much longer time scales. Their intrinsically greater level of fluorescence would also increase imaging capabilities. In addition when imaging fluorescently labelled cells, the slide on which they are fixed must be scanned for a single cell or group of cells of sufficient quality to use for experimental purposes. Classical fluorophores fade quickly during this process and well labelled cells must be located and imaged quickly to avoid losing image quality. QD-IgG conjugates would overcome this problem and the slide can be scanned for long periods, without any noticeable decrease in fluorescence intensity. QDs would also allow the possibility of storing fixed calls for re-imaging for longer than cells labelled with classical fluorophores.

In order to compare relative resistance to photobleaching of the QD-IgG conjugate and classical fluorophore, a bleaching experiment was performed. Equivalent samples of an FITC conjugated anti-rabbit antibody (Sigma) and a QD-IgG conjugate (produced using optimum conditions – see section 5.3.4.) were Illuminated with a white light source in a fluorescence microscope (see materials and methods section 2.4.1.) Fluorescence intensity for the two materials recorded over time. The values were normalised by expressing each intensity value as a decimal of the maximum observed intensity, and plotted as a graph (figure 5.5). While the FITC had 'bleached' to background level with in 200 seconds, the QD still remained fluorescent after 600 seconds.
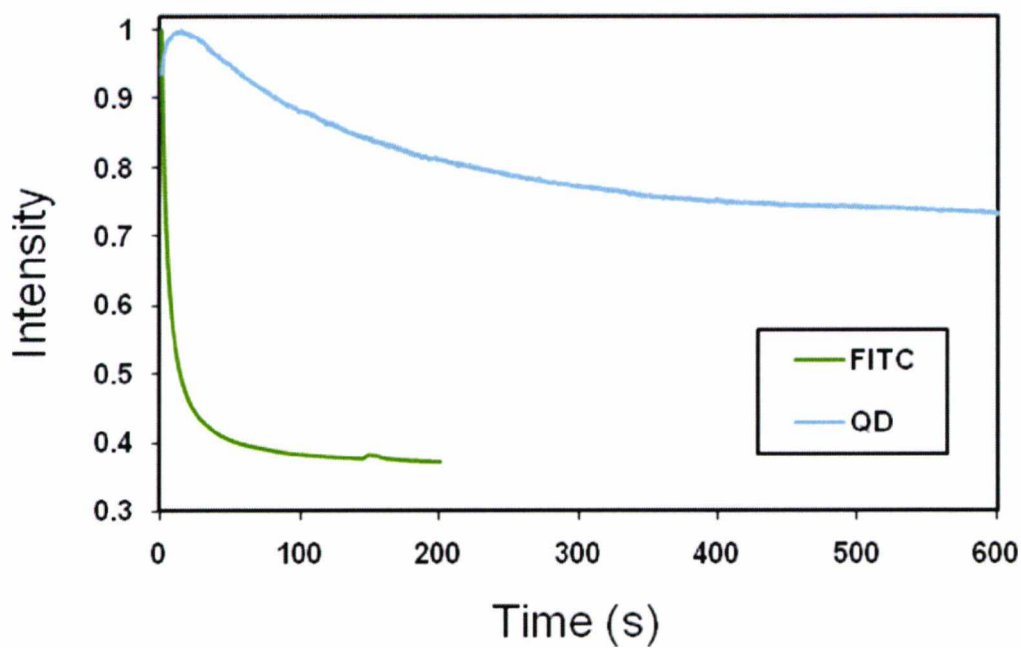
Figure 5.5. The effects of photo bleaching on a QD-IgG conjugate and a FITC-IgG conjugate.

Fluorescent intensity of a QD-IgG conjugate and a FITC-IgG conjugate over time. Values for intensity have been normalised against the maximum for each fluorophore.

5.5. Cellular imaging using quantum dot-antibody conjugates.

To assess the optimised QD-IgG conjugate in an imaging application, immunofluorescence microscopy was used. As a consequence of Evident Technologies Evitags® withdrawing from the bioscience market, the recommended alternative, eBioscience's eflour™ nanocrystals were used in the production of conjugates used in these experiments.

WT *S. pombe* cells were grown to mid log phase, were fixed, permeablised (see materials and methods 2.4.2.). and incubated with conjugates produced using the optimum conditions, highlighted green in table 5.5. An additional step to quench EDC activated, but non antibody conjugated QD surface groups was included in the production of these conjugates.(Such groups could have potentially reacted with any amine group on the cell surface or its interior leading to a decrease in the labelling efficiency through non specific chemisorptions). This involved incubating the conjugate with 50mM Tris pH 7.0 for 15 minutes after separation and before washing steps. In cells probed with QD-IgG conjugates not subject to this step non specific background fluorescence was observed (data not shown).

Images were taken from cells labelled with a QD-IgG conjugate, and compared with images from cells probed with an unlabelled primary antibody and complimentary FITC labelled secondary antibody. In a control experiment cells probed with EDC activated, but IgG free QDs, no discrete fluorescent labelling was observed (data not shown).

The top 2 panels of figure 5.6 show cells imaged with FITC and QDs. The CAR is clearly visible. These images are composites composed of multiple images taken at different focal planes throughout the cell, which are then flattened into a two dimensional image (maximum projection). Images were captured under the identical exposure conditions, and are directly comparable. It is immediately evident that the image acquired with the QDs is significantly brighter than the FITC image. The bottom panels show the digitally deconvolved version of the image (see materials
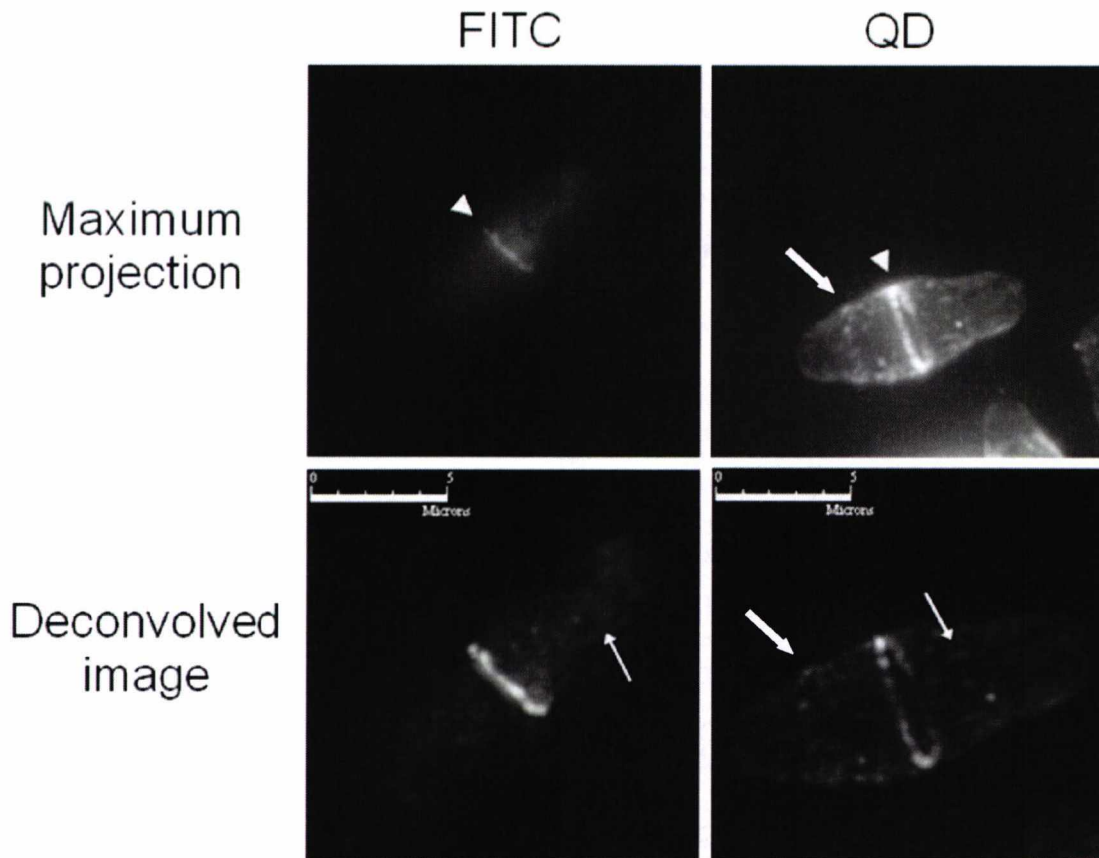
Figure 5.6. A comparison of Quantum dot and FITC immunofluorescence.

Immunofluorescence microscopy was performed against Cdc8 in WT *S. pombe* cells using a QD labelled primary antibody (direct), and a FITC labelled secondary antibody (indirect). The top two panels show a maximum projection of 21 sections taken at separate focal planes, using identical exposure settings. The CAR is clearly visible (arrow heads). The bottom two panels show the same cells after deconvolution by imaging software. Cdc8 decorated actin filaments can be seen (fine arrows). An unknown structure can be observed in the images produced with QDs (thick arrows). Scale bar equal to 5 microns.

and methods 2.4.1.). Digital deconvolution is a process that removes background fluorescence and sharpens the image to produce the best possible picture. In this process contrast and brightness is automatically adjusted to an optimum, and it is not therefore possible to directly compare fluorescence intensity between the two methods. However the image produced using QDs is at least as good as the FITC image, and the signal appears sharper and more detailed in the case of the QD conjugate. Cdc8 localised to actin filaments around the cell periphery can also be observed in both images, but appears more discrete in the image produced using QD-IgG conjugates. Cdc8 decorated actin cables can also be observed in the QD composite image, in the FITC image however they are indistinguishable from the background.

Another distinct structure can also be observed in the images produced using the QD-IgG conjugates. The structure resembles as cortical ring, located close to the cell tip (figure 5.6, thick arrows) however the only structure like this previously reported is the acto-myosin ring at the medial plane of cells undergoing mitosis This structure is as yet unknown, however it has been observed previously when imaging other actin associated proteins with classical fluorophores (Dan Mulvihill, personal communication). One possibility is that this structure is a 'scar' of CAR proteins left from a previous cell division. This structure has never been observed when imaging Cdc8 with classical fluorophores. This implies that QDs maybe advantageous for imaging previously unseen cellular structures.

Summary

During this part of the project a thorough investigation into the variables involved in producing quantum-antibody conjugates, was undertaken. It was evident from early experiments that the manufacturer's literature regarding conjugation and separation of QD-IgG conjugates was unreliable.

Through a logical series of experiments, the optimum conditions for conjugate production were elucidated, yielding a product with high fluorescence intensity and greatest antibody content. It was observed that the antibodies can cause fluorescence quenching of QDs in a concentration dependent manner. Alone, the EDC crosslinker did not have a quenching effect, however in conjunction with IgG, a fluorescence quenching effect was observed. QD-IgG conjugates produced underoptimum conditions were successfully used in immunoflourescence microscopy experiments. They produced an image that was brighter than a classical organic fluorophore, with sharper details enabling an as yet unidentified structure to be resolved. The QD-IgG conjugates were also substantially more resistant to photobleaching than the organic fluorophore.

Chapter 6: Discussion

Introduction

During the course of this study mutations were introduced in to the amino terminus of the fission yeast Tm Cdc8 to investigate the importance of this region for protein function. Biochemical analysis of the properties and function of these mutant Cdc8 proteins revealed that modification of the amino terminus affected the thermostability of the protein and its ability to form end-to-end interactions. In addition amino terminal modification altered the affinity of the protein for actin. Changes in affinity were subsequently reflected in the ability of the mutant Cdc8 proteins to regulate myosin S1 ATPase activity.

Despite changes to their biochemical properties, Cdc8 proteins expressed in a temperature sensitive *S. pombe* strain were able to complement function at the restrictive temperature. However, when expressed in a N α-acetyltransferase deficient strain of *S. pombe* the mutant Cdc8 proteins were unable to rescue the growth defects associated with this strain.

Finally a method of conjugating QDs to anti-Cdc8 antibodies was developed along with a detailed understanding of the variables involved in the conjugation process. The conjugates produced superior images when compared to organic fluorophores and were significantly more resistant to photobleaching.

6.1. Thermostability of wild type and mutant Cdc8 proteins.

In order to assess the effect of single amino acid substitutions at the amino terminus of Cdc8 on protein stability, thermal unfolding studies were performed using circular dichroism. At the salt concentration used in these experiments (500 mM) end-to-end interaction between Cdc8

dimers would have been absent (figure 3.5). The observed results therefore are a result of dimer dissociation and denaturation of the α-helices, and not of dissociation of end-to-end interactions. For each protein single phase curves indicated that the Cdc8 dimer dissociated at the same time as the protein denatured (figure 3.4).

Acetylation of Cdc8 increased mid-point melting temperature (T_m) only slightly (0.7^0C) however the change in enthalpy (ΔH) was increased by approximately 27 kJ mol^{-1}, compared to the unacetylated protein, suggesting that while acetylation does not convey resistance to higher temperatures it stabilises Cdc8 requiring more energy to melt the protein. This is consistent with observations that acetylation masks the charge of the amino terminal methionine allowing the amino terminus to adopt a more stable, fully helical conformation (Brown et al., 2001). It has also been reported that the acetyl group on one Tm α-helix can participate in an inter-helix hydrophobic interaction with the first methionine from the other α-helix (Greenfield et al., 1994). This effect could also account for the stabilising effect of amino terminal acetylation in Cdc8.

The lower ΔH of the unacetylated Cdc8 could be explained by the observation that in an unacetylated Tm the first two residues are predicted to be non helical and therefore do not form a coiled-coil or have inter-chain interactions (Brown et al., 2001). The dimer and individual helices in this case are partially disordered at the amino terminus and less energy is required to melt the protein. A more dramatic effect was observed with the Cdc8-D2A protein. The T_m dropped by over 2^0C (table 3.3) with a corresponding decrease in ΔH of approximately 16 kJ mol^{-1}. The first methionine in Tms beginning in sequence with Met-Ala, is cleaved when produced in *E. coli* (Monteiro et al., 1994) and this is also true for the Cdc8-D2A mutant (table 3.2.). This observation suggests that the first methionine, or having a complete heptad sequence at the amino terminus is important for α-helix and dimer stabilisation.

The removal of the negative charge at the E6 position of Cdc8 (E6A) had no effect on T_m or ΔH. The reversal of charge at the E6 position of Cdc8

	A	**B**	**C**
	abcdefg	abcdefg	abcdefg
1	MDKLREK	MDKLREK	MDKLREK
8	INAARAE	INAARAE	INAARAE
15	TDEAVAR	TDEAVAR	TDEAVAR
22	AEAAEAK	AEAAEAK	AEAAEAK
29	LKEVELQ	LKEVELQ	LKEVELQ
36	LSLKEQE	LSLKEQE	LSLKEQE
43	YESLSRK	YESLSRK	YESLSRK
50	SEAAESQ	SEAAESQ	SEAAESQ
57	LEELEEE	LEELEEE	LEELEEE
64	TKQLRLK	TKQLRLK	TKQLRLK
71	ADNEDIQ	ADNEDIQ	ADNEDIQ
78	KTEAEQL	KTEAEQL	KTEAEQL
85	SRKVELL	SRKVELL	SRKVELL
92	EEELETN	EEELETN	EEELETN
99	DKLLRET	DKLLRET	DKLLRET
106	TEKMRQT	TEKMRQT	TEKMRQT
113	DVKAEHF	DVKAEHF	DVKAEHF
120	ERRVQSL	ERRVQSL	ERRVQSL
127	ERERDDM	ERERDDM	ERERDDM
134	EQKLEEM	EQKLEEM	EQKLEEM
141	TDKYTKV	TDKYTKV	TDKYTKV
148	KAELDEV	KAELDEV	KAELDEV
155	HQALEDL	HQALEDL	HQALEDL

Figure 6.1. Alignment of Cdc8 heptad repeats

The amino acid sequence of Cdc8 aligned vertically in groups of heptad repeats. Mutations introduced in this study are highlighted in bold. Mutations identified in the *cdc8-110* gene are marked in blue font colour. (A) Alanine residues in 'core' positions are highlighted in grey. (B) Positively and negatively charged amino acid residues predicted to be involved in inter-chain ionic interactions are highlighted in green and red respectively. (C) Acidic, negatively charged amino acid residues, predicted to interact with actin are highlighted in red. Residues marked in red font colour are close to the predicted overlap region and less likely to be involved in actin interactions.

(E6K) decreased ΔH whereas the removal of the negative charge at the D16 position (D16A) increased ΔH. In coiled-coils inter-chain stability is increased by ionic interactions ('salt bridges') between residues in *e* and *g* positions (McLachlan et al., 1975, figure 1.16). As neither of these modifications are to residues predicted to be in salt bridge-forming positions the effect is likely due to stabilising or destabilising effects on the α-helix and not inter-chain interactions.

The Cdc8-LKL mutation substantially increased T_m by 2.6 ^{0}C and ΔH by approximately 33 kJ mol^{-1}. Coiled-coil dimers are stabilised by hydrophobic interactions between amino acid side chains in 'core' *a* and *d* positions (Crick., 1953, figure 1.16) and Tms contain alanine residues in some 'core' positions to introduce local instability and impart a bend in the coiled coil (Brown et al., 2005; Kwok and Hodges, 2004). The substitution of alanine, a destabilising residue at *d* position 11, (figure 6.1.A.), for Leucine, a stabilising residue, might improve thermostability by improving amino acid side chain packing in at the helix interface.

Also, in wild type Cdc8 the residues at salt bridge forming positions 7 and 12 (*g* and *e* respectively) are both positively charged (figure 6.1.B.). Substitution of Arginine at position 12, with lysine which is less positively charged, might reduce electrostatic repulsion between these positions and increase dimer stability. In addition to inter-helix stabilisation the change in relative residue size at each position (11,12,13) could affect α-helical stability; the wild type ARA motif is 'small-big-small' where as the LKL motif is 'bigger-smaller-bigger'.

From these results it is impossible to determine which of these factors is responsible for the effect observed. Additional studies substituting single amino acids at these positions would be useful in determining the importance of each amino acid residue. In addition a more definitive explanation for the effects of each amino terminal mutation could be achieved through a structural study of the Cdc8 overlap complex.

6.2. End-to-end interaction of wild type and mutant Cdc8 proteins.

The amino terminus of Tm is required for the formation of end-to-end interactions and modifications to the amino acid sequence can alter the ability to form polymers (Coulton et al., 2008; Hitchcock-DeGregori and Heald, 1987; Sano et al., 2000). A viscosity assay was used to study the effect the amino terminal amino acid substitutions on the ability of Cdc8 to form end-to-end connections, and the strength of these interactions.

The carboxyl terminus of Tms splay apart to allow the insertion of the amino terminus of another Tm dimer (Greenfield et al., 2006) and acetylated Tm is fully helical to the amino terminus where as the first 2 residues in an unacetylated Tm are non helical (Brown et al., 2001). It has been suggested that the amino terminus of Tm must be able to form a fully folded α-helical coiled coil to form a strong overlap with the carboxyl terminus (Palm et al., 2003). Consistent with this, acetylation of Cdc8 greatly increases its ability to polymerise and the strength of the end-to-end interactions (figure 3.5), as much higher salt concentrations are required to disrupt end-to-end binding. The acetylated Cdc8 is presumably fully helical at the amino terminus allowing unhindered insertion into the carboxyl terminal cleft, whereas the unacetylated protein is likely to be non helical at the amino terminus and as such interacts more weakly with other Tm dimers. However the Cdc8-D2A mutant which lacks the amino terminal methionine, is unable to form end-to-end interactions. Hydrophobic interactions between dimers is reported in Tm overlap complexes (Greenfield et al., 2006). The inability of Cdc8-D2A to form filaments suggests that the first methionine (a hydrophobic residue) may be important for end-to-end interaction possibly by forming hydrophobic interaction with the chains of the adjoining dimer. Equally an aspartic acid residue at position 2 may be required for formation of an overlap complex.

In addition to hydrophobic interactions in the Tm overlap complex, ionic interactions between charged amino acid residues are thought to play a role in the affinity of the Tm amino terminus for the carboxyl terminus

(Greenfield et al., 2006). The number of amino acid residues involved in the overlap varies between Tm isoforms (Tobacman, 2008) but is approximately 11 residues in muscle Tm. The overlap region between *S. cerevisiae* Tms is much shorter than in muscle Tm (Tobacman, 2008), as Cdc8 is similar in size to *S. cerevisiae* Tms the Cdc8 overlap region is likely to be correspondingly shorter. Nonetheless, the negatively charged glutamic acid at position 6 is likely to be within, or close to, the Cdc8 overlap region. Removal of this negative charge or its reversal, in the Cdc8-E6A and -E6K mutants respectively, increased the viscosity of the proteins to a value comparable with the acetylated Cdc8 (table 3.4). This suggests that the negative charge at this position in the wild type protein reduces end-to-end interactions possibly by an electrostatic repulsion between Tm dimers or between residues in the in the α-helix.

Interestingly the Cdc8-D16A and Cdc8–LKL mutants, where the residues involved are unlikely to be in the overlap complex, were able to increase end-to end interaction (table 3.4). The Cdc8-D16A mutation which falls in the *b* position of the heptad repeat, is unlikely to have hydrophobic or inter-chain interactions, therefore the effect is more likely a consequence of sequence changes transmitted along the structure of the alpha helix. The Cdc8-LKL mutation significantly increased the ability of the protein to polymerise and the strength of the interactions (figure 3.4), due to a less obvious consequences of this 3 amino acid substitution. The first substitution (Ala to Leu) at position 11 is part of an alanine cluster (figure 6.1.A.) thought to cause local instability and impart bends to vertebrate Tm dimers, facilitating their superhelical shape when bound to actin (Brown et al., 2005; Kwok and Hodges, 2004). The minimum effective size of alanine clusters is thought to be three residues (Lu and Hodges, 2004). If Cdc8 has a specific bend close to the amino terminus resulting from the cluster of 3 'core' positions alanines, replacement of a destabilising alanine with a stabilising leucine, could disrupt the formation of a bend. In doing so the conformational change could enhance end-to-end binding. Additionally replacement of positively charged arginine with the less positively charged lysine at *e* position 12 could favour end-to-end

interaction by reducing inter chain electrostatic repulsion, in a mechanism similar to the one proposed for increasing thermostability (section 6.1). The exact means by which the –LKL mutation favours end-to-end binding is unclear and mutation of individual amino acids at these positions could provide information on the importance of each residue. Again, a structural study of the Cdc8 overlap would offer a more definitive explanation of the effects observed.

6.3. Direct observation of Cdc8 polymers by electron microscopy.

Consistent with Skoumpla and colleagues (2007) it was possible to directly observe Cdc8 polymers by electron microscopy. Acetylated and unacetylated Cdc8 as well as Cdc8-LKL proteins were examined and these observations supported viscometry measurements. The majority of unacetylated Cdc8 was seen as single dimers, reflecting weak end-to-end interactions. Acetylated Cdc8 was observed to form longer polymers than the unacetylated protein (figure 3.5, table 3.5) consistent with the increased end-to-end interactions observed by viscometry.

The Cdc8-LKL mutant was observed to form 10 fold more polymers, of 4 or more dimers in length (figure 3.6, table 3.5), compared to the acetylated Cdc8, supporting the observed increase in viscosity. While it is evident that the Cdc8-LKL protein forms longer polymers by specific end-to-end binding, longer polymers may be more likely to interact in a non-specific manner. A 'tangle' of Cdc8-LKL polymers in solution may account partially for the increased viscosity of the protein. It may also explain the tolerance of Cdc8-LKL to higher salt concentrations (figure 3.5). Increased ionic concentrations affect specific end-to-end interactions, but may not have such an effect on non-specific 'tangling'.

Persistence length is the measure of the 'stiffness' of a polymer and can be calculated for Tm (Li et al., 2010a; Phillips and Chacko, 1996; Wolgemuth and Sun, 2006). Persistence length can extend beyond a single Tm dimer as the overlap can transmit mechanical forces between

Tm molecules. Tms with stronger end-to-end interactions have increased persistence lengths, for example skeletal muscle Tm forms end-to end interactions more readily than smooth muscle Tms and correspondingly has a greater persistence length (Coulton et al., 2008; Swenson and Stellwagen, 1989) The persistence length for unacetylated Cdc8 was calculated as 50 nm which is approximately twice the length of a Cdc8 dimer (24 nm) and consistent with the inability of unacetylated Cdc8 to form polymers longer than 2 dimers. The persistence length of Cdc8-LKL was equal (90 nm, ≈ 4 dimers) to that of the acetylated protein suggesting that the Cdc8-LKL mutation does not stiffen the protein and increased polymer length is not a result of stronger end-to-end interactions.

6.4. Actin affinity of wild type and mutant Cdc8 proteins.

Consistent with the results Skoumpla et al (2007) acetylated Cdc8 had a greater affinity for actin than the unacetylated protein, however the affinities were slightly tighter for each protein than previously reported. The binding affinities reported by Skoumpla and colleagues were calculated in the presence of 30 mM NaCl whereas binding experiments in this study were performed with 100 mM NaCl. There are several reports of reduced affinity of Tm for actin at lower ionic concentrations (reviewed in Perry., 2001), which likely accounts for the slight discrepancy between the two studies.

The affinity of the Cdc8-D2A protein for actin was extremely weak (table 4.1). The affinity of individual Tm dimers for actin is low (Wegner, 1980) and only becomes high when Tm dimers are joined end-to-end (Vilfan, 2001). Additionally small alterations to the amino terminus of Tm that impair its ability to from end-to-end interactions also have a negative impact on actin binding (Coulton et al., 2008; Heald and Hitchcock-DeGregori, 1988; Monteiro et al., 1994). The weak affinity of the Cdc8-D2A protein, which is unable to from end-to-end interactions (table 3.4), is supported by these observations. Conversely the increased viscosity of the Cdc8-E6A and –E6K proteins is reflected in increased affinities for

actin (table 4.1) when compared to the unacetylated protein. Interestingly, the Cdc-D16A protein which forms end-to-end interactions as readily as acetylated Cdc8 and the E6 position mutants (figure 3.5), had an approximately 5 fold weaker affinity for actin (table 4.1). Tm has repeating groups of negatively charged amino acids that are thought to play a role in actin interaction (Brown et al., 2005; Lorenz et al., 1995; McLachlan and Stewart, 1976), and Cdc8 has similar groups of acidic amino acids residues (figure 6.1.C.). The Cdc8-D16A mutation falls in a group of acidic residues close to the amino terminus. It is possible that while the mutation increases end-to-end interaction, the removal of the negative charge in this potential actin interacting site lowers the overall affinity for actin. To clarify if this region is important for actin binding, experiments to substitute other acidic residues in this part of the protein could be undertaken.

It was not possible to determine the affinity of Cdc8-LKL for actin using co-sedimentation assays. The protein was seen to pellet during centrifugation in the absence of actin (figure 4.1.C.), even at high salt concentrations. The Cdc8-LKL protein forms longer polymers than the other Cdc8 proteins studied (table 3.5) and these long polymers may 'tangle' in solution to an extent where they pellet in the absence of actin. This observation also lends support to the theory that the increased viscosity and resistance to higher salt concentration of the Cdc8-LKL protein may be attributable to the 'tangling' of long polymers.

6.5. The effect of Cdc8 on actin filaments

Observation of actin by electron microscopy revealed that actin decorated with cardiac Tm formed long, straight, continuous filaments (figure 4.3.), and is consistent with previous reports (Perry, 2001). When acetylated Cdc8 was added, although filaments remained long and continuous they were 'wavy' in appearance. Cdc8 has weak homology to vertebrate Tm and is shorter at 161 amino acids in length (Balasubramanian et al., 1992). In addition S. pombe actin is not identical to skeletal muscle actin,

non muscle β-actin or budding yeast actin, with a 10-12% discrepancy (Takaine and Mabuchi, 2007). Areas of marked inconsistency are found in sub-domains 3 and 4 (Mertins and Gallwitz, 1987) which are thought to be important for electrostatic interactions between actin and Tm (Lorenz et al., 1995). The observed 'waviness' could be the result of some incompatibility between fission yeast Tm and vertebrate actin. It would be interesting to see if the same effect was observed using actin purified from *S. pombe*.

Surprisingly, unacetylated Cdc8 was seen to have a dramatic effect on actin filaments which appeared brittle and broken into short filaments (figure 4.2). In *S. pombe* cells acetylated Cdc8 is found predominantly at the CAR, while unacetylated Cdc8 localises exclusively to interphase actin filaments (Coulton et al., 2010. Submitted). Interphase actin filaments are a dynamic system and one possibility is that unacetylated Cdc8 contributes to these dynamics by favoring or increasing shorter filaments with more actin ends available for polymerisation and depolymerisation. Another is that in the absence of other ABPs Cdc8 causes actin to become brittle. For example it is known that the formin remains associated or incorporated into F-actin in *S. pombe* (Skau et al., 2009) and that formins increase the flexibility of F-actin, while Tms tend to stabilise and stiffen actin filaments (Ujfalusi et al., 2009). Without this balance between flexibility and stiffness, unacetylated Cdc8 may cause F-actin to break.

Finally it may again be a result of an incompatibility of fission yeast Tm binding to vertebrate actin. The 'waviness' imparted to actin by acetylated Cdc8 may not break the filaments due to stabilization by the stronger end-to-end interaction. The weaker interactions between unacetylated Cdc8 dimers however, may be insufficient to prevent breakage of the filament. Again it would be interesting to see if the same effect was observed using unacetylated Cdc8 and actin purified from *S. pombe*.

6.6. Inhibition of myosin ATPase activity by wild type and mutant Cdc8 proteins

Acetylated Cdc8 binding to actin is able to inhibit the actin induced ATPase activity of myosin sub-fragment 1 (S1), and is consistent with reported findings that Cdc8 reduced fission yeast Myo2-driven actin filament gliding in motility assays (Stark et al., 2010). The unacetylated Cdc8, which has weaker end-to-end interactions, lower affinity for actin (table 3.4., table 4.1.) and a higher occupancy of the 'open' position on actin (Skoumpla et al., 2007), had a correspondingly reduced inhibitory effect on S1 ATPase rate (table 4.3).

The inhibition of S1 ATPase rate by Cdc8-E6A and Cdc8-E6K was reflected in their other biochemical properties. Both proteins had viscosities close to that of the acetylated Cdc8, slightly higher actin affinities (table 3.4., table 4.1), and as a result were able to inhibit ATPase rate slightly more than acetylated Cdc8 (table 4.2). Interestingly Cdc8-D16A, which has an equivalent end-to-end interaction as the 'E6' proteins, but an actin affinity comparable with unacetylated Cdc8, inhibited the S1 ATPase to a rate approximately half-way between acetylated and unacetylated Cdc8. This suggests that if the D16A mutation increases end-to-end interactions but reduces overall actin affinity, the ability to regulate myosin suffers as a consequence.

In contrast to the Cdc8-E6A and Cdc8-E6K proteins, despite increased end-to-end interactions the Cdc8-LKL protein only weakly inhibited S1 ATPase rate (table 4.2.). Different Tms occupy different positions on actin filaments (Lehman et al., 2000; Pittenger et al., 1994) and changes in one part of the molecule can have significant effects further along. One hypothesis is that the substitution of 3 amino acids (ARA to LKL) and the 'straightening' of a possible bend induced by the amino terminal alanine cluster affects the molecule in such a way that it occupies a more 'open' position on the actin filament, and as a result is less able to inhibit myosin ATPase rate.

It was established that a large concentration of Cdc8-LKL was required to fully saturate actin filaments (figure 4.5.) during the ATPase assays. As a result of this observation it was possible to determine the affinity of Cdc8-LKL for actin as the concentration of Cdc8-LKL which produced half the maximum inhibition of S1 ATPase rate .The subsequently determined weak affinity (5.2 µM) is likely attributable to the exceptionally long polymers that Cdc8-LKL forms. Tm dimers are thought to have a natural curvature that facilitates their binding to actin (Brown et al., 2005; Lorenz et al., 1995). It is hard to envisage how long polymers of Cdc8-LKL that form a 'coiled coiled-coil' would be able to easily physically associate around the actin filaments. This hypothesis is consistent with the 'gestalt' model of Tm binding (Holmes and Lehman, 2008), in which the overall shape of the Tm dimer is important for actin binding and that inherent helical contour of Tm dimer is an essential feature that facilitates the binding of the elongated protein on actin.

6.7. *In vivo* function of Cdc8 amino terminal mutants

To assess the function of each Cdc8 amino terminal mutant *in vivo* fission yeast expression plasmids containing each Cdc8 mutation were introduced into a *cdc8* temperature sensitive strain (*Cdc8-110*). At the restrictive temperature (36^0C) the endogenous Cdc8-110 protein is non-functional, cells fail to complete cytokinesis, become elongated and die. During this study the *cdc8-110* gene was amplified and sequenced and the sequence data (data not shown) confirmed two mutations in the protein, A18T and E31K. These mutations fall in the Cdc8 amino terminal alanine cluster and in region which interacts with actin (figure 6.1.A,C.) which might explain the dramatic effect of these temperature sensitive mutations. The exact role of each of the amino acid substitutions is unclear and is an area for further investigation.

The Cdc8-D2A mutant was unable to rescue Cdc8-110 function at the restrictive temperature (figure 4.7.), which is expected due to its inability to polymerise or bind actin. This is supported by the absence of actin

filaments and contractile rings in actin stained cells (figure 4.9) characteristic phenotype of loss of Cdc8 function (Chang et al., 1996; Pelham and Chang, 2001). Each of the other mutants however were able to rescue Cdc8-110 function at 36^0C (figure 4.7.) and actin staining indicated that these proteins had no significant detrimental effect on the actin cytoskeleton (figure 4.9). There were slight increases in the percentages of misplaced septa for each *cdc8* mutant when compared to the wild type gene, indicating that the Cdc8 mutants had a small impact on accurate septa placement. To have total confidence, these experiments should be repeated in a *cdc8⁺* deletion strain. The effects of stress conditions (e.g. osmotic, heat, starvation) on cell viability could also be examined. During this study the creation of a *cdc8* deletion strain was attempted, but was unsuccessful.

Although expression of *cdc8-D16A* was able to rescue function in the *cdc8-110* strain, the rate of growth was reduced by approximately 20% compared to the wild type gene (figure 4.8B.). The Cdc8-D16A protein had a reduced affinity for actin *in vitro* (table 4.1), if the same is true *in vivo* a lower affinity for actin could negatively influence actin dynamics resulting in slower growth. Interestingly expression of *cdc8-E6K* increased growth rate by approximately 20% compared to the wild type gene (figure 4.8B.), whereas the E6A mutation had no effect on growth rate. The E6K has the lowest enthalpy of unfolding of all the Cdc8 proteins studied, if this property in some way increases the dynamics of actin association *in vivo*, it may increase actin dynamics overall resulting in the observed increase in growth rate. This hypothesis could be tested using live cell imagining of fluorescently labelled actin, in a *cdc8⁺* deletion background, to measure actin dynamics in cells expressing Cdc8 mutants. However this is not currently possible as all current actin labels affect actin filament dynamics. Altered interactions of Cdc8 mutants with other actin binding proteins such as ADF/cofilin could also be partly responsible for the observed differences in growth rate, and could be investigated by measuring actin dynamics in cells expressing mutant

Cdc8 and increased or decreased levels of different actin binding proteins.

Most surprisingly, *cdc8-110* cells expressing *cdc8-LKL*, which had weak actin affinity in vitro increased growth rate by 50%. It is therefore likely that Cdc8-LKL was able to associate with actin filaments *in vivo* due to the mechanism of F-actin polymerisation by formins (section 1.6.3, figure 1.22.). Part of a long Cdc8-LKL polymer could bind to short, newly formed actin filament which could continue to be polymerised 'inside' the helical Cdc8-LKL polymer. The method used to determine the actin affinity of Cdc8-LKL in this study could be employed to test this hypothesis experimentally. In this case Cdc8-LKL should be initially incubated with monomeric G-actin, which would be induced to polymerise before use in the assay reaction.

The Cdc8-LKL protein was least able to inhibit myosin S1 ATPase activity *in vitro.* Type II myosins in S. pombe are important for assembly and construction of the CAR (Kitayama et al., 1997; May et al., 1997; Stark et al., 2010), and the inability of Cdc8-LKL to regulate their function could result in more rapid cell division and increased growth rate. Live cell imaging of CAR construction and constriction could help to test this theory.

6.8. The requirement for Cdc8 acetylation *in vivo.*

When mutant Cdc8 proteins were assessed for their ability to rescue the growth defects associated with *S. pombe* strain lacking amino terminal acetyltransferase activity (*arm1Δ*) none of the mutant proteins were able to rescue the *arm1Δ* phenotype. It is interesting that although end-to-end interactions were increased by the Cdc8-E6A, –E6K, –D16A and –LKL mutations, to values comparable to the acetylated protein *in vitro,* this was insufficient to complement loss of acetylation *in vivo.* Acetylated Cdc8 is found predominantly at the CAR, while unacetylated Cdc8

T

Table 6.1. A summary of Cdc8 mutant biochemical and cell biology data

Tropomyosin	Mass (Da)	T_m (°C)	ΔH (kJ mol-1)	Viscosity (cSt)	Persistance length (nm)	$K_{50\%}$	ATPase rate (nM Pi sec^{-1} µM S1^{-1})	Rescue of *cdc8-110*	Growth rate *cdc8-110* (Δ OD$_{600}$ hours^{-1})	Growth rate *Δarm1* (Δ OD$_{600}$ hours^{-1})
Cdc8	18,964	34.7	144.7	1.08	50 ± 10	2.76 ±0.22	44.4	n.d.	n.d.	0.042 ±0.002
Cdc8^{ACE}	19,005	35.4	171.8	1.15	90 ± 20	0.46 ±0.10	17.1	++	0.050 ±0.003	n.d.
Cdc8-D2A	18,788	32.4	128.3	1.05	n.d.	>20	n.d.	-	-	0.044 ±0.003
Cdc8-E6A	18,905	34.4	143.5	1.13	n.d.	0.32 ±0.14	14.2	++	0.052 ±0.001	0.039 ±0.003
Cdc8-E6K	18,963	35.4	130.2	1.15	n.d.	0.45 ±0.10	14.5	++	0.061 ±0.003	0.031 ±0.002
Cdc8-D16A	18,919	35.9	159.8	1.14	n.d.	2.27 ±0.31	28.3	+	0.040 ±0.004	0.043 ±0.001
Cdc8-LKL	19,020	37.3	177.4	1.22	90 ± 20	5.19*	86.8	++	0.075 ±0.004	0.044 ±0.002

localises exclusively to interphase actin filaments (Coulton et al., 2010. Submitted). Acetylation is known to influence the cytoplasmic localization of cellular components in other organisms (di Bari et al., 2006; Gay et al., 2003; Thevenet et al., 2004) and may be required to signal Cdc8 localisation to the CAR.

The growth rate of arm1Δ cells was unaffected by expression of Cdc8 mutants, with the exception of the Cdc8-E6K mutant. In this case the growth rate of arm1 cells was reduced, in contrast to its effect in cdc8-110 cells. It is difficult to understand why this mutation would have the opposite effect in an acetylase deficient background. It is possible that the low enthalpy of unfolding and lack of a fully helical amino terminal perturbs its interaction with actin, or actin dynamics in some way, resulting in a slower rate of growth. Although a reduced interaction with actin was not observed in vitro, however the combination of many factors must be considered in the cellular environment.

6.9. Quantum dot conjugates for cellular imaging.

Overall this project was successful in developing a method for conjugating quantum dots to antibodies, and demonstrating that conjugates produced under optimum conditions produced images of Tm localization in S. pombe cells that were significantly brighter and more resistant to photobleaching than organic fluorophores. An attractive quality of QDs is the ability to excite different (emission wavelength) QDs with a single wavelength (Bruchez et al., 1998), which is beneficial for multiplex fluorescence imaging. Dual labeling of two distinct cellular targets with QDs of different 'colours' was attempted during this study (data not shown) but was unsuccessful. If an optimised protocol for multiplex fluorescent labeling of S. pombe cells with QD-IgG conjugates could be developed, it would be a useful tool for cellular imaging. In addition if a technique for introducing QD-IgG conjugates into live fission yeast cells could be developed, it would allow long term imaging of live

cells, which is currently limited with organic fluorophores due to photobleaching. Cell permeabilisation techniques similar to those used for plasmid transformation (section 2.3.2.) might serve as a foundation to accomplish this objective.

However a number of issues arose during these experiments whose resolution was necessary for this successful outcome. These are described briefly below.

6.10. Nonspecific binding of quantum dots

At several stages during this study the tendency of QDs to bind nonspecifically to substrates was noted. This trend was initially observed while following the QD manufacturer's method for separating QD-IgG conjugates from un-reacted reactants; size exclusion chromatography. There have been reports of success using size exclusion chromatography for separation (Hua et al., 2006) while others specifically highlight difficulties encountered eluting QD fractions (Fernandez-Arguelles et al., 2008). In this study it was not possible to elute QD-IgG conjugates or QDs alone from the size exclusion column, therefore ultrafiltration was found to be a more satisfactory method. Consistent with this, in literature where groups have produced their own QD conjugates, ultrafiltration is a common method of separation (Bruchez et al., 1998; Kaul et al., 2007; Yu et al., 2009).

Although ultrafiltration proved a reliable method for separating QD-IgG conjugates from un-reacted reaction components, it was not without fault. If a sample of QD alone were subjected to ultrafiltration, combined fluorescence of the retentate and flow-through did not equal the total fluorescence of the sample prior to ultrafiltration (table 5.5. rows 12 & 13) and suggested that some of the QDs were 'lost' on the filter membrane. In support of this hypothesis, when observed closely QDs (slightly yellow in colour) could be observed adsorbed to the filter membrane and could not be removed by washing. This nonspecific adsorption of QDs to the

filter membrane could potentially have reduced conjugate yield in the small reaction volumes used in this study.

There are several reports of surface functionalised QDs binding nonspecifically to proteins and cellular membranes (Bentzen et al., 2005; Kairdolf et al., 2008) and examples of each were encountered during this study. While attempting to develop a well-plate based assay for determination of conjugate IgG content (section 5.3.1), QDs were observed to bind non-specifically to wells coated with Cdc8 protein. This nonspecific binding was abolished by the addition of a blocking agent (BSA) to the reaction, however ultimately the assay was unsuccessful as fluorescence was undetectable. Additionally during fluorescence microscopy experiments it was observed that QD-IgG conjugates frequently bound nonspecifically to *S. pombe* cells resulting in fluorescence background when imaging. The issue was resolved by quenching EDC activated but non-reacted QD surface carboxyl groups but incubating the conjugates with a 50 mM Tris solution.

Overall the tendency of QD to bind nonspecifically likely contributed to the degree of variation between batches of QD-IgG produced during this investigation.

6.11. The importance of reactant stoichiometry and effects on fluorescence quenching

The work carried out during this study highlighted the importance of achieving the optimum ratio of reactants, when conjugating IgG to QDs using EDC mediated coupling, due to the effects of the reactants on fluorescence quenching and conjugation efficiency. EDC alone did not significantly affect fluorescence intensity of the QD (table 5.4.) in the presence of IgG however a decrease in fluorescence was observed as EDC concentration increased.

IgG quenched QD fluorescence in a concentration dependent manner where higher concentrations of IgG resulted in lower QD fluorescence

intensity (table 5.2, table 5.3). Some recent reports (Dennis and Bao, 2008; Hering et al., 2009) have detailed the use of QDs and fluorescent proteins for FRET (Förster resonance energy transfer) applications. When excited by light, the energy emitted by QDs can be absorbed by fluorescent proteins in close proximity, which in turn fluoresce at a separate wavelength. Up to 90% quenching of QD fluorescence has been reported in these applications (Hering et al., 2007). Antibodies however are not fluorescent proteins, but if fluorescent energy could be transferred between QDs and antibodies, in a non emissive pathway, it would explain the quenching effect of IgG on QDs observed in this study This hypothesis is supported by reports of FRET based fluorescence quenching of QDs by carbon nanotubes (Biju et al., 2006) metal nanoparticles (Dyadyusha et al., 2005; Zhang et al., 2008) and also by modified oligonucleotides in FRET based assays for DNA detection (Lee et al., 2009).

A specific ratio of EDC to QDs was required for the most efficient conjugation regardless of antibody concentration. Ratios of EDC to QD higher or lower than this optimum resulted in resulted in conjugates possessing little to no IgG. This corresponds to findings from other studies of EDC mediated coupling, in which the EDC concentration must be high enough in order to obtain a complete reaction with carboxyl groups, but small enough to prevent formation of an unreactive N-acylurea group (Nakajima and Ikada, 1995; Sam et al., 2009). Overall the efficiency of conjugation was low; the percentage of IgG incorporated into the 'best' conjugate was only 11%.EDC reacts with carboxyl groups most efficiently between pH 3.5 and pH 4.5, additionally amide formation occurs optimally at pH 5.0 (Nakajima and Ikada, 1995). What is more after activation of carboxyl groups by EDC, the efficiency of amide formation at 25^0C decreases rapidly with time after 5 minutes; carboxyl groups will react with water and yield carboxylate.

It was not possible to perform conjugation reaction in this pH range due to the risk of antibody damage at low pH which undoubtedly had a negative effect on conjugation efficiency. What is more, although the protocol

developed during this study for QD-IgG conjugation included a 5 minute incubation of carboxyl functionalized QD with EDC, experimental error and local temperature fluctuations likely contributed to the degree of variation between batches of QD-IgG produced during this investigation

The failure of several assays to measure the IgG content of QD-IgG conjugates (sections 5.3.1., 5.3.2 & 5.3.3) could be attributable to this low conjugations efficiency, and as such there was simply not enough QD conjugated IgG to produce a detectable signal using these methods. Without time and resource constraints it would have been worthwhile investigating EDC:QD:IgG concentrations around the optimal ratio to see if conjugation efficiency could be improved.

6.12. Towards a model for Cdc8 end-to-end interaction

Before the atomic structure of a Tm overlap complex was available (Greenfield et al., 2006) a compelling line of evidence for the important role played by the end-to-end overlap was that Tms are slightly longer than needed to span integer numbers of actin monomers. Muscle Tm is 284 amino acid in length, whereas approximately 274 are sufficient to span 7 actin monomers ($\approx$ 39 residues per actin monomer) (Tobacman, 2008). The 'extra' 10 to 11 residues therefore are likely to accommodate each other (Greenfield et al., 2006). This logic can be applied to Cdc8. Cdc8 is 161 amino acids in length and predicted to span 4 actin monomers (Balasubramanian et al., 1992). However approximately 156 residues are sufficient to span 4 actin monomers. This suggests that 5 amino acid residues are involved in the Cdc8 overlap complex. A theoretical model of this complex is shown in figure 6.2.

In this model the amino terminal methionine could be close enough to the 'd' position leucine of the carboxyl terminus to form a hydrophobic interaction. In addition the amino terminal 'c' position lysine close enough to the 'e' position glutamic acid of the carboxyl terminus to form an ionic
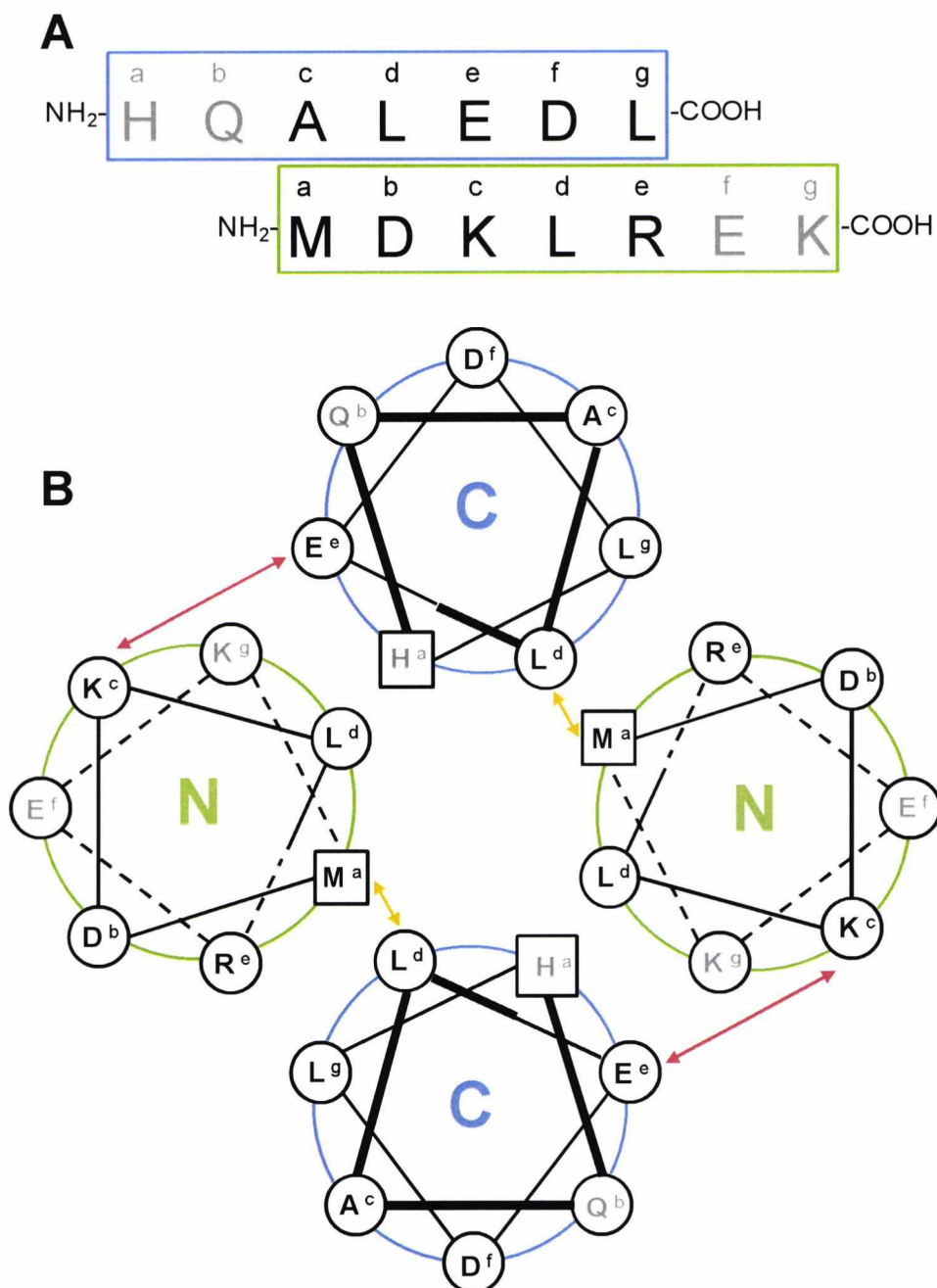
Figure 6.2. A model of the Cdc8 overlap complex

Diagrammatic representations of the last 7 amino acids of the Cdc8 carboxyl terminus and first 7 amino acids of the amino terminus (capitals) and their corresponding positions in the heptad repeat (lower case). Residues in grey are not in the predicted overlap. (A) Linear single chain representation of the predicted Cdc8 overlap complex.(B) Cross section of a double chain representation of the Cdc8 overlap complex. Thick lines represent helix closest to view and dashed line furthest from view. Possible interchain hydrophobic and ionic interactions are highlighted with yellow and red arrows respectively.

interaction. This theory is partially supported by some data obtained in this study. The Cdc8-D2A protein lacks the amino terminal methionine and was unable to form end-to-end interactions or bind actin. This could be the result of the inability to form inter-dimer hydrophobic interactions. The Cdc8-E6A and Cdc8-E6K mutants each had both an increase in the strength of end-to-end interactions and affinity for actin. Although these mutations are not in the hypothesised overlap, the removal or reversal of the negative charge at 'f' position could cause the positively charged, 'c' position lysine to interact more strongly the glutamic acid of the carboxyl terminus, and in doing so increase the strength of end-to-end interactions.

Although purely theoretical, this model does not seem implausible. It would be interesting to see what effect removal or reversal of charge at the amino terminal 'c' position has on the strength of end-to-end interactions and affinity for actin. An atomic structure of the Cdc8 overlap complex would be useful to test this hypothesis and is an area for future research.

Summary

Overall this study has made several significant contributions to the field. It has increased our understanding of the fission yeast Tm, which since its discovery has been largely unexplored (Balasubramanian et al., 1992; Skoumpla et al., 2007). It has provided evidence that Cdc8 behaves in a similar manner to previously studied metazoan Tms and like animal Tms the amino terminus of Cdc8 is important for it function. Modifications are reflected in the biochemical properties of the protein, its affinity for actin and its ability to regulate acto-myosin interactions.

This study has given insights into some of the amino acid residues that are important for the end-to-end interactions between Cdc8 dimers, and highlighted interesting areas for further investigation. It has also provided additional evidence for the 'gestalt' model of Tm-actin interaction (Holmes

and Lehman, 2008) arguing that the helical contour of Tm is important for association with actin. Importantly this study provides further evidence that actelylation is crucial for correct protein function. Mutation causing unacetylated Cdc8 to behave similarly to acetylated Cdc8 were insufficient in compensating for loss of this post translational modification

In addition the methodical approach to developing QD-IgG conjugates has identified several important factors involved in EDC mediated coupling. The study has highlighted the importance of reaction stoichiometry, and the difficulties arising from QD non-specific binding and quenching of fluorescence intensity.

Bibliography

Alberts, B., Bray, D., Lewis, J., Raff, M., Roberts, K. and Watson, J. (1994) *Molecular Biology of the Cell*. Garland Publishing.

Alivisatos, A.P. (1996) Semiconductor clusters, Nanocrystals and Quantum Dots. *Science*, **271**, 933-937.

Alivisatos, A.P., Gu, W. and Larabell, C. (2005) Quantum dots as cellular probes. *Annu Rev Biomed Eng*, **7**, 55-76.

Allen, C. and Borisy, G.G. (1974) Structural polarity and directional growth of microtubules of Chlamydomonas flagella. *J Mol Biol*, **90**, 381-402.

Ampe, C., Markey, F., Lindberg, U. and Vandekerckhove, J. (1988) The primary structure of human platelet profilin: reinvestigation of the calf spleen profilin sequence. *FEBS Lett*, **228**, 17-21.

Andrianantoandro, E. and Pollard, T.D. (2006) Mechanism of actin filament turnover by severing and nucleation at different concentrations of ADF/cofilin. *Mol Cell*, **24**, 13-23.

Ansari, S., El-Mezgueldi, M. and Marston, S. (2003) Cooperative inhibition of actin filaments in the absence of tropomyosin. *J Muscle Res Cell Motil*, **24**, 513-520.

Arai, R. and Mabuchi, I. (2002) F-actin ring formation and the role of F-actin cables in the fission yeast Schizosaccharomyces pombe. *J Cell Sci*, **115**, 887-898.

Arai, R., Nakano, K. and Mabuchi, I. (1998) Subcellular localization and possible function of actin, tropomyosin and actin-related protein 3 (Arp3) in the fission yeast Schizosaccharomyces pombe. *Eur J Cell Biol*, **76**, 288-295.

Araya, E., Berthier, C., Kim, E., Yeung, T., Wang, X. and Helfman, D.M. (2002) Regulation of coiled-coil assembly in tropomyosins. *J Struct Biol*, **137**, 176-183.

Astbury, W.T., Reed, R. and Spark, L.C. (1948) An X-ray and electron microscope study of tropomyosin. *Biochem J*, **43**, 282-287.

Attanapola, S.L., Alexander, C.J. and Mulvihill, D.P. (2009) Ste20-kinase-dependent TEDS-site phosphorylation modulates the dynamic localisation and endocytic function of the fission yeast class I myosin, Myo1. *J Cell Sci*, **122**, 3856-3861.

Aznar, S. and Lacal, J.C. (2001) Rho signals to cell growth and apoptosis. *Cancer Lett*, **165**, 1-10.

Bacchiocchi, C. and Lehrer, S.S. (2002) Ca(2+)-induced movement of tropomyosin in skeletal muscle thin filaments observed by multi-site FRET. *Biophys J*, **82**, 1524-1536.

Bahler, J., Steever, A.B., Wheatley, S., Wang, Y., Pringle, J.R., Gould, K.L. and McCollum, D. (1998) Role of polo kinase and Mid1p in determining the site of cell division in fission yeast. *J Cell Biol*, **143**, 1603-1616.

Bailey, K. (1948) Tropomyosin; a new asymmetric protein component of the muscle fibril. *Biochem J*, **43**, 271-279.

Balasubramanian, M.K., Feoktistova, A., McCollum, D. and Gould, K.L. (1996) Fission yeast Sop2p: a novel and evolutionarily conserved protein that interacts with Arp3p and modulates profilin function. *Embo J*, **15**, 6426-6437.

Balasubramanian, M.K., Helfman, D.M. and Hemmingsen, S.M. (1992) A new tropomyosin essential for cytokinesis in the fission yeast S. pombe. *Nature*, **360**, 84-87.

Balasubramanian, M.K., Hirani, B.R., Burke, J.D. and Gould, K.L. (1994) The Schizosaccharomyces pombe cdc3+ gene encodes a profilin essential for cytokinesis. *J Cell Biol*, **125**, 1289-1301.

Bamburg, J.R., Harris, H.E. and Weeds, A.G. (1980) Partial purification and characterization of an actin depolymerizing factor from brain. *FEBS Lett*, **121**, 178-182.

Bashour, A.M., Fullerton, A.T., Hart, M.J. and Bloom, G.S. (1997) IQGAP1, a Rac- and Cdc42-binding protein, directly binds and cross-links microfilaments. *J Cell Biol*, **137**, 1555-1566.

Bentzen, E.L., Tomlinson, I.D., Mason, J., Gresch, P., Warnement, M.R., Wright, D., Sanders-Bush, E., Blakely, R. and Rosenthal, S.J. (2005) Surface modification to reduce nonspecific binding of quantum dots in live cell assays. *Bioconjug Chem*, **16**, 1488-1494.

Berg, J.S., Powell, B.C. and Cheney, R.E. (2001) A millennial myosin census. *Mol Biol Cell*, **12**, 780-794.

Bernstein, B.W. and Bamburg, J.R. (1982) Tropomyosin binding to F-actin protects the F-actin from disassembly by brain actin-depolymerizing factor (ADF). *Cell Motil*, **2**, 1-8.

Bezanilla, M., Forsburg, S.L. and Pollard, T.D. (1997) Identification of a second myosin-II in Schizosaccharomyces pombe: Myp2p is conditionally required for cytokinesis. *Mol Biol Cell*, **8**, 2693-2705.

Bezanilla, M. and Pollard, T.D. (2000) Myosin-II tails confer unique functions in Schizosaccharomyces pombe: characterization of a novel myosin-II tail. *Mol Biol Cell*, **11**, 79-91.

Biju, V., Itoh, T., Baba, Y. and Ishikawa, M. (2006) Quenching of Photoluminescence in Conjugates of Quantum Dots and Single-Walled Carbon Nanotube. *J. Phys. Chem. B*, **110**, 26068-26074.

Blanchoin, L. and Pollard, T.D. (2002) Hydrolysis of ATP by polymerized actin depends on the bound divalent cation but not profilin. *Biochemistry*, **41**, 597-602.

Blanchoin, L., Pollard, T.D. and Hitchcock-DeGregori, S.E. (2001) Inhibition of the Arp2/3 complex-nucleated actin polymerization and branch formation by tropomyosin. *Curr Biol*, **11**, 1300-1304.

Brown, H.R. and Schachat, F.H. (1985) Renaturation of skeletal muscle tropomyosin: implications for in vivo assembly. *Proc Natl Acad Sci U S A*, **82**, 2359-2363.

Brown, J.H., Kim, K.H., Jun, G., Greenfield, N.J., Dominguez, R., Volkmann, N., Hitchcock-DeGregori, S.E. and Cohen, C. (2001) Deciphering the design of the tropomyosin molecule. *Proc Natl Acad Sci U S A*, **98**, 8496-8501.

Brown, J.H., Zhou, Z., Reshetnikova, L., Robinson, H., Yammani, R.D., Tobacman, L.S. and Cohen, C. (2005) Structure of the mid-region of tropomyosin: bending and binding sites for actin. *Proc Natl Acad Sci U S A*, **102**, 18878-18883.

Bruchez, M., Jr., Moronne, M., Gin, P., Weiss, S. and Alivisatos, A.P. (1998) Semiconductor nanocrystals as fluorescent biological labels. *Science*, **281**, 2013-2016.

Bryce, N.S., Schevzov, G., Ferguson, V., Percival, J.M., Lin, J.J., Matsumura, F., Bamburg, J.R., Jeffrey, P.L., Hardeman, E.C., Gunning, P. and Weinberger, R.P. (2003) Specification of actin filament function and molecular composition by tropomyosin isoforms. *Mol Biol Cell*, **14**, 1002-1016.

Bugyi, B., Papp, G., Hild, G., Lorinczy, D., Nevalainen, E.M., Lappalainen, P., Somogyi, B. and Nyitrai, M. (2006) Formins regulate actin filament flexibility through long range allosteric interactions. *J Biol Chem*, **281**, 10727-10736.

Carlier, M.F., Valentin-Ranc, C., Combeau, C., Fievez, S. and Pantoloni, D. (1994) Actin polymerization: regulation by divalent metal ion and nucleotide binding, ATP hydrolysis and binding of myosin. *Adv Exp Med Biol*, **358**, 71-81.

Carnahan, R.H. and Gould, K.L. (2003) The PCH family protein, Cdc15p, recruits two F-actin nucleation pathways to coordinate cytokinetic actin ring formation in Schizosaccharomyces pombe. *J Cell Biol*, **162**, 851-862.

Casella, J.F., Craig, S.W., Maack, D.J. and Brown, A.E. (1987) Cap Z(36/32), a barbed end actin-capping protein, is a component of the Z-line of skeletal muscle. *J Cell Biol*, **105**, 371-379.

Casella, J.F. and Torres, M.A. (1994) Interaction of Cap Z with actin. The NH2-terminal domains of the alpha 1 and beta subunits are not required for actin capping, and alpha 1 beta and alpha 2 beta heterodimers bind differentially to actin. *J Biol Chem*, **269**, 6992-6998.

Castrillon, D.H. and Wasserman, S.A. (1994) Diaphanous is required for cytokinesis in Drosophila and shares domains of similarity with the products of the limb deformity gene. *Development*, **120**, 3367-3377.

Chacko, S. (1981) Effects of phosphorylation, calcium ion, and tropomyosin on actin-activated adenosine 5'-triphosphatase activity of mammalian smooth muscle myosin. *Biochemistry*, **20**, 702-707.

Chan, C., Beltzner, C.C. and Pollard, T.D. (2009) Cofilin dissociates Arp2/3 complex and branches from actin filaments. *Curr Biol*, **19**, 537-545.

Chan, W.C., Maxwell, D.J., Gao, X., Bailey, R.E., Han, M. and Nie, S. (2002) Luminescent quantum dots for multiplexed biological detection and imaging. *Curr Opin Biotechnol*, **13**, 40-46.

Chang, F., Drubin, D. and Nurse, P. (1997) cdc12p, a protein required for cytokinesis in fission yeast, is a component of the cell division ring and interacts with profilin. *J Cell Biol*, **137**, 169-182.

Chang, F., Woollard, A. and Nurse, P. (1996) Isolation and characterization of fission yeast mutants defective in the assembly and placement of the contractile actin ring. *J Cell Sci*, **109**, 131-142.

Cheney, R.E. and Mooseker, M.S. (1992) Unconventional myosins. *Curr Opin Cell Biol*, **4**, 27-35.

Chhabra, E.S. and Higgs, H.N. (2007) The many faces of actin: matching assembly factors with cellular structures. *Nat Cell Biol*, **9**, 1110-1121.

Cho, Y.J. and Hitchcock-DeGregori, S.E. (1991) Relationship between alternatively spliced exons and functional domains in tropomyosin. *Proc Natl Acad Sci U S A*, **88**, 10153-10157.

Cho, Y.J., Liu, J. and Hitchcock-DeGregori, S.E. (1990) The amino terminus of muscle tropomyosin is a major determinant for function. *J Biol Chem*, **265**, 538-545.

Collins, K. and Matsudaira, P. (1991) Differential regulation of vertebrate myosins I and II. *J Cell Sci Suppl*, **14**, 11-16.

Colote, S., Widada, J.S., Ferraz, C., Bonhomme, F., Marti, J. and Liautard, J.P. (1988) Evolution of tropomyosin functional domains: differential splicing and genomic constraints. *J Mol Evol*, **27**, 228-235.

Coulton, A.T., Koka, K., Lehrer, S.S. and Geeves, M.A. (2008) Role of the head-to-tail overlap region in smooth and skeletal muscle beta-tropomyosin. *Biochemistry*, **47**, 388-397.

Dabrowska, R., Goch, A., Galazkiewicz, B. and Osinska, H. (1985) The influence of caldesmon on ATPase activity of the skeletal muscle actomyosin and bundling of actin filaments. *Biochim Biophys Acta*, **842**, 70-75.

Dabrowska, R., Nowak, E. and Drabikowski, W. (1983) Some functional properties of nonpolymerizable and polymerizable tropomyosin. *J Muscle Res Cell Motil*, **4**, 143-161.

Dalby-Payne, J.R., O'Loughlin, E.V. and Gunning, P. (2003) Polarization of specific tropomyosin isoforms in gastrointestinal epithelial cells and their impact on CFTR at the apical surface. *Mol Biol Cell*, **14**, 4365-4375.

Dalgaard, J.Z. and Klar, A.J. (2001) Does S. pombe exploit the intrinsic asymmetry of DNA synthesis to imprint daughter cells for mating-type switching? *Trends Genet*, **17**, 153-157.

David-Pfeuty, T., Erickson, H.P. and Pantaloni, D. (1977) Guanosinetriphosphatase activity of tubulin associated with microtubule assembly. *Proc Natl Acad Sci U S A*, **74**, 5372-5376.

Dennis, A.M. and Bao, G. (2008) Quantum dot-fluorescent protein pairs as novel fluorescence resonance energy transfer probes. *Nano Lett*, **8**, 1439-1445.

DePina, A.S. and Langford, G.M. (1999) Vesicle transport: the role of actin filaments and myosin motors. *Microsc Res Tech*, **47**, 93-106.

Derfus, A., Chan, W. and Bhatia, S. (2004) Intracellular delivery of quantum dots for live cell labeling and organelle tracking. *Adv. Mater.*, **16**, 961-966.

di Bari, M.G., Ciuffini, L., Mingardi, M., Testi, R., Soddu, S. and Barila, D. (2006) c-Abl acetylation by histone acetyltransferases regulates its nuclear-cytoplasmic localization. *EMBO Rep*, **7**, 727-733.

Djinovic-Carugo, K., Young, P., Gautel, M. and Saraste, M. (1999) Structure of the alpha-actinin rod: molecular basis for cross-linking of actin filaments. *Cell*, **98**, 537-546.

Doberstein, S.K. and Pollard, T.D. (1992) Localization and specificity of the phospholipid and actin binding sites on the tail of Acanthamoeba myosin IC. *J Cell Biol*, **117**, 1241-1249.

dos Remedios, C.G., Chhabra, D., Kekic, M., Dedova, I.V., Tsubakihara, M., Berry, D.A. and Nosworthy, N.J. (2003) Actin binding proteins: regulation of cytoskeletal microfilaments. *Physiol Rev*, **83**, 433-473.

Doyle, A., Martin-Garcia, R., Coulton, A.T., Bagley, S. and Mulvihill, D.P. (2009) Fission yeast Myo51 is a meiotic spindle pole body component with discrete roles during cell fusion and spore formation. *J Cell Sci*, **122**, 4330-4340.

Drees, B., Brown, C., Barrell, B.G. and Bretscher, A. (1995) Tropomyosin is essential in yeast, yet the TPM1 and TPM2 products perform distinct functions. *J Cell Biol*, **128**, 383-392.

Dyadyusha, L., Yin, H., Jaiswal, S., Brown, T., Baumberg, J.J., Booy, F.P. and Melvin, T. (2005) Quenching of CdSe quantum dot emission, a new approach for biosensing. *Chem Commun (Camb)*, 3201-3203.

El-Mezgueldi, M., Copeland, O., Fraser, I.D., Marston, S.B. and Huber, P.A. (1998) Characterization of the functional properties of smooth muscle caldesmon domain 4a: evidence for an independent inhibitory actin-tropomyosin binding domain. *Biochem J*, **332**, 395-401.

Evangelista, M., Pruyne, D., Amberg, D.C., Boone, C. and Bretscher, A. (2002) Formins direct Arp2/3-independent actin filament assembly to polarize cell growth in yeast. *Nat Cell Biol*, **4**, 32-41.

Fankhauser, C., Reymond, A., Cerutti, L., Utzig, S., Hofmann, K. and Simanis, V. (1995) The S. pombe cdc15 gene is a key element in the reorganization of F-actin at mitosis. *Cell*, **82**, 435-444.

Fanning, A.S., Wolenski, J.S., Mooseker, M.S. and Izant, J.G. (1994) Differential regulation of skeletal muscle myosin-II and brush border myosin-I enzymology and mechanochemistry by bacterially produced tropomyosin isoforms. *Cell Motil Cytoskeleton*, **29**, 29-45.

Feierbach, B. and Chang, F. (2001) Roles of the fission yeast formin for3p in cell polarity, actin cable formation and symmetric cell division. *Curr Biol*, **11**, 1656-1665.

Fernandez-Arguelles, M.T., Costa-Fernandez, J.M., Pereiro, R. and Sanz-Medel, A. (2008) Simple bio-conjugation of polymer-coated quantum dots with antibodies for fluorescence-based immunoassays. *Analyst*, **133**, 444-447.

Fujisawa, T., Kostyukova, A. and Maeda, Y. (2001) The shapes and sizes of two domains of tropomodulin, the P-end-capping protein of actin-tropomyosin. *FEBS Lett*, **498**, 67-71.

Fujiwara, K. and Pollard, T.D. (1976) Fluorescent antibody localization of myosin in the cytoplasm, cleavage furrow, and mitotic spindle of human cells. *J Cell Biol*, **71**, 848-875.

Gao, X., Cui, Y., Levenson, R.M., Chung, L.W. and Nie, S. (2004) In vivo cancer targeting and imaging with semiconductor quantum dots. *Nat Biotechnol*, **22**, 969-976.

Gay, F., Calvo, D., Lo, M.C., Ceron, J., Maduro, M., Lin, R. and Shi, Y. (2003) Acetylation regulates subcellular localization of the Wnt signaling nuclear effector POP-1. *Genes Dev*, **17**, 717-722.

Geeves, M.A. and Lehrer, S.S. (1994) Dynamics of the muscle thin filament regulatory switch: the size of the cooperative unit. *Biophys J*, **67**, 273-282.

Gillespie, P.G., Wagner, M.C. and Hudspeth, A.J. (1993) Identification of a 120 kd hair-bundle myosin located near stereociliary tips. *Neuron*, **11**, 581-594.

Gimona, M., Watakabe, A. and Helfman, D.M. (1995) Specificity of dimer formation in tropomyosins: influence of alternatively spliced exons on homodimer and heterodimer assembly. *Proc Natl Acad Sci U S A*, **92**, 9776-9780.

Goldman, E., Balighian, E., Mattoussi, H. and Kuno, M. (2002) Avidin: A Natural Bridge for Quantum Dot-Antibody Conjugates *J. Am. Chem. Soc.*, **124**, 6378-6382.

Goldschmidt-Clermont, P.J., Machesky, L.M., Baldassare, J.J. and Pollard, T.D. (1990) The actin-binding protein profilin binds to PIP2 and inhibits its hydrolysis by phospholipase C. *Science*, **247**, 1575-1578.

Gordon, A.M., Homsher, E. and Regnier, M. (2000) Regulation of contraction in striated muscle. *Physiol Rev*, **80**, 853-924.

Gordon, A.M., Regnier, M. and Homsher, E. (2001) Skeletal and cardiac muscle contractile activation: tropomyosin "rocks and rolls". *News Physiol Sci*, **16**, 49-55.

Grallert, A., Martin-Garcia, R., Bagley, S. and Mulvihill, D.P. (2007) In vivo movement of the type V myosin Myo52 requires dimerisation but is independent of the neck domain. *J Cell Sci*, **120**, 4093-4098.

Greaser, M.L. and Gergely, J. (1971) Reconstitution of troponin activity from three protein components. *J Biol Chem*, **246**, 4226-4233.

Greenfield, N.J., Huang, Y.J., Swapna, G.V., Bhattacharya, A., Rapp, B., Singh, A., Montelione, G.T. and Hitchcock-DeGregori, S.E. (2006) Solution NMR structure of the junction between tropomyosin molecules: implications for actin binding and regulation. *J Mol Biol*, **364**, 80-96.

Greenfield, N.J., Stafford, W.F. and Hitchcock-DeGregori, S.E. (1994) The effect of N-terminal acetylation on the structure of an N-terminal tropomyosin peptide and alpha alpha-tropomyosin. *Protein Sci*, **3**, 402-410.

Gunning, P., Hardeman, E., Jeffrey, P. and Weinberger, R. (1998) Creating intracellular structural domains: spatial segregation of actin and tropomyosin isoforms in neurons. *Bioessays*, **20**, 892-900.

Gunning, P., O'Neill, G. and Hardeman, E. (2008) Tropomyosin-based regulation of the actin cytoskeleton in time and space. *Physiol Rev*, **88**, 1-35.

Gunning, P.W., Schevzov, G., Kee, A.J. and Hardeman, E.C. (2005) Tropomyosin isoforms: divining rods for actin cytoskeleton function. *Trends Cell Biol*, **15**, 333-341.

Gutz, H., Heslot, H., Leupold, U. and Loprieno, N. (1976) *Handbook of Genetics*. Plenum, New York.

Hagan, I. and Yanagida, M. (1997) Evidence for cell cycle-specific, spindle pole body-mediated, nuclear positioning in the fission yeast Schizosaccharomyces pombe. *J Cell Sci*, **110 (Pt 16)**, 1851-1866.

Hammell, R.L. and Hitchcock-DeGregori, S.E. (1996) Mapping the functional domains within the carboxyl terminus of alpha-tropomyosin encoded by the alternatively spliced ninth exon. *J Biol Chem*, **271**, 4236-4242.

Hanahan, D. (1983) Studies on transformation of Escherichia coli with plasmids. *J Mol Biol*, **166**, 557-580.

Hanson, J. and Lowy, J. (1964) The Structure of Actin Filaments and the Origin of the Axial Periodicity in the I-Substance of Vertebrate Striated Muscle. *Proc R Soc Lond B Biol Sci*, **160**, 449-460.

Haselgrove, J.C. (1975) X-ray evidence for conformational changes in the myosin filaments of vertebrate striated muscle. *J Mol Biol*, **92**, 113-143.

Heald, R.W. and Hitchcock-DeGregori, S.E. (1988) The structure of the amino terminus of tropomyosin is critical for binding to actin in the absence and presence of troponin. *J Biol Chem*, **263**, 5254-5259.

Hering, V.R., Faulin, T.E., Triboni, E.R., Rodriguez, S.D., Bernik, D.L., Schumacher, R.I., Mammana, V.P., Faljoni-Alario, A., Abdalla, D.S., Gibson, G. and Politi, M.J. (2009) Violet ZnSe/ZnS as an alternative to

green CdSe/ZnS in nanocrystal-fluorescent protein FRET systems. *Bioconjug Chem*, **20**, 1237-1241.

Hering, V.R., Gibson, G., Schumacher, R.I., Faljoni-Alario, A. and Politi, M.J. (2007) Energy transfer between CdSe/ZnS core/shell quantum dots and fluorescent proteins. *Bioconjug Chem*, **18**, 1705-1708.

Herrmann, H., Bar, H., Kreplak, L., Strelkov, S.V. and Aebi, U. (2007) Intermediate filaments: from cell architecture to nanomechanics. *Nat Rev Mol Cell Biol*, **8**, 562-573.

Higgs, H.N. and Peterson, K.J. (2005) Phylogenetic analysis of the formin homology 2 domain. *Mol Biol Cell*, **16**, 1-13.

Hines, M. and Guyot-Sionnest, P. (1996) Synthesis and characterization of strongly luminescent ZnS-capped CdSe Nanocrystals. *Journal of Physical Chemistry*, **100**, 468-471.

Hinkle, A., Goranson, A., Butters, C.A. and Tobacman, L.S. (1999) Roles for the troponin tail domain in thin filament assembly and regulation. A deletional study of cardiac troponin T. *J Biol Chem*, **274**, 7157-7164.

Hirano, K., Derkach, D.N., Hirano, M., Nishimura, J. and Kanaide, H. (2003) Protein kinase network in the regulation of phosphorylation and dephosphorylation of smooth muscle myosin light chain. *Mol Cell Biochem*, **248**, 105-114.

Hitchcock-DeGregori, S.E. and Heald, R.W. (1987) Altered actin and troponin binding of amino-terminal variants of chicken striated muscle alpha-tropomyosin expressed in Escherichia coli. *J Biol Chem*, **262**, 9730-9735.

Hitchcock-DeGregori, S.E., Song, Y. and Greenfield, N.J. (2002) Functions of tropomyosin's periodic repeats. *Biochemistry*, **41**, 15036-15044.

Hitchcock, S.E., Huxley, H.E. and Szent-Gyorgyi, A.G. (1973) Calcium sensitive binding of troponin to actin-tropomyosin: a two-site model for troponin action. *J Mol Biol*, **80**, 825-836.

Hodges, A.R., Bookwalter, C.S., Krementsova, E.B. and Trybus, K.M. (2009) A nonprocessive class V myosin drives cargo processively when a kinesin- related protein is a passenger. *Curr Biol*, **19**, 2121-2125.

Holland, P.W. (1999) Gene duplication: past, present and future. *Semin Cell Dev Biol*, **10**, 541-547.

Holmes, K.C. and Lehman, W. (2008) Gestalt-binding of tropomyosin to actin filaments. *J Muscle Res Cell Motil*, **29**, 213-219.

Holmes, K.C., Popp, D., Gebhard, W. and Kabsch, W. (1990) Atomic model of the actin filament. *Nature*, **347**, 44-49.

Holthauzen, L.M., Correa, F. and Farah, C.S. (2004) Ca2+-induced rolling of tropomyosin in muscle thin filaments: the alpha- and beta-band hypothesis revisited. *J Biol Chem*, **279**, 15204-15213.

Hua, X., Liu, T., Cao, Y., Liu, B., Wang, H., Wang, J., Huang, Z. and Zhao, Y. (2006) Characterization of the coupling of quantum dots and immunoglobulin antibodies. *Anal Bioanal Chem*, **386**, 1665–1671.

Huckaba, T.M., Lipkin, T. and Pon, L.A. (2006) Roles of type II myosin and a tropomyosin isoform in retrograde actin flow in budding yeast. *J Cell Biol*, **175**, 957-969.

Huxley, A.F. and Niedergerke, R. (1954) Structural changes in muscle during contraction; interference microscopy of living muscle fibres. *Nature*, **173**, 971-973.

Huxley, H. and Hanson, J. (1954) Changes in the cross-striations of muscle during contraction and stretch and their structural interpretation. *Nature*, **173**, 973-976.

Huxley, H.E. (1963) Electron Microscope Studies on the Structure of Natural and Synthetic Protein Filaments from Striated Muscle. *J Mol Biol*, **7**, 281-308.

Ishikawa, H., Bischoff, R. and Holtzer, H. (1968) Mitosis and intermediate-sized filaments in developing skeletal muscle. *J Cell Biol*, **38**, 538-555.

Jaiswal, J.K., Mattoussi, H., Mauro, J.M. and Simon, S.M. (2003) Long-term multiple color imaging of live cells using quantum dot bioconjugates. *Nat Biotechnol*, **21**, 47-51.

Jancso, A. and Graceffa, P. (1991) Smooth muscle tropomyosin coiled-coil dimers. Subunit composition, assembly, and end-to-end interaction. *J Biol Chem*, **266**, 5891-5897.

Jochova, J., Rupes, I. and Streiblova, E. (1991) F-actin contractile rings in protoplasts of the yeast Schizosaccharomyces. *Cell Biol Int Rep*, **15**, 607-610.

Johnson, P. and Smillie, L.B. (1977) Polymerizability of rabbit skeletal tropomyosin: effects of enzymic and chemical modifications. *Biochemistry*, **16**, 2264-2269.

Kabsch, W., Mannherz, H.G., Suck, D., Pai, E.F. and Holmes, K.C. (1990) Atomic structure of the actin:DNase I complex. *Nature*, **347**, 37-44.

Kagawa, H., Sugimoto, K., Matsumoto, H., Inoue, T., Imadzu, H., Takuwa, K. and Sakube, Y. (1995) Genome structure, mapping and expression of the tropomyosin gene tmy-1 of Caenorhabditis elegans. *J Mol Biol*, **251**, 603-613.

Kairdolf, B.A., Mancini, M.C., Smith, A.M. and Nie, S. (2008) Minimizing nonspecific cellular binding of quantum dots with hydroxyl-derivatized surface coatings. *Anal Chem*, **80**, 3029-3034.

Kammerer, R.A., Schulthess, T., Landwehr, R., Lustig, A., Engel, J., Aebi, U. and Steinmetz, M.O. (1998) An autonomous folding unit mediates the assembly of two-stranded coiled coils. *Proc Natl Acad Sci U S A*, **95**, 13419-13424.

Karlik, C.C. and Fyrberg, E.A. (1986) Two Drosophila melanogaster tropomyosin genes: structural and functional aspects. *Mol Cell Biol*, **6**, 1965-1973.

Kaul, Z., Yaguchi, T., Harada, J.I., Ikeda, Y., Hirano, T., Chiura, H.X., Kaul, S.C. and Wadhwa, R. (2007) An antibody-conjugated internalizing quantum dot suitable for long-term live imaging of cells. *Biochem Cell Biol*, **85**, 133-140.

Kaul, Z., Yaguchi, T., Kaul, S.C., Hirano, T., Wadhwa, R. and Taira, K. (2003) Mortalin imaging in normal and cancer cells with quantum dot immuno-conjugates. *Cell Res*, **13**, 503-507.

Kee, A.J., Schevzov, G., Nair-Shalliker, V., Robinson, C.S., Vrhovski, B., Ghoddusi, M., Qiu, M.R., Lin, J.J., Weinberger, R., Gunning, P.W. and Hardeman, E.C. (2004) Sorting of a nonmuscle tropomyosin to a novel cytoskeletal compartment in skeletal muscle results in muscular dystrophy. *J Cell Biol*, **166**, 685-696.

Kim, S.V. and Flavell, R.A. (2008) Myosin I: from yeast to human. *Cell Mol Life Sci*, **65**, 2128-2137.

Kitayama, C., Sugimoto, A. and Yamamoto, M. (1997) Type II myosin heavy chain encoded by the myo2 gene composes the contractile ring during cytokinesis in Schizosaccharomyces pombe. *J Cell Biol*, **137**, 1309-1319.

Kobori, H., Yamada, N., Taki, A. and Osumi, M. (1989) Actin is associated with the formation of the cell wall in reverting protoplasts of the fission yeast Schizosaccharomyces pombe. *J Cell Sci*, **94**, 635-646.

Kollmar, M., Durrwang, U., Kliche, W., Manstein, D.J. and Kull, F.J. (2002) Crystal structure of the motor domain of a class-I myosin. *Embo J*, **21**, 2517-2525.

Kostyukova, A.S., Choy, A. and Rapp, B.A. (2006) Tropomodulin binds two tropomyosins: a novel model for actin filament capping. *Biochemistry*, **45**, 12068-12075.

Kostyukova, A.S., Hitchcock-Degregori, S.E. and Greenfield, N.J. (2007) Molecular basis of tropomyosin binding to tropomodulin, an actin-capping protein. *J Mol Biol*, **372**, 608-618.

Kovar, D.R., Kuhn, J.R., Tichy, A.L. and Pollard, T.D. (2003) The fission yeast cytokinesis formin Cdc12p is a barbed end actin filament capping protein gated by profilin. *J Cell Biol*, **161**, 875-887.

Kovar, D.R., Wu, J.Q. and Pollard, T.D. (2005) Profilin-mediated competition between capping protein and formin Cdc12p during cytokinesis in fission yeast. *Mol Biol Cell*, **16**, 2313-2324.

Kremneva, E., Nikolaeva, O., Maytum, R., Arutyunyan, A.M., Kleimenov, S.Y., Geeves, M.A. and Levitsky, D.I. (2006) Thermal unfolding of smooth muscle and nonmuscle tropomyosin alpha-homodimers with alternatively spliced exons. *Febs J*, **273**, 588-600.

Krendel, M. and Mooseker, M.S. (2005) Myosins: tails (and heads) of functional diversity. *Physiology (Bethesda)*, **20**, 239-251.

Kuhn, T.B. and Bamburg, J.R. (2008) Tropomyosin and ADF/cofilin as collaborators and competitors. *Adv Exp Med Biol*, **644**, 232-249.

Kurahashi, H., Imai, Y. and Yamamoto, M. (2002) Tropomyosin is required for the cell fusion process during conjugation in fission yeast. *Genes Cells*, **7**, 375-384.

Kwok, S.C. and Hodges, R.S. (2004) Stabilizing and destabilizing clusters in the hydrophobic core of long two-stranded alpha-helical coiled-coils. *J Biol Chem*, **279**, 21576-21588.

Le Goff, X., Motegi, F., Salimova, E., Mabuchi, I. and Simanis, V. (2000) The S. pombe rlc1 gene encodes a putative myosin regulatory light chain that binds the type II myosins myo3p and myo2p. *J Cell Sci*, **113**, 4157-4163.

Lee, J., Choi, Y., Kim, J., Park, E. and Song, R. (2009) Positively charged compact quantum Dot-DNA complexes for detection of nucleic acids. *Chemphyschem*, **10**, 806-811.

Lee, W.L., Bezanilla, M. and Pollard, T.D. (2000) Fission yeast myosin-I, Myo1p, stimulates actin assembly by Arp2/3 complex and shares functions with WASp. *J Cell Biol*, **151**, 789-800.

Lees-Miller, J.P. and Helfman, D.M. (1991) The molecular basis for tropomyosin isoform diversity. *Bioessays*, **13**, 429-437.

Lehman, W., Craig, R. and Vibert, P. (1994) Ca(2+)-induced tropomyosin movement in Limulus thin filaments revealed by three-dimensional reconstruction. *Nature*, **368**, 65-67.

Lehman, W., Hatch, V., Korman, V., Rosol, M., Thomas, L., Maytum, R., Geeves, M.A., Van Eyk, J.E., Tobacman, L.S. and Craig, R. (2000) Tropomyosin and actin isoforms modulate the localization of tropomyosin strands on actin filaments. *J Mol Biol*, **302**, 593-606.

Lehman, W., Vibert, P. and Craig, R. (1997) Visualization of caldesmon on smooth muscle thin filaments. *J Mol Biol*, **274**, 310-317.

Lehman, W., Vibert, P., Uman, P. and Craig, R. (1995) Steric-blocking by tropomyosin visualized in relaxed vertebrate muscle thin filaments. *J Mol Biol*, **251**, 191-196.

Lehrer, S.S. and Qian, Y. (1990) Unfolding/refolding studies of smooth muscle tropomyosin. Evidence for a chain exchange mechanism in the preferential assembly of the native heterodimer. *J Biol Chem*, **265**, 1134-1138.

Leupold, U. (1957) [Physiologic and genetic studies of adenine-dependant mutants of Schizosaccharomyces pombe; a contribution to the problem of pseudoallele.]. *Schweiz Z Pathol Bakteriol*, **20**, 535-544.

Leupold, U. (1970) Genetical methods for *S. Pombe*. *Methods in Cell Physiology*, **4**, 169-175.

Li, X., Lehman, W. and Fischer, S. (2010a) The Relationship between Curvature, Flexibility and Persistence Length in the Tropomyosin Coiled-Coil. *J Struct Biol*, **170**, 313-318.

Li, X.D., Jung, H.S., Mabuchi, K., Craig, R. and Ikebe, M. (2006) The globular tail domain of myosin Va functions as an inhibitor of the myosin Va motor. *J Biol Chem*, **281**, 21789-21798.

Li, X.E., Holmes, K.C., Lehman, W., Jung, H. and Fischer, S. (2010b) The shape and flexibility of tropomyosin coiled coils: implications for actin filament assembly and regulation. *J Mol Biol*, **395**, 327-339.

Li, X.E., Lehman, W. and Fischer, S. (2010c) The relationship between curvature, flexibility and persistence length in the tropomyosin coiled-coil. *J Struct Biol*, **170**, 313-318.

Lieto-Trivedi, A., Dash, S. and Coluccio, L.M. (2007) Myosin surface loop 4 modulates inhibition of actomyosin 1b ATPase activity by tropomyosin. *Biochemistry*, **46**, 2779-2786.

Lin, J.J., Eppinga, R.D., Warren, K.S. and McCrae, K.R. (2008) Human tropomyosin isoforms in the regulation of cytoskeleton functions. *Adv Exp Med Biol*, **644**, 201-222.

Liu, H. and Bretscher, A. (1992) Characterization of TPM1 disrupted yeast cells indicates an involvement of tropomyosin in directed vesicular transport. *J Cell Biol*, **118**, 285-299.

Liu, H.P. and Bretscher, A. (1989a) Disruption of the single tropomyosin gene in yeast results in the disappearance of actin cables from the cytoskeleton. *Cell*, **57**, 233-242.

Liu, H.P. and Bretscher, A. (1989b) Purification of tropomyosin from Saccharomyces cerevisiae and identification of related proteins in Schizosaccharomyces and Physarum. *Proc Natl Acad Sci U S A*, **86**, 90-93.

Lorenz, M., Poole, K.J., Popp, D., Rosenbaum, G. and Holmes, K.C. (1995) An atomic model of the unregulated thin filament obtained by X-ray fiber diffraction on oriented actin-tropomyosin gels. *J Mol Biol*, **246**, 108-119.

Loudon, R.P., Silver, L.D., Yee, H.F., Jr. and Gallo, G. (2006) RhoA-kinase and myosin II are required for the maintenance of growth cone polarity and guidance by nerve growth factor. *J Neurobiol*, **66**, 847-867.

Lu, S.M. and Hodges, R.S. (2004) Defining the minimum size of a hydrophobic cluster in two-stranded alpha-helical coiled-coils: effects on protein stability. *Protein Sci*, **13**, 714-726.

Lymn, R.W. and Taylor, E.W. (1971) Mechanism of adenosine triphosphate hydrolysis by actomyosin. *Biochemistry*, **10**, 4617-4624.

Mabuchi, I. and Okuno, M. (1977) The effect of myosin antibody on the division of starfish blastomeres. *J Cell Biol*, **74**, 251-263.

Machesky, L.M., Atkinson, S.J., Ampe, C., Vandekerckhove, J. and Pollard, T.D. (1994) Purification of a cortical complex containing two unconventional actins from Acanthamoeba by affinity chromatography on profilin-agarose. *J Cell Biol*, **127**, 107-115.

Machesky, L.M. and Insall, R.H. (1998) Scar1 and the related Wiskott-Aldrich syndrome protein, WASP, regulate the actin cytoskeleton through the Arp2/3 complex. *Curr Biol*, **8**, 1347-1356.

Madigan, M., Martinko, J. and Parker, J. (2003) *Brock Biology of Microorganisms*. Pearson Education.

Maekawa, S., Nishida, E., Ohta, Y. and Sakai, H. (1984) Isolation of low molecular weight actin-binding proteins from porcine brain. *J Biochem*, **95**, 377-385.

Mahtab, R., Harden, H. and Murphy, C. (2000) Temperature- and salt-dependent binding of DNA to protein sized quantum dots: thermodynamics of 'inorganic protein' -DNA interactions. *J. Am. Chem. Soc.*, **122**, 14-17.

Mak, A.S. and Smillie, L.B. (1981) Non-polymerizable tropomyosin: preparation, some properties and F-actin binding. *Biochem Biophys Res Commun*, **101**, 208-214.

Mandelkow, E. and Mandelkow, E.M. (1995) Microtubules and microtubule-associated proteins. *Curr Opin Cell Biol*, **7**, 72-81.

Margossian, S.S. and Lowey, S. (1982) Preparation of myosin and its subfragments from rabbit skeletal muscle. *Methods Enzymol*, **85**, 55-71.

Marks, J., Hagan, I.M. and Hyams, J.S. (1986) Growth polarity and cytokinesis in fission yeast: the role of the cytoskeleton. *J Cell Sci Suppl*, **5**, 229-241.

Marks, J. and Hyams, J.S. (1985) Localization of F-actin through the cell division cycle of Schizosaccharomyces pombe. *Eur. J. Cell. Biol*, 27-32.

Marston, S. and El-Mezgueldi, M. (2008) Role of tropomyosin in the regulation of contraction in smooth muscle. *Adv Exp Med Biol*, **644**, 110-123.

Martin-Garcia, R. and Mulvihill, D.P. (2009) Myosin V spatially regulates microtubule dynamics and promotes the ubiquitin-dependent degradation of the fission yeast CLIP-170 homologue, Tip1. *J Cell Sci*, **122**, 3862-3872.

Martin, C. and Gunning, P. (2008) Isoform sorting of tropomyosins. *Adv Exp Med Biol*, **644**, 187-200.

Martin, S.R. and Schilstra, M.J. (2008) Circular dichroism and its application to the study of biomolecules. *Methods Cell Biol*, **84**, 263-293.

Mason, J.M. and Arndt, K.M. (2004) Coiled coil domains: stability, specificity, and biological implications. *Chembiochem*, **5**, 170-176.

Matsudaira, P. (1994a) Actin crosslinking proteins at the leading edge. *Semin Cell Biol*, **5**, 165-174.

Matsudaira, P. (1994b) The fimbrin and alpha-actinin footprint on actin. *J Cell Biol*, **126**, 285-287.

Mattoussi, H., Mauro, J., Goldman, E., Anderson, G. and Vikram. (2000) Self-Assembly of CdSe-ZnS Quantum Dot Bioconjugates Using an Engineered Recombinant Protein. *J. Am. Chem. Soc.*, **122,**, 12142-12150.

Maundrell, K. (1993) Thiamine-repressible expression vectors pREP and pRIP for fission yeast. *Gene*, **123**, 127-130.

May, K.M., Watts, F.Z., Jones, N. and Hyams, J.S. (1997) Type II myosin involved in cytokinesis in the fission yeast, Schizosaccharomyces pombe. *Cell Motil Cytoskeleton*, **38**, 385-396.

Maytum, R., Bathe, F., Konrad, M. and Geeves, M.A. (2004) Tropomyosin exon 6b is troponin-specific and required for correct acto-myosin regulation. *J Biol Chem*, **279**, 18203-18209.

Maytum, R., Geeves, M.A. and Konrad, M. (2000) Actomyosin regulatory properties of yeast tropomyosin are dependent upon N-terminal modification. *Biochemistry*, **39**, 11913-11920.

McCollum, D., Balasubramanian, M.K., Pelcher, L.E., Hemmingsen, S.M. and Gould, K.L. (1995) Schizosaccharomyces pombe cdc4+ gene encodes a novel EF-hand protein essential for cytokinesis. *J Cell Biol*, **130**, 651-660.

McCollum, D., Feoktistova, A., Morphew, M., Balasubramanian, M. and Gould, K.L. (1996) The Schizosaccharomyces pombe actin-related protein, Arp3, is a component of the cortical actin cytoskeleton and interacts with profilin. *Embo J*, **15**, 6438-6446.

McGough, A. (1998) F-actin-binding proteins. *Curr Opin Struct Biol*, **8**, 166-176.

McGough, A., Pope, B., Chiu, W. and Weeds, A. (1997) Cofilin changes the twist of F-actin: implications for actin filament dynamics and cellular function. *J Cell Biol*, **138**, 771-781.

McKillop, D.F. and Geeves, M.A. (1993) Regulation of the interaction between actin and myosin subfragment 1: evidence for three states of the thin filament. *Biophys J*, **65**, 693-701.

McLachlan, A.D. and Stewart, M. (1975) Tropomyosin coiled-coil interactions: evidence for an unstaggered structure. *J. Mol. Biol*, **98**, 293–304.

McLachlan, A.D. and Stewart, M. (1976) The 14-fold periodicity in alpha-tropomyosin and the interaction with actin. *J Mol Biol*, **103**, 271-298.

Mehta, A.D., Rock, R.S., Rief, M., Spudich, J.A., Mooseker, M.S. and Cheney, R.E. (1999) Myosin-V is a processive actin-based motor. *Nature*, **400**, 590-593.

Mertins, P. and Gallwitz, D. (1987) A single intronless action gene in the fission yeast Schizosaccharomyces pombe: nucleotide sequence and transcripts formed in homologous and heterologous yeast. *Nucleic Acids Res*, **15**, 7369-7379.

Mitchison, J.M. (1957) The growth of single cells. I. Schizosaccharomyces pombe. *Exp Cell Res*, **13**, 244-262.

Mitchison, J.M. and Nurse, P. (1985) Growth in cell length in the fission yeast Schizosaccharomyces pombe. *J Cell Sci*, **75**, 357-376.

Mitchison, M. (1970) Physiological and cytological methods for *Schizosaccharomyces pombe*. *Methods in Cell Physiology*, **4**, 131-168.

Monteiro, P.B., Lataro, R.C., Ferro, J.A. and Reinach Fde, C. (1994) Functional alpha-tropomyosin produced in Escherichia coli. A dipeptide extension can substitute the amino-terminal acetyl group. *J Biol Chem*, **269**, 10461-10466.

Moraczewska, J., Nicholson-Flynn, K. and Hitchcock-DeGregori, S.E. (1999) The ends of tropomyosin are major determinants of actin affinity and myosin subfragment 1-induced binding to F-actin in the open state. *Biochemistry*, **38**, 15885-15892.

Moreno, S., Klar, A. and Nurse, P. (1991) Molecular genetic analysis of fission yeast Schizosaccharomyces pombe. *Methods Enzymol*, **194**, 795-823.

Motegi, F., Arai, R. and Mabuchi, I. (2001) Identification of two type V myosins in fission yeast, one of which functions in polarized cell growth and moves rapidly in the cell. *Mol Biol Cell*, **12**, 1367-1380.

Motegi, F., Mishra, M., Balasubramanian, M.K. and Mabuchi, I. (2004) Myosin-II reorganization during mitosis is controlled temporally by its dephosphorylation and spatially by Mid1 in fission yeast. *J Cell Biol*, **165**, 685-695.

Mullins, R.D., Heuser, J.A. and Pollard, T.D. (1998a) The interaction of Arp2/3 complex with actin: nucleation, high affinity pointed end capping, and formation of branching networks of filaments. *Proc Natl Acad Sci U S A*, **95**, 6181-6186.

Mullins, R.D., Kelleher, J.F., Xu, J. and Pollard, T.D. (1998b) Arp2/3 complex from Acanthamoeba binds profilin and cross-links actin filaments. *Mol Biol Cell*, **9**, 841-852.

Mulvihill, D.P., Barretto, C. and Hyams, J.S. (2001a) Localization of fission yeast type II myosin, Myo2, to the cytokinetic actin ring is regulated by phosphorylation of a C-terminal coiled-coil domain and requires a functional septation initiation network. *Mol Biol Cell*, **12**, 4044-4053.

Mulvihill, D.P., Pollard, P.J., Win, T.Z. and Hyams, J.S. (2001b) Myosin V-mediated vacuole distribution and fusion in fission yeast. *Curr Biol*, **11**, 1124-1127.

Murray, A. and Hunt, T. (1993) *The Cell Cycle: An Introduction*. Oxford University Press.

Murray, C., Norris, D. and Bawendi, M.G. (1993) Synthesis and characterization of nearly monodisperse CdE (E = S, Se, Te) semiconductor nanocrystalites. *J. Am. Chem. Soc.*, **115**, 8706-8715.

Nakajima, N. and Ikada, Y. (1995) Mechanism of amide formation by carbodiimide for bioconjugation in aqueous media. *Bioconjug Chem*, **6**, 123-130.

Nakano, K. and Mabuchi, I. (2006a) Actin-capping protein is involved in controlling organization of actin cytoskeleton together with ADF/cofilin, profilin and F-actin crosslinking proteins in fission yeast. *Genes Cells*, **11**, 893-905.

Nakano, K. and Mabuchi, I. (2006b) Actin-depolymerizing protein Adf1 is required for formation and maintenance of the contractile ring during cytokinesis in fission yeast. *Mol Biol Cell*, **17**, 1933-1945.

Ness, J.M., Akhtar, R.S., Latham, C.B. and Roth, K.A. (2003) Combined tyramide signal amplification and quantum dots for sensitive and photostable immunofluorescence detection. *J Histochem Cytochem*, **51**, 981-987.

Nirmal, M. and Brus, L. (1999) Luminescence Photophysics in Semiconductor Nanocrystals. *Acc. Chem. Res*, **32**, 407-414.

Nishida, E., Maekawa, S. and Sakai, H. (1984) Cofilin, a protein in porcine brain that binds to actin filaments and inhibits their interactions with myosin and tropomyosin. *Biochemistry*, **23**, 5307-5313.

Noguchi, T., Arai, R., Motegi, F., Nakano, K. and Mabuchi, I. (2001) Contractile ring formation in Xenopus egg and fission yeast. *Cell Struct Funct*, **26**, 545-554.

Novy, R.E., Liu, L.F., Lin, C.S., Helfman, D.M. and Lin, J.J. (1993) Expression of smooth muscle and nonmuscle tropomyosins in Escherichia coli and characterization of bacterially produced tropomyosins. *Biochim Biophys Acta*, **1162**, 255-265.

Nurse, P. (1975) Genetic control of cell size at cell division in yeast. *Nature*, **256**, 547-551.

Nurse, P. (1990) Universal control mechanism regulating onset of M-phase. *Nature*, **344**, 503-508.

Nurse, P., Thuriaux, P. and Nasmyth, K. (1976) Genetic control of the cell division cycle in the fission yeast Schizosaccharomyces pombe. *Mol Gen Genet*, **146**, 167-178.

Oakley, B.R., Oakley, C.E., Yoon, Y. and Jung, M.K. (1990) Gamma-tubulin is a component of the spindle pole body that is essential for microtubule function in Aspergillus nidulans. *Cell*, **61**, 1289-1301.

Odronitz, F. and Kollmar, M. (2007) Drawing the tree of eukaryotic life based on the analysis of 2,269 manually annotated myosins from 328 species. *Genome Biol*, **8**, R196.

Ohkura, H., Hagan, I.M. and Glover, D.M. (1995) The conserved Schizosaccharomyces pombe kinase plo1, required to form a bipolar spindle, the actin ring, and septum, can drive septum formation in G1 and G2 cells. *Genes Dev*, **9**, 1059-1073.

Okada, K., Ravi, H., Smith, E.M. and Goode, B.L. (2006) Aip1 and cofilin promote rapid turnover of yeast actin patches and cables: a coordinated mechanism for severing and capping filaments. *Mol Biol Cell*, **17**, 2855-2868.

Ostap, E.M. (2008) Tropomyosins as discriminators of myosin function. *Adv Exp Med Biol*, **644**, 273-282.

Palm, T., Greenfield, N.J. and Hitchcock-DeGregori, S.E. (2003) Tropomyosin ends determine the stability and functionality of overlap and troponin T complexes. *Biophys J*, **84**, 3181-3189.

Parry, D.A. and Squire, J.M. (1973) Structural role of tropomyosin in muscle regulation: analysis of the x-ray diffraction patterns from relaxed and contracting muscles. *J Mol Biol*, **75**, 33-55.

Pashkova, N., Jin, Y., Ramaswamy, S. and Weisman, L.S. (2006) Structural basis for myosin V discrimination between distinct cargoes. *Embo J*, **25**, 693-700.

Pelham, R.J., Jr. and Chang, F. (2001) Role of actin polymerization and actin cables in actin-patch movement in Schizosaccharomyces pombe. *Nat Cell Biol*, **3**, 235-244.

Pelham, R.J., Jr., Lin, J.J. and Wang, Y.L. (1996) A high molecular mass non-muscle tropomyosin isoform stimulates retrograde organelle transport. *J Cell Sci*, **109**, 981-989.

Pellegrin, S. and Mellor, H. (2007) Actin stress fibres. *J Cell Sci*, **120**, 3491-3499.

Pellegrino, T., Manna, L., Kudera, S., Liedl, T. and Koktysh, D. (2004) Hydrophobic nanocrystals coated with an amphiphilic polymer shell: a general route to water-soluable nanocrystals. *Nano Lett*, **4**, 703-707.

Peng, X., Wickham, J. and Alivisatos, A.P. (1998) Kinetics of II-VI and III-V colloidal semiconductor nanocrystal growth - focusing of size distributions. *J. Am. Chem. Soc.*, **120**, 5343-5344.

Peng, Z. and Peng, X. (2001) Formation of high-quality CdTe, CdSe, and CdS nanocrystals using CdO as precursor. *J Am Chem Soc* **123**, 183-184.

Perry, S.V. (2001) Vertebrate tropomyosin: distribution, properties and function. *J Muscle Res Cell Motil*, **22**, 5-49.

Petersen, J., Weilguny, D., Egel, R. and Nielsen, O. (1995) Characterization of fus1 of Schizosaccharomyces pombe: a developmentally controlled function needed for conjugation. *Mol Cell Biol*, **15**, 3697-3707.

Phillips, G.N., Jr. (1986) Construction of an atomic model for tropomyosin and implications for interactions with actin. *J Mol Biol*, **192**, 128-131.

Phillips, G.N., Jr. and Chacko, S. (1996) Mechanical properties of tropomyosin and implications for muscle regulation. *Biopolymers*, **38**, 89-95.

Phillips, G.N., Jr., Fillers, J.P. and Cohen, C. (1986) Tropomyosin crystal structure and muscle regulation. *J Mol Biol*, **192**, 111-131.

Pittenger, M.F., Kazzaz, J.A. and Helfman, D.M. (1994) Functional properties of non-muscle tropomyosin isoforms. *Curr Opin Cell Biol*, **6**, 96-104.

Pittenger, M.F., Kistler, A. and Helfman, D.M. (1995) Alternatively spliced exons of the beta tropomyosin gene exhibit different affinities for F-actin and effects with nonmuscle caldesmon. *J Cell Sci*, **108**, 3253-3265.

Polevoda, B., Cardillo, T.S., Doyle, T.C., Bedi, G.S. and Sherman, F. (2003) Nat3p and Mdm20p are required for function of yeast NatB Nalpha-terminal acetyltransferase and of actin and tropomyosin. *J Biol Chem*, **278**, 30686-30697.

Pollard, T.D. (2007) Regulation of actin filament assembly by Arp2/3 complex and formins. *Annu Rev Biophys Biomol Struct*, **36**, 451-477.

Pollard, T.D. and Korn, E.D. (1973) Acanthamoeba myosin. I. Isolation from Acanthamoeba castellanii of an enzyme similar to muscle myosin. *J Biol Chem*, **248**, 4682-4690.

Pollard, T.D. and Wu, J.Q. (2010) Understanding cytokinesis: lessons from fission yeast. *Nat Rev Mol Cell Biol*, **11**, 149-155.

Poole, K.J., Lorenz, M., Evans, G., Rosenbaum, G., Pirani, A., Craig, R., Tobacman, L.S., Lehman, W. and Holmes, K.C. (2006) A comparison of muscle thin filament models obtained from electron microscopy reconstructions and low-angle X-ray fibre diagrams from non-overlap muscle. *J Struct Biol*, **155**, 273-284.

Poole, K.J.V., Evans, G., Rosenbaum, G., Lorenz, M. and Holmes, K. (1995) The effect of crossbridges on the calcium sensitivity of the structural change of the regulated thin filament. *Biophys. J*, **68**, 365.

Potter, J.D. and Gergely, J. (1974) Troponin, tropomyosin, and actin interactions in the Ca2+ regulation of muscle contraction. *Biochemistry*, **13**, 2697-2703.

Pruyne, D. (2008) Tropomyosin function in yeast. *Adv Exp Med Biol*, **644**, 168-186.

Pruyne, D., Evangelista, M., Yang, C., Bi, E., Zigmond, S., Bretscher, A. and Boone, C. (2002) Role of formins in actin assembly: nucleation and barbed-end association. *Science*, **297**, 612-615.

Pruyne, D.W., Schott, D.H. and Bretscher, A. (1998) Tropomyosin-containing actin cables direct the Myo2p-dependent polarized delivery of secretory vesicles in budding yeast. *J Cell Biol*, **143**, 1931-1945.

Purves, W., Sadava, D., Orians, G. and Heller, H. (2001) *Life: The science of biology*. Sinauer Associates.

Qin, Z., Kreplak, L. and Buehler, M.J. (2009) Hierarchical structure controls nanomechanical properties of vimentin intermediate filaments. *PLoS One*, **4**, e7294.

Raven, P.H., Evert, R.F. and Eichhorn, S.E. (1992) *The Biology of Plants*. W.H. Freeman & Co.

Rayment, I., Holden, H.M., Whittaker, M., Yohn, C.B., Lorenz, M., Holmes, K.C. and Milligan, R.A. (1993) Structure of the actin-myosin complex and its implications for muscle contraction. *Science*, **261**, 58-65.

Reck-Peterson, S.L., Tyska, M.J., Novick, P.J. and Mooseker, M.S. (2001) The yeast class V myosins, Myo2p and Myo4p, are nonprocessive actin-based motors. *J Cell Biol*, **153**, 1121-1126.

Reisler, E. and Egelman, E.H. (2007) Actin structure and function: what we still do not understand. *J Biol Chem*, **282**, 36133-36137.

Robertson, A.S., Smythe, E. and Ayscough, K.R. (2009) Functions of actin in endocytosis. *Cell Mol Life Sci*, **66**, 2049-2065.

Robinow, C.F. (1977) The Number of Chromosomes in *Schizosaccharomyces pombe*: Light Microscopy of Stained Preparations. *Genetics*, **87**, 491-497.

Rohatgi, R., Ho, H.Y. and Kirschner, M.W. (2000) Mechanism of N-WASP activation by CDC42 and phosphatidylinositol 4, 5-bisphosphate. *J Cell Biol*, **150**, 1299-1310.

Romero, S., Le Clainche, C., Didry, D., Egile, C., Pantaloni, D. and Carlier, M.F. (2004) Formin is a processive motor that requires profilin to accelerate actin assembly and associated ATP hydrolysis. *Cell*, **119**, 419-429.

Ross, J.L., Ali, M.Y. and Warshaw, D.M. (2008) Cargo transport: molecular motors navigate a complex cytoskeleton. *Curr Opin Cell Biol*, **20**, 41-47.

Sagot, I., Klee, S.K. and Pellman, D. (2002a) Yeast formins regulate cell polarity by controlling the assembly of actin cables. *Nat Cell Biol*, **4**, 42-50.

Sagot, I., Rodal, A.A., Moseley, J., Goode, B.L. and Pellman, D. (2002b) An actin nucleation mechanism mediated by Bni1 and profilin. *Nat Cell Biol*, **4**, 626-631.

Sam, S., Touahir, L., Salvador Andresa, J., Allongue, P., Chazalviel, J.N., Gouget-Laemmel, A.C., Henry de Villeneuve, C., Moraillon, A., Ozanam, F., Gabouze, N. and Djebbar, S. (2009) Semiquantitative study of the EDC/NHS activation of acid terminal groups at modified porous silicon surfaces. *Langmuir*, **26**, 809-814.

Sano, K., Maeda, K., Oda, T. and Maeda, Y. (2000) The effect of single residue substitutions of serine-283 on the strength of head-to-tail interaction and actin binding properties of rabbit skeletal muscle alpha-tropomyosin. *J Biochem*, **127**, 1095-1102.

Schafer, D.A. and Cooper, J.A. (1995) Control of actin assembly at filament ends. *Annu Rev Cell Dev Biol*, **11**, 497-518.

Schevzov, G., Gunning, P., Jeffrey, P.L., Temm-Grove, C., Helfman, D.M., Lin, J.J. and Weinberger, R.P. (1997) Tropomyosin localization

reveals distinct populations of microfilaments in neurites and growth cones. *Mol Cell Neurosci*, **8**, 439-454.

Sellers, J.R. and Veigel, C. (2006) Walking with myosin V. *Curr Opin Cell Biol*, **18**, 68-73.

Singer, J.M. and Shaw, J.M. (2003) Mdm20 protein functions with Nat3 protein to acetylate Tpm1 protein and regulate tropomyosin-actin interactions in budding yeast. *Proc Natl Acad Sci U S A*, **100**, 7644-7649.

Singh, A. and Hitchcock-DeGregori, S.E. (2003) Local destabilization of the tropomyosin coiled coil gives the molecular flexibility required for actin binding. *Biochemistry*, **42**, 14114-14121.

Singh, A. and Hitchcock-DeGregori, S.E. (2006) Dual requirement for flexibility and specificity for binding of the coiled-coil tropomyosin to its target, actin. *Structure*, **14**, 43-50.

Singh, A. and Hitchcock-DeGregori, S.E. (2007) Tropomyosin's periods are quasi-equivalent for actin binding but have specific regulatory functions. *Biochemistry*, **46**, 14917-14927.

Skau, C.T., Neidt, E.M. and Kovar, D.R. (2009) Role of tropomyosin in formin-mediated contractile ring assembly in fission yeast. *Mol Biol Cell*, **20**, 2160-2173.

Skoumpla, K., Coulton, A.T., Lehman, W., Geeves, M.A. and Mulvihill, D.P. (2007) Acetylation regulates tropomyosin function in the fission yeast Schizosaccharomyces pombe. *J Cell Sci*, **120**, 1635-1645.

Smith, C.L., Matsumoto, T., Niwa, O., Klco, S., Fan, J.B., Yanagida, M. and Cantor, C.R. (1987a) An electrophoretic karyotype for Schizosaccharomyces pombe by pulsed field gel electrophoresis. *Nucleic Acids Res*, **15**, 4481-4489.

Smith, C.W., Pritchard, K. and Marston, S.B. (1987b) The mechanism of Ca2+ regulation of vascular smooth muscle thin filaments by caldesmon and calmodulin. *J Biol Chem*, **262**, 116-122.

Spudich, J.A. and Watt, S. (1971) The regulation of rabbit skeletal muscle contraction. I. Biochemical studies of the interaction of the tropomyosin-troponin complex with actin and the proteolytic fragments of myosin. *J Biol Chem*, **246**, 4866-4871.

Stark, B.C., Sladewski, T.E., Pollard, L.W. and Lord, M. (2010) Tropomyosin and Myosin-II Cellular Levels Promote Actomyosin Ring Assembly in Fission Yeast. *Mol Biol Cell*, **21**, 989-1000.

Stone, D. and Smillie, L.B. (1978) The amino acid sequence of rabbit skeletal alpha-tropomyosin. The NH2-terminal half and complete sequence. *J Biol Chem*, **253**, 1137-1148.

Strand, J., Nili, M., Homsher, E. and Tobacman, L.S. (2001) Modulation of myosin function by isoform-specific properties of Saccharomyces cerevisiae and muscle tropomyosins. *J Biol Chem*, **276**, 34832-34839.

Suresh, P. and Arp, L.H. (1993) A monoclonal antibody-based latex bead agglutination test for the detection of Bordetella avium. *Avian Dis*, **37**, 767-772.

Svitkina, T.M. and Borisy, G.G. (1999) Arp2/3 complex and actin depolymerizing factor/cofilin in dendritic organization and treadmilling of actin filament array in lamellipodia. *J Cell Biol*, **145**, 1009-1026.

Swenson, C.A. and Stellwagen, N.C. (1989) Flexibility of smooth and skeletal tropomyosins. *Biopolymers*, **28**, 955-963.

Szpacenko, A. and Dabrowska, R. (1986) Functional domain of caldesmon. *FEBS Lett*, **202**, 182-186.

Takaine, M. and Mabuchi, I. (2007) Properties of actin from the fission yeast Schizosaccharomyces pombe and interaction with fission yeast profilin. *J Biol Chem*, **282**, 21683-21694.

Takaine, M., Numata, O. and Nakano, K. (2009) Fission yeast IQGAP arranges actin filaments into the cytokinetic contractile ring. *Embo J*, **28**, 3117-3131.

Tanaka, K., Petersen, J., MacIver, F., Mulvihill, D.P., Glover, D.M. and Hagan, I.M. (2001) The role of Plo1 kinase in mitotic commitment and septation in Schizosaccharomyces pombe. *Embo J*, **20**, 1259-1270.

Tang, N. and Ostap, E.M. (2001) Motor domain-dependent localization of myo1b (myr-1). *Curr Biol*, **11**, 1131-1135.

Thevenet, L., Mejean, C., Moniot, B., Bonneaud, N., Galeotti, N., Aldrian-Herrada, G., Poulat, F., Berta, P., Benkirane, M. and Boizet-Bonhoure, B. (2004) Regulation of human SRY subcellular distribution by its acetylation/deacetylation. *Embo J*, **23**, 3336-3345.

Thirumurugan, K., Sakamoto, T., Hammer, J.A., 3rd, Sellers, J.R. and Knight, P.J. (2006) The cargo-binding domain regulates structure and activity of myosin 5. *Nature*, **442**, 212-215.

Tilney, L.G., Bryan, J., Bush, D.J., Fujiwara, K., Mooseker, M.S., Murphy, D.B. and Snyder, D.H. (1973) Microtubules: evidence for 13 protofilaments. *J Cell Biol*, **59**, 267-275.

Tirnauer, J.S. (2004) A new cytoskeletal connection for APC: linked to actin through IQGAP. *Dev Cell*, **7**, 778-780.

Titus, M.A. (2000) The role of unconventional myosins in Dictyostelium endocytosis. *J Eukaryot Microbiol*, **47**, 191-196.

Tobacman, L.S. (2008) Cooperative binding of tropomyosin to actin. *Adv Exp Med Biol*, **644**, 85-94.

Tokumasu, F. and Dvorak, J. (2003) Development and application of quantum dots for immunocytochemistry of human erythrocytes. *J Microsc*, **211**, 256-261.

Toramoto, T., Ikeda, D., Ochiai, Y., Minoshima, S., Shimizu, N. and Watabe, S. (2004) Multiple gene organization of pufferfish Fugu rubripes tropomyosin isoforms and tissue distribution of their transcripts. *Gene*, **331**, 41-51.

Toth, J., Kovacs, M., Wang, F., Nyitray, L. and Sellers, J.R. (2005) Myosin V from Drosophila reveals diversity of motor mechanisms within the myosin V family. *J Biol Chem*, **280**, 30594-30603.

Tran, P.T., Marsh, L., Doye, V., Inoue, S. and Chang, F. (2001) A mechanism for nuclear positioning in fission yeast based on microtubule pushing. *J Cell Biol*, **153**, 397-411.

Trybus, K.M. (2008) Myosin V from head to tail. *Cell Mol Life Sci*, **65**, 1378-1389.

Tyska, M.J., Mackey, A.T., Huang, J.D., Copeland, N.G., Jenkins, N.A. and Mooseker, M.S. (2005) Myosin-1a is critical for normal brush border structure and composition. *Mol Biol Cell*, **16**, 2443-2457.

Ujfalusi, Z., Vig, A., Hild, G. and Nyitrai, M. (2009) Effect of tropomyosin on formin-bound actin filaments. *Biophys J*, **96**, 162-168.

Umemoto, S., Bengur, A.R. and Sellers, J.R. (1989) Effect of multiple phosphorylations of smooth muscle and cytoplasmic myosins on movement in an in vitro motility assay. *J Biol Chem*, **264**, 1431-1436.

Urbancikova, M. and Hitchcock-DeGregori, S.E. (1994) Requirement of amino-terminal modification for striated muscle alpha-tropomyosin function. *J Biol Chem*, **269**, 24310-24315.

Van Troys, M., Huyck, L., Leyman, S., Dhaese, S., Vandekerkhove, J. and Ampe, C. (2008) Ins and outs of ADF/cofilin activity and regulation. *Eur J Cell Biol*, **87**, 649-667.

Vibert, P., Craig, R. and Lehman, W. (1997) Steric-model for activation of muscle thin filaments. *J Mol Biol*, **266**, 8-14.

Vicente-Manzanares, M., Ma, X., Adelstein, R.S. and Horwitz, A.R. (2009) Non-muscle myosin II takes centre stage in cell adhesion and migration. *Nat Rev Mol Cell Biol*, **10**, 778-790.

Vilfan, A. (2001) The binding dynamics of tropomyosin on actin. *Biophys J*, **81**, 3146-3155.

Vinson, V.K., De La Cruz, E.M., Higgs, H.N. and Pollard, T.D. (1998) Interactions of Acanthamoeba profilin with actin and nucleotides bound to actin. *Biochemistry*, **37**, 10871-10880.

Walker, R.A., O'Brien, E.T., Pryer, N.K., Soboeiro, M.F., Voter, W.A., Erickson, H.P. and Salmon, E.D. (1988) Dynamic instability of individual microtubules analyzed by video light microscopy: rate constants and transition frequencies. *J Cell Biol*, **107**, 1437-1448.

Wang, N. and Stamenovic, D. (2002) Mechanics of vimentin intermediate filaments. *J Muscle Res Cell Motil*, **23**, 535-540.

Watanabe, N., Madaule, P., Reid, T., Ishizaki, T., Watanabe, G., Kakizuka, A., Saito, Y., Nakao, K., Jockusch, B.M. and Narumiya, S. (1997) p140mDia, a mammalian homolog of Drosophila diaphanous, is a target protein for Rho small GTPase and is a ligand for profilin. *Embo J*, **16**, 3044-3056.

Wawro, B., Greenfield, N.J., Wear, M.A., Cooper, J.A., Higgs, H.N. and Hitchcock-DeGregori, S.E. (2007) Tropomyosin regulates elongation by formin at the fast-growing end of the actin filament. *Biochemistry*, **46**, 8146-8155.

Weber, A., Pennise, C.R. and Fowler, V.M. (1999) Tropomodulin increases the critical concentration of barbed end-capped actin filaments by converting ADP.P(i)-actin to ADP-actin at all pointed filament ends. *J Biol Chem*, **274**, 34637-34645.

Weeds, A.G. and Taylor, R.S. (1975) Separation of subfragment-1 isoenzymes from rabbit skeletal muscle myosin. *Nature*, **257**, 54-56.

Wegner, A. (1980) The interaction of alpha, alpha- and alpha , beta-tropomyosin with actin filaments. *FEBS Lett*, **119**, 245-248.

Wegner, A. and Walsh, T.P. (1981) Interaction of tropomyosin-troponin with actin filaments. *Biochemistry*, **20**, 5633-5642.

Weisenberg, R.C., Borisy, G.G. and Taylor, E.W. (1968) The colchicine-binding protein of mammalian brain and its relation to microtubules. *Biochemistry*, **7**, 4466-4479.

Weisenberg, R.C. and Deery, W.J. (1976) Role of nucleotide hydrolysis in microtubule assembly. *Nature*, **263**, 792-793.

Welch, M.D., DePace, A.H., Verma, S., Iwamatsu, A. and Mitchison, T.J. (1997) The human Arp2/3 complex is composed of evolutionarily conserved subunits and is localized to cellular regions of dynamic actin filament assembly. *J Cell Biol*, **138**, 375-384.

Wen, K.K., Kuang, B. and Rubenstein, P.A. (2000) Tropomyosin-dependent filament formation by a polymerization-defective mutant yeast actin (V266G,L267G). *J Biol Chem*, **275**, 40594-40600.

Wessels, D., Soll, D.R., Knecht, D., Loomis, W.F., De Lozanne, A. and Spudich, J. (1988) Cell motility and chemotaxis in Dictyostelium amebae lacking myosin heavy chain. *Dev Biol*, **128**, 164-177.

Whitby, F.G., Kent, H., Stewart, F., Stewart, M., Xie, X., Hatch, V., Cohen, C. and Phillips, G.N., Jr. (1992) Structure of tropomyosin at 9 angstroms resolution. *J Mol Biol*, **227**, 441-452.

Whitby, F.G. and Phillips, G.N., Jr. (2000) Crystal structure of tropomyosin at 7 Angstroms resolution. *Proteins*, **38**, 49-59.

Wieczorek, D.F., Smith, C.W. and Nadal-Ginard, B. (1988) The rat alpha-tropomyosin gene generates a minimum of six different mRNAs coding for striated, smooth, and nonmuscle isoforms by alternative splicing. *Mol Cell Biol*, **8**, 679-694.

Willard, D., Carillo, L., Jung, J. and Van Orden, A. (2001) CdSe-ZnS Quantum Dots as Resonance Energy Transfer Donors in a Model Protein-Protein Binding Assay. *Nano Lett*, **1**, 469-474.

Win, T.Z., Gachet, Y., Mulvihill, D.P., May, K.M. and Hyams, J.S. (2001) Two type V myosins with non-overlapping functions in the fission yeast Schizosaccharomyces pombe: Myo52 is concerned with growth polarity and cytokinesis, Myo51 is a component of the cytokinetic actin ring. *J Cell Sci*, **114**, 69-79.

Win, T.Z., Mulvihill, D.P. and Hyams, J.S. (2002) Take five: a myosin class act in fission yeast. *Cell Motil Cytoskeleton*, **51**, 53-56.

Wolfe, B.A. and Gould, K.L. (2005) Split decisions: coordinating cytokinesis in yeast. *Trends Cell Biol*, **15**, 10-18.

Wolgemuth, C.W. and Sun, S.X. (2006) Elasticity of alpha-helical coiled coils. *Phys Rev Lett*, **97**, 248101.

Wood, V., Gwilliam, R., Rajandream, M.A., Lyne, M., Lyne, R., Stewart, A., Sgouros, J., Peat, N., Hayles, J., Baker, S., Basham, D., Bowman, S., Brooks, K., Brown, D., Brown, S., Chillingworth, T., Churcher, C., Collins, M., Connor, R., Cronin, A., Davis, P., Feltwell, T., Fraser, A., Gentles, S., Goble, A., Hamlin, N., Harris, D., Hidalgo, J., Hodgson, G., Holroyd, S., Hornsby, T., Howarth, S., Huckle, E.J., Hunt, S., Jagels, K., James, K., Jones, L., Jones, M., Leather, S., McDonald, S., McLean, J., Mooney, P., Moule, S., Mungall, K., Murphy, L., Niblett, D., Odell, C., Oliver, K., O'Neil, S., Pearson, D., Quail, M.A., Rabbinowitsch, E., Rutherford, K.,

Rutter, S., Saunders, D., Seeger, K., Sharp, S., Skelton, J., Simmonds, M., Squares, R., Squares, S., Stevens, K., Taylor, K., Taylor, R.G., Tivey, A., Walsh, S., Warren, T., Whitehead, S., Woodward, J., Volckaert, G., Aert, R., Robben, J., Grymonprez, B., Weltjens, I., Vanstreels, E., Rieger, M., Schafer, M., Muller-Auer, S., Gabel, C., Fuchs, M., Dusterhoft, A., Fritzc, C., Holzer, E., Moestl, D., Hilbert, H., Borzym, K., Langer, I., Beck, A., Lehrach, H., Reinhardt, R., Pohl, T.M., Eger, P., Zimmermann, W., Wedler, H., Wambutt, R., Purnelle, B., Goffeau, A., Cadieu, E., Dreano, S., Gloux, S., Lelaure, V., Mottier, S., Galibert, F., Aves, S.J., Xiang, Z., Hunt, C., Moore, K., Hurst, S.M., Lucas, M., Rochet, M., Gaillardin, C., Tallada, V.A., Garzon, A., Thode, G., Daga, R.R., Cruzado, L., Jimenez, J., Sanchez, M., del Rey, F., Benito, J., Dominguez, A., Revuelta, J.L., Moreno, S., Armstrong, J., Forsburg, S.L., Cerutti, L., Lowe, T., McCombie, W.R., Paulsen, I., Potashkin, J., Shpakovski, G.V., Ussery, D., Barrell, B.G. and Nurse, P. (2002) The genome sequence of Schizosaccharomyces pombe. *Nature*, **415**, 871-880.

Woychik, R.P., Maas, R.L., Zeller, R., Vogt, T.F. and Leder, P. (1990) 'Formins': proteins deduced from the alternative transcripts of the limb deformity gene. *Nature*, **346**, 850-853.

Wu, J.Q., Bahler, J. and Pringle, J.R. (2001) Roles of a fimbrin and an alpha-actinin-like protein in fission yeast cell polarization and cytokinesis. *Mol Biol Cell*, **12**, 1061-1077.

Wu, J.Q., Kuhn, J.R., Kovar, D.R. and Pollard, T.D. (2003a) Spatial and temporal pathway for assembly and constriction of the contractile ring in fission yeast cytokinesis. *Dev Cell*, **5**, 723-734.

Wu, X., Liu, H., Liu, J., Haley, K.N., Treadway, J.A., Larson, J.P., Ge, N., Peale, F. and Bruchez, M.P. (2003b) Immunofluorescent labeling of cancer marker Her2 and other cellular targets with semiconductor quantum dots. *Nat Biotechnol*, **21**, 41-46.

Xu, C., Craig, R., Tobacman, L., Horowitz, R. and Lehman, W. (1999) Tropomyosin positions in regulated thin filaments revealed by cryoelectron microscopy. *Biophys J*, **77**, 985-992.

Yamamoto, M. (1996) Regulation of meiosis in fission yeast. *Cell Struct Funct*, **21**, 431-436.

Yamashiro-Matsumura, S. and Matsumura, F. (1988) Characterization of 83-kilodalton nonmuscle caldesmon from cultured rat cells: stimulation of actin binding of nonmuscle tropomyosin and periodic localization along microfilaments like tropomyosin. *J Cell Biol*, **106**, 1973-1983.

Yonemura, S. and Pollard, T.D. (1992) The localization of myosin I and myosin II in Acanthamoeba by fluorescence microscopy. *J Cell Sci*, **102**, 629-642.

Yu, H., Lee, J., Kim, S., Nguyen, G. and Kim, I. (2009) Electrochemical immunoassay using quantum dot/antibody probe for identification of cyanobacterial hepatotoxin microcystin-LR. *Anal Bioanal Chem*, **394**, 2173–2181.

Zhang, J., Badugu, R. and Lakowicz, J.R. (2008) Fluorescence Quenching of CdTe Nanocrystals by Bound Gold Nanoparticles in Aqueous Solution. *Plasmonics*, **3**, 3-11.